Spacecraft Attitude and Power Control Using Variable Speed Control Moment Gyros

A Thesis
Presented to
The Academic Faculty

by

Hyungjoo Yoon

In Partial Fulfillment
of the Requirements for the Degree
Doctor of Philosophy in the
School of Aerospace Engineering

Georgia Institute of Technology
December 2004

Spacecraft Attitude and Power Control Using Variable Speed Control Moment Gyros

Approved by:

Dr. Panagiotis Tsiotras, Advisor

Dr. Eric Johnson

Dr. J.V.R. Prasad

Dr. Robert Braun

Dr. David G. Taylor

November 12. 2004

TABLE OF CONTENTS

LIST OF TABLES

LIST OF FIGURES

SUMMARY

A Variable Speed Control Moment Gyro (VSCMG) is a recently introduced actuator for spacecraft attitude control. It generates a torque by exchanging angular momentum with the spacecraft body. As its name implies, a VSCMG is essentially a single-gimbal control moment gyro (CMG) with a flywheel allowed to have variable spin speed. In other words, it is a hybrid between two types of internal torque generators; namely, a conventional control moment gyro and a reaction wheel. Thanks to its extra degrees of freedom, a VSCMGs cluster can be used to achieve additional objectives, such as power tracking and/or singularity avoidance, as well as attitude control.

In this thesis, control laws for an integrated power/attitude control system (IPACS) for a satellite using VSCMGs are introduced. The gimbal rates of the VSCMGs are used to provide the reference-tracking torques, while the wheel accelerations are used for both attitude and power reference tracking. The power tracking objective is achieved by storing or releasing the kinetic energy in the wheels. The proposed control algorithms perform both the attitude and power tracking goals simultaneously. A model-based control and an indirect adaptive control for a spacecraft with uncertain inertia properties are developed. Moreover, control laws for equalization of the wheel speeds are also proposed. Wheel speed equalization distributes evenly the kinetic energy among the wheels, thus minimizing the possibility of wheel speed saturation and the occurrence of zero-speed singularities.

This thesis also provides a singularity avoidance method using VSCMGs. Single-gimbal CMGs have many advantages over other actuator systems for attitude control of spacecraft. However, their use as torque actuators is hindered by the presence of singularities which, when encountered, do not allow a CMG cluster to generate torques about arbitrary directions. In this thesis, the singularity avoidance problem using a VSCMGs cluster is

studied in detail for both the cases of attitude tracking with and without a power tracking requirement. A null motion method to avoid singularities is presented, and a criterion is developed to determine the momentum region over which this method will successfully avoid singularities. This criterion can be used to size the wheels and develop appropriate momentum damping strategies tailored to the specific mission requirements.

The spacecraft angular velocity and attitude control problem using a single VSCMG is addressed. Complete attitude control of a spacecraft is not possible with only one VSCMG, because of the conservation of the angular momentum. However, angular velocity stabilization and/or partial attitude control are still possible without violating the momentum conservation law. Both liner and nonlinear controllers which stabilize the angular velocity of the spacecraft, while achieving partial attitude regulation are provided. In partial attitude regulation, a body-fixed axis, chosen to be perpendicular to the gimbal axis, is controlled to aim at an arbitrarily given direction, while the spacecraft angular velocity is stabilized. This study can be used to characterize the types of missions that are possible when some of the VSCMG actuators used for spacecraft attitude control fail.

Finally, an adaptive control algorithm for the spacecraft attitude tracking in case when the actuator parameters, for instance the spin axis directions, are uncertain is developed. The spacecraft equations of motion in this case are fully nonlinear and represent a Multi-Input-Multi-Output (MIMO) system, thus adaptive tracking control is a challenging problem. The second-order equation of motion is converted to the first-order state space form, an then an adaptive controller is designed based on Lyapunov stability theorem. The smooth projection algorithm is applied to keep the parameter estimates inside a singularity-free region. The proposed controller successfully deals with unknown misalignments of the axis directions of the actuators. The design procedure can also be easily applied to general MIMO dynamical systems.

CHAPTER I

INTRODUCTION

1.1 Motivation

A single-gimbal control moment gyro (SGCMG) is a torque generating device used for the attitude control of a spacecraft. It operates in a continuous manner and can produce a large output torque. Thus, it has been regarded as an ideal actuator for spacecraft attitude control, especially for large-sized and/or large-angle maneuvering spacecraft. However, a SGCMG inherently contains a critical drawback of the 'singularity' problem, which limits practical application of the SGCMG for real missions. A variable speed control moment gyro (VSCMG) is an improved device to solve this problem, keeping the advantages of SGCMGs. It has a large number of control inputs, thus it may not have a singularity, or it can easily avoid a singularity. However, very little is known in the literature so far on the singularity problem of VSCMGs. In addition, the excess number of inputs of VSCMGs may be used for additional purposes other than attitude control. In particular, the VSCMGs can be used as so-called 'mechanical batteries', and can replace conventional chemical batteries. Such chemical batteries currently occupy a large portion of total weigh of a spacecraft. This means that the usage of VSCMGs as an mechanical battery can significantly improve the mass balance of a spacecraft. However, no one has seriously dealt with this issues in the literature thus far.

These two issues, the singularity problem and the usage of VSCMGs devices as energy storage, are the main topics of this thesis. Along with other additional issues, such as adaptive tracking control and underactuated attitude control etc., they are dealt in a mathematically rigorous manner. All the proposed control techniques and methods are also tested by several numerical simulations.

The following sections in this chapter introduce the VSCMG actuator system and the related topics dealt with in this thesis.

1.2 Control Moment Gyros (CMGs) and Variable Speed CMGs (VSCMGs)

A control moment gyro (CMG) is a device used as an actuator for the attitude control of a spacecraft. It generates torques through angular momentum transfer to and from the main spacecraft body. This is achieved by changing the direction of the angular momentum vector of a gimballed flywheel. Since a CMG operates in a continuous manner – contrary to the on/off operation of gas jets – it can achieve very precise attitude control. Moreover, as with other momentum exchange devices (e.g. reaction wheels), it does not consume any propellant, thus prolonging the life of the spacecraft. CMGs essentially act as torque amplifiers due to their torque amplification property [56]. This property makes them especially advantageous as attitude control actuators for large space spacecraft and space structures, e.g. a space station. In fact, CMGs have been used for attitude control in Skylab, MIR and the International Space Station (ISS).

There exist two types of control moment gyros, namely, the single gimbal CMGs (SGCMGs) and the double gimbal CMGs (DGCMGs), shown in Fig.1. The SGCMGs have several advantages over DGCMGs. First, they have a simpler mechanical structure. Second, their "torque amplification property" allows a small gimbal motor control (input) torque to generate a large (output) torque on the spacecraft. On the other hand, a SGCMGs system has the disadvantage of nontrivial singular gimbal states, which are mentioned in chapter IV.

In this thesis, a SGCMG and its variation, a variable speed CMG (VSCMG), are investigated. In order to keep the terminology simple, in the sequel the term CMG will be synonymous to a SGCMG system unless specifically stated otherwise. The concept of a VSCMG was first introduced by Ford and Hall [28] where it was called "gimballed momentum wheel." Whereas the wheel speed of a conventional CMG is kept constant, the wheel speed of a VSCMG is allowed to vary smoothly. A VSCMG can thus be considered as a hybrid device between a reaction wheel and a conventional CMG. VSCMGs have extra degrees of freedom and can be used for additional objectives such as energy storage, singularity avoidance, as well as attitude control.

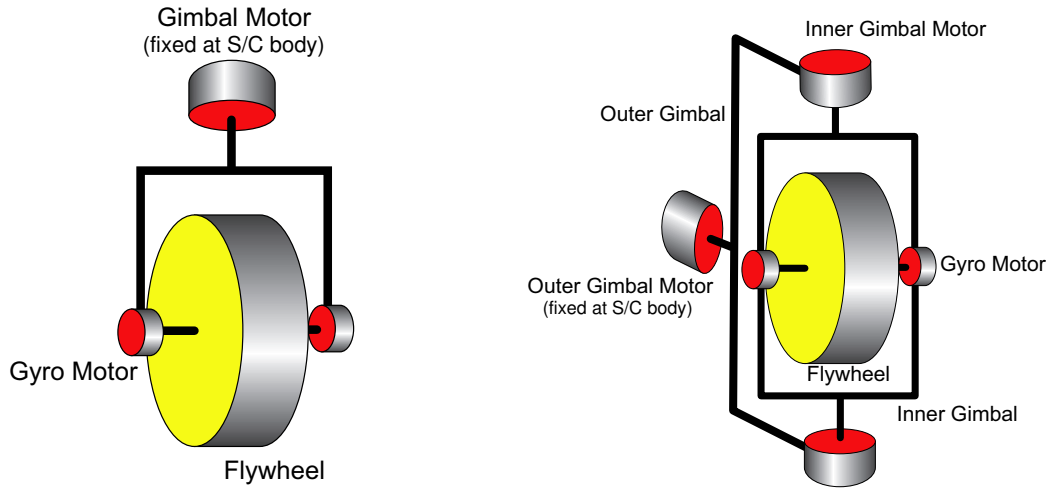

(a) Single Gimbal CMG

(b) Double Gimbal CMG

Figure 1: Two Types of CMG System

1.3 Adaptive Attitude Tracking Control of Spacecraft

The main purpose of CMG/VSCMG actuator systems is to generate a torque for attitude control of a spacecraft. Many works have been published on attitude control of spacecraft, and some of them [73, 71, 28, 29] used CMG/VSCMGs for the torque generator. In contrast to previous relevant results, the model-based control presented in this thesis achieves tracking of arbitrary trajectories as opposed to only attitude stabilization/regulation. Moreover, Refs. [28, 29] concentrate on rest-to-rest maneuvers using CMGs with a perfectly known spacecraft model. While Ref. [67] presents a general trajectory tracking VSCMG control law, none of the cited references treats the simultaneous attitude and power tracking problem with VSCMGs, as in Chapter 3 of this thesis.

In addition to model-based attitude and power tracking control law presented in Chapter 3, an adaptive control concept is also derived to deal with the uncertainty of the inertia properties of the spacecraft. For exact attitude tracking, the inertia of spacecraft should be known. However, the inertia of spacecraft may change considerably due to docking, releasing a payload, retrieving a satellite, sloshing and/or consumption of fuel etc., so an adaptive control scheme is chosen for precise attitude tracking control. Several adaptive control laws for the attitude tracking problem have been reported in the literature [5, 12, 74, 3, 82, 108, 69]

However, most of the previous results use variable thrust gas jets, momentum or reaction wheels or conventional CMGs as actuators. The adaptive tracking controller in Ref. [82] uses Euler angles and Rodriguez parameters (Gibbs vector) to describe the attitude of the spacecraft, so it is valid only in a narrow range due to the kinematic singularity. Reference [74] uses conventional CMGs and requires that the angular acceleration be measurable. In case the angular acceleration is not measurable, approximation schemes are needed. The adaptive controller developed in Ref. [108] has four asymptotically stable states, one of which is the desired state and the others are obtained through the rotation by an angle $\pm\pi$ around the axes of the desired frame. These undesired states become unstable if the reference motions are persistently exciting. The adaptive control law in Ref. [5] can be simplified if knowledge of the largest and smallest principal moments of inertia is available. In addition, it is shown that the products of inertia can be identified by constant tracking maneuvers. Reference [69] also deals with the attitude tracking controller which asymptotically approaches a specified linear PID response in the presence of the inertia errors.

Most references mentioned above assume that the unknown inertia parameters are constant, which is not valid for the CMG or VSCMG systems. As far as the author knows there are no results for adaptive attitude control for a VSCMG system. There have been a few results on the adaptive control for a conventional CMG system, but most of them use the linearized or simplified equations of motion [12, 74]. Of particular interest is Ref. [3], where adaptation is used to control a double-gimballed CMG with uncertain inertia properties. The present thesis offers the first design of an adaptive control using the complete nonlinear equations of motion for a rigid spacecraft with a VSCMG cluster, considering the variable moment of inertia due to the gimbal angle change. In addition, this control law achieves both attitude and power tracking.

1.4 Integrated Power and Attitude Control System (IPACS)

Current spacecraft are complex systems composed of several subsystems. They use chemical batteries to store excess energy generated by the solar panels during the period of exposure

to the sun; see Fig. 3. A typical example of a chemical battery is shown in Fig. 2. These batteries are used to provide power for the spacecraft subsystems during eclipse and are re-charged when the spacecraft is in the sunlight. However, the use of chemical batteries introduces several problems such as limited life cycle (less than 5 years), shallow depth of discharge (approximately 20-30% of their rated energy-storage capacity), large weight and strict temperature limits (at or below 20°C in a low-Earth orbit). As a matter of fact, these limitations often drive the entire spacecraft thermal design. Moreover, the use of chemical batteries requires additional system mass for controlling the charging and discharging cycles.

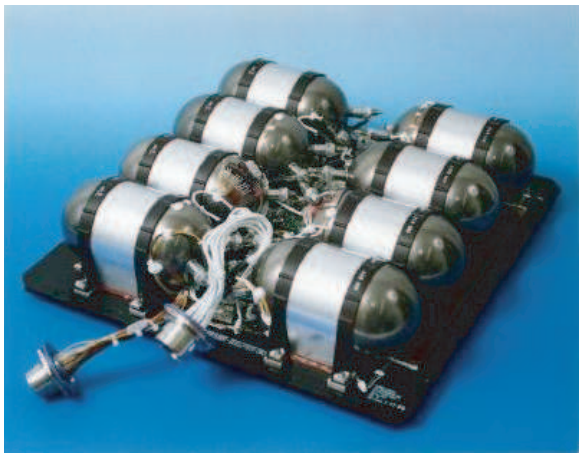

Figure 2: Typical Chemical Battery Used in a Satellite System

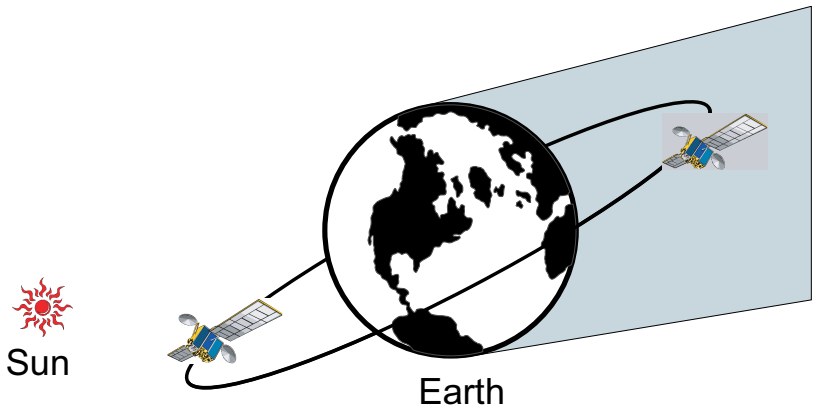

Figure 3: Typical Orbit of a Satellite

An alternative to chemical batteries is the use of flywheels to store energy. The use of flywheels as "mechanical batteries" has several significant benefits over the conventional

chemical battery systems, such as increased efficiency (up to 90% depth of discharge), longer lifetime (virtually unlimited), and the ability to operate in a relatively hot (up to 40°C) environment. It also has higher specific energy and specific power, and can be charged/discharged rapidly. Moreover, these mechanical battery systems can generate high-peak/impulse electric power, which is not easy to get from the chemical batteries. This benefit enables the mechanical batteries to be used to power space-based radar systems.

Most importantly, flywheels offer the potential to combine the energy-storage and the attitude-control functions into a single device, thus increasing reliability and significantly reducing the overall weight and spacecraft size. This means increased payload capacity and significant reduction of launch and fabrication costs.

This concept, termed the Integrated Power and Attitude Control System (IPACS) has been studied since the 1960s, but it has become particularly popular during the last decade. The use of flywheels instead of batteries to store energy on spacecraft was suggested as early as 1961 in a paper by Roes [66], where a 17 Wh/kg composite flywheel spinning at 10,000-20,000 rpm on magnetic bearings was proposed. The configuration included two counter-rotating flywheels, but the author did not mention the possibility of using the momentum stored in the wheels for attitude control. This idea grew over the next three decades. References [7, 20, 59] are representative of the period from 1970-1977, during which the term IPACS was coined [7]. Reference [51] addresses the optimal bearing control for high-speed momentum wheels. A complete survey on IPACS is given in Refs. [92] and [33].

To this date, this well-documented IPACS concept has never been implemented on an actual spacecraft mainly because of the high flywheel spin rates required for an efficient IPACS system [65] (on the order of 40,000 to 80,000 rpm - versus less than 6,500 rpm for conventional control moment gyros or momentum wheel actuators). At such high speeds, the actuators quickly wear out traditional mechanical bearings. Additional challenges include flywheel material mass/durability and stiffness inadequacies. Recently, the advances in composite materials and magnetic bearing technology promise to enable a realistic IPACS development. NASA Glenn Research Center announced that a flywheel energy storage

system recently achieved full-speed operation at 60,000 rpm [18].

Since flywheels are typically used onboard orbiting satellites to control the attitude, a suitable algorithm must be used to simultaneously meet the attitude torques and the power requirements. In Ref. [92], a control law was presented for an IPACS with momentum wheels. In the present thesis, a control law for an IPACS using Variable-Speed Single-Gimballed Control Moment Gyros (VSCMGs) is introduced. In addition to the ability to store a kinetic energy, single-gimbal VSCMGs still have the capability of producing large torques due to their torque amplification property, similarly to the SGCMGs. This makes them ideal for several commercial and military missions. On the other hand, VSCMG motors have to be stronger than for standard CMGs [73]. Due to the higher speeds of the VSCMGs (compared to low-speed momentum of CMG wheels) the power consumption for the VSCMG motors is expected to be several times larger than the one for CMGs (standard CMG motors are optimized for low power consumption at constant speed operation). Moreover, a significant component of the CMG power consumption – not present in fixed-wheel IPACS – is the power required to provide the gimbal holding torque against the gyroscopic torque along the bearing axis. A comparative study in terms of *total* power requirements between fixed-wheel, CMGs and VSCMGs seems to be desirable in this context.

The VSCMG cluster stores kinetic energy by spinning up its wheels during exposure to the sunlight. It provides power for the satellite subsystems by despinning the wheels during the eclipse. The spinning-up/spinning-down operation has to be coordinated in such a manner that the generated torques do not disturb the attitude. Most conventional control designs for the IPACS problem use the linearized equations of motion, but this thesis uses the complete, nonlinear equations with minimal assumptions. The derived equations of motion used in this thesis for a cluster of VSCMGs are similar to those in Refs. [73] and [29]. The only mild assumptions made in deriving these equations are that the spacecraft, flywheels, and gimbal frames are rigid and that the flywheels and gimbals are balanced. In addition, Ref. [73] imposes the assumption that the gimbal frame inertia is negligible. Without loss of generality, in the present developments, the gimbal angle rates and reaction wheel accelerations are taken as control inputs to the VSCMG system. That is, as is often

done in practice, a velocity steering law is assumed. This implies that the gimbal angle acceleration is kept small. An inner servo loop is used to ensure that the actual gimbal angle rate converges to the desired rate. This is somewhat different than commanding directly gimbal accelerations (i.e., acceleration steering law) that typically results in excessive gimbal torque commands [73, 60].

1.5 Singularity of CMGs and VSCMGs

The most serious obstacle in using a CMGs system in practice is the existence of singular gimbal angle states for which the CMGs system cannot generate a torque along arbitrary directions. At each singular state, all admissible torque directions lie on a two-dimensional surface in the three-dimensional angular momentum space. As a result, the CMG system cannot generate a torque normal to this surface. Because a CMG system changes only the direction and not the magnitude of the angular momentum vector of each wheel, there exists a maximum workspace for the total angular momentum of the CMG cluster. This workspace is the "angular momentum envelope." The gimbal angles for which the total angular momentum reaches this envelope are obviously singular, since the CMGs cannot generate a torque outward the envelope. These gimbal angle states are called "external singularities," and the CMG system is said to be "saturated." One can calculate the momentum envelope for a given CMG configuration, and thus anticipate the occurrence and location of the external singularities. These singularities can then be taken into account at the design step. Another approach is to use a momentum management scheme to dump the excess angular momentum of the CMG cluster before it becomes saturated. Nonetheless, there are also "internal singularities" inside the envelope, which are generally difficult to anticipate. Avoiding such internal singularities has been a long-standing problem in the CMG attitude control literature [56, 21, 85].

Although both SGCMGs and DGCMGs have singular gimbal angle states, the singularities of DGCMGs are trivial (i.e., external) or easily avoidable [49, 63]. On the other hand, SGCMGs have internal singularities which cannot be avoided without generating an output torque error. Although one can reduce the possibility of encountering singularities

by increasing the number of CMG wheels, it is, in general, impossible to completely eliminate the possibility of encountering singular states. For the special type of a "roof type," or "multiple type" SGCMG configuration [107, 49], which has no less than six wheels with three wheels having an identical gimbal axis direction, it has been shown that all internal singularities are avoidable without generating torque error; see Refs. [47, 49]. This wheel configuration is inefficient, however, in the sense that the radius of the momentum envelope is small despite the redundant number of wheels [46]. To make matters worse, the most popular steering law for SGCMGs (i.e., the minimum norm steering law) renders the singular states attractive thus exacerbating the steering problem [56, 21, 35].

The internal unavoidable singularities make SGCMGs less popular for typical space missions despite their other advantages. DGCMGs have been used in Skylab [49, 99, 101] and in the International Space Station (ISS) [101], whereas the Russian space station MIR used a cluster of six SGCMGs [101, 48]. MIR used a skew-configured, redundant, six-wheel SGCMGs cluster, with only four CMGs being active at a time. In this system, there still exist unavoidable internal singularities, but all of them lie near the envelope. This configuration is intentionally oversized in order to place all unavoidable singularities outside the required momentum reservoir [63].

A theory for the singularities of a CMG system was first established by Margulies and Aubrun [56]. They examined the geometric properties of the singular states, and introduced some important concepts such as the momentum envelope. They also introduced the *null motion* technique to avoid certain singular states. The term null motion refers to any strategy that changes the gimbal angles without generating any torque. Based on the work of Ref. [56] several authors have refined and improved the analysis of the singularities of CMGs. Tokar and Platonov [85] showed that a CMG system in a pyramid configuration (Fig. 7) has singular states at which a null motion strategy does not work. Kurokawa [47, 46, 45, 49] published several papers studying the characteristics of the singularities both from a mathematical and a geometric point of view. Specifically, Kurokawa presented a method to distinguish between hyperbolic (i.e., avoidable) and elliptical (unavoidable) singularities. Bedrossian et al [10] also introduced a method for classifying singularities and demonstrated

an analogy between the singularities of a CMG system and those of a robot manipulator. Most recently, Wie [106] provided a comprehensive mathematical treatment of the nature of singularities of a CMG system, emphasizing their characterization and visualization.

Most methods developed so far to tackle the CMG singularity problem can be divided into three categories. The first category consists of the so-called "singularity robust (SR)" methods [60, 29, 101], which produce a torque error when encountering singular states. These methods are relatively simple but they cannot generate the commanded torque exactly in the vicinity of the singular states. In particular, Wie [105] recently provided a steering law which avoids all singularities, albeit only for a case of spacecraft reorientation where precision tracking is not required during the whole duration of the maneuver. The second category uses local gradient methods which rely on null motion. If the CMG cluster has a redundant number of wheels (i.e., more than three) there exist null motions which do not affect the total angular momentum and thus output torque. (Figure 4 demonstrates the singular configurations and the null motions of a robot manipulator and a CMGs systems in 2-dimensional cases. In Fig. 4(b), each arrow indicates an angular momentum vector of each CMG flywheel.) The gradient methods search for a direction along which an objective function, containing information about the singularity, increases (or decreases) locally. One then applies a null motion along this direction. This method produces an output torque exactly equal to the required torque. However, as mentioned above, it is known that there are singular states which cannot be avoided using null motion methods [85, 10, 49].

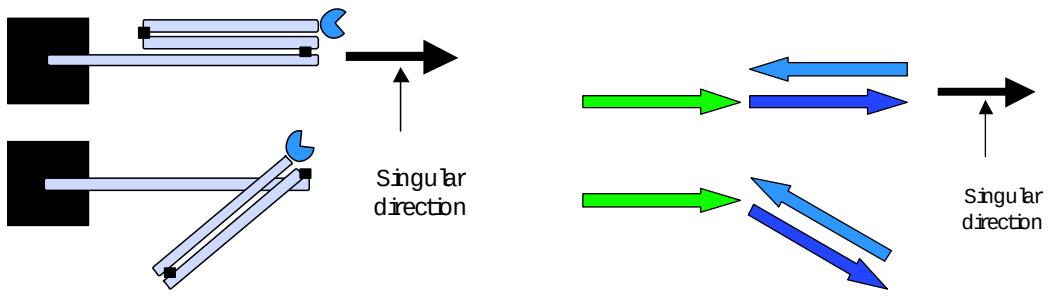

(a) 3-Link Manipulator (b) 3-CMGs System

Figure 4: Examples of Singularity and Null Motion.

The third category uses global avoidance methods, which include path planning [63], preferred gimbal angle [97], workspace restriction [48, 49] etc. These global methods anticipate the singular states and then they steer the gimbal angles so that the CMG system does not encounter any singularities. However, some of these methods need off-line calculation [63, 97] while others do not fully utilize the angular momentum capacity of the CMG cluster [48, 49].

In the present thesis, a singularity avoidance method using single gimbal variable speed control moment gyros (VSCMGs) is presented. First, a mathematical analysis for the singularities of a VSCMG cluster and a singularity avoidance method using null motion are presented. Although Schaub and Junkins [71] have also introduced a singularity avoidance method using VSCMGs, nonetheless, no conditions are provided in Ref. [71] under which such a strategy is possible. Moreover, in Ref. [71] the authors restrict the discussion to the case of attitude tracking, whereas in the present thesis the author includes the case of simultaneous attitude and power tracking. As shown in Section 5.2, this has several important repercussions to the singularity classification and avoidance problem.

1.6 Angular Velocity and Line-of-Sight Control Using A Single VSCMG

Recent advances in spacecraft and satellite control systems have succeeded in solving several challenging problems dealing with the attitude tracking and robust control of rigid and flexible spacecraft, optimal slew maneuvers, precision pointing, formation flying, etc. Techniques from nonlinear [103, 102, 94, 26, 75, 55], adaptive [80, 98, 78, 27, 4, 68], optimal [38, 25, 72, 23, 96, 14, 76, 61] and robust control [78, 50, 54, 13, 100] have been used to his end with success. Most, if not all, of these results have been developed under the assumption that the spacecraft is actively controlled with a sufficient number of actuators, which is equal to, or even larger than, the number of the degrees of freedom of the system. Although this is certainly the case with most current spacecraft, the issue of controlling a rigid spacecraft with less than three control torques has recently aroused the interest of many researchers, as it provides the theoretical foundation to account for unexpected

actuator failures. It also allows the minimization of the required number of actuators to perform certain missions.

Several papers have been published on the stabilization of the angular velocity (or detumbling) of a rigid spacecraft with less than three control torques [15, 1, 2, 83, 62, 8, 57, 91]. In these works only the dynamic (or kinetic) equations are under consideration, and the objective is to null the angular velocity vector of the spacecraft. Stabilization of the much more difficult complete equations (dynamics and kinematics) has also been addressed [17, 44, 87, 22, 58, 84, 90]; the objective of these references is to stabilize a spacecraft about a desired reference attitude with less than three control torques. See Ref. [88] for a full survey of the underactuated spacecraft control literature up to that time. In all previous references, the control torques are assumed to be provided by some external mechanism (e.g., gas jets or magnetotorquers, etc). Alternatively, internal torques generated by momentum exchange devices, such as reaction or momentum wheels or control moment gyros (CMGs) can also be used for attitude control of a spacecraft. Only few researchers have worked on the attitude stabilization [43, 42], detumbling and/or angular velocity control [95, 32, 9] problem using two or one reaction wheels.

Recently, Tsiotras et al. have addressed the stabilization of a spacecraft via a single VSCMG actuator [93]. In Ref. [93], it is shown that complete attitude stabilization may not always be possible due to the angular momentum conservation constraint (see Fig. 5), but the angular velocity system is linearly controllable, hence stabilizable. Both linear LQR feedback controllers and a nonlinear controller were designed in Ref. [93] for stabilizing the angular velocity equations.

The present thesis provides some new results for the angular velocity stabilization of a spacecraft via a single VSCMG, while also achieving partial attitude control. Even though complete attitude control is impossible due to the momentum conservation constraint, it is still possible to achieve stabilization about certain orientations lying in a feasible orientation manifold. The author investigates this possibility and provides both linear and nonlinear controllers which locally and globally stabilize the angular velocity system. These controllers also regulate the spacecraft attitude so that a body-fixed axis aims at a given inertial

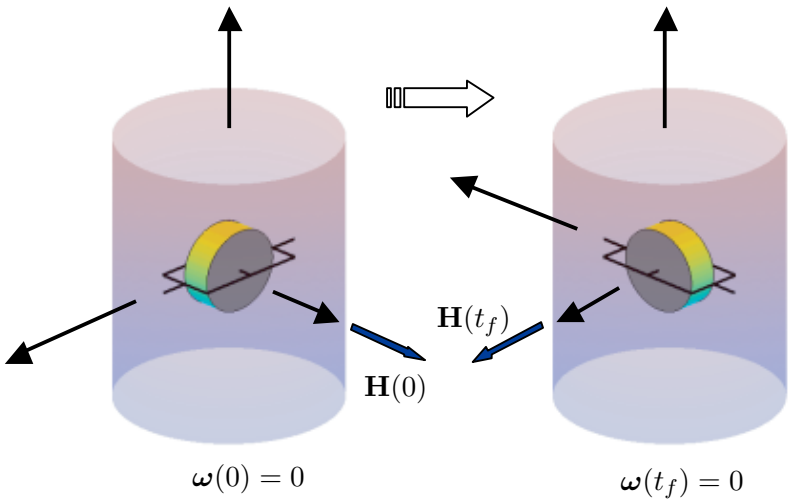

Figure 5: Examples of Infeasible Rest-to-Rest Maneuvering via a Single VSCMG.

direction. This problem is of interest not only from a theoretical point of view, but also from a practical point of view. For instance, if one installs a camera or an antenna fixed on the spacecraft, then one can control the line-of-sight of this camera/antenna so that it points along a desired direction with a single VSCMG. Therefore, if for a specific mission one does not need to track the complete attitude, then a single VSCMG is sufficient to achieve this control objective. Moreover, the present study also characterizes the types of missions that are possible when some of the VSCMG actuators used for the spacecraft attitude control fail.

1.7 Adaptive Spacecraft Attitude Tracking Control with Actuator Uncertainties

Adaptive attitude control of a spacecraft with uncertain parameters has been studied intensively in the past few decades [79, 12, 74, 108, 3, 5, 69]. This problem is also treated in this thesis, in Chapter 3. However, most (if not all) of these research copes with only the uncertainties in the inertia matrix of the spacecraft, assuming that an exact model of the actuator is available. In other words, these results have been derived under the assumption that the torque axis directions and/or input scalings of the actuators, (such as gas jets, reaction wheels, or CMGs/VSCMGs etc.) are exactly known. This assumption, however, is rarely satisfied in practice, because of misalignment of the actuator during the installation, aging

and wearing out of the mechanical/electrical parts, etc. The effect of these uncertainties on the overall system performance may be negligible for most cases. When the internal torque generators are used for Integrated Power and Attitude Control System (IPACS), however, the flywheels spins at high speeds to store kinetic energy. As a result, the effect of actuator modelling errors may cause large performance deterioration. In order to store large amount of kinetic energy while not generating large output torques, the flywheels have to cancel their angular momentum. If the exact direction of axes of the flywheels are unknown, such precise cancellation is impossible, causing large output torque errors.

One of the difficulties in designing adaptive controllers dealing with actuator uncertainties is that the spacecraft equations of motion represent a Multi-Input-Multi-Output (MIMO) system. The controller has to track at least three attitude parameters for full three-axis attitude control, and it generally needs three or more actuator torques. A lot of research has been published on the adaptive tracking problem, but most of them are only for Single-Input-Single-Output (SISO) or uncoupled multi-input systems. Slotine et. al. [81, 79] proposed adaptive controllers for MIMO systems, but these systems must be Hamiltonian, and the uncertainties are in the inertia term and/or Coriolis/centrifugal terms, but not in the actuator term. Ge [30] derived an adaptive control law for multi-link robot manipulator systems with uncertainties in the control input term, but the uncertainty must be in the input scalings. That is, the uncertainty matrix is diagonal if represented in a multiplicative form.

Recently, Chang [19] has provided an adaptive and robust tracking control for nonlinear MIMO systems. His work is based on the "smooth projection algorithm," which was also used in Refs. [64] and [41] for adaptive control design for SISO systems. This algorithm plays a key role in order to keep the parameter estimations inside a properly defined convex set, so that the estimations do not drift into a region where the control law may become singular.

In this thesis, an adaptive control law is designed for spacecraft attitude tracking using VSCMGs whose axis directions are not exactly known. The equations of motion of a spacecraft with VSCMGs is highly complicated, thus a set of slightly simplified equations is

used to design the control law. Even though the control design is provided for a spacecraft with VSCMGs, it can be easily applied to other dynamical systems, whose equations of motion can be written in the standard 2nd-order form, for instance, a spacecraft controlled by other types of actuators or a multi-link robot manipulator.

1.8 Outline of this Thesis

This thesis is organized as follows. In Chapter 2, the author provides the equations of motion of a spacecraft with a VSCMG cluster. In Chapter 3, two kinds of attitude tracking control laws are developed: One is a model-based control under the assumption that the exact inertia of the spacecraft is known, and the other is an adaptive control to handle uncertainty in the inertial matrix. These control laws are extended for the integrated power and attitude control system (IPACS). A wheel speed equalization method is also provided in this chapter. In Chapter 4, the author provides a review on the singularities of a conventional CMG cluster, focusing on the standard pyramid configuration. In addition, a new approach to classify the singularities into avoidable and unavoidable ones is presented. Figures of the singularities are also provided here. This chapter sets the stage for the singularity analysis of a VSCMG system given in Chapter 5. A singularity avoidance scheme using null motion and based on the gradient method is proposed. The analysis is extended to the case of combined attitude and power constraints. The author shows that there exist singularities in this case, and these are studied in detail. Chapter 6 provides an LQR controller which steers a body-fixed line-of-sight so that it aims at an arbitrarily given direction while stabilizing the angular velocity of a spacecraft. A multi-stage nonlinear controller is also designed to globally achieve this control objective. Chapter 7 outlines an adaptive control problem for attitude tracking when there exist uncertain parameters in the actuator modelling. Finally, Chapter 8 summarizes the main results of this thesis, and proposes several issues for the future study.

1.9 Contributions

This thesis presents a theoretical development of usage of the VSCMG for the simultaneous attitude and power control purpose. The following summary lists the contribution of this work.

- Adaptive control of spacecraft with varying moment of inertia :

  Many researchers have proposed adaptive control algorithms to deal with the unknown inertia problem. While they assumed that the unknown inertia of a spacecraft are constant, the total moments of inertia of a spacecraft with CMGs/VSCMGs are functions of the gimbal angle. The present thesis offers the first design of an adaptive control, considering the variable moment of inertia due to the gimbal angle change.

- IPACS using VSCMGs :

  Recently, the usage of flywheels as mechanical batteries has been extensively studied by many researchers in various fields. In particular, the application for a spacecraft is more challenging, because the speed changes of the flywheels will also generate output torque and may cause large attitude errors, unless they are properly controlled. The present thesis is the first published work to provide a control algorithm to meet simultaneously both attitude and power requirements using the flywheels of VSCMGs.

- Singularity Analysis of CMGs :

  The single-gimbaled CMGs have many advantages over other actuators, but they have a singularity problem. Some researchers have suggested to use the null motion to avoid the singularities, but found that there are singularities which cannot be avoided using the null motion. The present thesis derives a criterion for the existence of null motion, which is identical with that in the previous works, but it is derived under a more mathematically straightforward procedure. The thesis also provides a 3-dimensional visualization of the singular configurations with high quality.

- Singularity Analysis of VSCMGs (with and without the power constraints) :

  The present thesis also extends the singularity analysis of CMGs to the VSCMGs

case. This work is the first published result which unveils the characteristics of the singularities of VSCMGs. Moreover, the thesis also provides an important corollary for designing fail safe modes, by showing that only a certain number of CMGs need to operate as VSCMGs in order to avoid the singularities. In addition, the thesis presents a similar analysis for the case where the VSCMGs are used for power tracking as well. The analysis can be used to determine the wheel design specifications (size and/or number of wheels and the skew angle) or dictate the initiation of momentum dumping.

- Line-of-sight regulation with angular velocity stabilization with a single VSCMG :

  The control problem with only one VSCMG is first dealt with in this thesis. It is a kind of the underactuated spacecraft control problem, where less than three control inputs are used for the attitude control. It is shown that only a certain type of partial attitude control is available. As an example for such partial attitude control, the line-of-sight regulation with angular velocity stabilization is introduced and solved. This result can be used for real spacecraft missions where only the direction of cammer/antenna is considered.

- Adaptive control with actuator uncertainties :

  The present thesis provides the first adaptive control method of a spacecraft with uncertainties in the actuator model. The suggested adaptive method attenuates the tracking error caused by unknown actuator parameters, for instance, misaligned axis directions and/or the unknown gains due to aging and/or wearing. Though the method still leaves room for improvements (for instance, the reductions of the number of the estimates), the present thesis provides a first step in this direction.

CHAPTER II

SYSTEM MODEL

2.1 Dynamics

Consider a rigid spacecraft with a cluster of N single-gimbal VSCMGs used to provide internal torques, as shown in Fig. 6*.

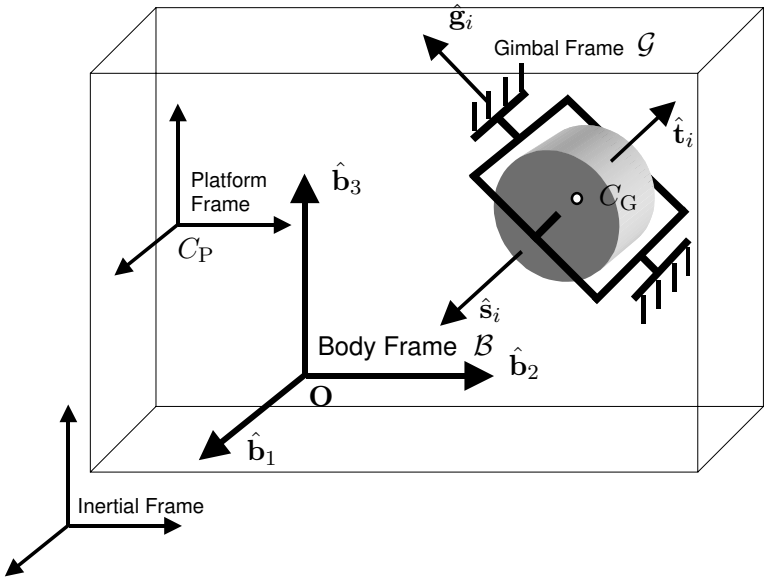

Figure 6: Spacecraft Body with a Single VSCMG

The definition of the axes are as follows.

$\hat{\mathbf{g}}_i$: gimbal axis vector

$\hat{\mathbf{s}}_i$: spin axis vector

$\hat{\mathbf{t}}_i$: transverse axis vector (torque vector) given as $\hat{\mathbf{t}}_i = \hat{\mathbf{g}}_i \times \hat{\mathbf{s}}_i$.

The total angular momentum of a spacecraft with a VSCMG cluster consisting of N wheels can be expressed in the spacecraft body frame as

$$\mathbf{h} = J\boldsymbol{\omega} + A_g I_{\mathrm{cg}} \dot{\boldsymbol{\gamma}} + A_s I_{\mathrm{ws}} \boldsymbol{\Omega} \tag{1}$$

*Some symbols shown in this figure are not defined in this section, but will be later.

where $\boldsymbol{\gamma} = (\gamma_1, \ldots, \gamma_N)^T \in \mathbb{R}^N$ and $\boldsymbol{\Omega} = (\Omega_1, \ldots, \Omega_N)^T \in \mathbb{R}^N$ are column vectors whose elements are the gimbal angles and the wheel speeds of the VSCMGs with respect to the gimbals, respectively. See Appendix A for the detail procedure to derive it. In (1) the matrix J, is the inertia matrix of the whole spacecraft, defined as

$$J = {}^{B}I + A_s I_{\mathrm{cs}} A_s^T + A_t I_{\mathrm{ct}} A_t^T + A_g I_{\mathrm{cg}} A_g^T \tag{2}$$

where ${}^{B}I$ is the combined matrix of inertia of the spacecraft platform and the point-masses of the VSCMGs. The matrices $I_{c\star}$ and $I_{w\star}$ are diagonal with elements the values of the inertias of the gimbal plus wheel structure and wheel-only-structure of the VSCMGs, respectively. Specifically, $I_{\mathrm{c}\star} = I_{\mathrm{g}\star} + I_{\mathrm{w}\star}$ where $I_{\mathrm{g}\star} = \mathrm{diag}[I_{\mathrm{c}\star_1}, \ldots, I_{\mathrm{c}\star_{\mathrm{N}}}]$ and $I_{\mathrm{w}\star} = \mathrm{diag}[I_{\mathrm{w}\star_1}, \ldots, I_{\mathrm{w}\star_{\mathrm{N}}}]$, where $\star$ is g, s or t. The matrices $A_\star \in \mathbb{R}^{3\times N}$ have as columns the gimbal, spin and transverse directional unit vectors expressed in the body-frame. Thus, $A_s = [\hat{\mathbf{s}}_1, \cdots, \hat{\mathbf{s}}_N]$, $A_t = \left[\hat{\mathbf{t}}_1, \cdots, \hat{\mathbf{t}}_N\right]$, and $A_g = [\hat{\mathbf{g}}_1, \cdots, \hat{\mathbf{g}}_N]$. Note that $A_s = A_s(\boldsymbol{\gamma})$ and $A_g = A_g(\boldsymbol{\gamma})$ and thus both matrices A_s and A_g are functions of the gimbal angles. Consequently, the inertia matrix $J = J(\boldsymbol{\gamma})$ is also a function of the gimbal angles $\boldsymbol{\gamma}$, whereas the matrix ${}^{B}I$ is constant.

The equations of motion are derived by taking the time derivative of the total angular momentum of the system. If $\mathbf{h}_c$ is defined as $\mathbf{h}_c = A_g I_{\mathrm{cg}} \dot{\boldsymbol{\gamma}} + A_s I_{\mathrm{ws}} \boldsymbol{\Omega}$ then $\mathbf{h} = J\boldsymbol{\omega} + \mathbf{h}_c$ and the time derivative of $\mathbf{h}$ with respect to the body B-frame is $\dot{\mathbf{h}} = \dot{J}\boldsymbol{\omega} + J\dot{\boldsymbol{\omega}} + \dot{\mathbf{h}}_c = -[\boldsymbol{\omega}^{\times}]\,\mathbf{h} + \boldsymbol{g}_e$ where $\boldsymbol{g}_e$ is an external torque (assumed here to be zero for simplicity), and where for any vector $\boldsymbol{x} = (x_1, x_2, x_3)^T \in \mathbb{R}^3$, the notation $[\boldsymbol{x}^{\times}]$ denotes the skew-symmetric matrix

$$[\boldsymbol{x}^{\times}] = \begin{bmatrix} 0 & -x_3 & x_2 \\ x_3 & 0 & -x_1 \\ -x_2 & x_1 & 0 \end{bmatrix}.$$

The matrices A_g, A_s, and A_t can be written using their initial values at time $t = 0$, A_{g0}, A_{s0}, A_{t0} and the gimbal angles as [28]

$$A_g = A_{g0} \tag{3}$$

$$A_s = A_{s0}[\cos\boldsymbol{\gamma}]^d + A_{t0}[\sin\boldsymbol{\gamma}]^d \tag{4}$$

$$A_t = A_{t0}[\cos\boldsymbol{\gamma}]^d - A_{s0}[\sin\boldsymbol{\gamma}]^d \tag{5}$$

where $\cos\boldsymbol{\gamma} = (\cos\boldsymbol{\gamma}_1, \ldots, \cos\boldsymbol{\gamma}_N)^T \in \mathbb{R}^N$ and $\sin\boldsymbol{\gamma} = (\sin\boldsymbol{\gamma}_1, \ldots, \sin\boldsymbol{\gamma}_N)^T \in \mathbb{R}^N$, and where $[\boldsymbol{x}]^d \in \mathbb{R}^{N\times N}$ denotes a diagonal matrix with its elements the components of the vector $\boldsymbol{x} \in \mathbb{R}^N$, i.e., $[\boldsymbol{x}]^d = \text{diag}(x_1, x_2, \ldots, x_N)$. Using Eqs. (3)-(5), a simple calculation shows that $\dot{A}_s = A_t[\dot{\boldsymbol{\gamma}}]^d$ and $\dot{A}_t = -A_s[\dot{\boldsymbol{\gamma}}]^d$. The time derivatives of J and $\mathbf{h}_c$ are then calculated as

$$\dot{\mathbf{h}}_c = A_g I_{\text{cg}}\ddot{\boldsymbol{\gamma}} + A_t I_{\text{ws}}[\boldsymbol{\Omega}]^d\dot{\boldsymbol{\gamma}} + A_s I_{\text{ws}}\dot{\boldsymbol{\Omega}} \tag{6}$$

and

$$\dot{J} = A_t[\dot{\boldsymbol{\gamma}}]^d(I_{\text{cs}} - I_{\text{ct}})A_s^T + A_s[\dot{\boldsymbol{\gamma}}]^d(I_{\text{cs}} - I_{\text{ct}})A_t^T, \tag{7}$$

where we have made use of the obvious fact that $[\dot{\boldsymbol{\gamma}}]^d\boldsymbol{\Omega} = [\boldsymbol{\Omega}]^d\dot{\boldsymbol{\gamma}}$. Finally, the dynamic equations take the form

$$\begin{aligned}\Big(A_t[\dot{\boldsymbol{\gamma}}]^d(I_{\text{cs}} - I_{\text{ct}})A_s^T + A_s[\dot{\boldsymbol{\gamma}}]^d(I_{\text{cs}} - I_{\text{ct}})A_t^T\Big)\boldsymbol{\omega} + J\dot{\boldsymbol{\omega}} \\ + A_g I_{\text{cg}}\ddot{\boldsymbol{\gamma}} + A_t I_{\text{ws}}[\boldsymbol{\Omega}]^d\dot{\boldsymbol{\gamma}} + A_s I_{\text{ws}}\dot{\boldsymbol{\Omega}} + [\boldsymbol{\omega}^\times]\Big(J\boldsymbol{\omega} + A_g I_{\text{cg}}\dot{\boldsymbol{\gamma}} + A_s I_{\text{ws}}\boldsymbol{\Omega}\Big) = 0\end{aligned} \tag{8}$$

Note that the equations for a VSCMG system can also be applied to a reaction/momemtum wheel system by letting the gimbal angles $\boldsymbol{\gamma}$ be constant. They can also be applied to a conventional CMG system by letting the wheel rotation speeds $\boldsymbol{\Omega}$ be constant.

2.2 Kinematics

There are various ways to represent the attitude of a rigid body. In this thesis, the Euler parameters and the so-called modified Rodrigues parameters (MRPs) are mainly used in designing controllers and conducting simulations.

The Euler parameters, also known as 'Quaternions', is invented by Hamilton as a result of searching for hypercomplex numbers that could be represented by points in three dimensional space [104]. The quaternion parametrization is closely related with Euler's eigenaxis rotation theorem. When a attitude is represented by the Euler principal unit vector $\hat{\eta}$ and angle ϕ, the Euler parameters are defined by

$$[q_1, q_2, q_3]^T = \hat{\eta}\sin(\phi/2) \tag{9a}$$

$$q_4 = \cos(\phi/2) \tag{9b}$$

and there is a constraint between these parameters as

$$q_1^2 + q_2^2 + q_3^2 + q_4^2 = 1. \tag{10}$$

The quaternion with four Euler parameters is widely used because it is singularity-free while it has a minimum redundancy of one.

The modified Rodrigues parameters (MRPs) given in Refs. [86, 70] and [77] are also used to describe the attitude kinematics error of the spacecraft. The MRPs are defined in terms of the Euler principal unit vector $\hat{\eta}$ and angle ϕ by

$$\boldsymbol{\sigma} = [\sigma_1, \sigma_2, \sigma_3]^T = \hat{\eta} \tan(\phi/4). \tag{11}$$

The MRPs have the advantage of being well defined for the whole range for rotations [86, 70, 89], i.e., $\phi \in [0, 2\pi)$, while they have no redundancy. There is a relationship between the Euler parameters and MRPs as

$$\sigma_i = \frac{q_i}{1 + q_4}, \quad i = 1, 2, 3. \tag{12}$$

The differential equation that governs the kinematics in terms of the MRPs is given by

$$\dot{\boldsymbol{\sigma}} = G(\boldsymbol{\sigma})\boldsymbol{\omega} \tag{13}$$

where $G(\boldsymbol{\sigma}) = \frac{1}{2}\Big(\mathbf{I} + [\boldsymbol{\sigma}^{\times}] + \boldsymbol{\sigma}\boldsymbol{\sigma}^T - [\frac{1}{2}(1 + \boldsymbol{\sigma}^T\boldsymbol{\sigma})]\,\mathbf{I}\Big)$ and $\mathbf{I}$ is the 3×3 identity matrix.

It has to be mentioned that the use of the MRPs to describe the kinematics is done without loss of generality. Any other suitable kinematic description could have been used with the conclusions of the thesis remaining essentially the same.

CHAPTER III

ATTITUDE AND POWER TRACKING CONTROL OF A SPACECRAFT

3.1 Model-Based Attitude Tracking Controller

In this section a control law based on Lyapunov stability theory is derived for the attitude tracking problem. In the sequel, it is assumed that the spacecraft and VSCMGs inertia properties are exactly known.

3.1.1 Lyapunov Stability Condition for Attitude Tracking

Assume that the attitude to be tracked is given in terms of the dynamics and kinematics of a desired reference frame (D-frame), i.e., in terms of some known functions $\boldsymbol{\sigma}_d(t)$, $\boldsymbol{\omega}_d(t)$ and $\dot{\boldsymbol{\omega}}_d(t)$ for $t \geq 0$. Here $\boldsymbol{\sigma}_d$ is the MRP vector presenting the attitude of the D-frame w.r.t the inertial frame (N-frame) and $\boldsymbol{\omega}_d$ is the angular velocity of the D-frame w.r.t the N-frame expressed in the B-frame. Let $\boldsymbol{\omega}_d^D$ denote the angular velocity of the D-frame expressed in its own frame, and let $\dot{\boldsymbol{\omega}}_d^D$ denote the time derivative w.r.t. the D-frame, assumed to be known. It follows that $\boldsymbol{\omega}_d = C_D^B\,\boldsymbol{\omega}_d^D$ and $\dot{\boldsymbol{\omega}}_d = C_D^B\,\dot{\boldsymbol{\omega}}_d^D - [\boldsymbol{\omega}^\times]\,C_D^B\,\boldsymbol{\omega}_d^D$.

The angular-velocity tracking error written in the body frame (B-frame) is defined as $\boldsymbol{\omega}_e = \boldsymbol{\omega} - \boldsymbol{\omega}_d$ and $\boldsymbol{\sigma}_e$ is the Modified Rodrigues Parameters error between the reference frame and the body frame, calculated from $C_D^B(\boldsymbol{\sigma}_e) = C_N^B(\boldsymbol{\sigma})C_D^N(\boldsymbol{\sigma}_d)$. The kinematics of the MRP error is then $\dot{\boldsymbol{\sigma}}_e = G(\boldsymbol{\sigma}_e)\,\boldsymbol{\omega}_e$.

A feedback control law to render $\boldsymbol{\omega}_e \to 0$ and $\boldsymbol{\sigma}_e \to 0$ is found using the following Lyapunov function [86, 92, 73]

$$V = \tfrac{1}{2}\boldsymbol{\omega}_e^T J \boldsymbol{\omega}_e + 2k_0 \ln\left(1 + \boldsymbol{\sigma}_e^T \boldsymbol{\sigma}_e\right) \tag{14}$$

where $k_0 > 0$. This function is positive definite and radially unbounded in terms of the

tracking errors $\boldsymbol{\omega}_e$ and $\boldsymbol{\sigma}_e$. The time derivative of V is

$$\begin{aligned}\dot{V} &= \tfrac{1}{2}(\boldsymbol{\omega}-\boldsymbol{\omega}_d)^T\dot{J}(\boldsymbol{\omega}-\boldsymbol{\omega}_d)+(\boldsymbol{\omega}-\boldsymbol{\omega}_d)^T J(\dot{\boldsymbol{\omega}}-\dot{\boldsymbol{\omega}}_d)+2k_o\frac{2\boldsymbol{\sigma}_e^T\dot{\boldsymbol{\sigma}}_e}{1+\boldsymbol{\sigma}_e^T\boldsymbol{\sigma}_e}\\ &= -(\boldsymbol{\omega}-\boldsymbol{\omega}_d)^T\left\{-\tfrac{1}{2}\dot{J}(\boldsymbol{\omega}-\boldsymbol{\omega}_d)-J(\dot{\boldsymbol{\omega}}-\dot{\boldsymbol{\omega}}_d)-k_0\boldsymbol{\sigma}_e\right\}\end{aligned}$$

The previous equation suggests that for Lyapunov stability, the choice

$$-\tfrac{1}{2}\dot{J}(\boldsymbol{\omega}-\boldsymbol{\omega}_d)-J(\dot{\boldsymbol{\omega}}-\dot{\boldsymbol{\omega}}_d)-k_0\boldsymbol{\sigma}_e=K_1(\boldsymbol{\omega}-\boldsymbol{\omega}_d) \tag{15}$$

where K_1 is a 3×3 positive definite matrix results in global asymptotic stability of the closed-loop system*. Simple calculations show that

$$\dot{\mathbf{h}}_c+\tfrac{1}{2}\dot{J}(\boldsymbol{\omega}+\boldsymbol{\omega}_d)+[\boldsymbol{\omega}^\times]A_gI_{\rm cg}\dot{\boldsymbol{\gamma}}=K_1(\boldsymbol{\omega}-\boldsymbol{\omega}_d)+k_0\boldsymbol{\sigma}_e-J\dot{\boldsymbol{\omega}}_d-[\boldsymbol{\omega}^\times]\left(J\boldsymbol{\omega}+A_sI_{\rm ws}\boldsymbol{\Omega}\right) \tag{16}$$

The lhs of the previous equation contains the control inputs $\dot{\boldsymbol{\gamma}}$ and $\dot{\boldsymbol{\Omega}}$. In particular, it can be shown that

$$\dot{\mathbf{h}}_c+\tfrac{1}{2}\dot{J}(\boldsymbol{\omega}+\boldsymbol{\omega}_d)+[\boldsymbol{\omega}^\times]A_gI_{\rm cg}\dot{\boldsymbol{\gamma}}=B\ddot{\boldsymbol{\gamma}}+C\dot{\boldsymbol{\gamma}}+D\dot{\boldsymbol{\Omega}}$$

where $B=A_gI_{\rm cg}$, $D=A_sI_{\rm ws}$ and

$$\begin{aligned}C &= A_tI_{\rm ws}[\boldsymbol{\Omega}]^d+[\boldsymbol{\omega}^\times]A_gI_{\rm cg}\\ &\quad+\tfrac{1}{2}[(\mathbf{s}_1\mathbf{t}_1^T+\mathbf{t}_1\mathbf{s}_1^T)(\boldsymbol{\omega}+\boldsymbol{\omega}_d),\cdots,(\mathbf{s}_N\mathbf{t}_N^T+\mathbf{t}_N\mathbf{s}_N^T)(\boldsymbol{\omega}+\boldsymbol{\omega}_d)](I_{\rm cs}-I_{\rm ct})\end{aligned} \tag{17}$$

By denoting the rhs of Eq. (16) as the *required control torque* $\boldsymbol{L}_{\rm rm}$ for attitude tracking

$$\boldsymbol{L}_{\rm rm}=K_1(\boldsymbol{\omega}-\boldsymbol{\omega}_d)+k_0\boldsymbol{\sigma}_e-J\dot{\boldsymbol{\omega}}_d-[\boldsymbol{\omega}\times]\left(J\boldsymbol{\omega}+A_sI_{\rm ws}\boldsymbol{\Omega}\right)$$

one obtains that the control inputs must be chosen as

$$B\ddot{\boldsymbol{\gamma}}+C\dot{\boldsymbol{\gamma}}+D\,\dot{\boldsymbol{\Omega}}=\boldsymbol{L}_{\rm rm} \tag{18}$$

3.1.2 Velocity-Based Steering Law for Attitude Tracking

Typically, the gimbal acceleration term $B\ddot{\boldsymbol{\gamma}}$ can be ignored since the matrix B is small compared to the matrices C and D [73]. In this case $\dot{\boldsymbol{\gamma}}$ and $\dot{\boldsymbol{\Omega}}$ can be used as control inputs

*Strictly speaking, the choice of Eq. (15) proves only Lyapunov stability. Asymptotic convergence to the origin follows from a straightforward argument using La Salle's invariant set theory; see, for instance, Refs. [92, 41]. For the sake of brevity, the details of the proof is omited.

instead of $\ddot{\boldsymbol{\gamma}}$ and $\dot{\boldsymbol{\Omega}}$. This is referred to in the literature as (gimbal) velocity-based steering law. Letting $B\ddot{\boldsymbol{\gamma}} \approx 0$ in Eq. (18) the condition for stabilization then becomes

$$[C \quad D] \begin{bmatrix} \dot{\boldsymbol{\gamma}} \\ \dot{\boldsymbol{\Omega}} \end{bmatrix} = \boldsymbol{L}_{\mathrm{rm}} \tag{19}$$

Since I_{ws} and $[\boldsymbol{\Omega}]^d$ are diagonal matrices and the second and third terms in the rhs of Eq. (17) are relatively small, it follows that the column vectors of the C matrix are almost parallel to the transverse axes of the gimbal structure and the column vectors of the D matrix are parallel to the spin axes of the gimbal structure. Therefore, if there are at least two VSCMGs and their (fixed) gimbal axes are not parallel to each other, and if none of the wheel spin rates becomes zero, the column vectors of C and D always span the 3-dimensional space. It follows that this VSCMG system can generate control torques along an arbitrary direction. In other words, such a VSCMG system never falls into the singularity (gimbal lock) of a conventional CMG system owing to the extra degrees of freedom provided by the wheel speed control [73]. Moreover, if one has three or more VSCMGs, Eq. (19) is underdetermined and there exist null-motion solutions which do not have any effect on the generated control torque [71, 29]. Therefore, one can use this null-motion for power tracking and/or wheel speed equalization. This is discussed in the 'Power Tracking' section (Sec. 3.3) below.

3.1.3 Acceleration-Based Steering Law for Attitude Tracking

The gimbal motors require angle acceleration (equivalently, torque) commands instead of gimbal rate commands. The control law in terms of $\dot{\boldsymbol{\gamma}}$ has then to be implemented via another feedback loop around the gimbal angle *acceleration*. For instance, once the reference or desired gimbal rate command $\dot{\boldsymbol{\gamma}}_d$ has been determined from, say, (19) or (30), (36) below, the gimbal acceleration (and hence torque) command can be computed from

$$\ddot{\boldsymbol{\gamma}} = K_a(\dot{\boldsymbol{\gamma}} - \dot{\boldsymbol{\gamma}}_d) + \ddot{\boldsymbol{\gamma}}_d \approx K_a(\dot{\boldsymbol{\gamma}} - \dot{\boldsymbol{\gamma}}_d) \tag{20}$$

where K_a is a 4×4 matrix of controller gains. By choosing the matrix K_a to be Hurwitz, this control law will force the actual gimbal rates $\dot{\boldsymbol{\gamma}}$ to track $\dot{\boldsymbol{\gamma}}_d$ as $t \to \infty$.

3.2 Adaptive Attitude Tracking Controller

In this section, a control law is designed to deal with the uncertainty associated with the spacecraft inertia matrix. Several research results have been published on adaptive attitude control of spacecraft, but most of these results use gas jets and/or reaction/momentum wheels as actuators. In all these cases, the spacecraft inertia matrix J is constant. As stated previously, a difficulty arises from the fact that in the VSCMG (and CMG) case the spacecraft inertia matrix J is not constant because it depends on the gimbal angles $\boldsymbol{\gamma}$.

Next, an adaptive control law is proposed for the VSCMG case. The approach follows arguments that are similar (but not identical) to standard adaptive control design techniques. In the sequel it is assumed that the VSCMG cluster inertia properties are exactly known.

3.2.1 Adaptive Control with VSCMGs

In the VSCMG mode, the inertia matrix J is not constant because it depends on the gimbal angles $\boldsymbol{\gamma}$. However, the *derivative* of J is known since it is determined by the control gimbal commands $\dot{\boldsymbol{\gamma}}$. In this section the author uses this observation to design an adaptive control law which uses estimates of the elements of J. Although direct adaptive schemes that do not identify the moments of inertia are also possible, knowledge of the inertia matrix is often required to meet other mission objectives. Such direct adaptive schemes is not pursued in this work. Of course, as with all typical adaptive control schemes, persistency of excitation of the trajectory is required to identify the correct values of the inertia matrix. Nonetheless, in all cases it is shown that the controller stabilizes the system.

First, the equations of the system (8) is rewritten as follows

$$\tfrac{1}{2}\dot{J}\boldsymbol{\omega} + J\dot{\boldsymbol{\omega}} + [\boldsymbol{\omega}^{\times}](J\boldsymbol{\omega} + A_s I_{\mathrm{ws}}\boldsymbol{\Omega}) + B\ddot{\boldsymbol{\gamma}} + \tilde{C}\dot{\boldsymbol{\gamma}} + D\dot{\boldsymbol{\Omega}} = 0 \tag{21}$$

where B and D as before, and where

$$\begin{aligned}\tilde{C} &= A_t I_{\mathrm{ws}}[\boldsymbol{\Omega}]^d + [\boldsymbol{\omega}^{\times}]A_g I_{\mathrm{cg}} \\ &\quad + \tfrac{1}{2}[(\mathbf{s}_1\mathbf{t}_1^T + \mathbf{t}_1\mathbf{s}_1^T)\boldsymbol{\omega}, \cdots, (\mathbf{s}_N\mathbf{t}_N^T + \mathbf{t}_N\mathbf{s}_N^T)\boldsymbol{\omega}](I_{\mathrm{cs}} - I_{\mathrm{ct}})\end{aligned} \tag{22}$$

It is again assumed that the term $B\ddot{\boldsymbol{\gamma}}$ can be neglected and hence the system dynamics reduce to

$$\tfrac{1}{2}\dot{J}\,\boldsymbol{\omega} + J\dot{\boldsymbol{\omega}} + [\boldsymbol{\omega}^{\times}](J\boldsymbol{\omega} + A_s I_{\mathrm{ws}}\boldsymbol{\Omega}) + \tilde{C}\dot{\boldsymbol{\gamma}} + D\dot{\boldsymbol{\Omega}} = 0 \tag{23}$$

By differentiating now Eq. (13), one obtains $\boldsymbol{\omega} = G^{-1}(\boldsymbol{\sigma})\dot{\boldsymbol{\sigma}}$ and $\ddot{\boldsymbol{\sigma}} = G(\boldsymbol{\sigma})\dot{\boldsymbol{\omega}} + \dot{G}(\boldsymbol{\sigma},\dot{\boldsymbol{\sigma}})\,\boldsymbol{\omega}$ and using Eq. (23),

$$JG^{-1}(\boldsymbol{\sigma})\ddot{\boldsymbol{\sigma}} = JG^{-1}(\boldsymbol{\sigma})\dot{G}(\boldsymbol{\sigma},\dot{\boldsymbol{\sigma}})\boldsymbol{\omega} - [\boldsymbol{\omega}^{\times}](J\boldsymbol{\omega} + A_s I_{\mathrm{ws}}\boldsymbol{\Omega}) - \tilde{C}\dot{\boldsymbol{\gamma}} - D\dot{\boldsymbol{\Omega}} - \tfrac{1}{2}\dot{J}\,\boldsymbol{\omega}.$$

Let now $\mathbf{h}_1 = J\boldsymbol{\omega}$ and $\mathbf{h}_2 = A_s I_{\mathrm{ws}}\boldsymbol{\Omega}$. The equation of the system can then be written in the standard form,

$$H^*(\boldsymbol{\sigma})\,\ddot{\boldsymbol{\sigma}} + C^*(\boldsymbol{\sigma},\dot{\boldsymbol{\sigma}})\,\dot{\boldsymbol{\sigma}} = F \tag{24}$$

where

$$\begin{aligned} H^*(\boldsymbol{\sigma}) &= G^{-T}(\boldsymbol{\sigma})JG^{-1}(\boldsymbol{\sigma}) \\ C^*(\boldsymbol{\sigma},\dot{\boldsymbol{\sigma}}) &= -G^{-T}(\boldsymbol{\sigma})JG^{-1}(\boldsymbol{\sigma})\dot{G}(\boldsymbol{\sigma},\dot{\boldsymbol{\sigma}})G^{-1}(\boldsymbol{\sigma}) - G^{-T}(\boldsymbol{\sigma})[h_1^{\times}]G^{-1}(\boldsymbol{\sigma}) \\ F &= G^{-T}(\boldsymbol{\sigma})[h_2^{\times}]\,\boldsymbol{\omega} - G^{-T}(\boldsymbol{\sigma})\,(\tilde{C}\dot{\boldsymbol{\gamma}} + D\dot{\boldsymbol{\Omega}}) - \tfrac{1}{2}G^{-T}(\boldsymbol{\sigma})\dot{J}\,\boldsymbol{\omega} \end{aligned}$$

Note that the lhs of Eq. (24) is linear in terms of the elements of J which are the unknown parameters to be estimated.

The term $\dot{G}(\boldsymbol{\sigma},\dot{\boldsymbol{\sigma}})$ can be derived by differentiating the expression for $G(\boldsymbol{\sigma})$ as

$$\dot{G}(\boldsymbol{\sigma},\dot{\boldsymbol{\sigma}}) = \tfrac{1}{2}\Big([\dot{\boldsymbol{\sigma}}^{\times}] + \dot{\boldsymbol{\sigma}}\boldsymbol{\sigma}^T + \boldsymbol{\sigma}\dot{\boldsymbol{\sigma}}^T - \dot{\boldsymbol{\sigma}}^T\boldsymbol{\sigma}\,\mathbf{I}\Big) \tag{25}$$

Using now the fact that $\frac{d}{dt}(G^{-1}) = -G^{-1}\dot{G}G^{-1}$ one has

$$\dot{H}^* - 2C^* = \frac{d}{dt}(G^{-T})JG^{-1} - G^{-T}J\frac{d}{dt}(G^{-1}) + 2G^{-T}[h_1^{\times}]G^{-1} + G^{-T}(\boldsymbol{\sigma})\dot{J}G^{-1}(\boldsymbol{\sigma})$$

which implies that the matrix $(\dot{H}^* - 2C^* - G^{-T}\dot{J}G^{-1})$ is skew-symmetric.

The remaining procedure follows one of the standard adaptive control design methods [82]. To this end, let the parameter vector $\boldsymbol{a} = (J_{11}\ J_{12}\ J_{13}\ J_{22}\ J_{23}\ J_{33})^T \in \mathbb{R}^6$ and let $\hat{\boldsymbol{a}}$ be the parameter vector estimate. The parameter estimation error is $\tilde{\boldsymbol{a}} = \hat{\boldsymbol{a}} - \boldsymbol{a}$ and $\tilde{\boldsymbol{\sigma}} = \boldsymbol{\sigma} - \boldsymbol{\sigma}_d$ is the attitude tracking error. Consider now the Lyapunov-like function

$$V_a = \tfrac{1}{2}\boldsymbol{s}^T H^*(\boldsymbol{\sigma})\boldsymbol{s} + \tfrac{1}{2}\tilde{\boldsymbol{a}}^T\Gamma^{-1}\tilde{\boldsymbol{a}} \tag{26}$$

where Γ is a strictly positive constant matrix and where $\boldsymbol{s} = \dot{\tilde{\boldsymbol{\sigma}}} + \lambda\tilde{\boldsymbol{\sigma}} = \dot{\boldsymbol{\sigma}} - \dot{\boldsymbol{\sigma}}_r$ ($\lambda > 0$) is a measure of the attitude tracking error. Note that $\dot{\boldsymbol{\sigma}}_r = \dot{\boldsymbol{\sigma}}_d - \lambda\tilde{\boldsymbol{\sigma}}$ is the reference velocity vector. Differentiating V, and using the skew-symmetry of the matrix $(\dot{H}^* - 2C^* - G^{-T}\dot{J}G^{-1})$, one obtains

$$\dot{V}_a = \boldsymbol{s}^T\Big(F - H^*(\boldsymbol{\sigma})\ddot{\boldsymbol{\sigma}}_r - C^*(\boldsymbol{\sigma},\dot{\boldsymbol{\sigma}})\dot{\boldsymbol{\sigma}}_r + \tfrac{1}{2}G^{-T}(\boldsymbol{\sigma})\dot{J}G^{-1}(\boldsymbol{\sigma})\boldsymbol{s}\Big) + \tilde{\boldsymbol{a}}^T\Gamma^{-1}\dot{\tilde{\boldsymbol{a}}}$$

Let a control law such that

$$F = \hat{H}^*(\boldsymbol{\sigma})\ddot{\boldsymbol{\sigma}}_r + \hat{C}^*(\boldsymbol{\sigma},\dot{\boldsymbol{\sigma}})\dot{\boldsymbol{\sigma}}_r - K_D\boldsymbol{s} - \tfrac{1}{2}G^{-T}(\boldsymbol{\sigma})\dot{J}G^{-1}(\boldsymbol{\sigma})\boldsymbol{s} \tag{27}$$

where $\hat{H}^* = G^{-T}\hat{J}G^{-1}$ and $\hat{C}^* = -G^{-T}\hat{J}G^{-1}\dot{G}G^{-1} - G^{-T}[\hat{\mathbf{h}}_1^{\times}]G^{-1}$ and where K_D is a symmetric positive definite matrix. Then it follows that

$$\dot{V}_a = \boldsymbol{s}^T\Big(\tilde{H}^*(\boldsymbol{\sigma})\ddot{\boldsymbol{\sigma}}_r + \tilde{C}^*(\boldsymbol{\sigma},\dot{\boldsymbol{\sigma}})\dot{\boldsymbol{\sigma}}_r - K_D\boldsymbol{s}\Big) + \tilde{\boldsymbol{a}}^T\Gamma^{-1}(\dot{\hat{\boldsymbol{a}}} - \dot{\boldsymbol{a}})$$

where $\tilde{H}^*(\boldsymbol{\sigma}) = \hat{H}^*(\boldsymbol{\sigma}) - H^*(\boldsymbol{\sigma})$ and $\tilde{C}^*(\boldsymbol{\sigma},\dot{\boldsymbol{\sigma}}) = \hat{C}^*(\boldsymbol{\sigma},\dot{\boldsymbol{\sigma}}) - C^*(\boldsymbol{\sigma},\dot{\boldsymbol{\sigma}})$. The expression for $\dot{J}$ implies that $\dot{\boldsymbol{a}}$ is known if $\dot{\boldsymbol{\gamma}}$ is known.

The linear parametrization of the dynamics allows us to define a *known* matrix $Y^*(\boldsymbol{\sigma},\dot{\boldsymbol{\sigma}},\dot{\boldsymbol{\sigma}}_r,\ddot{\boldsymbol{\sigma}}_r)$ such that

$$\tilde{H}^*(\boldsymbol{\sigma})\ddot{\boldsymbol{\sigma}}_r + \tilde{C}^*(\boldsymbol{\sigma},\dot{\boldsymbol{\sigma}})\dot{\boldsymbol{\sigma}}_r = Y^*(\boldsymbol{\sigma},\dot{\boldsymbol{\sigma}},\dot{\boldsymbol{\sigma}}_r,\ddot{\boldsymbol{\sigma}}_r)\,\tilde{\boldsymbol{a}} \tag{28}$$

Choosing the adaptation law as

$$\dot{\hat{\boldsymbol{a}}} = -\Gamma(Y^*)^T\boldsymbol{s} + \dot{\boldsymbol{a}} \tag{29}$$

yields $\dot{V}_a = -\boldsymbol{s}^T K_D\boldsymbol{s} \leq 0$. The last inequality implies boundedness of $\boldsymbol{s}$ and $\tilde{\boldsymbol{a}}$ and, in addition, that $\boldsymbol{s} \to 0$. Using standard arguments [82, 41] it follows that $\boldsymbol{\sigma} \to \boldsymbol{\sigma}_d$. Therefore, global asymptotic stability of the attitude tracking error is guaranteed.

From Eq. (27) it follows that the required control inputs are obtained by solving

$$[C \quad D]\begin{bmatrix}\dot{\boldsymbol{\gamma}}\\ \dot{\boldsymbol{\Omega}}\end{bmatrix} = \boldsymbol{L}_{\mathrm{ra}} \tag{30}$$

where $D = A_s I_{\mathrm{ws}}$ and

$$\begin{aligned} C = {} & A_t I_{\mathrm{ws}}[\boldsymbol{\Omega}]^d + [\boldsymbol{\omega}^{\times}]A_g I_{\mathrm{cg}} \\ & + \tfrac{1}{2}[(\mathbf{s}_1\mathbf{t}_1^T + \mathbf{t}_1\mathbf{s}_1^T)(\boldsymbol{\omega} + G^{-1}\dot{\boldsymbol{\sigma}}_r), \cdots, (\mathbf{s}_N\mathbf{t}_N^T + \mathbf{t}_N\mathbf{s}_N^T)(\boldsymbol{\omega} + G^{-1}\dot{\boldsymbol{\sigma}}_r)](I_{\mathrm{cs}} - I_{\mathrm{ct}}) \end{aligned} \tag{31}$$

and where

$$L_{\text{ra}} = -G^T(\boldsymbol{\sigma})\Big(\hat{H}^*(\boldsymbol{\sigma})\ddot{\boldsymbol{\sigma}}_r + \hat{C}^*\dot{\boldsymbol{\sigma}}_r - K_D\boldsymbol{s}\Big) + [\mathbf{h}_2^{\times}]\,\boldsymbol{\omega} \tag{32}$$

Once $\dot{\boldsymbol{\gamma}}$ is known from the solution of Eq. (30), it can be substituted in the adaptive control law in Eq. (29).

Remark: Usually the combined matrix of inertia of the spacecraft platform and the point-masses of VSCMGs, ${}^{B}I$, occupies most of the total matrix of inertia $J(\boldsymbol{\gamma})$, and the $\boldsymbol{\gamma}$-dependent part of the inertia matrix is relatively small. In such a case, one can assume that J is a constant matrix. With this assumption, the equation of the system (21) can be written in a simplified form as

$$J\dot{\boldsymbol{\omega}} + [\boldsymbol{\omega}^{\times}](J\boldsymbol{\omega} + A_s I_{\text{ws}}\boldsymbol{\Omega}) + B\ddot{\boldsymbol{\gamma}} + \tilde{C}_s\dot{\boldsymbol{\gamma}} + D\dot{\boldsymbol{\Omega}} = 0 \tag{33}$$

where $\tilde{C}_s = A_t I_{\text{ws}}[\boldsymbol{\Omega}]^d + [\boldsymbol{\omega}^{\times}]A_g I_{\text{cg}}$. The equation in the standard form (24) remains the same, except that now F becomes

$$F_s = G^{-T}(\boldsymbol{\sigma})[\mathbf{h}_2^{\times}]\,\boldsymbol{\omega} - G^{-T}(\boldsymbol{\sigma})\,(\tilde{C}_s\dot{\boldsymbol{\gamma}} + D\dot{\boldsymbol{\Omega}})$$

Moreover, it can be easily shown that the matrix $\dot{H}^* - 2C^*$ is skew-symmetric. Therefore, the required control input is obtained by solving Eq. (30) with $\tilde{C}_s$ instead of C. The adaptation law also simplifies to

$$\dot{\hat{\boldsymbol{a}}} = -\Gamma(Y^*)^T\boldsymbol{s} \tag{34}$$

3.3 Power Tracking

In Ref. [92] a solution to the simultaneous attitude and power tracking problem was given for the case of a rigid spacecraft with N momentum wheels. In this section these results are extended to the case of N VSCMGs. By setting the gimbal angles to a constant value, one can retrieve the results of Ref. [92] as a special case.

The total (useful) kinetic energy E stored in the momentum wheels is

$$E = \tfrac{1}{2}\boldsymbol{\Omega}^T I_{\mathrm{ws}} \boldsymbol{\Omega}$$

Hence, the power (rate of change of the energy) is given by

$$P = \frac{\mathrm{d}E}{\mathrm{d}t} = \begin{bmatrix} 0 & \boldsymbol{\Omega}^T I_{\mathrm{ws}} \end{bmatrix} \begin{bmatrix} \dot{\boldsymbol{\gamma}} \\ \dot{\boldsymbol{\Omega}} \end{bmatrix} \tag{35}$$

This equation is augmented to the attitude tracking equation (19) or (30), to obtain the equation for IPACS with VSCMG as follows

$$Q\boldsymbol{u} = \boldsymbol{L}_{\mathrm{rp}} \tag{36}$$

where

$$\boldsymbol{u} = \begin{bmatrix} \dot{\boldsymbol{\gamma}} \\ \dot{\boldsymbol{\Omega}} \end{bmatrix}, \qquad Q_{4\times 2N} = \begin{bmatrix} C_{3\times N} & D_{3\times N} \\ 0_{1\times N} & (\boldsymbol{\Omega}^T I_{\mathrm{ws}})_{1\times N} \end{bmatrix}, \qquad \boldsymbol{L}_{\mathrm{rp}} = \begin{bmatrix} \boldsymbol{L}_r \\ P \end{bmatrix} \tag{37}$$

and P is the required power and $\boldsymbol{L}_{\mathrm{r}}$ is either $\boldsymbol{L}_{\mathrm{rm}}$ or $\boldsymbol{L}_{\mathrm{ra}}$, depending on the attitude controller used.

3.4 Solution of Velocity Steering Law for IPACS

If the Q matrix has rank 4 (is full row rank), Eq. (36) has infinitely many solutions and the minimum norm solution, which is generally chosen among the solutions to reduce the input, can be calculated from

$$\boldsymbol{u} = Q^T (QQ^T)^{-1} \boldsymbol{L}_{\mathrm{rp}} \tag{38}$$

If the C matrix in Eq. (37) has rank 3 (is full row rank), then the matrix Q is also full row rank, i.e., rank $Q = 4$. This can be shown as follows. If Q is not full rank (rank $Q \neq 4$),

the row vectors of Q are linearly dependent, thus the last row vector of Q can be expressed as a linear combination of the other three row vectors. It implies that a zero row vector, $0_{1\times N}$, can be written as a linear combination of the three row vectors of C. However, this can happen only if C is not full rank.

If, however, the C matrix has rank 2, then Q may be rank deficient and an exact solution which satisfies Eq. (36) does not exist unless $\boldsymbol{L}_{\text{rp}}$ is in the range of Q. Otherwise, only an approximate solution can be calculated from $\boldsymbol{u} = Q^{\dagger}\boldsymbol{L}_{\text{rp}}$, where $Q^{\dagger}$ is the Moore-Penrose inverse of $Q^{\dagger}$. In this case, simultaneous attitude and power tracking is not possible, except in very special cases [92].

Although the rank deficiency of the C matrix can be reduced using more VSCMGs, the possibility of a singularity still remains. Moreover, if the minimum norm solution of Eq. (36) is used for control, this solution tends to steer the gimbals toward the rank deficiency states [56, 21, 35]. This happens because the projection of the generated torques along the required torque direction is maximum when the transverse axis of the gimbal (the axis along which torque can be generated in CMG mode) is close to the required torque. Thus, the minimum norm solution tends to use the gimbals whose configuration is far from the rank deficiency states. Several methods have been proposed for keeping the matrix C full rank using null-motion [29, 73, 71, 35]. In Chapter 5, a singularity avoidance method using a VSCMG system is provided with rigorous mathematical and geometrical analysis.

It is advantageous for the VSCMGs to act as conventional CMGs in order to make the most out of the torque amplification effect, which is the most significant merit of the CMGs. A weighted minimum norm solution, which minimizes the weighted cost

$$\mathcal{J}_2 = \tfrac{1}{2}\boldsymbol{u}^T W^{-1}\boldsymbol{u} \tag{39}$$

can be used to operate between the CMG and MW modes [73]. For example, if the weighting matrix W is defined as

$$W = \begin{bmatrix} w_1 e^{-w_2\sigma_c}\mathbf{I}_N & 0_N \\ 0_N & \mathbf{I}_N \end{bmatrix} \tag{40}$$

[†]Since the Moore-Penrose inverse solution becomes equal to Eq. (38) when Q is full row rank, one can always choose this solution regardless of the rank of Q.

where $\mathbf{I}_N$ is the $N \times N$ identity matrix and where σ_c is the condition number of C (the ratio of the largest to the smallest singular value) and w_1 and w_2 are positive gains chosen by the user, the weighted minimum norm solution control law is given by

$$\boldsymbol{u} = WQ^T(QWQ^T)^{-1}\boldsymbol{L}_{\text{rp}} \tag{41}$$

In case Q is not full row rank, the approximate solution can be obtained from

$$\boldsymbol{u} = W^{\frac{1}{2}}(QW^{\frac{1}{2}})^{\dagger}\boldsymbol{L}_{\text{rp}} \tag{42}$$

Note that according to the condition number of the matrix C, the VSCMG can operate either as a MW (close to a CMG singularity, i.e., when σ_c is large) or as a regular CMG (away from a singularity i.e., when σ_c is small). As a CMG singularity is approached, the VSCMG's will smoothly switch to a momentum wheel mode. As a result, this method can also handle temporary rank deficiencies of the matrix C [73]. In this work, the condition number of the matrix C is used as a measure of closeness of the matrix C to being rank-deficient. Larger condition numbers mean a more "singular" matrix C. This is a more reliable measure of rank-deficiency of a matrix than, say, the determinant of the matrix [36]. The condition numbers have also been used in Refs. [29] and [71].

Notice that a purely MW mode can be enforced by letting W in (41) be

$$W_{\text{MW}} = \begin{bmatrix} 0_N & 0_N \\ 0_N & \mathbf{I}_N \end{bmatrix}.$$

A conventional CMG operation is enforced if W in (41) is chosen as

$$W_{\text{CMG}} = \begin{bmatrix} \mathbf{I}_N & 0_N \\ 0_N & 0_N \end{bmatrix}.$$

As alluded to in the Introduction, in MW mode the VSCMGs are power-inefficient (when compared to low-speed flywheels). Under normal conditions, however, the MW mode will be engaged only sporadically, and for short periods of time, in order to provide the necessary torque (albeit in a power-inefficient manner) near singularities.

3.5 Wheel Speed Equalization

If some of the wheel spin rates become too small, a change of the gimbal angle cannot generate the required torque. If this is the case, the remaining degrees of freedom may not be enough to allow exact attitude and power tracking. On the other hand, if some of the wheel spin rates become too high, some of the wheels may saturate. Desaturation of the wheels requires thruster firing, thus depleting valuable fuel. To minimize the possibility of singularity and/or wheel saturation, it is desirable to equalize the wheel spinning rates of the VSCMGs, whenever possible. Next, two control laws are proposed to achieve wheel speed equalization for a VSCMG-based IPACS.

The first method adds an extra constraint that forces the wheel speeds to converge to the average wheel speed of the cluster. By introducing

$$\mathcal{J}_{w1}(\Omega_1, \cdots, \Omega_N) = \tfrac{1}{2}\sum_{i=1}^{N}(\Omega_i - \bar{\Omega})^2 = \tfrac{1}{2}\boldsymbol{\Omega}_e^T\boldsymbol{\Omega}_e \tag{43}$$

where $\bar{\Omega} = \frac{1}{N}\sum_{i=1}^{N}\Omega_i$, $\boldsymbol{\Omega}_e = \boldsymbol{\Omega} - \bar{\boldsymbol{\Omega}}\mathbf{1}_{N\times 1}$, and $\mathbf{1}_{N\times 1}$ is $N\times 1$ vector whose elements are 1's, the condition for equalization is expressed as the requirement that

$$\frac{d}{dt}\mathcal{J}_{w1} = \nabla\mathcal{J}_{w1}\,\dot{\boldsymbol{\Omega}} = \sum_{i=1}^{N}\frac{\partial\mathcal{J}_{w1}}{\partial\Omega_i}\dot{\Omega}_i = -k_2\mathcal{J}_{w1}$$

where $k_2 > 0$. This condition is augmented in Eq. (36) and the control input u is calculated from this augmented equation. Summarizing, the control law that achieves attitude and power tracking with wheel speed equalization is given by

$$\begin{bmatrix} C & D \\ 0 & \boldsymbol{\Omega}^T I_{\mathrm{ws}} \\ 0 & \nabla\mathcal{J}_{w1} \end{bmatrix}\begin{bmatrix} \dot{\boldsymbol{\gamma}} \\ \dot{\boldsymbol{\Omega}} \end{bmatrix} = \begin{bmatrix} \boldsymbol{L}_{\mathrm{r}} \\ P \\ -k_2\mathcal{J}_{w1} \end{bmatrix} \tag{44}$$

and the use of (41). Using the fact that $\boldsymbol{\Omega}_e = [\mathbf{I}_N - \frac{1}{N}\mathbf{1}_{N\times N}]\boldsymbol{\Omega}$ where $\mathbf{1}_{N\times N}$ is $N\times N$ matrix whose elements are 1's and the matrix $[\mathbf{I}_N - \frac{1}{N}\mathbf{1}_{N\times N}]$ is idempotent[‡], it can be easily shown that $\nabla\mathcal{J}_{w1} = \boldsymbol{\Omega}_e^T$.

The second method uses a modified cost of (39) in which the directions of wheel speed

[‡]A matrix A is idempotent if $A^2 = A$.

changes are considered. The cost to be minimized in this case is expressed as

$$\mathcal{J}_{w2} = \tfrac{1}{2}\boldsymbol{u}^T W^{-1}\,\boldsymbol{u} + R\,\boldsymbol{u} \tag{45}$$

The weighting matrix R is determined so that the wheels which rotate faster or slower than the average wheel speed are suitably penalized. For instance, one may choose $R = \begin{bmatrix}0_{1\times N} & k_3\boldsymbol{\Omega}_e^T\end{bmatrix}$ where $k_3 > 0$ The motivation for this choice for R stems from the following observation. Notice that with the previous choice of R one has $R\boldsymbol{u} = \sum_{i=1}^{N}(\Omega_i - \bar{\Omega})\dot{\Omega}_i$. If $\Omega_i > \bar{\Omega}$ for some i, then $R\boldsymbol{u}$ is minimized by choosing $\dot{\Omega}_i < 0$, i.e, by making Ω_i tend closer to $\bar{\Omega}$. If, on the other hand $\Omega_i < \bar{\Omega}$ then $R\boldsymbol{u}$ is minimized by choosing $\dot{\Omega}_i > 0$ forcing again Ω_i towards $\bar{\Omega}$. Of course, the linear term $R\boldsymbol{u}$ does not have an unconstrained minimum hence a quadratic term is included in (45) to ensure that the minimization problem has a solution.

The solution that minimizes the cost (45) subject to the equality constraint (36) is

$$\boldsymbol{u} = W\Big(Q^T(QWQ^T)^{-1}(\boldsymbol{L}_{\rm rp} + QWR^T) - R^T\Big) \tag{46}$$

In case Q is not full row rank, the equation

$$\boldsymbol{u} = W^{\frac{1}{2}}(QW^{\frac{1}{2}})^{\dagger}\boldsymbol{L}_{\rm rp} - [\mathbf{I} - W^{1/2}(QW^{1/2})^{\dagger}Q]WR^T \tag{47}$$

can be used, instead. Note that this method is identical with the control law without wheel speed equalization if $k_3 = 0$.

It can be shown that with the choice $W = \alpha\mathbf{I}$ ($\alpha > 0$), the second method is basically equivalent to so-called the *gradient method* [49], which was originally devised for the singularity avoidance problem of conventional CMGs [49, 71] using the null motion. The null motion does not have any effect on the generated output torque but has the effect of increasing (or decreasing) the cost function. Using the general gradient method, and with $W = \alpha\mathbf{I}$, the null motion of Eq. (36) can be written as

$$\begin{bmatrix}\dot{\boldsymbol{\gamma}}\\ \dot{\boldsymbol{\Omega}}\end{bmatrix}_{\rm null} = [\mathbf{I} - Q^{\dagger}Q]\boldsymbol{d} = \mathcal{P}\boldsymbol{d}, \qquad \boldsymbol{d} \in \mathbb{R}^{2N\times 1} \tag{48}$$

It can be easily shown that $Q[\dot{\boldsymbol{\gamma}}^T, \dot{\boldsymbol{\Omega}}^T]^T_{\text{null}} = 0$, and the projection matrix $\mathcal{P} = [\mathbf{I} - Q^\dagger Q]$ is idempotent. It is also a symmetric matrix (and hence positive semi-definite) since it represents an orthogonal projection onto the null subspace of the matrix Q.

If now the vector $\boldsymbol{d}$ is selected as

$$\boldsymbol{d} = -k_3 \begin{bmatrix} \frac{\partial \mathcal{J}_{w1}}{\partial \gamma}^T \\ \frac{\partial \mathcal{J}_{w1}}{\partial \Omega}^T \end{bmatrix} \tag{49}$$

then the rate of change of $\mathcal{J}_{w1}$ due to the null motion is

$$\begin{aligned} \dot{\mathcal{J}}_{w1}|_{\text{null}} &= \begin{bmatrix} \frac{\partial \mathcal{J}_{w1}}{\partial \gamma} & \frac{\partial \mathcal{J}_{w1}}{\partial \Omega} \end{bmatrix} \begin{bmatrix} \dot{\boldsymbol{\gamma}} \\ \dot{\boldsymbol{\Omega}} \end{bmatrix}_{\text{null}} \\ &= -k_3 \begin{bmatrix} \frac{\partial \mathcal{J}_{w1}}{\partial \gamma} & \frac{\partial \mathcal{J}_{w1}}{\partial \Omega} \end{bmatrix} \mathcal{P} \begin{bmatrix} \frac{\partial \mathcal{J}_{w1}}{\partial \gamma}^T \\ \frac{\partial \mathcal{J}_{w1}}{\partial \Omega}^T \end{bmatrix} \leq 0 \end{aligned}$$

Thus, it is expected that the wheel speeds will be equalized. We also see that in this case WR^T in Eq. (47) is equal to $-\boldsymbol{d}$ in Eq. (49). Since $\frac{\partial \mathcal{J}_{w1}}{\partial \gamma} = 0$, it follows that the second method is equal to the gradient method.

Each of the previous two wheel speed equalization algorithms has its own merits and pitfalls. The first one guarantees exact equalization for the IPACS. However, this method uses an additional degree of freedom since one has to solve the augmented linear system (44). Thus, it may lead the VSCMGs system to another singularity problem. The second method, on the other hand, shows a tendency for wheel speed equalization but it does not guarantee perfect equalization of wheel speeds, in general. The wheel speeds tend to become equal away from the CMG singularity, but they exhibit a bifurcation near the singularity, since the torques for attitude control must be generated from changes of wheel speeds. However, this method does not use any additional degrees of freedom. If some other objectives such as a singularity avoidance strategy is desired, the second method may be preferable.

3.6 Numerical Examples

A numerical example for a satellite in a low Earth orbit is provided to test the proposed IPACS algorithm. Similar to Refs. [73, 65], a standard four-VSCMG pyramid configuration,

Table 1: Simulation Parameters

Symbol	Value	Units
N	4	–
θ	54.75	deg
$\omega(0)$	$[0,0,0]^T$	rad/sec
$\dot{\omega}(0)$	$[0,0,0]^T$	rad/sec^2
$\sigma(0)$	$[0,0,0]^T$	–
$\gamma(0)$	$[\pi/2,-\pi/2,-\pi/2,\pi/2]^T$	rad
$\dot{\gamma}(0)$	$[0,0,0]^T$	rad/sec^2
${}^B I$	$\begin{bmatrix} 15053 & 3000 & -1000 \\ 3000 & 6510 & 2000 \\ -1000 & 2000 & 11122 \end{bmatrix}$	kg m^2
$I_{\rm ws}$	diag$\{0.7,\ 0.7,\ 0.7,\ 0.7\}$	kg m^2
$I_{\rm wt}, I_{\rm wg}$	diag$\{0.4,\ 0.4,\ 0.4,\ 0.4\}$	kg m^2
$I_{\rm gs}, I_{\rm gt}, I_{\rm gg}$	diag$\{0.1,\ 0.1,\ 0.1,\ 0.1\}$	kg m^2

shown in Fig. 7 is used. In this configuration the VSCMGs are installed so that the four gimbal axes form a pyramid with respect to the body. The angle of each of the pyramid sides to its base (assumed to be parallel to the spacecraft $x-y$ plane) is given by θ. Table 1 contains the parameters used for the simulations. These parameters closely parallel those used in Refs. [73, 65].

Two simulation scenarios are presented to demonstrate the validity of the adaptive IPACS and speed equalization control algorithms given in the previous sections. In the first scenario, a satellite in a near-polar orbit with a period of 98 min is considered (the orbital data are chosen as in Ref. [92]). The satellite's boresight axis is required to track a ground station, and the satellite is required to rotate about its boresight axis so that the solar panel axis is perpendicular to the satellite-sun axis in order to maximize the efficiency of the panel. For simplicity, it is assumed that the satellite keeps tracking the ground station and the Sun even when these are not directly visible due to the location of the Earth.

During the eclipse (which lasts approximately 35 min), the nominal power requirement is 680 W, with an additional requirement of 4-kW power for 5 min. During sunlight (which lasts approximately 63 min), the wheels are charged with a power level of 1 kW until the total energy stored in the wheels reaches 1.5 kWh. These attitude and power tracking

requirements are the same as in Ref. [92]. The details of the method used to generated the required attitude, body rate and body acceleration are also given in the same reference. In this scenario, the spacecraft body frame is initially aligned with the inertial frame. The control gains are chosen as

$$K_D = 4 \times 10^3\, \mathbf{I}_{3\times 3}, \quad \Gamma = 1 \times 10^7\, \mathbf{I}_{6\times 6}, \quad \lambda = 0.01, \qquad k_2 = 2 \times 10^{-3}$$
$$k_3 = 2 \times 10^{-3}, \qquad K_a = -2\, \mathbf{I}_{4\times 4}, \qquad w_1 = 1 \times 10^{-4}, \quad w_2 = 1$$

based on trial and error. As a challenging case, all of the initial parameter estimates are chosen to be zero, which means no initial information about the inertia matrix is available. In practice, any educated estimate of the inertia parameters (or prior experience) can be used to choose the controller gains or the initial parameter estimates accordingly. The results of the numerical simulations are shown below. Figure 8 shows the attitude error. The spacecraft attitude tracks the desired attitude exactly after a short period of time. Figure 9 shows that the actual power profile also tracks the required power command exactly. The crosses indicate the desired power history and the solid line indicates the actual power history. These figures show that the goal of IPACS is achieved successfully. Figure 10 shows the wheel speed histories when each of the two wheel equalization methods is applied. The corresponding gimbal angles and control signals for both methods are shown in Fig. 11 and 12. The attitude histories are similar for both cases.

As seen from the top plot of Fig. 10, the first method achieves exact speed equalization, whereas the second method equalizes the wheels only approximately; see bottom plot of Fig. 10. In fact, after the condition number of the matrix C becomes large – lower right plot in Fig. 12 – the second method switches to a MW mode and thus the wheel speeds deviate from each other. The first method still keeps the wheel speeds equalized after the sudden change of the required power profile, whereas the second method shows a tendency of divergence. As expected, in both cases, the wheels spin-up (charge) during sunlight and despin (discharge) during the eclipse.

It is worth pointing out that in all simulations the moment of inertia matrix has been assumed to be completely unknown. Despite this fact, the adaptive control law achieves

both attitude and power tracking while equalizing the wheel speeds, as desired. Although the control algorithm shows excellent attitude/power tracking performance, the reference attitude trajectory in this scenario is too slow to achieve parameter convergence. In order to emphasize the performance of the adaptive controller, another scenario in which the reference trajectory varies much faster is considered. For illustration purposes, a reference trajectory similar to the coning motion of Ref. [5] is chosen. Initially, the reference attitude is aligned with the actual attitude, and the angular velocity of the reference attitude is chosen as

$$\omega_d(t) = 0.02 \times (\ \sin(2\pi t/800),\ \ \sin(2\pi t/600),\ \ \sin(2\pi t/400)\ )^T \text{rad/sec}$$

A 20% uncertainty in the spacecraft nominal inertia matrix ${}^{B}I$ is assumed. Figure 13 shows the attitude error trajectories with and without adaptation. These simulation results show that the designed adaptive control gives significantly improved performance over the controller without adaptation. The time history of the inertia parameters are shown in Fig. 14. The horizontal lines are the actual values of the parameters. As shown in this figure, parameter convergence is achieved for this maneuver.

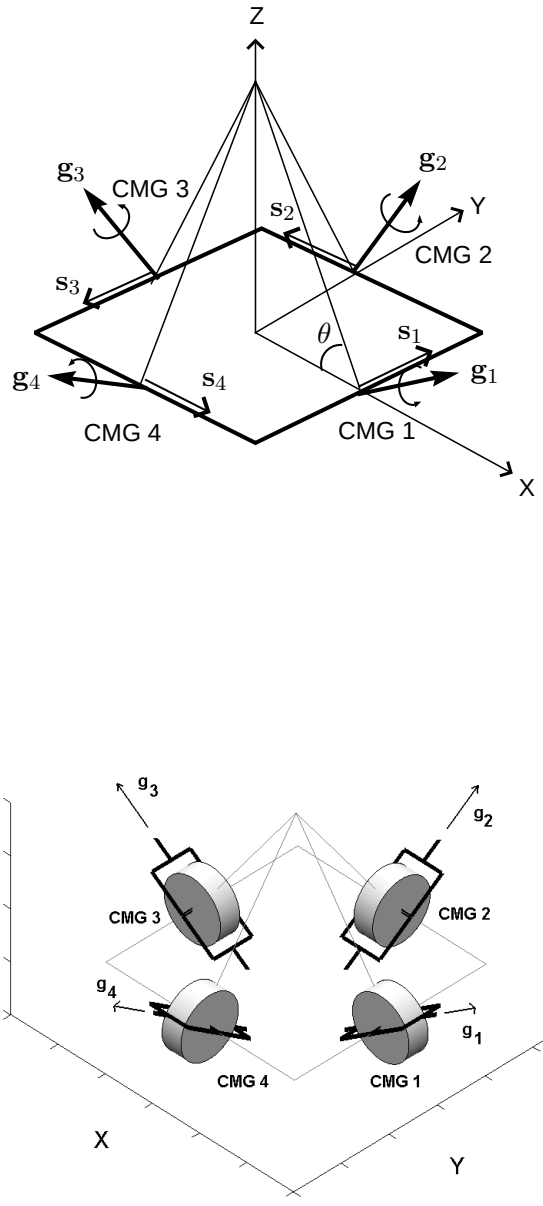

Figure 7: A VSCMGs System with Pyramid Configuration

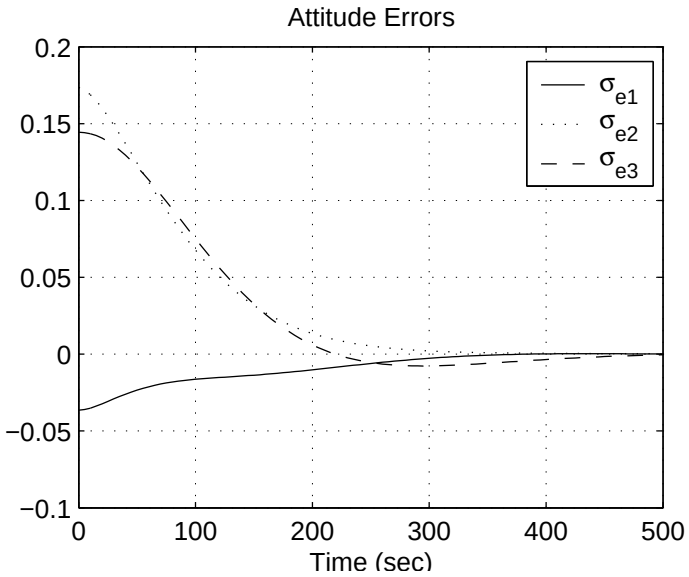

Figure 8: Attitude Error Trajectory.

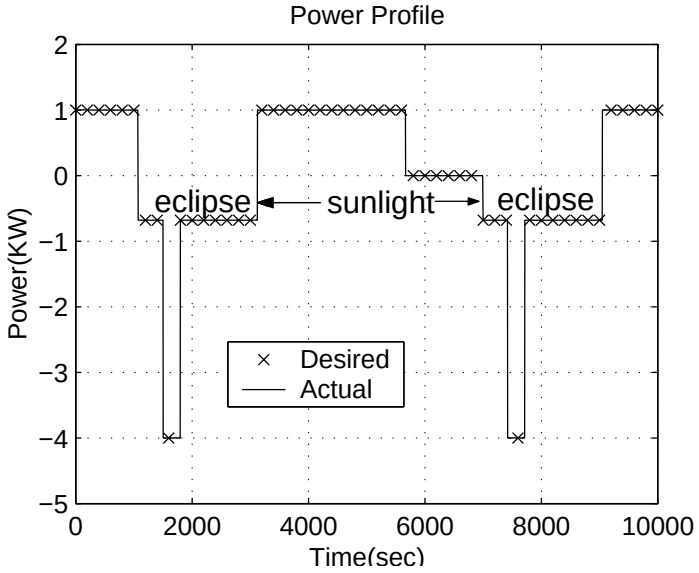

Figure 9: Desired (circle) and Actual (solid line) Power Profiles.

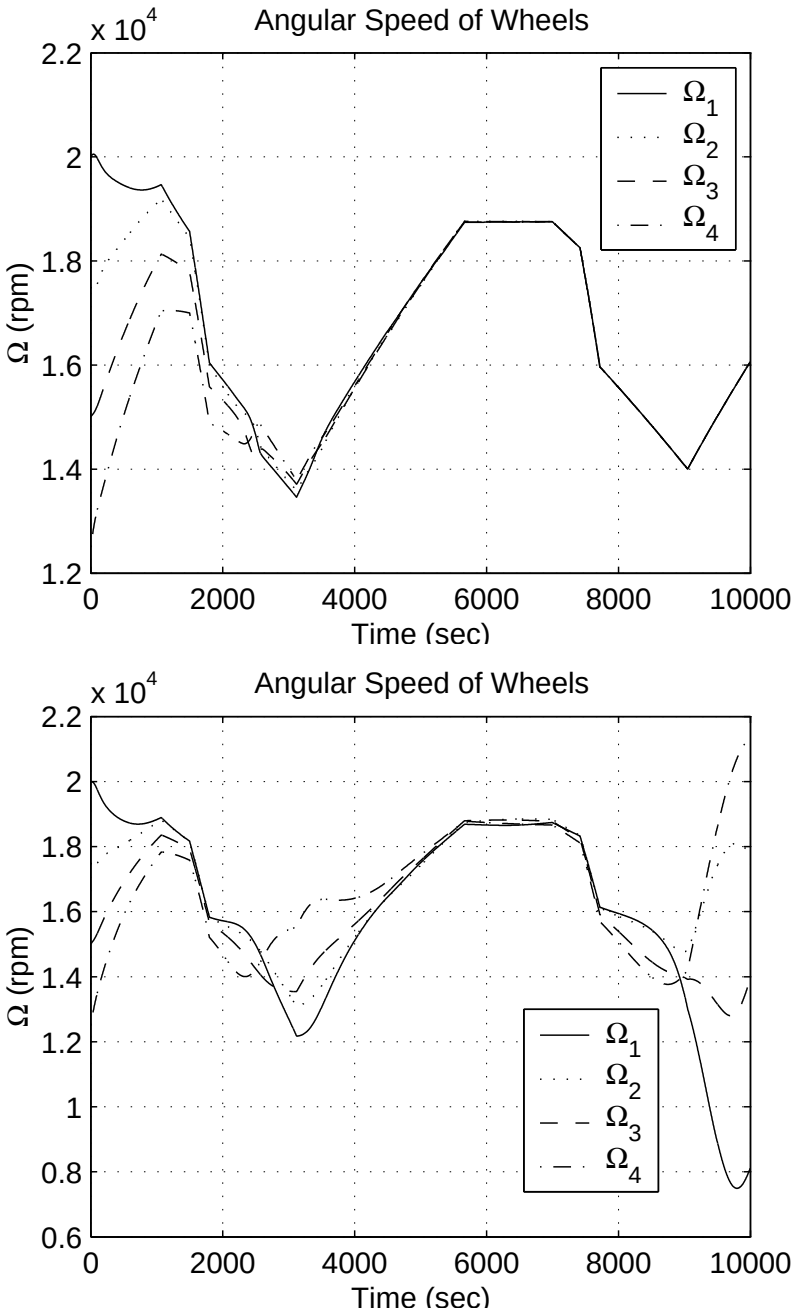

Figure 10: Angular Wheel Speeds with Speed Equalization: Method 1 (top) and Method 2 (bottom).

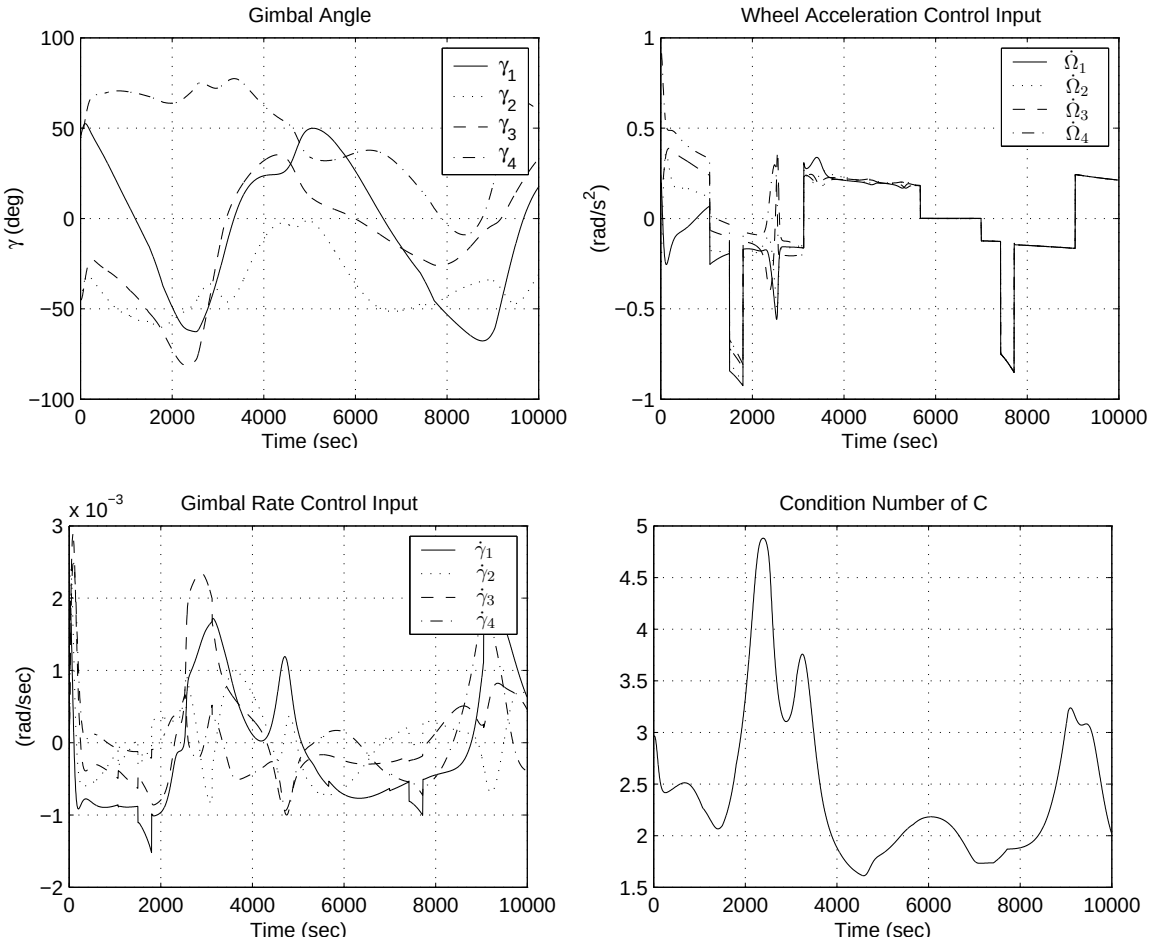

Figure 11: Gimbal Angles, Control Inputs and Condition Number of Matrix C (Method 1).

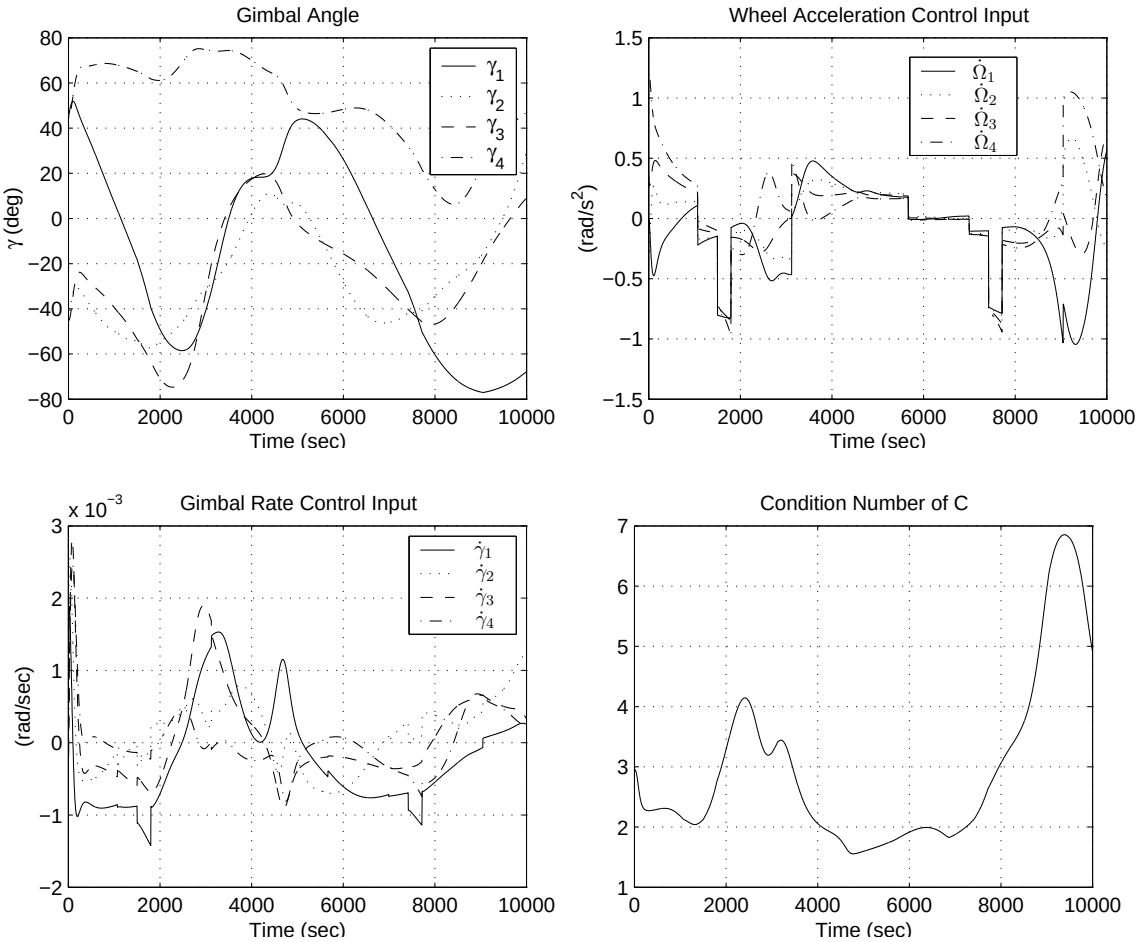

Figure 12: Gimbal Angles, Control Inputs and Condition Number of Matrix C (Method 2).

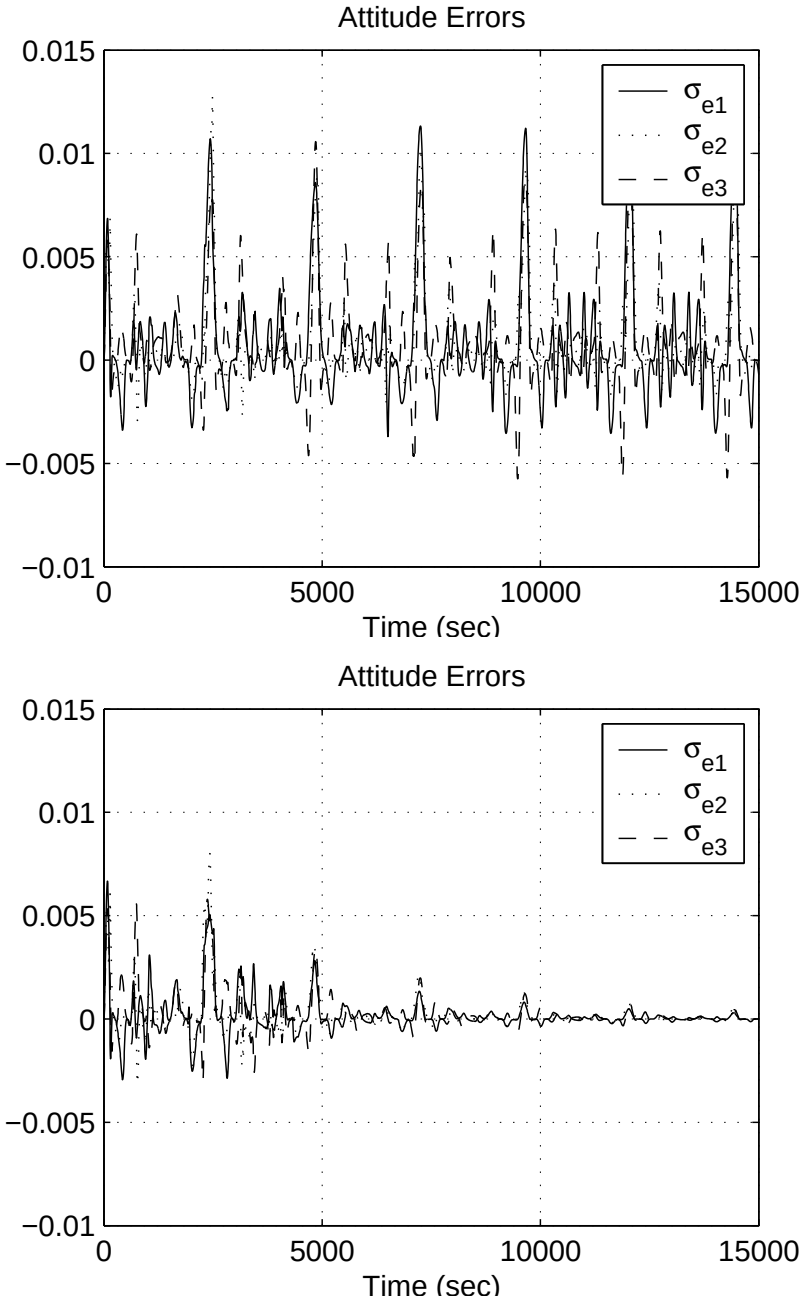

Figure 13: Attitude Error Trajectories. Without Adaptation (top) and With Adaptation (bottom).

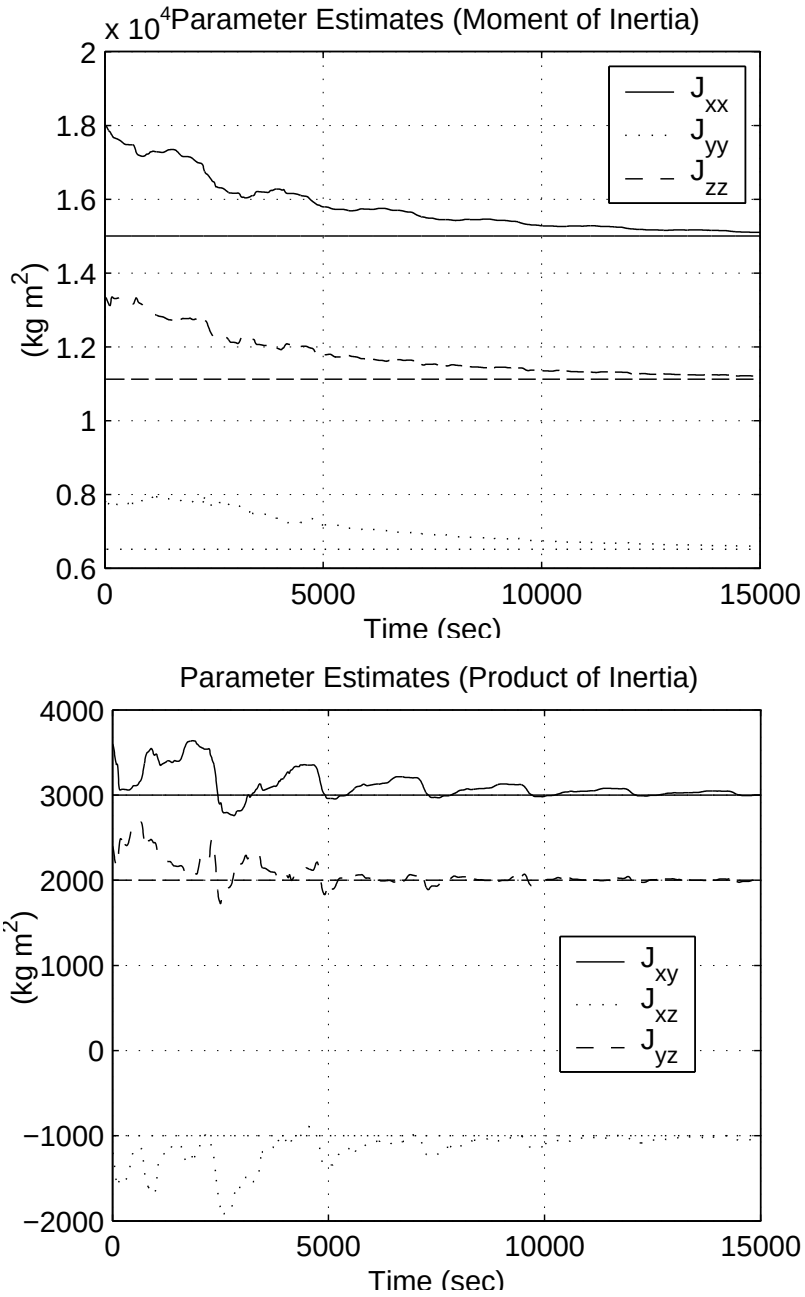

Figure 14: Parameter Convergence for Coning Motion: J_{xx}, J_{yy}, J_{zz} (top) and J_{xy}, J_{xz}, J_{yz} (bottom).

CHAPTER IV

SINGULARITY ANALYSIS OF CONVENTIONAL CMG SYSTEM

4.1 CMGs/VSCMGs System Modelling

Even though an exact nonlinear equation of motion has been derived in Chapter 2, it is too complicated for the analysis of the singularity problem of CMGs/VSCMGs systems. Therefore, a simplified equation of motion in which the dynamics of spacecraft is not considered is derived in this section, as done in most, if not all, of the previous works.

Consider again a rigid spacecraft with a cluster of N single-gimbal VSCMGs used to produce internal torques, as did in Chapter 2. The mutually orthogonal unit vectors of the ith VSCMG are shown in Fig. 6.

The VSCMG can rotate about the gimbal axis $\hat{\mathbf{g}}_i$ with a gimbal angle γ_i, and the wheel rotates about the spin axis $\hat{\mathbf{s}}_i$ with a angular speed Ω_i. The unit vectors $\hat{\mathbf{s}}_i$ and $\hat{\mathbf{t}}_i$ depend on the gimbal angle γ_i, while the gimbal axis vector $\hat{\mathbf{g}}_i$ is fixed in the body frame. The relationship between the derivatives of these unit vectors can be written as

$$\dot{\hat{\mathbf{s}}}_i = \dot{\gamma}_i \hat{\mathbf{t}}_i, \quad \dot{\hat{\mathbf{t}}}_i = -\dot{\gamma}_i \hat{\mathbf{s}}_i, \quad \dot{\hat{\mathbf{g}}}_i = 0, \quad i = 1, \cdots, N. \tag{50}$$

There are several ways to configure a number of VSCMG units. The standard pyramid configuration with four VSCMG units is emphasized in this chapter (see Fig. 7). The skew angle θ in Fig. 7 is chosen as $\cos\theta = 1/\sqrt{3}$ ($\theta \approx 54.74°$) so that the pyramid becomes half of a regular octahedron. This configuration has been studied extensively because it is only once-redundant and its momentum envelope (see Section 4.2-B) is nearly spherical [101] and three-axis symmetric [11].

In deriving the equations for a VSCMG actuator it will be assumed that the gimbal rates $\dot{\gamma}_i$ are much smaller than the wheel speeds Ω_i, so that $\dot{\gamma}_i$ do not add to the total angular momentum. Hence, one can neglect the angular momentum induced by the gimbal

rates $\dot{\gamma}_i$. The moments of inertia of the gimbal frame structures is also neglected. These assumptions have been widely used in the studies on CMGs/VSCMGs systems and they are accurate for typical CMG/spacecraft configurations. For the exact equations of motion of a spacecraft with VSCMG actuators without these assumptions, see Chapter 2.

The angular momentum vector of each wheel can be expressed as $h_i \hat{\mathbf{s}}_i$, for $i = 1, \ldots, N$, where $h_i = I_{\mathrm{w}s_i} \Omega_i$ and with $I_{\mathrm{w}s_i}$ denoting the moment of inertia of the ith VSCMG about its spin axis. The total angular momentum $\mathbf{H}$ of the VSCMG system is the vector sum of the individual momenta of each wheel

$$\mathbf{H}(\gamma_1, \cdots, \gamma_N; \Omega_1, \cdots, \Omega_N) = \sum_{i=1}^{N} h_i \hat{\mathbf{s}}_i. \tag{51}$$

The time derivative of $\mathbf{H}$ is equal to the torque $\mathbf{T}$ applied from the spacecraft main body to the VSCMG system, which is equal and opposite to the output torque from the VSCMG to the spacecraft body. This relation is written as

$$\mathbf{T} = \dot{\mathbf{H}} = \sum_{i=1}^{N} h_i \hat{\mathbf{t}}_i \dot{\gamma}_i + \sum_{i=1}^{N} \hat{\mathbf{s}}_i I_{\mathrm{w}s_i} \dot{\Omega}_i \tag{52}$$

and in matrix form,

$$\begin{bmatrix} C(\boldsymbol{\Omega}, \boldsymbol{\gamma}) & D(\boldsymbol{\gamma}) \end{bmatrix} \begin{bmatrix} \dot{\boldsymbol{\gamma}} \\ \dot{\boldsymbol{\Omega}} \end{bmatrix} = \mathbf{T} \tag{53}$$

where $C : \mathbb{R}^N \times [0, 2\pi)^N \to \mathbb{R}^{3 \times N}$ and $D : [0, 2\pi)^N \to \mathbb{R}^{3 \times N}$ are matrix-valued functions given by

$$C(\boldsymbol{\Omega}, \boldsymbol{\gamma}) \triangleq [I_{\mathrm{w}s_1} \Omega_1 \hat{\mathbf{t}}_1, \cdots, I_{\mathrm{w}s_N} \Omega_N \hat{\mathbf{t}}_N] \tag{54}$$

$$D(\boldsymbol{\gamma}) \triangleq [I_{\mathrm{w}s_1} \hat{\mathbf{s}}_1, \cdots, I_{\mathrm{w}s_N} \hat{\mathbf{s}}_N] \tag{55}$$

and where $\boldsymbol{\gamma} \triangleq (\gamma_1, \ldots, \gamma_N)^T \in [0, 2\pi)^N$ and $\boldsymbol{\Omega} \triangleq (\Omega_1, \ldots, \Omega_N)^T \in \mathbb{R}^N$. Notice that equations (53) are also valid for a conventional CMG system, if one sets the wheel speeds Ω_i to be constant ($\dot{\boldsymbol{\Omega}} = 0$), and for a reaction wheel system, if one sets the gimbal angles γ_i to be constant ($\dot{\boldsymbol{\gamma}} = 0$).

4.2 Review of a Conventional CMG System

4.2.1 Singularities of a CMG System

In this section, the basic terminology is introduced and the singularity problem of a conventional CMG system, which is based mainly on the results of Refs. [49, 10, 56] are reviewed. The ensuing analysis will be used to set the stage for the singularity analysis of the VSCMG case.

For simplicity, let us assume that $h_i = 1$ for $i = 1, \cdots, N$. The total angular momentum in (51) becomes

$$\mathbf{H}(\gamma_1, ..., \gamma_N) = \sum_{i=1}^{N} \hat{\mathbf{s}}_i \tag{56}$$

and the torque equation (53) becomes

$$C(\boldsymbol{\gamma})\, \dot{\boldsymbol{\gamma}} = \mathbf{T} \tag{57}$$

where $C(\boldsymbol{\gamma}) = [\hat{\mathbf{t}}_1, \cdots, \hat{\mathbf{t}}_N]$. In order to generate a torque $\mathbf{T}$ along an arbitrary direction, we need $C(\boldsymbol{\gamma})$ to be full rank for all $\boldsymbol{\gamma} \in [0, 2\pi)^N$. Then, the gimbal rate $\dot{\boldsymbol{\gamma}}$ can be computed from a *steering law*, for instance, one that provides the minimum norm solution to (57)

$$\dot{\boldsymbol{\gamma}} = C^T (C C^T)^{-1} \mathbf{T}. \tag{58}$$

If $\operatorname{rank} C(\boldsymbol{\gamma}_s) \neq 3$ for some $\boldsymbol{\gamma}_s$, $\dot{\boldsymbol{\gamma}}$ cannot be calculated for arbitrary torque commands.* Notice that $\operatorname{rank} C = 1$ implies that all $\hat{\mathbf{t}}_i$ are aligned in the same direction, and this can happen only if all $\hat{\mathbf{g}}_i$ are lying on a same plane, as is the case for a roof-type system [49]. Such a rather special case is not dealt with in this thesis. Thus, henceforth the singularities of a CMG system are defined as the gimbal states $\boldsymbol{\gamma}_s$ for which $\operatorname{rank} C(\boldsymbol{\gamma}_s) = 2$.

In the singular states all unit vectors $\hat{\mathbf{t}}_i$ lie on the same plane, and we can thus define a singular direction vector $\hat{\mathbf{u}}$ which is normal to this plane. That is,

$$\hat{\mathbf{u}} \cdot \hat{\mathbf{t}}_i = 0, \quad \forall\, i = 1, \cdots, N. \tag{59}$$

The previous conditions imply, in particular, that $\hat{\mathbf{u}} \in \mathcal{R}^{\perp}(C)$, the perpendicular complement to the range space of the matrix C. Moreover, $\hat{\mathbf{t}}_i$ is normal to $\hat{\mathbf{g}}_i$ by definition, so $\hat{\mathbf{t}}_i$ is

*Even in this case, there may exist a solution $\dot{\boldsymbol{\gamma}}$ to (57), if the required torque $\mathbf{T}$ lies in the two-dimensional range of $C(\boldsymbol{\gamma}_s)$, but this can be treated as an exceptional case.

normal to the plane spanned by $\hat{\mathbf{g}}_i$ and $\hat{\mathbf{u}}$. Therefore, $\hat{\mathbf{s}}_i$ must lie on this plane as shown in Fig. 15. Geometrically this means that each $\hat{\mathbf{s}}_i$ has a maximal or minimal (negatively maximal) projection onto the singular vector $\hat{\mathbf{u}}$, i.e., the dot product $\hat{\mathbf{u}}\cdot\hat{\mathbf{s}}_i$ is maximal or minimal. It follows that the component of the total angular momentum along a singular direction, $\mathbf{H_u} \triangleq \mathbf{H}\cdot\hat{\mathbf{u}} = \sum_{i=1}^{N} \hat{\mathbf{u}}\cdot\hat{\mathbf{s}}_i$, takes a stationary value at the singular states corresponding to the singular vector $\hat{\mathbf{u}}$. Therefore, we have again

$$\frac{\partial \mathbf{H_u}}{\partial \gamma_i} = \hat{\mathbf{u}}\cdot\frac{\partial \hat{\mathbf{s}}_i}{\partial \gamma_i} = \hat{\mathbf{u}}\cdot\hat{\mathbf{t}}_i = 0, \quad i = 1, \cdots, N \tag{60}$$

for all singular configurations.

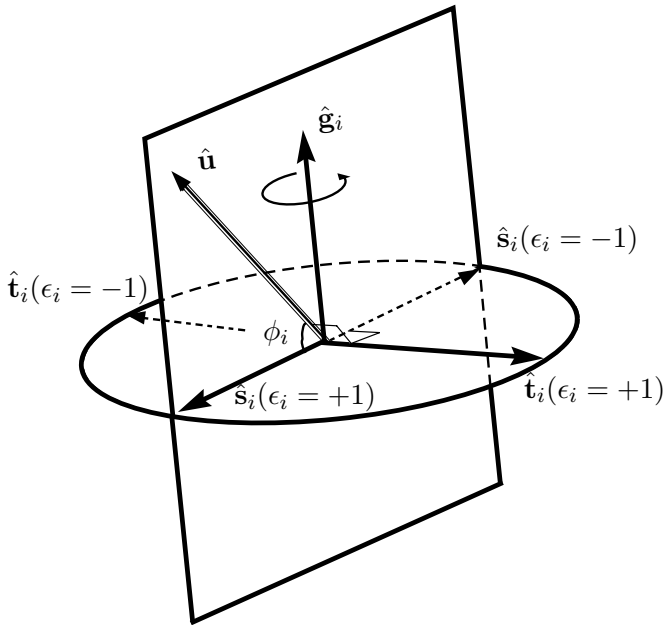

Figure 15: Vectors at a Singular Gimbal State.

For a given singular vector $\hat{\mathbf{u}} \neq \pm\hat{\mathbf{g}}_i$, there are two possibilities:

$$\hat{\mathbf{t}}_i\cdot\hat{\mathbf{u}} = 0 \text{ and } \hat{\mathbf{s}}_i\cdot\hat{\mathbf{u}} > 0, \quad \text{or} \quad \hat{\mathbf{t}}_i\cdot\hat{\mathbf{u}} = 0 \text{ and } \hat{\mathbf{s}}_i\cdot\hat{\mathbf{u}} < 0. \tag{61}$$

For a CMG cluster with N wheels there is a total of 2^N combinations of singular states for a given singular direction $\hat{\mathbf{u}}$. Defining $\epsilon_i = \text{sign}(\hat{\mathbf{s}}_i\cdot\hat{\mathbf{u}})$, the torque axis vector and the spin axis vector at a singular state can be obtained as

$$\hat{\mathbf{t}}_i = \epsilon_i\ \hat{\mathbf{g}}_i\times\hat{\mathbf{u}}/|\hat{\mathbf{g}}_i\times\hat{\mathbf{u}}|, \quad \hat{\mathbf{u}} \neq \pm\hat{\mathbf{g}}_i, \quad i = 1, \cdots, N \tag{62}$$

$$\hat{\mathbf{s}}_i = \hat{\mathbf{t}}_i \times \hat{\mathbf{g}}_i = \epsilon_i \, (\hat{\mathbf{g}}_i \times \hat{\mathbf{u}}) \times \hat{\mathbf{g}}_i / |\hat{\mathbf{g}}_i \times \hat{\mathbf{u}}|, \quad \hat{\mathbf{u}} \neq \pm \hat{\mathbf{g}}_i, \quad i = 1, \cdots, N \tag{63}$$

and therefore the total angular momentum at the singular states corresponding to a singular direction $\hat{\mathbf{u}}$ is expressed as

$$\mathbf{H} = \sum_{i=1}^{N} \hat{\mathbf{s}}_i = \sum_{i=1}^{N} \epsilon_i \, (\hat{\mathbf{g}}_i \times \hat{\mathbf{u}}) \times \hat{\mathbf{g}}_i / |\hat{\mathbf{g}}_i \times \hat{\mathbf{u}}|, \quad \hat{\mathbf{u}} \neq \pm \hat{\mathbf{g}}_i. \tag{64}$$

This equation defines a mapping from $\hat{\mathbf{u}} \neq \pm \hat{\mathbf{g}}_i$ to the total momentum $\mathbf{H}$ at the corresponding singular state. Hence, given a set of ϵ_i's, we can draw a singular surface, which is defined as the locus of the total momentum vector at the singular states, for all $\hat{\mathbf{u}} \in \mathbb{R}^3$ with $\|\hat{\mathbf{u}}\| = 1, \hat{\mathbf{u}} \neq \pm \hat{\mathbf{g}}_i$ where $\|\cdot\|$ denotes the Euclidian norm. Figure 16 shows examples of these singular surfaces for a pyramid configuration for two different combinations of $\epsilon_1, \epsilon_2, \epsilon_3, \epsilon_4$.

4.2.2 The Angular Momentum Envelope of a CMG

The angular momentum envelope is defined as the boundary of the maximum workspace of the total angular momentum $\mathbf{H}$. The angular momentum envelope of a CMGs cluster in a pyramid configuration consists of two types of singular surfaces which are connected to each other smoothly. The first type corresponds to the case when all ϵ_i are positive, i.e., the angular momentum of each CMG unit has a maximal projection onto the singular direction[†]. Figure 16(a) shows the singular surface for all ϵ_i positive, drawn for all $\hat{\mathbf{u}} \in \mathbb{R}^3, \|\hat{\mathbf{u}}\| = 1$.

Notice that this singular surface does not cover the whole momentum envelope, and there exist holes on the surface. The reason is as follows. If $\hat{\mathbf{u}}$ is along a gimbal axis $\hat{\mathbf{g}}_k$, $k \in \{1, \cdots, N\}$, then $\hat{\mathbf{t}}_k$ is normal to $\hat{\mathbf{u}}$ for any gimbal angle γ_k. Moreover, $\hat{\mathbf{s}}_k$ is also normal to $\hat{\mathbf{u}}$. Therefore, while every CMG except the kth wheel must satisfy the conditions for singularity in (61) with positive ϵ_i, $i \neq k$, the gimbal angle γ_k does not have any effect on $\mathbf{H} \cdot \hat{\mathbf{u}}$. As the vector $\hat{\mathbf{s}}_k$ rotates about $\hat{\mathbf{g}}_k$, the total angular momentum $\mathbf{H}$ forms a unit circle as shown Fig. 16(a). The center of each circle is given by the vector sum of the remaining $N-1$ momentum vectors ($i = 1, \ldots, N$, $i \neq k$) in the singular configuration, and the edge of each hole is the image of a mapping from the singular directions $\hat{\mathbf{u}} = \pm \hat{\mathbf{g}}_i$ to the total momentum vector.

[†]The case of all negative ϵ_i is also on the angular momentum envelope due to symmetry.

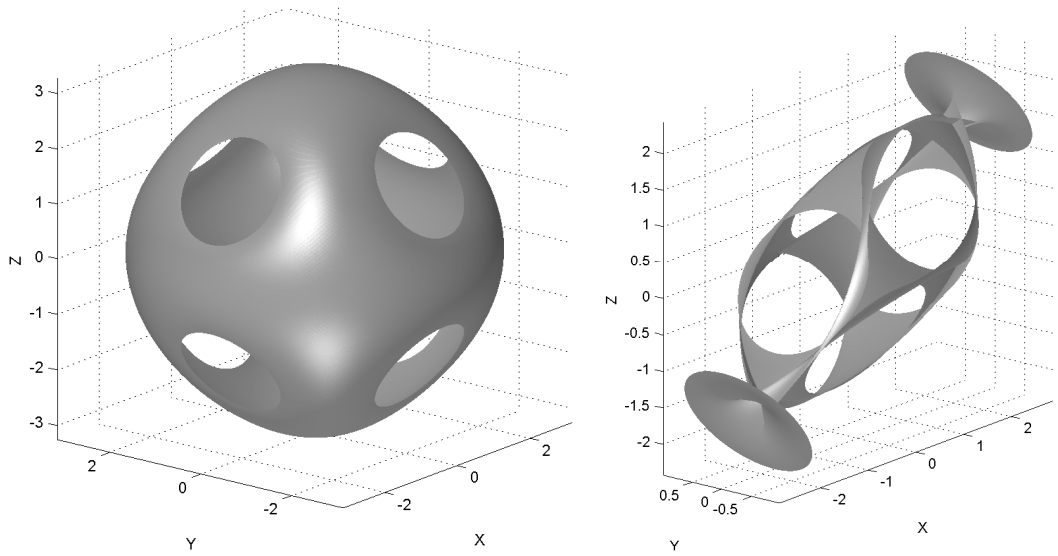

(a) $\epsilon_i = +1,\ i = 1, \cdots, 4$ (b) $\epsilon_1 = -1,\ \epsilon_2 = \epsilon_3 = \epsilon_4 = +1$

Figure 16: Singular Surfaces of CMGs in Pyramid Configuration

These holes are smoothly connected to the second type of the singular surface, for which one and only one of the $\epsilon_i,\ i \in \{1, \cdots, N\}$ is negative (or only one positive due to symmetry). This singular surface produces a trumpet-like funnel at the holes and part of it lies inside the momentum envelope. Figure 16(b) shows a singular surface for a four-wheel CMG cluster in a pyramid configuration with $\epsilon_1 = -1$. As shown in this figure, this surface consists with two portions: an external portion, which is part of the envelope, and an internal portion, which lies entirely inside the momentum envelope.

In conclusion, the complete momentum envelope is composed of the singular surface with $\epsilon_i > 0$ for $i = 1, \cdots, N$ and the external portion of the singular surface with one and only one negative ϵ_i, i.e., $\epsilon_i < 0$ and $\epsilon_j > 0$ for $j = 1, \cdots, N,\ j \neq i$. The complete momentum envelope is shown in Fig. 17. The internal portion of the singular surface with one and only one negative ϵ as well as the singular surface with more than one negative ϵ_i's are inside the momentum envelope. Figure 18 shows a cut of the angular momentum envelop revealing its rather complicated internal structure.

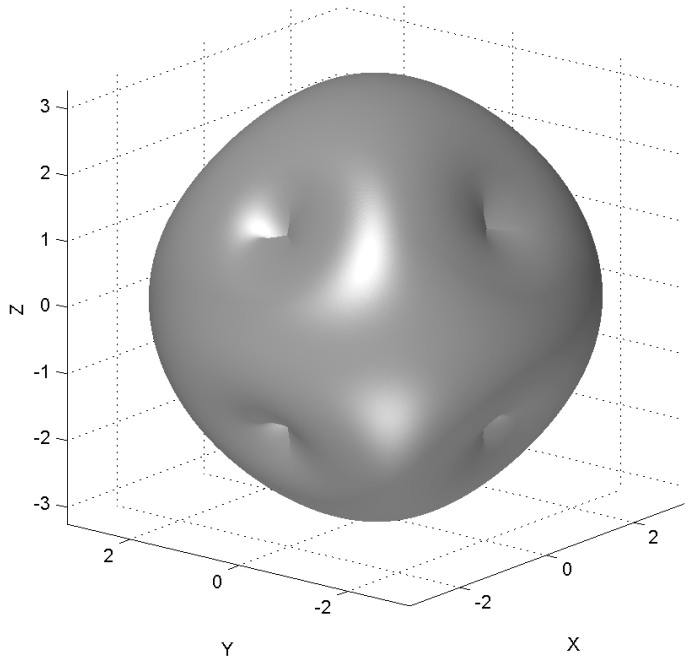

Figure 17: Angular Momentum Envelope of CMGs

4.2.3 Escape from Singularity using Null Motion

It may be possible to develop a gimbal angle reconfiguration strategy from a singular state $\boldsymbol{\gamma}_s$ without generating a torque, equivalently, without changing the total angular momentum. Since the size of matrix C in Eq. (54) is $3 \times N$ and its rank is at most three, there may exist a solution $\dot{\boldsymbol{\gamma}}$ of (57) (which must necessarily lie in the null space of $C(\boldsymbol{\gamma})$) if N is greater than three. Such a null motion strategy can be written as

$$\dot{\boldsymbol{\gamma}}_{\text{null}} = [\mathbf{I}_N - C^{\dagger}(\boldsymbol{\gamma})C(\boldsymbol{\gamma})]\mathbf{d}, \qquad \mathbf{d} \in \mathbb{R}^{N\times 1} \tag{65}$$

where $C^{\dagger}(\cdot)$ is the Moore-Penrose inverse of the matrix $C(\cdot)$ and $\mathbf{I}_N$ is the $N \times N$ identity matrix. It can be easily shown that $C(\boldsymbol{\gamma})\dot{\boldsymbol{\gamma}}_{\text{null}} = 0$. We are interested in investigating the possibility of the existence of null motions for escaping a singular state $\boldsymbol{\gamma}_s$ in such a way that no torque is generated on the spacecraft.

To this end, assume that at some time, say t, the CMG cluster is at a singular orientation, say $\boldsymbol{\gamma}(t) \triangleq \boldsymbol{\gamma}_s$. By definition, this implies that $\operatorname{rank} C(\boldsymbol{\gamma}(t)) = 2$. In order to escape this

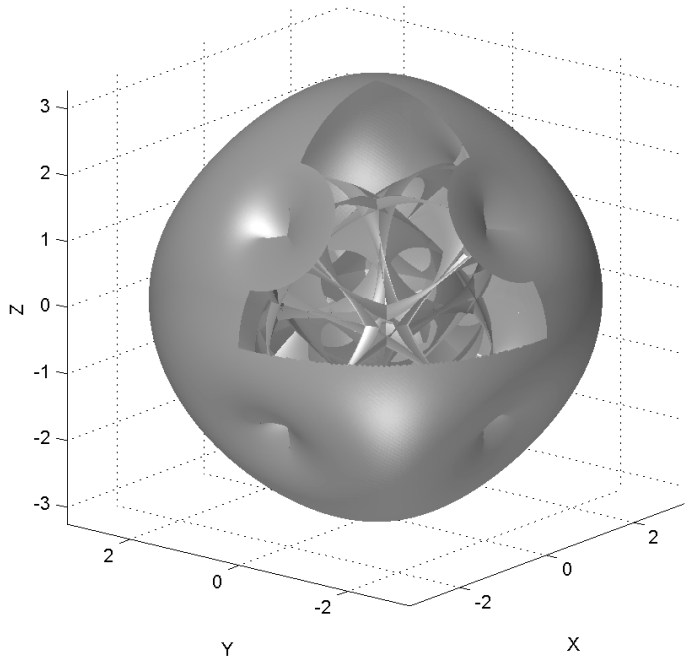

Figure 18: Singular Surfaces of CMGs ((i) $\epsilon_i = +1$ for all i, and (ii) ϵ_i's $= +1$ except one i)

singularity using null motion the following to be true

$$C(\boldsymbol{\gamma}(t))\dot{\boldsymbol{\gamma}}(t) = 0, \qquad \text{at time } t \tag{66}$$

$$C(\boldsymbol{\gamma}(t+\mathrm{d}t))\dot{\boldsymbol{\gamma}}(t+\mathrm{d}t) = 0, \qquad \text{at time } t+\mathrm{d}t \tag{67}$$

Taylor's theorem allows us to write

$$\boldsymbol{\gamma}(t+\mathrm{d}t) = \boldsymbol{\gamma}(t) + \dot{\boldsymbol{\gamma}}(t)\mathrm{d}t + r_1(\mathrm{d}t), \qquad \dot{\boldsymbol{\gamma}}(t+\mathrm{d}t) = \dot{\boldsymbol{\gamma}}(t) + \ddot{\boldsymbol{\gamma}}(t)\mathrm{d}t + r_2(\mathrm{d}t)$$

where $\lim_{\mathrm{d}t\to 0} \|r_i(\mathrm{d}t)\|/\mathrm{d}t = 0$ for $i = 1, 2$. The question of existence of null motion therefore reduces to one of finding $\ddot{\boldsymbol{\gamma}}(t) \in \mathbb{R}^N$ such that (67) holds, given that (66) holds. From (67) we have that

$$0 = C(\boldsymbol{\gamma}(t+\mathrm{d}t))\dot{\boldsymbol{\gamma}}(t+\mathrm{d}t) = C(\boldsymbol{\gamma}(t+\mathrm{d}t))(\dot{\boldsymbol{\gamma}}(t) + \ddot{\boldsymbol{\gamma}}(t)\mathrm{d}t + r_2(\mathrm{d}t))$$

Noticing that

$$\begin{aligned} C(\boldsymbol{\gamma}(t+\mathrm{d}t)) &= C(\boldsymbol{\gamma}(t) + \dot{\boldsymbol{\gamma}}(t)\mathrm{d}t + r_1(\mathrm{d}t)) \\ &= C(\boldsymbol{\gamma}(t)) + \sum_{i=1}^{N} \frac{\partial C}{\partial \gamma_i}\dot{\gamma}_i(t)\mathrm{d}t + r_3(\mathrm{d}t) \end{aligned}$$

where $\lim_{\mathrm{d}t\to 0} \|r_3(\mathrm{d}t)\|/\mathrm{d}t = 0$ and using (66) we therefore have that

$$\begin{aligned} 0 &= C(\boldsymbol{\gamma}(t+\mathrm{d}t))\dot{\boldsymbol{\gamma}}(t+\mathrm{d}t) \\ &= C(\boldsymbol{\gamma}(t))\dot{\boldsymbol{\gamma}}(t) + \left(\sum_{i=1}^{N} \frac{\partial C}{\partial \gamma_i}\dot{\gamma}_i(t)\mathrm{d}t\right)\dot{\boldsymbol{\gamma}}(t) + C(\boldsymbol{\gamma}(t))\ddot{\boldsymbol{\gamma}}(t)\mathrm{d}t + r_4(\mathrm{d}t) \end{aligned}$$

where $\lim_{\mathrm{d}t\to 0} \|r_4(\mathrm{d}t)\|/\mathrm{d}t = 0$. Taking the limit as $\mathrm{d}t \to 0$ one obtains that a null motion exists if and only if there exist $\ddot{\boldsymbol{\gamma}}(t)$ such that the following is true

$$\left(\sum_{i=1}^{N} \frac{\partial C}{\partial \gamma_i}\dot{\gamma}_i(t)\right)\dot{\boldsymbol{\gamma}}(t) + C(\boldsymbol{\gamma}(t))\,\ddot{\boldsymbol{\gamma}}(t) = 0 \tag{68}$$

where $\dot{\boldsymbol{\gamma}}(t) \in \mathcal{N}[C(\boldsymbol{\gamma}(t))]$. Noticing that

$$\sum_{i=1}^{N} \frac{\partial C}{\partial \gamma_i}\dot{\gamma}_i(t) = -\sum_{i=1}^{N} \dot{\gamma}_i \hat{\mathbf{s}}_i$$

condition (68) can be written in the form

$$-D(\boldsymbol{\gamma}(t))\dot{\boldsymbol{\gamma}}^2(t) + C(\boldsymbol{\gamma}(t))\,\ddot{\boldsymbol{\gamma}}(t) = 0, \qquad \forall \dot{\boldsymbol{\gamma}}(t) \in \mathcal{N}[C(\boldsymbol{\gamma}(t))] \tag{69}$$

where $\dot{\boldsymbol{\gamma}}^2 \triangleq [\dot{\gamma}_1^2,\ \cdots\ , \dot{\gamma}_N^2]^T$ and $D \triangleq [\hat{\mathbf{s}}_1,\ \hat{\mathbf{s}}_2,\ \cdots\ ,\ \hat{\mathbf{s}}_N]$. Equation (69) has a solution for $\ddot{\boldsymbol{\gamma}}(t)$ if and only if $\mathcal{R}[D(\boldsymbol{\gamma}(t))] \subseteq \mathcal{R}[C(\boldsymbol{\gamma}(t))]$, equivalently, $\mathcal{R}^{\perp}[C(\boldsymbol{\gamma}(t))] \subseteq \mathcal{R}^{\perp}[D(\boldsymbol{\gamma}(t))]$. Now recall that $\mathcal{R}^{\perp}[C(\boldsymbol{\gamma}(t))] = \mathrm{span}\{\hat{\mathbf{u}}\}$ hence the condition for existence of a solution to (69) is that $\hat{\mathbf{u}} \in \mathcal{R}^{\perp}[D(\boldsymbol{\gamma}(t))]$. Multiplying (69) on the left with $\hat{\mathbf{u}}^T$ we therefore get

$$\hat{\mathbf{u}}^T D(\boldsymbol{\gamma}(t))\dot{\boldsymbol{\gamma}}^2 = 0, \qquad \forall \dot{\boldsymbol{\gamma}} \in \mathcal{N}[C(\boldsymbol{\gamma}(t))] \tag{70}$$

or, finally, that

$$\dot{\boldsymbol{\gamma}}^T \mathcal{P}\dot{\boldsymbol{\gamma}} = 0, \qquad \forall \dot{\boldsymbol{\gamma}} \in \mathcal{N}[C(\boldsymbol{\gamma}(t))] \tag{71}$$

where $\mathcal{P} \triangleq \mathrm{diag}[\hat{\mathbf{u}}^T\hat{\mathbf{s}}_1, \cdots, \hat{\mathbf{u}}^T\hat{\mathbf{s}}_N]$. Condition (71) for existence of null motion is identical to the condition obtained by Ref. [10] using the concept of "virtual" gimbal angle displacements, which is to some degree, a mathematical artifact; see also Ref. [106]. In the above derivation, no such assumptions are made. This results to a derivation of (71) which more straightforward and which also allows connections to the existence of null motions in practice. For example, from the previous derivation it is evident that the existence of null motions, *in practice* depends, to a large extend, also on the torque capability of the gimbal

motors to provide the necessary torque $\ddot{\boldsymbol{\gamma}}$ to solve (69), something which is not directly evident from (71).

Clearly, equation (71) may not hold for every singular state. Hence, one can classify singular states into two types: The first type contains all singular states whose quadratic term $\mathcal{P}$ is sign-definite on the null space of $C(\boldsymbol{\gamma}_s)$. For these singular states, an escape from a singular state using null motion is impossible since the quadratic term in Eq. (71) cannot become zero by any nonzero gimbal angle change in $\mathcal{N}[C(\boldsymbol{\gamma}_s)]$. These singularities are called "definite", "elliptic" or "impassable" [10, 49]. Any singularity avoidance method using null motion fails if the CMGs encounter a singular state of this type. The other type contains all singularities whose quadratic term $\mathcal{P}$ is not sign-definite on $\mathcal{N}[C(\boldsymbol{\gamma}_s)]$. In this case, Eq. (71) may hold and thus there exist null motions $\dot{\boldsymbol{\gamma}}_{\text{null}}$ as in (65) which can be used to escape from the singular gimbal angles. These are called "indefinite", "hyperbolic" or "passable" singular gimbal states [46, 49, 10].

Note that a sufficient (but not necessary) condition for an elliptic singularity is that $\mathcal{P} > 0$, i.e., $\epsilon_i = \text{sign}(\hat{\mathbf{u}} \cdot \hat{\mathbf{s}}_i) > 0$ (or < 0 due to the symmetry) for all $i = 1, \ldots, N$. These states are obviously on the momentum envelope. However, the quadratic term in (71) can be sign definite on the null space of C even if $\mathcal{P}$ itself is not sign-definite on $\mathbb{R}^N$. In this case at least one of the ϵ_i is negative. As already mentioned some of the singular states with one negative ϵ_i are still on the envelope but those with two negative ϵ_i (the case with only three negative ϵ_i is the same as the case with only three positive ϵ_i) are inside the momentum envelope. All states on the envelope are elliptic but these are easily predictable. The internal elliptic singularities are not easily predictable and they are the main cause of concern during the implementation of the CMG steering algorithms in practice.

CHAPTER V

SINGULARITY ANALYSIS OF VSCMG SYSTEM

5.1 Singularity Analysis of VSCMGs Without Power Tracking

While the gimbal rates $\dot{\gamma}_i$ are the only control input variables in a CMG system, the wheel accelerations $\dot{\Omega}_i$ offer additional control variables in the case of a VSCMG system. The torque equation (57) for a CMGs cluster is modified in the case of VSCMGs as

$$[C \quad D] \begin{bmatrix} \dot{\boldsymbol{\gamma}} \\ \dot{\boldsymbol{\Omega}} \end{bmatrix} = \mathbf{T}.$$

If there are at least two wheels and their (fixed) gimbal axes are not parallel to each other, and if none of the wheel speeds becomes zero, the column vectors of $[C\ D]$ always span the three-dimensional space, i.e., $\text{rank}([C\ D]) = 3$ [73]. It follows that such a VSCMG system is always able to generate control torques along an arbitrary direction. In other words, such a VSCMG system never falls into a singularity, owing to the extra degrees of freedom provided by wheel speed control [73, 71]. However, it is still desirable to keep $\text{rank}\, C = 3$, because it is preferable to generate the required torque using gimbal angle changes rather than using wheel speed changes*. Hence, in the sequel we define as a "singularity of a VSCMG cluster" the rank deficiency of the matrix C, even though the VSCMGs will be able to generate an arbitrary torque at such cases. Notice that if none of the wheel speeds is zero, the matrix C defined in Eq.(54) becomes singular if and only if the unit vectors $\hat{\mathbf{t}}_i$ span a two-dimensional plane, similarly to the conventional CMGs. Hence, the rank of the matrix $C(\boldsymbol{\Omega}, \boldsymbol{\gamma})$ in (54) is independent of the (nonzero) wheel speeds. When $\text{rank}\, C(\boldsymbol{\Omega}, \boldsymbol{\gamma}) = 2$ there exists a singular direction $\hat{\mathbf{u}}$ perpendicular to this plane, i.e., $\hat{\mathbf{u}} \cdot \hat{\mathbf{t}}_i = 0$ for all $i = 1, \cdots, N$ and the condition for singularity remains therefore the same as for the CMG case.

*Owing to the torque amplification effect of a CMG. Also, for high wheel speeds it is power-inefficient to produce torques via wheel acceleration/deceleration.

As in section 3.4, Schaub et al [73] introduced a technique to cope with this type of singularity of the matrix C using the weighted minimum norm solution of (53), namely,

$$\begin{bmatrix} \dot{\boldsymbol{\gamma}} \\ \dot{\boldsymbol{\Omega}} \end{bmatrix} = WQ^T(QWQ^T)^{-1}\mathbf{T} \tag{72}$$

where $Q \triangleq [C\ D]$ and W is a weighting matrix which is function of the singularity index of the matrix C [73], for instance

$$W \triangleq \begin{bmatrix} w_1 e^{-w_2\kappa(C)}\mathbf{I}_N & 0_N \\ 0_N & \mathbf{I}_N \end{bmatrix} \tag{73}$$

where $\kappa(C)$ is the condition number of the matrix C and w_1 and w_2 are positive constants.

According to this approach, the VSCMGs operate as CMGs to take full advantage of the torque amplification effect under normal conditions (i.e., $\kappa(C)$ is small) but as the singularity is approached, $\kappa(C)$ becomes large and the VSCMGs smoothly switch to a momentum wheel mode [73]. However, this technique is a passive method which by itself does not ensure avoidance of singularities. Therefore, an active method to avoid the singularity is needed.

For this purpose, let us consider the possibility of null motion for a VSCMG system. Such a null motion must satisfy

$$[C \quad D] \begin{bmatrix} \dot{\boldsymbol{\gamma}} \\ \dot{\boldsymbol{\Omega}} \end{bmatrix}_{\text{null}} = \mathbf{0}_{3\times 1}. \tag{74}$$

Equivalently, a null motion strategy will not change the total angular momentum $\mathbf{H}$. Notice that $\dot{\boldsymbol{\gamma}} \in \mathcal{N}(C)$ and $\dot{\boldsymbol{\Omega}} \in \mathcal{N}(D)$ is a sufficient but not necessary condition for the existence of null motion. Even if $\dot{\boldsymbol{\gamma}} \notin \mathcal{N}(C)$ and $\dot{\boldsymbol{\Omega}} \notin \mathcal{N}(D)$, there still exists the possibility of satisfying Eq. (74). To check the possibility of escaping from a singular state by null motion in the case of VSCMGs, an approach similar to the CMGs case described in the previous section is used. To this end, we investigate whether to the following is true

$$C(\boldsymbol{\Omega}(t), \boldsymbol{\gamma}(t))\dot{\boldsymbol{\gamma}}(t) + D(\boldsymbol{\gamma}(t))\dot{\boldsymbol{\Omega}}(t) = 0, \quad \text{at time } t \tag{75}$$

$$C(\boldsymbol{\Omega}(t+\mathrm{d}t), \boldsymbol{\gamma}(t+\mathrm{d}t))\dot{\boldsymbol{\gamma}}(t+\mathrm{d}t) + D(\boldsymbol{\gamma}(t+\mathrm{d}t))\dot{\boldsymbol{\Omega}}(t+\mathrm{d}t) = 0, \quad \text{at time } t+\mathrm{d}t \tag{76}$$

where $C(\boldsymbol{\Omega}, \boldsymbol{\gamma})$ and $D(\boldsymbol{\gamma})$ as in (54)-(55). From Taylor's theorem,

$$\boldsymbol{\gamma}(t+\mathrm{d}t) = \boldsymbol{\gamma}(t) + \dot{\boldsymbol{\gamma}}(t)\mathrm{d}t + r_1(\mathrm{d}t), \qquad \dot{\boldsymbol{\gamma}}(t+\mathrm{d}t) = \dot{\boldsymbol{\gamma}}(t) + \ddot{\boldsymbol{\gamma}}(t)\mathrm{d}t + r_2(\mathrm{d}t),$$
$$\boldsymbol{\Omega}(t+\mathrm{d}t) = \boldsymbol{\Omega}(t) + \dot{\boldsymbol{\Omega}}(t)\mathrm{d}t + r_3(\mathrm{d}t), \qquad \dot{\boldsymbol{\Omega}}(t+\mathrm{d}t) = \dot{\boldsymbol{\Omega}}(t) + \ddot{\boldsymbol{\Omega}}(t)\mathrm{d}t + r_4(\mathrm{d}t).$$

where $\lim_{\mathrm{d}t\to 0} \|r_i(\mathrm{d}t)\|/\mathrm{d}t = 0, i = 1, \ldots, 4$. Noticing that

$$C(\boldsymbol{\Omega}(t+\mathrm{d}t), \boldsymbol{\gamma}(t+\mathrm{d}t)) = C(\boldsymbol{\Omega}(t), \boldsymbol{\gamma}(t)) + \sum_{i=1}^{N} \frac{\partial C}{\partial \gamma_i}\dot{\gamma}_i(t)\mathrm{d}t + \sum_{i=1}^{N} \frac{\partial C}{\partial \Omega_i}\dot{\Omega}_i(t)\mathrm{d}t + r_5(\mathrm{d}t)$$
$$D(\boldsymbol{\gamma}(t+\mathrm{d}t)) = D(\boldsymbol{\gamma}(t)) + \sum_{i=1}^{N} \frac{\partial D}{\partial \gamma_i}\dot{\gamma}_i(t)\mathrm{d}t + r_6(\mathrm{d}t),$$

where $\lim_{\mathrm{d}t\to 0} \|r_i(\mathrm{d}t)\|/\mathrm{d}t = 0, i = 5, 6$, one has that

$$\begin{aligned} 0 = {} & C(\boldsymbol{\Omega}(t), \boldsymbol{\gamma}(t))\dot{\boldsymbol{\gamma}}(t) + D(\boldsymbol{\gamma}(t))\dot{\boldsymbol{\Omega}}(t) \\ & + \left(\sum_{i=1}^{N} \frac{\partial C}{\partial \gamma_i}\dot{\gamma}_i(t)\mathrm{d}t\right)\dot{\boldsymbol{\gamma}}(t) + \left(\sum_{i=1}^{N} \frac{\partial C}{\partial \Omega_i}\dot{\Omega}_i(t)\mathrm{d}t\right)\dot{\boldsymbol{\gamma}}(t) + C(\boldsymbol{\Omega}(t), \boldsymbol{\gamma}(t))\ddot{\boldsymbol{\gamma}}(t)\mathrm{d}t \\ & + \left(\sum_{i=1}^{N} \frac{\partial D}{\partial \gamma_i}\dot{\gamma}_i(t)\mathrm{d}t\right)\dot{\boldsymbol{\Omega}}(t) + D(\boldsymbol{\gamma}(t))\ddot{\boldsymbol{\Omega}}(t)\mathrm{d}t + r_7(\mathrm{d}t) \end{aligned} \tag{77}$$

with $\lim_{\mathrm{d}t\to 0} \|r_7(\mathrm{d}t)\|/\mathrm{d}t = 0$. Using Eq.(75), dividing with $\mathrm{d}t$ and taking the limit as $\mathrm{d}t \to 0$, we have that a null motion exists if and only if there exist $\ddot{\boldsymbol{\gamma}}(t) \in \mathbb{R}^N$ and $\ddot{\boldsymbol{\Omega}}(t) \in \mathbb{R}^N$ such that the following is true

$$\begin{aligned} 0 = {} & C(\boldsymbol{\Omega}(t), \boldsymbol{\gamma}(t))\ddot{\boldsymbol{\gamma}}(t) + D(\boldsymbol{\gamma}(t))\ddot{\boldsymbol{\Omega}}(t) \\ & + \left(\sum_{i=1}^{N} \frac{\partial C}{\partial \gamma_i}\dot{\gamma}_i(t)\right)\dot{\boldsymbol{\gamma}}(t) + \left(\sum_{i=1}^{N} \frac{\partial C}{\partial \Omega_i}\dot{\Omega}_i(t)\right)\dot{\boldsymbol{\gamma}}(t) + \left(\sum_{i=1}^{N} \frac{\partial D}{\partial \gamma_i}\dot{\gamma}_i(t)\right)\dot{\boldsymbol{\Omega}}(t) \end{aligned} \tag{78}$$

Using now the facts that

$$\begin{aligned} \frac{\partial C}{\partial \gamma_i} &= [0, 0, \cdots, -I_{\mathrm{ws}i}\Omega_i\hat{\mathbf{s}}_i, \cdots, 0] \\ \frac{\partial C}{\partial \Omega_i} &= [0, 0, \cdots, I_{\mathrm{ws}i}\hat{\mathbf{t}}_i, \cdots, 0] \\ \frac{\partial D}{\partial \gamma_i} &= [0, 0, \cdots, I_{\mathrm{ws}i}\hat{\mathbf{t}}_i, \cdots, 0] \end{aligned} \tag{79}$$

condition (78) can be written as

$$[C(\boldsymbol{\Omega}(t), \boldsymbol{\gamma}(t)) \quad D(\boldsymbol{\gamma}(t))] \begin{bmatrix} \ddot{\boldsymbol{\gamma}}(t) \\ \ddot{\boldsymbol{\Omega}}(t) \end{bmatrix} = -2\sum_{i=1}^{N} I_{\mathrm{ws}i}\hat{\mathbf{t}}_i\dot{\gamma}_i\dot{\Omega}_i + \sum_{i=1}^{N} I_{\mathrm{ws}i}\Omega_i\hat{\mathbf{s}}_i\dot{\gamma}_i^2 \tag{80}$$

where $[\dot{\boldsymbol{\gamma}}^T(t), \dot{\boldsymbol{\Omega}}^T(t)]^T \in \mathcal{N}([C,\ D])$. Since the column vectors of $[C,\ D]$ always span the 3-dimensional space, there always exist vectors $\ddot{\boldsymbol{\gamma}}(t) \in \mathbb{R}^N$ and $\ddot{\boldsymbol{\Omega}}(t) \in \mathbb{R}^N$ which satisfy (80). Thus, a null motion always exists for the VSCMG case. Most interestingly, we do not need all N wheels operate as VSCMGs in order to avoid singularities. Only two out of all N wheels need to operate as VSCMGs while the remaining $N-2$ may operate as conventional CMGs. This is due to the fact that any two inner products $\hat{\mathbf{u}} \cdot \hat{\mathbf{s}}_i$ cannot be zero at a singularity simultaneously provided that no two gimbal directions are identical. We conclude that every singularity (in terms of the rank deficiency of C) is escapable with null motion $[\dot{\boldsymbol{\gamma}}^T, \dot{\boldsymbol{\Omega}}^T]^T_{\text{null}} \in \mathcal{N}(Q)$, if we have no less than two VSCMGs out of a total of N wheels.

5.1.1 Singularity Avoidance using Null Motion of VSCMGs Without Power Tracking

In this section a method to avoid singularities for VSCMGs using null motion is proposed. The method has several variations depending on the selection for measuring the vicinity to a singular state (for example, the minimum singular value of C, the determinant of CC^T, the condition number of C, etc.). A singularity avoidance scheme will tend to increase the measure of the singularity in some cases (e.g., the minimum singular value of C or the determinant of CC^T) and will tend to decrease it in other cases (e.g., the condition number of C).

Let $\kappa(\boldsymbol{\gamma}, \boldsymbol{\Omega})$ be a measure of the singularity of the matrix $C(\boldsymbol{\Omega}, \boldsymbol{\gamma})$ which is a function of gimbal angles and wheel speeds. The proposed method, commonly known as the "gradient method [49]," is to add a null motion which does not have any effect on the generated output torque but it increases (or decreases) the singularity measure $\kappa(\boldsymbol{\gamma}, \boldsymbol{\Omega})$. For example, if we let $Q = [C\ D]$, then any null motion can be written as

$$\begin{bmatrix} \dot{\boldsymbol{\gamma}} \\ \dot{\boldsymbol{\Omega}} \end{bmatrix}_{\text{null}} = [\mathbf{I}_{2N} - Q^{\dagger}Q]\mathbf{d}, \qquad \mathbf{d} \in \mathbb{R}^{2N \times 1} \tag{81}$$

It can be easily shown that $Q[\dot{\boldsymbol{\gamma}}^T, \dot{\boldsymbol{\Omega}}^T]^T_{\text{null}} = 0$, and the projection matrix $[\mathbf{I}_{2N} - Q^{\dagger}Q]$ is

symmetric and idempotent[†] and thus positive semi-definite. If the vector $\mathbf{d}$ is selected as

$$\mathbf{d} = \pm k_n \begin{bmatrix} \frac{\partial \kappa}{\partial \boldsymbol{\gamma}}^T \\ \frac{\partial \kappa}{\partial \boldsymbol{\Omega}}^T \end{bmatrix}, \quad k_n > 0 \tag{82}$$

then, the rate of change of $\kappa(\boldsymbol{\gamma}, \boldsymbol{\Omega})$ due to (81) is

$$\begin{aligned} \dot{\kappa}_{\text{null}} &= \begin{bmatrix} \frac{\partial \kappa}{\partial \boldsymbol{\gamma}} & \frac{\partial \kappa}{\partial \boldsymbol{\Omega}} \end{bmatrix} \begin{bmatrix} \dot{\boldsymbol{\gamma}} \\ \dot{\boldsymbol{\Omega}} \end{bmatrix}_{\text{null}} \\ &= \pm k_n \begin{bmatrix} \frac{\partial \kappa}{\partial \boldsymbol{\gamma}} & \frac{\partial \kappa}{\partial \boldsymbol{\Omega}} \end{bmatrix} [\mathbf{I}_{2N} - Q^\dagger Q] \begin{bmatrix} \frac{\partial \kappa}{\partial \boldsymbol{\gamma}}^T \\ \frac{\partial \kappa}{\partial \boldsymbol{\Omega}}^T \end{bmatrix} \\ &\leq 0 \quad (\text{or} \geq 0) \end{aligned} \tag{83}$$

Therefore, it is expected that the singularity will be avoided. However, this method does not necessarily guarantee singularity avoidance, since the change of $\kappa(\boldsymbol{\gamma}, \boldsymbol{\Omega})$ due to the torque-generating solution of Eq. (72) may dominate the change due to the null motion of Eq. (81). Nevertheless, singularity avoidance methods based on null motions have been successfully used in practice [49]. Appendix A presents the details for calculating the gradient of the condition number needed in Eq. (82).

Assuming Q is full rank a more general form than (81) can be used to generate null motions, as follows

$$\begin{bmatrix} \dot{\boldsymbol{\gamma}} \\ \dot{\boldsymbol{\Omega}} \end{bmatrix}_{\text{null}} = -k_n [\mathbf{I}_{2N} - W Q^T (Q W Q^T)^{-1} Q] W \begin{bmatrix} \frac{\partial \kappa}{\partial \boldsymbol{\gamma}}^T \\ \frac{\partial \kappa}{\partial \boldsymbol{\Omega}}^T \end{bmatrix}, \tag{84}$$

[†] A is an idempotent matrix if $A^2 = A$. All eigenvalues of an idempotent matrix are 1 or 0.

where $W > 0$ some weighting matrix. Then, $\dot{\kappa}_{\text{null}}$ becomes

$$\begin{aligned}
\dot{\kappa}_{\text{null}} &= \begin{bmatrix} \frac{\partial \kappa}{\partial \boldsymbol{\gamma}} & \frac{\partial \kappa}{\partial \boldsymbol{\Omega}} \end{bmatrix} \begin{bmatrix} \dot{\boldsymbol{\gamma}} \\ \dot{\boldsymbol{\Omega}} \end{bmatrix}_{\text{null}} \\
&= -k_n \begin{bmatrix} \frac{\partial \kappa}{\partial \boldsymbol{\gamma}} & \frac{\partial \kappa}{\partial \boldsymbol{\Omega}} \end{bmatrix} [\mathbf{I}_{2N} - WQ^T(QWQ^T)^{-1}Q]W \begin{bmatrix} \frac{\partial \kappa}{\partial \boldsymbol{\gamma}}^T \\ \frac{\partial \kappa}{\partial \boldsymbol{\Omega}}^T \end{bmatrix} \\
&= -k_n \begin{bmatrix} \frac{\partial \kappa}{\partial \boldsymbol{\gamma}} & \frac{\partial \kappa}{\partial \boldsymbol{\Omega}} \end{bmatrix} [W - WQ^T(QWQ^T)^{-1}QW] \begin{bmatrix} \frac{\partial \kappa}{\partial \boldsymbol{\gamma}}^T \\ \frac{\partial \kappa}{\partial \boldsymbol{\Omega}}^T \end{bmatrix} \\
&= -k_n \begin{bmatrix} \frac{\partial \kappa}{\partial \boldsymbol{\gamma}} & \frac{\partial \kappa}{\partial \boldsymbol{\Omega}} \end{bmatrix} W^{\frac{1}{2}} [\mathbf{I}_{2N} - W^{\frac{1}{2}}Q^T(QWQ^T)^{-1}QW^{\frac{1}{2}}]W^{\frac{1}{2}} \begin{bmatrix} \frac{\partial \kappa}{\partial \boldsymbol{\gamma}}^T \\ \frac{\partial \kappa}{\partial \boldsymbol{\Omega}}^T \end{bmatrix}
\end{aligned}$$

where $W^{\frac{1}{2}}W^{\frac{1}{2}} = W$ and $W^{\frac{T}{2}} = W^{\frac{1}{2}}$.

Let $P_1 = \mathbf{I}_{2N} - W^{\frac{1}{2}}Q^T(QWQ^T)^{-1}QW^{\frac{1}{2}}$, then $P_1^T = P_1$, and

$$\begin{aligned}
P_1P_1 &= [\mathbf{I}_{2N} - W^{\frac{1}{2}}Q^T(QWQ^T)^{-1}QW^{\frac{1}{2}}][\mathbf{I}_{2N} - W^{\frac{1}{2}}Q^T(QWQ^T)^{-1}QW^{\frac{1}{2}}] \\
&= \mathbf{I}_{2N} - W^{\frac{1}{2}}Q^T(QWQ^T)^{-1}QW^{\frac{1}{2}} - W^{\frac{1}{2}}Q^T(QWQ^T)^{-1}QW^{\frac{1}{2}} \\
&\quad + W^{\frac{1}{2}}Q^T(QWQ^T)^{-1}QWQ^T(QWQ^T)^{-1}QW^{\frac{1}{2}} \\
&= \mathbf{I}_{2N} - W^{\frac{1}{2}}Q^T(QWQ^T)^{-1}QW^{\frac{1}{2}} \\
&= P_1,
\end{aligned}$$

so P_1 is symmetric and idempotent and thus non-negative definite. Therefore, $\dot{\kappa}_{\text{null}} \leq 0$.

5.2 Singularity Analysis of VSCMGs With Power Tracking

In Ref. [92], Tsiotras et. al. have introduced a control method for the simultaneous attitude and power tracking problem for the case of a rigid spacecraft with N momentum wheels. These results have been extended to the case of N VSCMGs in Section 3.3. By setting the gimbal angles in Section 3.3 to be constant, one can retrieve the results of Ref. [92] as a special case.

The control law for IPACS with VSCMGs derived in Section 3.3 is

$$Q_p \boldsymbol{u} = \mathbf{L} \tag{85}$$

where

$$\boldsymbol{u} \triangleq \begin{bmatrix} \dot{\boldsymbol{\gamma}} \\ \dot{\boldsymbol{\Omega}} \end{bmatrix}, \quad Q_p \triangleq \begin{bmatrix} C & D \\ \mathbf{0}_{1\times N} & \boldsymbol{\Omega}^T I_{\mathrm{ws}} \end{bmatrix}, \quad \mathbf{L} \triangleq \begin{bmatrix} \mathbf{T} \\ P \end{bmatrix}$$

The existence of a solution to Eq. (85) depends on the rank of the coefficient matrix $Q_p \in \mathbb{R}^{4\times 2N}$. If $\operatorname{rank} Q_p = 4$, then Eq. (85) always has a solution, for example,

$$\begin{bmatrix} \dot{\boldsymbol{\gamma}} \\ \dot{\boldsymbol{\Omega}} \end{bmatrix} = W Q_p^T (Q_p W Q_p^T)^{-1} \mathbf{L}. \tag{86}$$

However, if $\operatorname{rank} Q_p = 3$, it is not possible to solve equation (85)[‡]. In Section 3.4, it has been shown that a sufficient (but not necessary) condition for $\operatorname{rank} Q_p = 4$ is that $\operatorname{rank} C = 3$.

In order to investigate the existence of null motion for the case of both attitude and power tracking problem, we first notice that in this case, in addition to (75)-(76) the following conditions must be true as well

$$\boldsymbol{\Omega}^T(t) I_{\mathrm{ws}} \dot{\boldsymbol{\Omega}}(t) = 0, \quad \text{at time } t \tag{87}$$

$$\boldsymbol{\Omega}^T(t+\mathrm{d}t) I_{\mathrm{ws}} \dot{\boldsymbol{\Omega}}(t+\mathrm{d}t) = 0, \quad \text{at time } t+\mathrm{d}t \tag{88}$$

leading to the condition that a null motion exists if and only if there exist $\ddot{\boldsymbol{\gamma}}(t) \in \mathbb{R}^N$ and $\ddot{\boldsymbol{\Omega}}(t) \in \mathbb{R}^N$ such that

$$\begin{bmatrix} C(\boldsymbol{\Omega}(t), \boldsymbol{\gamma}(t)) & D(\boldsymbol{\gamma}(t)) \\ \mathbf{0}_{1\times N} & \boldsymbol{\Omega}^T(t) I_{\mathrm{ws}} \end{bmatrix} \begin{bmatrix} \ddot{\boldsymbol{\gamma}}(t) \\ \ddot{\boldsymbol{\Omega}}(t) \end{bmatrix} = \begin{bmatrix} \boldsymbol{\zeta}_1 \\ \zeta_2 \end{bmatrix} \tag{89}$$

where

$$\boldsymbol{\zeta}_1 \triangleq -2\sum_{i=1}^{N} I_{\mathrm{ws}i} \hat{\mathbf{t}}_i \dot{\gamma}_i \dot{\Omega}_i + \sum_{i=1}^{N} I_{\mathrm{ws}i} \Omega_i \hat{\mathbf{s}}_i \dot{\gamma}_i^2 \tag{90}$$

$$\zeta_2 \triangleq -\dot{\boldsymbol{\Omega}}^T I_{\mathrm{ws}} \dot{\boldsymbol{\Omega}} = -\sum_{i=1}^{N} I_{\mathrm{ws}_i} \dot{\Omega}_i^2 \tag{91}$$

Now, let us show that a solution to (89) exists if and only if rank $M = 2$, where

$$M \triangleq \begin{bmatrix} I_{\mathrm{ws}_1} \hat{\mathbf{u}}^T \mathbf{s}_1 & I_{\mathrm{ws}_2} \hat{\mathbf{u}}^T \mathbf{s}_2 & \cdots & I_{\mathrm{ws}_N} \hat{\mathbf{u}}^T \mathbf{s}_N \\ I_{\mathrm{ws}_1} \Omega_1 & I_{\mathrm{ws}_2} \Omega_2 & \cdots & I_{\mathrm{ws}_N} \Omega_N \end{bmatrix} \tag{92}$$

[‡]Notice that rank $Q_p \geq 3$, since rank $[C\ D] = 3$.

A solution to (89) exists if and only if $\boldsymbol{\zeta} \triangleq [\boldsymbol{\zeta}_1^T \ \zeta_2]^T \in \mathcal{R}[Q_p]$, equivalently, if and only if $\mathbf{v}^T\boldsymbol{\zeta} = 0$ for all nonzero $\mathbf{v} \in \mathcal{R}^\perp[Q_p]$.

Notice that

$$\mathcal{R}^\perp[Q_p] = \{\, \mathbf{v} = [\mathbf{v}_1^T \ v_2]^T \in \mathbb{R}^4 : \mathbf{v}_1 \in \mathcal{R}^\perp(C),\ \mathbf{v}_1^T D(\boldsymbol{\gamma}) + v_2 \boldsymbol{\Omega}^T I_{\mathrm{ws}} = 0 \,\} \tag{93}$$

which, via the fact $\mathcal{R}^\perp(C) = \mathrm{span}\{\hat{\mathbf{u}}\}$ leads to the condition

$$[\hat{\mathbf{u}}^T \ \eta] \begin{bmatrix} \boldsymbol{\zeta}_1 \\ \zeta_2 \end{bmatrix} = \sum_{i=1}^{N} I_{\mathrm{ws}i} \hat{\mathbf{u}}^T \hat{\mathbf{s}}_i \, \Omega_i \dot{\gamma}_i^2 - \eta \left(\sum_{i=1}^{N} I_{\mathrm{ws}_i} \dot{\Omega}_i^2 \right) = 0 \tag{94}$$

for all η such that $\hat{\mathbf{u}}^T D(\boldsymbol{\gamma}) + \eta \, \boldsymbol{\Omega}^T I_{\mathrm{ws}} = 0$, that is, for all η such that

$$[I_{\mathrm{ws}_1} \hat{\mathbf{u}}^T \mathbf{s}_1, \cdots, I_{\mathrm{ws}_N} \hat{\mathbf{u}}^T \mathbf{s}_N] + \eta \, [I_{\mathrm{ws}_1} \Omega_1, \cdots, I_{\mathrm{ws}_N} \Omega_N] = 0. \tag{95}$$

If rank $M = 2$, then there does not exist η which satisfies (95), thus the sufficiency is shown. In the other hand, if rank $M = 1$, then there exists nonzero η satisfying (95). That means

$$I_{\mathrm{ws}_1} \hat{\mathbf{u}}^T \mathbf{s}_1 = -\eta I_{\mathrm{ws}_1} \Omega_1, \cdots, I_{\mathrm{ws}_N} \hat{\mathbf{u}}^T \mathbf{s}_N = -\eta I_{\mathrm{ws}_N} \Omega_N$$

Thus, Eq.(94) becomes

$$-\eta \left(\sum_{i=1}^{N} I_{\mathrm{ws}i} \Omega_i^2 \dot{\gamma}_i^2 + \sum_{i=1}^{N} I_{\mathrm{ws}_i} \dot{\Omega}_i^2 \right) = 0 \tag{96}$$

which cannot hold for any $[\dot{\boldsymbol{\gamma}}, \dot{\boldsymbol{\Omega}}] \neq 0$. This shows the necessity and the proof is completed.

In case rank $M = 1$ then it is impossible to satisfy both the angular momentum (torque) and the kinetic energy (power) requirement for singularity avoidance using null motion. Therefore, the inescapable singularities of a VSCMG system used for combined attitude control and power tracking is completely characterized by the rank of the matrix M in (92). Notice that since the wheel speeds Ω_i are all positive by definition[§], the rank deficiency of M can occur only when $\epsilon_i \triangleq \mathrm{sign}(\hat{\mathbf{u}} \cdot \hat{\mathbf{s}}_i) = +1$ for all $i = 1, \ldots, N$.

[§]If a wheel speed Ω_i is negative, we can redefine the direction of spin axis $\mathbf{s}_i$ in the opposite direction.

5.3 The Angular Momentum Envelope of a VSCMG Cluster

In this section, more details on the inescapable singularities and their relation to the rank deficiency of the matrix M in (92) are given. For this purpose, three singular surfaces are defined in the three-dimensional angular momentum space. The first surface is the momentum envelope for given kinetic energy, the second is the momentum envelope for given wheel speeds, and the third is the momentum envelope for given kinetic energy and gimbal angles.

5.3.1 The Momentum Envelope for Given Kinetic Energy

In this section the angular momentum envelope of a VSCMG cluster for a given kinetic energy is defined, and it is shown that the total angular momentum vector reaches this envelope if and only if the VSCMG cluster encounters an inescapable singularity (i.e., rank M=1).

To this end, consider the case when a power command $P(t)$ is given for all $t_0 \leq t \leq t_f$. Then the kinetic energy stored in the VSCMG cluster for $t \geq t_0$ can be computed from $E(t) = \int_{t_0}^{t} P(t)\mathrm{d}t + E(t_0)$. Suppose that $E(t) = E$ is given at some instant. The objective is to find the maximum workspace of $\mathbf{H}(t)$ with the given value of the kinetic energy E. The boundary of the maximum angular momentum workspace can be found by solving the following maximization problem.

For a given singular direction $\hat{\mathbf{u}}$, find the gimbal angles γ_i's and wheel speeds Ω_i's that maximize the function $\mathcal{J}_{\mathrm{ME}}$ defined by

$$\mathcal{J}_{\mathrm{ME}} \triangleq \mathbf{H} \cdot \hat{\mathbf{u}} = \sum_{i=1}^{N} I_{\mathrm{ws}_i} \Omega_i \hat{\mathbf{u}} \cdot \hat{\mathbf{s}}_i = \sum_{i=1}^{N} \alpha_i(\gamma_i) I_{\mathrm{ws}_i} \Omega_i \tag{97}$$

subject to the constraints

$$\sum_{i=1}^{N} I_{\mathrm{ws}_i} \Omega_i^2 = 2E \tag{98}$$

$$\alpha_i^2(\gamma_i) \leq {\alpha_{\max}}_i^2, \quad i = 1, \ldots, N \tag{99}$$

where $\alpha_i(\gamma_i) \triangleq \hat{\mathbf{u}} \cdot \hat{\mathbf{s}}_i$ and $\alpha_{\max i}$ is its maximum value. Since α_i becomes maximum when $\hat{\mathbf{s}}_i$ has a maximum projection onto $\hat{\mathbf{u}}$ as shown in Fig. 15, $\alpha_{\max i}$ is given by $\alpha_{\max i} = \sqrt{1 - (\hat{\mathbf{g}}_i \cdot \hat{\mathbf{u}})^2}$.

In Appendix B.2, it is shown that the solution to this maximization problem is

$$\alpha_i^* = \alpha_{\max i}, \quad i = 1, \cdots, N \tag{100}$$

$$\Omega_i^* = \frac{\alpha_{\max i}}{2\lambda_0}, \quad i = 1, \cdots, N \tag{101}$$

where

$$\lambda_0 \triangleq \frac{1}{\sqrt{8E}} \left(\sum_{i=1}^{N} I_{ws_i} {\alpha_{\max i}}^2 \right)^{\frac{1}{2}}.$$

Equation (100) implies that the gimbal angles of the VSCMGs are in a singular configuration with all $\epsilon_i = +1$, and Eq. (101) implies that each wheel has a speed which is proportional to $\hat{\mathbf{u}} \cdot \hat{\mathbf{s}}_i$. It can also be shown that the solution (100)-(101) corresponds to an inescapable singularity where rank $M = 1$ (see Appendix B for the details). In summary, an inescapable singularity for the case of attitude/power tracking for a VSCMG cluster occurs when the wheels have maximum angular momentum along the singular direction with the given kinetic energy constraint.

The above observations also lend themselves to a method for drawing the angular momentum envelope of a VSCMGs system with given kinetic energy constraint. Given a singular direction $\hat{\mathbf{u}}$, each spin axis $\hat{\mathbf{s}}_i$ is determined as in the conventional CMGs case, i.e., from Eq. (63) with all $\epsilon_i = +1$, and with the wheel speeds determined from Eq. (101). Hence, the total angular momentum at this singular configuration for a given singular direction $\hat{\mathbf{u}}$ can be expressed as

$$\mathbf{H} = \sum_{i=1}^{N} \frac{(\hat{\mathbf{g}}_i \times \hat{\mathbf{u}}) \times \hat{\mathbf{g}}_i}{|\hat{\mathbf{g}}_i \times \hat{\mathbf{u}}|} \Omega_i^* I_{ws i} = \frac{1}{2\lambda_0} \sum_{i=1}^{N} (\hat{\mathbf{u}} - \hat{\mathbf{g}}_i (\hat{\mathbf{g}}_i \cdot \hat{\mathbf{u}})) I_{ws i}, \tag{102}$$

where the last equality follows from $|\hat{\mathbf{g}}_i \times \hat{\mathbf{u}}| = \max\{\hat{\mathbf{s}}_i \cdot \hat{\mathbf{u}}\} = \alpha_{\max i}$.

Equation (102) defines an ellipsoid in the momentum space. If the total angular momentum vector reaches this surface and the reference attitude (torque requirement) forces it to go outside this surface, then the VSCMGs cluster cannot meet both attitude and power tracking requirements. Contrary to the CMGs case, shown in Fig. 16(a), the momentum envelop of a VSCMG cluster with given kinetic energy has no holes. The reason is that when the singular direction $\hat{\mathbf{u}}$ is along a gimbal axis $\hat{\mathbf{g}}_i$, the angular speed of the ith wheel does not have a component along $\hat{\mathbf{u}}$ since $\hat{\mathbf{s}}_i \perp \hat{\mathbf{g}}_i$ and thus $\hat{\mathbf{s}}_i \perp \hat{\mathbf{u}}$. Hence, the ith wheel speed

does not contribute to the maximization of the total angular momentum along $\hat{\mathbf{u}}$. Thus, Ω_i may be taken to be zero with all the other wheels having higher speeds (in order to satisfy the kinetic energy constraint).

5.3.2 A Geometric Picture of the Inescapable Singularity Case

A nice geometric picture emerges for describing the occurrence of inescapable singularities using the concept of the angular momentum envelope. In addition to the angular momentum envelope for given kinetic energy introduced in the previous section, one can also define the angular momentum envelope of a VSCMG system with given energy *and* a given set of gimbal angles. Given the total kinetic energy E and the gimbal angles, this envelope is defined as the boundary of the maximum workspace of the total momentum $\mathbf{H}$ as wheel speeds vary but the total energy E and the gimbal angles γ_i's are kept constant. This surface can be drawn by solving the following maximization problem which maximizes

$$\mathcal{J}_{\mathrm{ME}} \triangleq \mathbf{H} \cdot \hat{\mathbf{u}} = \sum_{i=1}^{N} I_{\mathrm{ws}_i} \Omega_i \hat{\mathbf{u}} \cdot \hat{\mathbf{s}}_i = \sum_{i=1}^{N} \alpha_i I_{\mathrm{ws}_i} \Omega_i \tag{103}$$

subject to the constraints

$$\sum_{i=1}^{N} I_{\mathrm{ws}_i} \Omega_i^2 = 2E$$

for each $\hat{\mathbf{u}} \in \mathbb{R}^3$, $\|\hat{\mathbf{u}}\| = 1$, while the gimbal angles γ_i's are fixed.

The solution to this maximization problem is similar to the one in Section 5.3.1 and thus, it is omitted. Its solution yields

$$\Omega_i^* = \frac{\alpha_i}{2\lambda_0}$$

where

$$\lambda_0 \triangleq \frac{1}{\sqrt{8E}} \left(\sum_{i=1}^{N} I_{\mathrm{ws}_i} \alpha_i^2 \right)^{\frac{1}{2}}.$$

In addition to the angular momentum envelop for given kinetic energy and given kinetic energy and gimbal angles, one can also construct the angular momentum envelope for given wheel speeds using the method described in Sections 4.2.1 and 4.2.2. The interplay between the latter two surfaces provides a clear picture for the occurrence of the inescapable singularities.

Figures 19 and 20 show the envelopes at a singular configuration corresponding to the singular direction $\hat{\mathbf{u}} = [0, 0, 1]^T$ with $\epsilon_i > 0$ for $i = 1, 2, 3, 4$. In these figures, surface A is the momentum envelope with given wheel speeds, surface B is with given energy and gimbal angles, and surface C is with given kinetic energy.

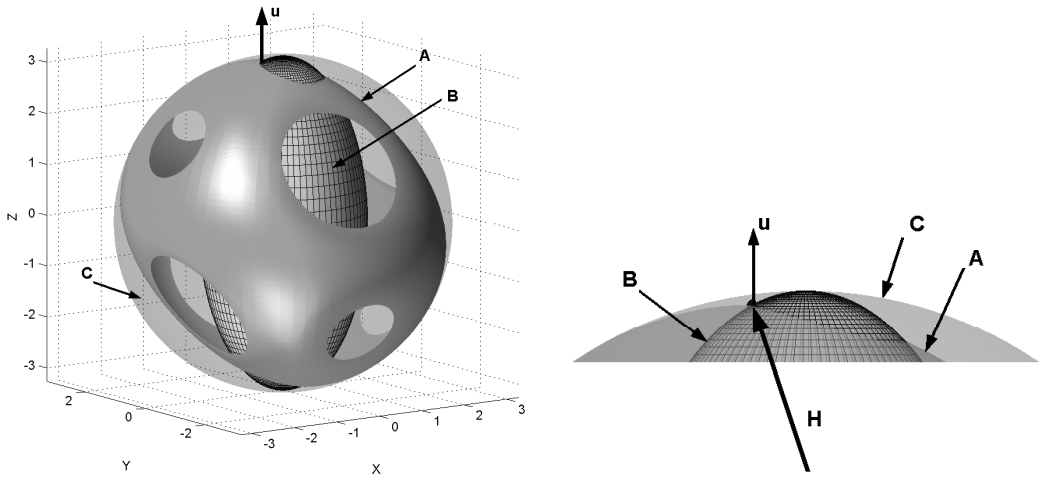

(a) (b)

Figure 19: Escapable Singularity of VSCMGs

Figure 19 shows a case when the gimbal angles are singulary configured with all $\epsilon_i > 0$, but the wheel speeds are not equal to the maximizing solution of Eq. (101) hence $\operatorname{rank} M \neq 1$. Notice that the total momentum vector $\mathbf{H}$ lies inside the momentum envelope with given energy (surface C). As the gimbal angles vary with the wheel speeds fixed, $\mathbf{H}$ will move inside the surface A, thus $\Delta\mathbf{H} \cdot \hat{\mathbf{u}} < 0$. As the wheel speeds vary with gimbal angles and total energy fixed, $\mathbf{H}$ will move inside the surface B, thus $\Delta\mathbf{H} \cdot \hat{\mathbf{u}}$ due to the wheel speeds changes can be either positive or negative as shown in this figure. Hence, this sign-indefinite term can cancel the negative definite term of $\Delta\mathbf{H} \cdot \hat{\mathbf{u}}$ due to the gimbal angle changes. Therefore, a gimbal angle change is possible without violating the angular momentum and energy constraints, and this singularity is escapable using null motion.

In the other hand, Fig. 20 shows an inescapable singularity when $\operatorname{rank} M = 1$. The momentum vector $\mathbf{H}$ reaches the envelope C. At this $\mathbf{H}$, both surface A and surface B are normal to the singular direction $\hat{\mathbf{u}}$, so both $\Delta\mathbf{H} \cdot \hat{\mathbf{u}}$ by gimbal angle change and $\Delta\mathbf{H} \cdot \hat{\mathbf{u}}$

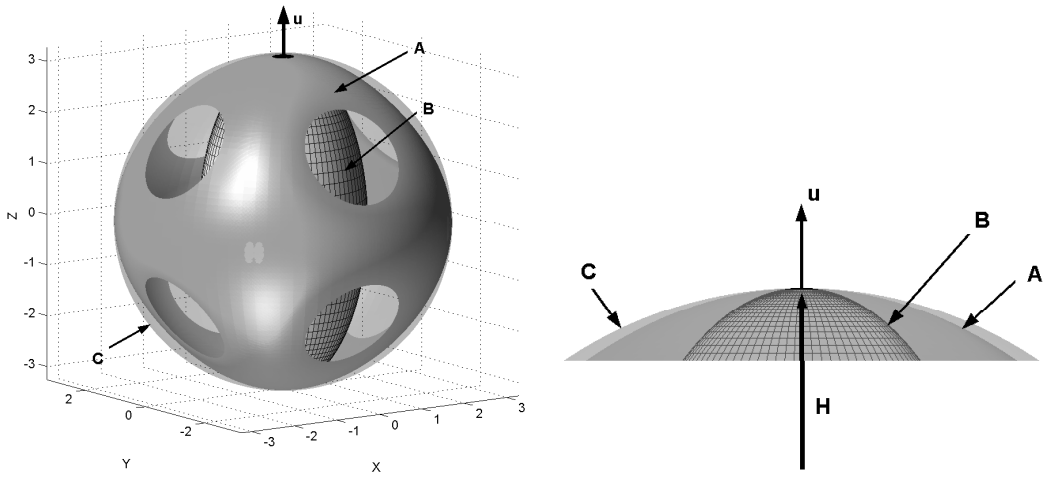

(a) (b)

Figure 20: Inescapable Singularity of VSCMGs

by wheel speed change are negative. Therefore, theses two $\Delta\mathbf{H} \cdot \hat{\mathbf{u}}$ cannot cancel to each other, and this means that gimbal angle changes and wheel speed changes with $\Delta\mathbf{H} = 0$ is impossible. Thus escaping from the singularity without violating either the momentum or the power constraints is impossible .

5.3.3 A Condition for Singularity Avoidance

If a VSCMGs cluster has a pyramid configuration with skew angle θ (see Fig. 7) and each wheel has the same moment of inertia $I_{\mathrm{w}} \triangleq I_{\mathrm{ws1}} = I_{\mathrm{ws2}} = I_{\mathrm{ws3}} = I_{\mathrm{ws4}}$, it can be shown that the momentum envelope with energy constraint E becomes an ellipsoid with the semi-axes of lengths $\sqrt{4EI_{\mathrm{w}}(1+\cos^2\theta)}$, $\sqrt{4EI_{\mathrm{w}}(1+\cos^2\theta)}$ and $\sqrt{8EI_{\mathrm{w}}}\sin\theta$ (see Appendix C for the proof of this fact). This provides a criterion for detecting whether the VSCMGs will encounter an inescapable singularity.

Theorem 1. *Consider a VSCMGs system used for attitude and power tracking. Assume that the VSCMG cluster has a pyramid configuration with angle θ and the wheels have the same moment of inertia I_{w}. Then, for a given energy command history $E(t)$ and angular momentum command history $\mathbf{H}(t)$ for $t_0 \leq t \leq t_f$, the VSCMGs encounters an inescapable*

singularity, if and only if there exist $\bar{t} \in [t_0, t_f]$ *such that*

$$\frac{H_x^2(\bar{t})}{4EI_{\rm w}(1+\cos^2\theta)} + \frac{H_y^2(\bar{t})}{4EI_{\rm w}(1+\cos^2\theta)} + \frac{H_z^2(\bar{t})}{8EI_{\rm w}\sin^2\theta} \geqslant 1 \tag{104}$$

where $H_x(\bar{t}), H_y(\bar{t}), H_z(\bar{t})$ *are the components of* $\mathbf{H}(\bar{t})$ *in the body frame.*

Specifically, when the skew angle is $\theta = 54.74^\circ$, then $\cos\theta = 1/\sqrt{3}$ and $\sin\theta = \sqrt{2/3}$ and the ellipsoid becomes a sphere with radius $\sqrt{\frac{16}{3}EI_{\rm w}}$. Therefore, the following is an immediate consequence of Theorem 1.

Corollary 1. *Consider a VSCMGs system used for attitude and power tracking. Assume that the VSCMG cluster has a regular pyramid configuration (skew angle* $\theta = 54.74^\circ$*) and the wheels have the same moment of inertia* $I_{\rm w}$*. Then, for a given energy command history* $E(t)$ *and angular momentum command history* $\mathbf{H}(t)$ *for* $t_0 \leq t \leq t_f$*, the VSCMGs encounters an inescapable singularity, if and only if there exist* $\bar{t} \in [t_0, t_f]$ *such that*

$$\|\mathbf{H}(\bar{t})\| \geqslant \sqrt{\frac{16}{3}E(\bar{t})I_{\rm w}}. \tag{105}$$

One method to solve the inescapable singularity problem for VSCMGs for an IPACS is to increase the workspace of the VSCMGs by increasing the inertia of the wheels. This means that the wheel size must be carefully determined depending on the spacecraft mission. Another possibility is to perform momentum dump/desaturation using external torque actuators such as magnetic torquers or gas thrusters. With this method, we can decrease $\|\mathbf{H}(t)\|$ thus keeping $\mathbf{H}(t)$ within the ellipsoid (or sphere) defined in Theorem 1 (or Corollary 1).

Once we know that the VSCMGs will never encounter inescapable singularities for a given attitude and power command from Theorem 1, we can apply the gradient method introduced in Eqs. (81) and (82), replacing Q with Q_p, i.e.,

$$\begin{bmatrix} \dot{\boldsymbol{\gamma}} \\ \dot{\boldsymbol{\Omega}} \end{bmatrix}_{\rm null} = k_n[\mathbf{I}_{2N} - Q_p^\dagger Q_p] \begin{bmatrix} \frac{\partial \kappa}{\partial \boldsymbol{\gamma}}^T \\ \frac{\partial \kappa}{\partial \boldsymbol{\Omega}}^T \end{bmatrix} \tag{106}$$

The control law (106) will escape all singularities of the VSCMG system while tracking the required attitude and power reference commands.

5.4 Numerical Examples

A numerical example is provided to test the proposed singularity avoidance method in Eq. (106). A spacecraft with four VSCMGs in a regular pyramid configuration is used for all numerical simulations. The simulation parameters of the spacecraft and VSCMGs system are identical with those used in the previous simulation in Section 3.6.

The exact equations of motion from Chapter 2 are used in all simulations in order to validate our approach. For all simulations the initial reference attitude is assumed to be aligned with the inertial frame and the angular velocity of the reference attitude is chosen as

$$\boldsymbol{\omega}_d(t) = \begin{bmatrix} 2 \times 10^{-3} \sin(2\pi t/9000) \\ -3 \times 10^{-3} \sin(2\pi t/12000) \\ 1 \times 10^{-3} \sin(2\pi t/10000) \end{bmatrix} \text{(rad/sec)}$$

The initial attitude of the spacecraft body frame is chosen as

$$\mathbf{q}_0 = [-1, 1, -1, 1]^T/\sqrt{4}$$

where $\mathbf{q}$ is the quaternion parameter vector with respect to the inertial frame. (This initial attitude is equivalent to 3-2-1 Euler angles, $\phi_0 = -90^\circ$, $\theta_0 = 0^\circ$, $\psi_0 = -90^\circ$). The initial angular velocity of the body frame is set to zero.

Two simulations are performed and the results are presented below. In the first case only the attitude and power tracking control of Section 3.6 is applied. In the second case the singularity avoidance control of Eq. (106) is used. The gain in the singularity avoidance control is chosen as $k = 0.005$. Figure 21 shows the reference and actual attitude histories. In these plots the subscript d means the desired quaternion history. The spacecraft attitude tracks the desired attitude exactly after a short period of time. The reference and the actual power profiles are shown in Fig. 22. The two profiles overlap each other perfectly and are shown as a single line. Figures 21 and 22 show that both attitude and power tracking are achieved successfully. However, Fig. 23 shows that the matrix C becomes close to being singular at approximately $t = 4000$ sec without the singularity avoiding algorithm. The control input $\dot{\boldsymbol{\Omega}}$ becomes very large during this period, since the weighting matrix W in

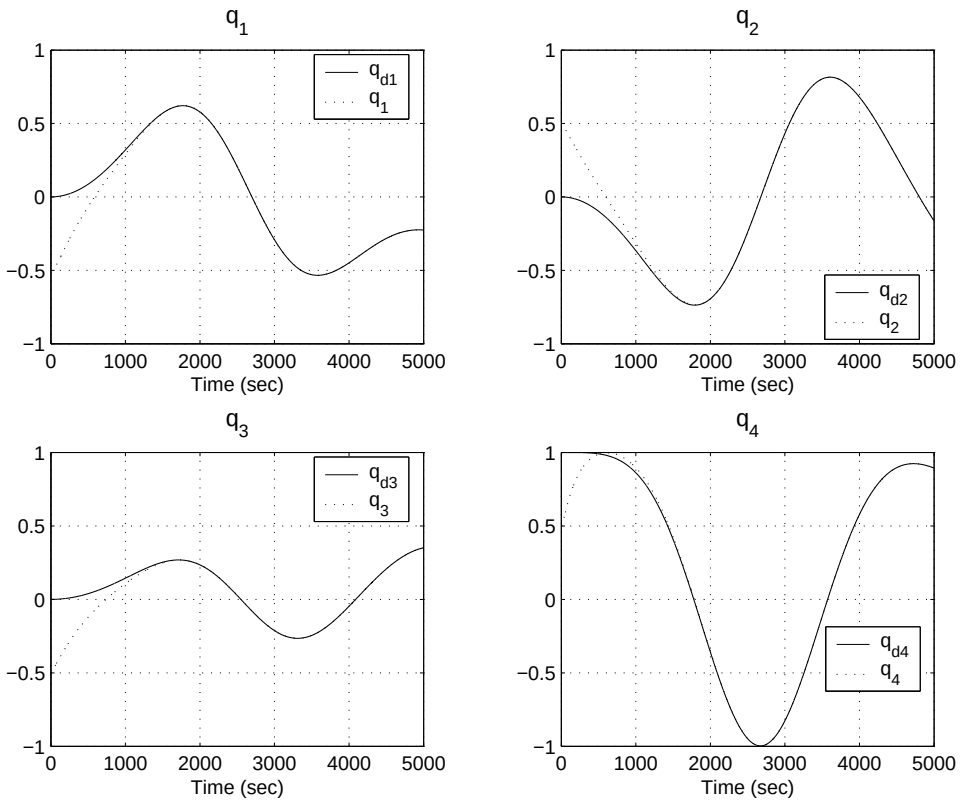

Figure 21: Reference and Actual Attitude Trajectory.

Eq. (86) makes the VSCMGs operate as reaction wheels, and so $\dot{\mathbf{\Omega}}$ has to generate the required output torque. Note that without the weighting matrix, the gimbal rate input $\dot{\boldsymbol{\gamma}}$ would become very large, instead of $\dot{\mathbf{\Omega}}$. Both cases are undesirable.

On the other hand, Fig. 24 shows that singularities are successfully avoided using the null motion algorithm of Eq. (106). Although slightly larger control inputs $\dot{\boldsymbol{\gamma}}$ are needed to reconfigure the gimbal angle configuration as the matrix C approach the singular states, the overall magnitudes of both $\dot{\boldsymbol{\gamma}}$ and $\dot{\mathbf{\Omega}}$ are kept within a reasonable range, contrary to the case without a singularity avoidance strategy. It should be pointed out that the attitude and the power time histories with null motion are identical to those without null motion, i.e., the null motion does not affect either the output torque or the delivered power to the spacecraft bus, as expected.

Figure 25 shows that the singularity cannot be avoided even using the null motion method, if the criterion in Theorem 1 is violated. In Fig. 25(a), $\|\mathbf{H}\|$ and the radius of the

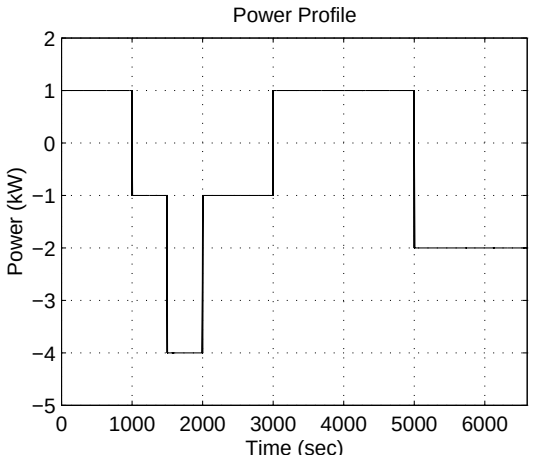

Figure 22: Desired and Actual Power Profile.

momentum envelope of the VSCMGs, which is equal to $\sqrt{\frac{16}{3}EI_{\rm w}}$, are plotted. During the period when $\|\mathbf{H}(t)\| < \sqrt{\frac{16}{3}E(t)I_{\rm w}}$, singularities are avoided using null motion, but when $\|\mathbf{H}(t)\| \approx \sqrt{\frac{16}{3}E(t)I_{\rm w}}$ (near $t = 6600\,\text{sec}$) the condition number $\kappa(\boldsymbol{\gamma}, \boldsymbol{\Omega})$ increases, as shown in Fig. 25(b). At this instant, the value of the matrix M defined in Eq. (92) is given by

$$M \approx \begin{bmatrix} 0.6844 & 0.6719 & 0.4073 & 0.4686 \\ \dfrac{0.6844}{0.0011} & \dfrac{0.6719}{0.0011} & \dfrac{0.4073}{0.0011} & \dfrac{0.4686}{0.0011} \end{bmatrix}.$$

It can be seen that at this instant the row vectors of the matrix M are parallel to each other, as expected by the analysis of Section 5.3.

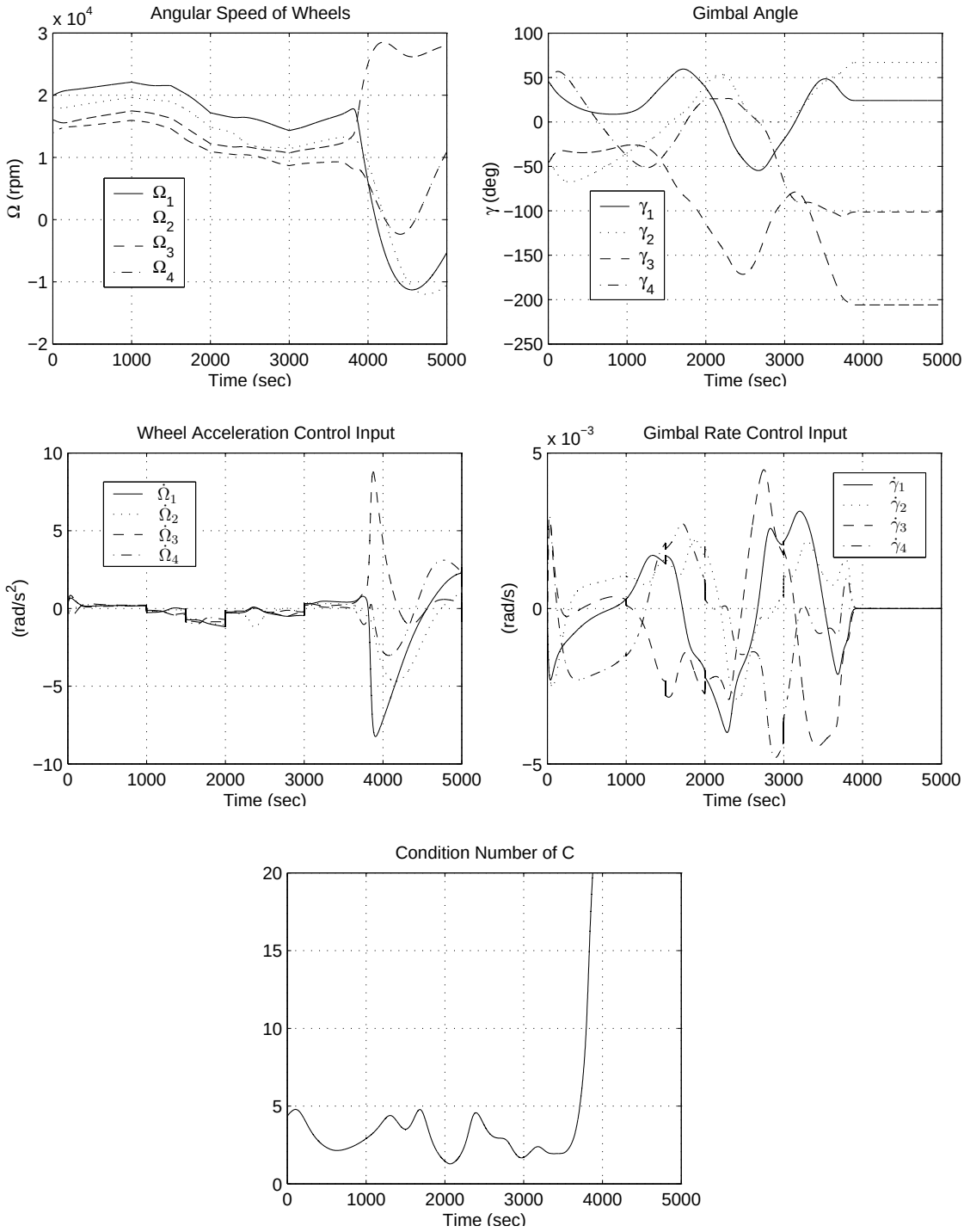

Figure 23: Simulation Without Singularity Avoidance.

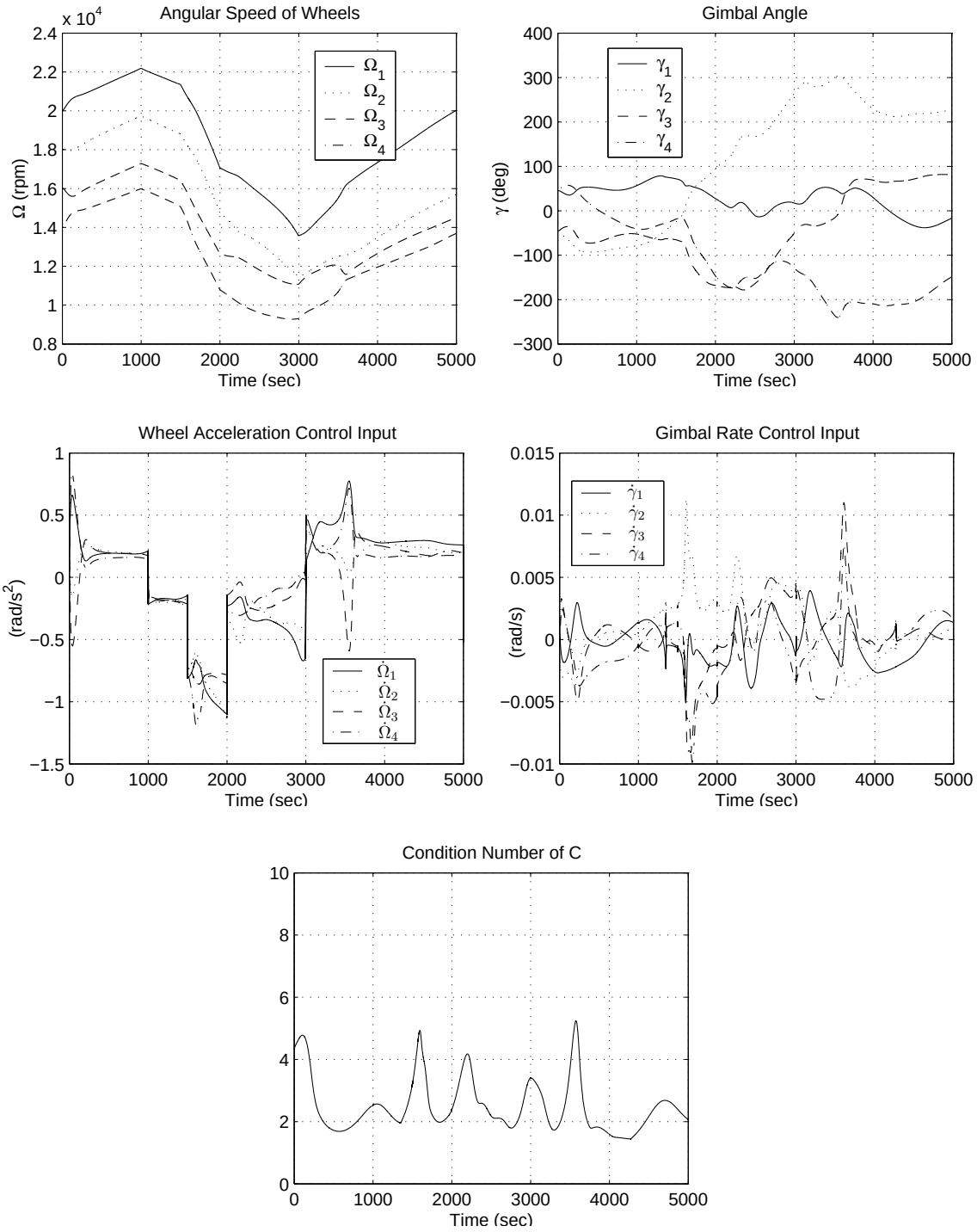

Figure 24: Simulation With Singularity Avoidance.

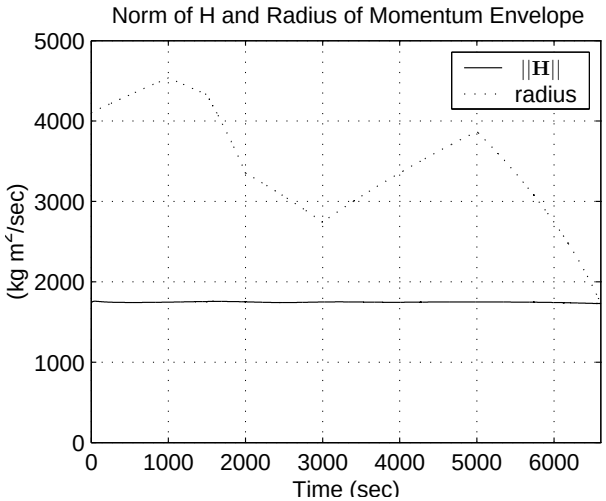

(a) Norm of $\mathbf{H}(t)$ and Radius of Momentum Envelope

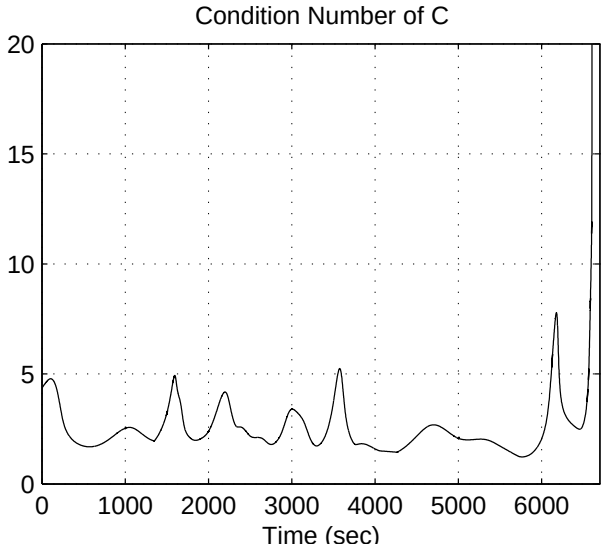

(b) Condition Number of C

Figure 25: Inescapable Singularity

CHAPTER VI

SPACECRAFT ANGULAR VELOCITY AND LINE-OF-SIGHT CONTROL USING A SINGLE-GIMBAL VARIABLE-SPEED CONTROL MOMENT GYRO

6.1 Equations of Motion

The dynamic equations of motion of a spacecraft with a cluster of VSCMGs have been fully derived in chapter 2. Figure 6 shows a schematic of a spacecraft with a single VSCMG. The body-frame $\mathcal{B}$ is represented by the orthonormal set of unit vectors $\hat{\mathbf{b}}_1$, $\hat{\mathbf{b}}_2$ and $\hat{\mathbf{b}}_3$, and its origin is located at the center of mass of the entire spacecraft. The gimbal frame $\mathcal{G}$ is represented by the orthonormal set of unit vectors $\hat{\mathbf{s}}$, $\hat{\mathbf{t}}$ and $\hat{\mathbf{g}}$, and it is located on the gimbal as shown in Fig. 6.

Specializing the dynamical equations of motion (8) of Chapter 2 to the single VSCMG case, one obtains,

$$J\dot{\boldsymbol{\omega}} + \dot{J}\boldsymbol{\omega} + I_{\mathrm{cg}}\ddot{\gamma}\hat{\mathbf{g}} + I_{\mathrm{ws}}\Omega\dot{\gamma}\hat{\mathbf{t}} + I_{\mathrm{ws}}\dot{\Omega}\hat{\mathbf{s}} + \boldsymbol{\omega}^{\times}\mathbf{h} = 0, \tag{107}$$

where the total angular momentum vector $\mathbf{h}$ of the spacecraft is expressed in the $\mathcal{B}$-frame as

$$\mathbf{h} \triangleq J\boldsymbol{\omega} + I_{\mathrm{cg}}\dot{\gamma}\hat{\mathbf{g}} + I_{\mathrm{ws}}\Omega\hat{\mathbf{s}}. \tag{108}$$

The total moment of inertia of the spacecraft will change, in general, as the VSCMG rotates about its gimbal axis, so the matrix $J = J(\gamma)$ is a function of a gimbal angle γ; see Eq. (7). However, the dependence of J on γ is weak, especially when the size of spacecraft main body is large. It will be therefore assumed that J is constant ($\dot{J} = 0$) during controller design. In addition, to simplify the analysis, it is assumed that the gimbal acceleration term $I_{\mathrm{cg}}\ddot{\gamma}\hat{\mathbf{g}}$ is ignored. This assumption is standard in the literature [28, 73, 65], and it amounts to gimbal angle rate servo control. Under these assumptions, the dynamic equation (107)

can be simplified as

$$\begin{aligned} J\dot{\boldsymbol{\omega}} &= -\boldsymbol{\omega}^{\times}\mathbf{h} - I_{\mathrm{ws}}\Omega\dot{\gamma}\hat{\mathbf{t}} - I_{\mathrm{ws}}\dot{\Omega}\hat{\mathbf{s}} \\ &= -\boldsymbol{\omega}^{\times}(J\boldsymbol{\omega} + I_{\mathrm{cg}}\dot{\gamma}\hat{\mathbf{g}} + I_{\mathrm{ws}}\Omega\hat{\mathbf{s}}) - I_{\mathrm{ws}}\Omega\dot{\gamma}\hat{\mathbf{t}} - I_{\mathrm{ws}}\dot{\Omega}\hat{\mathbf{s}} \\ &= -\boldsymbol{\omega}^{\times}(J\boldsymbol{\omega} + I_{\mathrm{cg}}\dot{\gamma}\hat{\mathbf{g}} + I_{\mathrm{ws}}\Omega\hat{\mathbf{s}}) - I_{\mathrm{ws}}\Omega\hat{\mathbf{t}}u_1 - I_{\mathrm{ws}}\hat{\mathbf{s}}u_2, \end{aligned} \tag{109}$$

where the control input is

$$\boldsymbol{u} \triangleq \begin{bmatrix} u_1 \\ u_2 \end{bmatrix} = \begin{bmatrix} \dot{\gamma} \\ \dot{\Omega} \end{bmatrix}. \tag{110}$$

6.2 Parametrization of the Spacecraft Orientations at Rest

Because the VSCMG is an internal momentum exchange actuator, the total angular momentum of the spacecraft is conserved (in both magnitude and direction) during a maneuver, assuming no external control/disturbance torques are applied to the spacecraft. Therefore, for a given initial total angular momentum vector $\mathbf{H}_0$ of the spacecraft including the platform and the VSCMG actuator, the final rest state of the spacecraft and the VSCMG is such that, the direction of the spin axis of the VSCMG is aligned with $\mathbf{H}_0$, and the magnitude of the angular momentum of the wheel is equal to the initial magnitude of the angular momentum vector $H_0 \triangleq \|\mathbf{H}_0\|$. That is,

$$\mathbf{H}_0 = I_{\mathrm{ws}}\Omega_{\mathrm{f}}\hat{\mathbf{s}}_{\mathrm{f}} = H_0 \cdot \mathrm{sgn}(\Omega_{\mathrm{f}})\hat{\mathbf{s}}_{\mathrm{f}} \tag{111}$$

where the subscript 'f' denotes the desired final state, when the spacecraft is at rest. Since the final spin axis of the VSCMG is determined by the initial angular momentum $\mathbf{H}_0$, the spacecraft attitude at rest can be determined via only two rotations: one is a rotation of the spacecraft about the gimbal axis, and the other is a rotation of the spacecraft about the final spin axis. Since at least three parameters are needed to express the complete orientation of a spacecraft, one expects that complete attitude control of the spacecraft is not possible using one VSCMG; see Ref. [93] for a formal proof of this claim. As a result, the set of all feasible final spacecraft orientations at rest for a given initial angular momentum $\mathbf{H}_0$ can be parameterized by a pair of two angles.

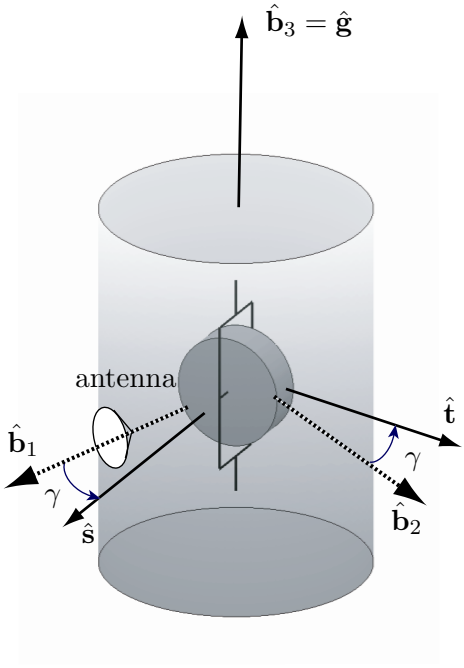

Figure 26: Axes Definition of a Spacecraft with a VSCMG and an Antenna.

Note that the geometric constraint that the wheel spin axis is aligned with $\mathbf{H}_0$ implies that the gimbal axis must be perpendicular to $\mathbf{H}_0$, whenever the spacecraft is at rest. Therefore, if we install a camera or an antenna on the spacecraft so that its line-of-sight is fixed in the plane normal to the gimbal axis, we can aim the line-of-sight at any given inertial direction $\hat{\mathbf{n}}$. Before providing a formal proof of the last statement, all possible final orientations of the spacecraft when it comes to rest are invetigated.

To this end, and without loss of generality, let us assume that the gimbal axis is fixed along the $\hat{\mathbf{b}}_3$-body axis, and the camera/antenna is fixed along the $\hat{\mathbf{b}}_1$-body axis, as shown in Fig. 26. The gimbal angle γ is defined as the angle from $\hat{\mathbf{b}}_1$ to $\hat{\mathbf{s}}$ about the $\hat{\mathbf{g}} = \hat{\mathbf{b}}_3$ axis. The spin axis of the VSCMG can then be written as

$$\hat{\mathbf{s}} = \cos\gamma\, \hat{\mathbf{b}}_1 + \sin\gamma\, \hat{\mathbf{b}}_2. \tag{112}$$

The author introduces the following parametrization of the spacecraft orientation. First, an inertial frame $\mathcal{H}$ with basis vectors $\hat{\mathbf{a}}_1, \hat{\mathbf{a}}_2, \hat{\mathbf{a}}_3$ is defined, so that the total angular momentum $\mathbf{H}_0$ is aligned along $\hat{\mathbf{a}}_3$, that is,

$$\hat{\mathbf{a}}_3 \triangleq \frac{\mathbf{H}_0}{H_0}. \tag{113}$$

Any spacecraft orientation can be described by a "3-1-3" body-axis angel sequence from frame $\mathcal{H}$ to frame $\mathcal{B}$ via the direction cosine matrix $R_{\mathcal{H}}^{\mathcal{B}}$ from $\mathcal{H}$ to $\mathcal{B}$, defined as $R_{\mathcal{H}}^{\mathcal{B}} = R_3(\psi)R_1(\theta)R_3(\phi)$, where R_i, for $i = 1, 2, 3$ is the rotational matrix about the ith body-axis. Componentwise, we can write

$$R_{\mathcal{H}}^{\mathcal{B}} = \begin{bmatrix} \mathrm{c}\phi\,\mathrm{c}\psi - \mathrm{s}\phi\,\mathrm{c}\theta\,\mathrm{s}\psi & \mathrm{s}\phi\,\mathrm{c}\psi + \mathrm{c}\phi\,\mathrm{c}\theta\,\mathrm{s}\psi & \mathrm{s}\theta\,\mathrm{s}\psi \\ -\mathrm{c}\phi\,\mathrm{s}\psi - \mathrm{s}\phi\,\mathrm{c}\theta\,\mathrm{c}\psi & -\mathrm{s}\phi\,\mathrm{s}\psi + \mathrm{c}\phi\,\mathrm{c}\theta\,\mathrm{c}\psi & \mathrm{s}\theta\,\mathrm{c}\psi \\ \mathrm{s}\phi\,\mathrm{s}\theta & -\mathrm{c}\phi\,\mathrm{s}\theta & \mathrm{c}\theta \end{bmatrix}, \tag{114}$$

where $\theta \in [0, \pi]$, and $\phi, \psi \in (-\pi, \pi]$, and $\mathrm{c}\phi \triangleq \cos\phi$, $\mathrm{s}\phi \triangleq \sin\phi$, etc. From (111) and (113), one now has

$$\mathrm{sgn}(\Omega_\mathrm{f}) \begin{bmatrix} \cos\gamma_\mathrm{f} \\ \sin\gamma_\mathrm{f} \\ 0 \end{bmatrix} = R_{\mathcal{H}}^{\mathcal{B}}\,\hat{\mathbf{a}}_3 = \begin{bmatrix} \sin\theta_\mathrm{f}\ \sin\psi_\mathrm{f} \\ \sin\theta_\mathrm{f}\ \cos\psi_\mathrm{f} \\ \cos\theta_\mathrm{f} \end{bmatrix} \tag{115}$$

for the case when the spacecraft and the VSCMG gimbal are both at rest. Comparing the third element of (115) yields $\cos\theta_\mathrm{f} = 0$, i.e., $\theta_\mathrm{f} = \pi/2$. Physically, this implies that the only orientations which are accessible at rest are those for which the total angular momentum is perpendicular to the $\hat{\mathbf{b}}_3$-axis (the gimbal axis). Therefore, all feasible spacecraft orientations at rest can be parameterized by the pair of the two Euler angles ϕ_f and ψ_f. Since $\theta_\mathrm{f} = \pi/2$ it follows that $\sin\theta_\mathrm{f} = 1$. Hence $\cos\gamma_\mathrm{f} = \mathrm{sgn}(\Omega_\mathrm{f})\sin\psi_\mathrm{f}$, and $\sin\gamma_\mathrm{f} = \mathrm{sgn}(\Omega_\mathrm{f})\cos\psi_\mathrm{f}$. This yields a relation between the final gimbal angle γ_f and the final Euler angle ψ_f as follows

$$\gamma_\mathrm{f} = \mathrm{sgn}(\Omega_\mathrm{f})\frac{\pi}{2} - \psi_\mathrm{f}. \tag{116}$$

This means that the final Euler angle ψ_f is determined by the final gimbal angle γ_f when $\boldsymbol{\omega} = 0$. Therefore, we can use the gimbal angle γ_f as one of the parameters to describe the spacecraft orientation at rest, in lieu of ψ_f. In the sequel, the author denotes $\gamma_\mathrm{f}^+ = \pi/2 - \psi_\mathrm{f}$ and $\gamma_\mathrm{f}^- = -\pi/2 - \psi_\mathrm{f} = \gamma_\mathrm{f}^+ - \pi$.

Next, an algorithm to find the values of the angles ϕ_f and ψ_f (or γ_f) is provided in order to make the line-of-sight (herein, the $\hat{\mathbf{b}}_1$-axis) aim at an arbitrarily given direction $\hat{\mathbf{n}}$. To this end, suppose that $\hat{\mathbf{n}}$ can be written in the inertial frame $\mathcal{H}$ as $\hat{\mathbf{n}} = n_1\,\hat{\mathbf{a}}_1 + n_2\,\hat{\mathbf{a}}_2 + n_3\,\hat{\mathbf{a}}_3$.

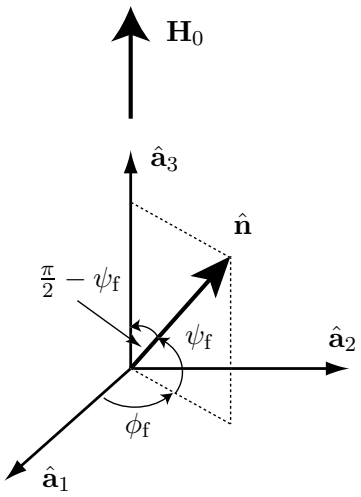

Figure 27: A Desired Inertial Direction $\hat{\mathbf{n}}$ in the Inertial Frame $\mathcal{H}$.

Then in order to make the body axis $\hat{\mathbf{b}}_1$ point at the inertial vector $\hat{\mathbf{n}}$, we require that

$$\begin{bmatrix} n_1 \\ n_2 \\ n_3 \end{bmatrix} = R_{\mathcal{B}}^{\mathcal{H}} \hat{\mathbf{b}}_1 = \begin{bmatrix} \cos\phi_\mathrm{f} \ \cos\psi_\mathrm{f} \\ \sin\phi_\mathrm{f} \ \cos\psi_\mathrm{f} \\ \sin\psi_\mathrm{f} \end{bmatrix}, \tag{117}$$

since $\cos\theta_\mathrm{f} = 0$ and $\sin\theta_\mathrm{f} = 1$. In fact, (117) is the expression of the vector $\hat{\mathbf{n}}$ in the spherical coordinate system, shown in Fig. 27. One can therefore specify the desired final value of the parameters ϕ_f and ψ_f for any given inertial vector $\hat{\mathbf{n}}$. Moreover, if one defines the inertial frame $\mathcal{H}$ so that

$$\hat{\mathbf{a}}_2 = \frac{\hat{\mathbf{a}}_3 \times \hat{\mathbf{n}}}{\|\hat{\mathbf{a}}_3 \times \hat{\mathbf{n}}\|}, \qquad \hat{\mathbf{a}}_1 = \hat{\mathbf{a}}_2 \times \hat{\mathbf{a}}_3, \tag{118}$$

along with Eq. (113), then the final required values of the Euler angles are

$$\phi_\mathrm{f} = 0, \quad \psi_\mathrm{f} = \arcsin n_3 = \arcsin(\hat{\mathbf{n}} \cdot \hat{\mathbf{a}}_3). \tag{119}$$

Next, it is shown that a camera/anntena must be installed so that its line-of-sight axis is normal to the gimbal axis in order to aim at an arbitrary inertial direction when $\boldsymbol{\omega} = 0$. To this end, let us define a body-fixed unit vector $\hat{\mathbf{b}} = b_1\hat{\mathbf{b}}_1 + b_2\hat{\mathbf{b}}_2 + b_3\hat{\mathbf{b}}_3$. When the spacecraft is at rest, and thus $\theta_\mathrm{f} = \pi/2$, the vector $\hat{\mathbf{b}}$ can be written in the $\mathcal{H}$-frame as

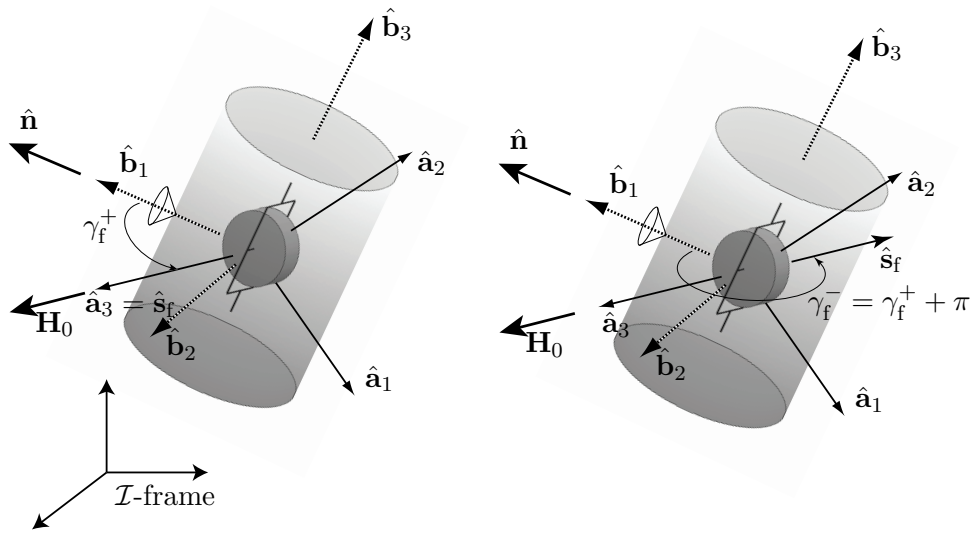

(a) $\Omega_{\mathrm{f}} = \Omega_{\mathrm{f}}^{+} > 0$. (b) $\Omega_{\mathrm{f}} = \Omega_{\mathrm{f}}^{-} < 0$.

Figure 28: Desired Attitudes with $\boldsymbol{\omega} = 0$ for Given $\mathbf{H}_0$ and $\hat{\mathbf{n}}$.

$\hat{\mathbf{b}} = a_1\hat{\mathbf{a}}_1 + a_2\hat{\mathbf{a}}_2 + a_3\hat{\mathbf{a}}_3$, where

$$\begin{bmatrix} a_1 \\ a_2 \\ a_3 \end{bmatrix} = R_{\mathcal{B}}^{\mathcal{H}}\hat{\mathbf{b}} = \begin{bmatrix} \mathrm{c}\phi_{\mathrm{f}}\,\mathrm{c}\psi_{\mathrm{f}} & -\mathrm{c}\phi_{\mathrm{f}}\,\mathrm{s}\psi_{\mathrm{f}} & \mathrm{s}\phi_{\mathrm{f}} \\ \mathrm{s}\phi_{\mathrm{f}}\,\mathrm{c}\psi_{\mathrm{f}} & -\mathrm{s}\phi_{\mathrm{f}}\,\mathrm{s}\psi_{\mathrm{f}} & -\mathrm{c}\phi_{\mathrm{f}} \\ \mathrm{s}\psi_{\mathrm{f}} & \mathrm{c}\psi_{\mathrm{f}} & 0 \end{bmatrix} \begin{bmatrix} b_1 \\ b_2 \\ b_3 \end{bmatrix}. \tag{120}$$

In order to make $\hat{\mathbf{b}}$ point at any inertial direction $\hat{\mathbf{n}}$, the final Euler angles ϕ_{f} and ψ_{f} must be such that $\hat{\mathbf{b}} \cdot \hat{\mathbf{n}} = a_1\, n_1 + a_2\, n_2 + a_3\, n_3 = 1$. In particular, let us consider the case when the line-of-sight axis (the $\hat{\mathbf{b}}$-axis) is commanded so that it aims at the direction of the total angular momentum, that is $\hat{\mathbf{n}} = \hat{\mathbf{a}}_3 = \mathbf{H}_0/H_0$. Then, $\hat{\mathbf{b}} \cdot \hat{\mathbf{n}} = \hat{\mathbf{b}} \cdot \hat{\mathbf{a}}_3 = a_3 = b_1\mathrm{s}\psi_{\mathrm{f}} + b_2\mathrm{c}\psi_{\mathrm{f}} = \sqrt{b_1^2 + b_2^2}\sin(\psi_{\mathrm{f}} + \alpha)$, where $\cos\alpha = b_1/\sqrt{b_1^2 + b_2^2}$, $\sin\alpha = b_2/\sqrt{b_1^2 + b_2^2}$. Since $\hat{\mathbf{b}} \cdot \hat{\mathbf{n}} = 1$ it follows that $b_1^2 + b_2^2 = 1$, and thus $b_3 = 0$, which implies that the body fixed vector $\hat{\mathbf{b}}$ must be perpendicular to the gimbal axis $\hat{\mathbf{b}}_3 = \hat{\mathbf{g}}$, thus completing the proof.

Figure 28 shows two final rest configurations for which $\hat{\mathbf{b}}_1$ points at the given inertial direction $\hat{\mathbf{n}}$. There are two possible cases, as expected from Eq. (116). One is with a positive final wheel speed, that is, $\Omega_{\mathrm{f}} = \Omega_{\mathrm{f}}^{+} \triangleq H_0/I_{\mathrm{ws}} > 0$. In this case, the final gimbal axis $\hat{\mathbf{s}}_{\mathrm{f}}$ is aligned along $\mathbf{H}_0$ in the same direction, as shown in Fig. 28(a). The other case is with a negative final wheel speed, that is, $\Omega_{\mathrm{f}} = \Omega_{\mathrm{f}}^{-} \triangleq -H_0/I_{\mathrm{ws}} < 0$. The final gimbal axis $\hat{\mathbf{s}}_{\mathrm{f}}$ is

aligned along $\mathbf{H}_0$ in the opposite direction, as shown in Fig. 28(b).

In both cases, the final $\hat{\mathbf{b}}_1$-axis points at the direction of $\hat{\mathbf{n}}$, as desired. Notice that the gimbal axis $\hat{\mathbf{g}} = \hat{\mathbf{b}}_3$ is perpendicular to the total angular momentum vector $\mathbf{H}_0 = H_0\hat{\mathbf{a}}_3$ because $\theta_\mathrm{f} = \pi/2$. Also notice that the final gimbal angle γ_f is the angle between the line-of-sight vector $\hat{\mathbf{n}}$ and the wheel spin axis $\hat{\mathbf{s}}_\mathrm{f}$. In fact, γ_f can be computed by Eqs. (116) and (119) as

$$\gamma_\mathrm{f}^+ = \arccos\left(\frac{\mathbf{H}_0 \cdot \hat{\mathbf{n}}}{H_0}\right), \qquad (\Omega_\mathrm{f} > 0), \tag{121a}$$

$$\gamma_\mathrm{f}^- = \gamma_\mathrm{f}^+ - \pi, \qquad (\Omega_\mathrm{f} < 0). \tag{121b}$$

If the sign of the final wheel speed is known, then the pair $(\phi_\mathrm{f}, \gamma_\mathrm{f})$ determines the final spacecraft orientation at rest. Furthermore, if we design a controller that achieves

$$\boldsymbol{\omega} \to 0, \tag{122a}$$

$$\gamma_e \triangleq \gamma - \gamma_\mathrm{f} \to 0, \tag{122b}$$

$$\phi_e \triangleq \phi - \phi_\mathrm{f} \to 0, \tag{122c}$$

then the spacecraft will be brought to rest and the $\hat{\mathbf{b}}_1$-axis will point at the desired inertial direction $\hat{\mathbf{n}}$.

6.3 Linearized System Analysis and Controller Design

The kinematic differential equation for the "3-1-3" rotational sequence is given by

$$\begin{bmatrix} \dot{\phi} \\ \dot{\theta} \\ \dot{\psi} \end{bmatrix} = \frac{1}{\sin\theta} \begin{bmatrix} \mathrm{s}\psi & \mathrm{c}\psi & 0 \\ \mathrm{c}\psi\ \mathrm{s}\theta & -\mathrm{s}\psi\ \mathrm{s}\theta & 0 \\ -\mathrm{s}\psi\ \mathrm{c}\theta & -\mathrm{c}\psi\ \mathrm{c}\theta & \mathrm{s}\theta \end{bmatrix} \begin{bmatrix} \omega_1 \\ \omega_2 \\ \omega_3 \end{bmatrix}, \tag{123}$$

and the differential equation of γ_e is

$$\dot{\gamma}_e = \dot{\gamma} = u_1. \tag{124}$$

In this section, the nonlinear equations of motion, given by (109), (123) and (124) are linearized. Then these equations is used to investigate the controllability properties of the system $(\boldsymbol{\omega}, \gamma_e, \phi_e)$. An LQR control law is also presented that satisfies the control objectives

(122) and thus stabilizes the angular velocity of spacecraft with a body-fixed axis aiming at a given inertial direction.

6.3.1 Controllability Analysis

The desired equilibrium points of Eqs. (109),(123) and (124) are given by $\boldsymbol{\omega} = 0$, $\gamma_e = 0$, $\phi_e = 0^*$, $\Omega = \Omega_\mathrm{f}$ and $\boldsymbol{u} = [u_1,\ u_2]^T = 0$. Moreover, we know that $\sin\theta \approx 1$, $\sin\psi \approx \mathrm{sgn}(\Omega_\mathrm{f})\cos\gamma$ and $\cos\psi \approx \mathrm{sgn}(\Omega_\mathrm{f})\sin\gamma$ near the equilibrium. Thus one can linearize the differential equation of ϕ_e as follows.

$$\dot{\phi}_e = \dot{\phi} \approx (\omega_1 \cos\gamma_\mathrm{f} \ + \omega_2 \sin\gamma_\mathrm{f}\ ) \cdot \mathrm{sgn}(\Omega_\mathrm{f}) = \boldsymbol{\omega} \cdot \hat{\mathbf{s}}_\mathrm{f}\ \ \mathrm{sgn}(\Omega_\mathrm{f}). \tag{125}$$

Therefore, we have two linearized systems depending on the sign of Ω_f, and the equations of motion are given by [93]

$$\begin{bmatrix} \dot{\boldsymbol{\omega}} \\ \dot{\gamma_e} \\ \dot{\phi_e} \end{bmatrix} = \begin{bmatrix} A_1 & 0 & 0 \\ 0 & 0 & 0 \\ A_2 & 0 & 0 \end{bmatrix} \begin{bmatrix} \Delta\boldsymbol{\omega} \\ \gamma_e \\ \phi_e \end{bmatrix} + \begin{bmatrix} B_1 & B_2 \\ 1 & 0 \\ 0 & 0 \end{bmatrix} \begin{bmatrix} u_1 \\ u_2^n \end{bmatrix} \tag{126}$$

where,

$$A_1 \triangleq J^{-1} I_\mathrm{ws} \Omega_\mathrm{f} \hat{\mathbf{s}}_\mathrm{f}^\times \tag{127a}$$

$$A_2 \triangleq \hat{\mathbf{s}}_\mathrm{f}^T\ \mathrm{sgn}(\Omega_\mathrm{f}) \tag{127b}$$

$$B_1 \triangleq -J^{-1} I_\mathrm{ws} \Omega_\mathrm{f} \hat{\mathbf{t}}_\mathrm{f} \tag{127c}$$

$$B_2 \triangleq -J^{-1} I_\mathrm{ws} \hat{\mathbf{s}}_\mathrm{f} \tag{127d}$$

$$u_2^n = \mathrm{sgn}(\Omega_\mathrm{f}) u_2, \tag{127e}$$

where all vectors are expressed in the $\mathcal{B}$-frame.

Proposition 1. *The linearized system described by Eqs. (126) and (127) is controllable for any* $\gamma_\mathrm{f} \in [0, 2\pi)$ *and* $\Omega_\mathrm{f} \in \mathbb{R}\backslash\{0\}$.

*In fact, the Euler angle ϕ does not appear in the right-hand-sides of the nonlinear equations (109), (123) and (124). That means ϕ is ignorable, i.e., the linearization is independent of ϕ_e. Therefore, the linearization does not need a condition that ϕ_e is small, and the linearized equation (126) is valid regardless of the magnitude of ϕ_e. This argument is used later in Sec. 6.4.5.

Proof. The controllability of Eqs. (126) and (127) can be shown using the Popov-Belevitch-Hautus (PBH) test [39]. A necessary and sufficient condition for the controllability of (126) and (127) is that the matrix $\mathcal{C}(\lambda)$ defined as

$$\mathcal{C}(\lambda) \triangleq \begin{bmatrix} A_1 - \lambda I & 0 & 0 & B_1 & B_2 \\ 0 & -\lambda & 0 & 1 & 0 \\ A_2 & 0 & -\lambda & 0 & 0 \end{bmatrix} \tag{128}$$

has rank 5 for all $\lambda \in \mathbb{C}$. It has already been proved in Ref. [93] that the linearized subsystem $(\boldsymbol{\omega}, \gamma_e)$ is controllable, that is, the pair of matrices $(\bar{A}, \bar{B})$, where

$$\bar{A} \triangleq \begin{bmatrix} A_1 & 0 \\ 0 & 0 \end{bmatrix}, \quad \bar{B} \triangleq \begin{bmatrix} B_1 & B_2 \\ 1 & 0 \end{bmatrix}, \tag{129}$$

is controllable. Therefore, it follows easily that rank $\mathcal{C}(\lambda) = 5$ for all $\lambda \neq 0$. We only need to check the rank of the matrix

$$\mathcal{C}'(0) \triangleq \begin{bmatrix} A_1 & B_1 & B_2 \\ 0 & 1 & 0 \\ \hat{\mathbf{s}}_{\mathrm{f}}^T \mathrm{sgn}(\Omega_{\mathrm{f}}) & 0 & 0 \end{bmatrix}. \tag{130}$$

Notice that

$$\operatorname{rank} \mathcal{C}'(0) = \operatorname{rank} \begin{bmatrix} \hat{\mathbf{s}}_{\mathrm{f}}^{\times} & \hat{\mathbf{t}}_{\mathrm{f}} & \hat{\mathbf{s}}_{\mathrm{f}} \\ 0 & 1 & 0 \\ \hat{\mathbf{s}}_{\mathrm{f}}^T & 0 & 0 \end{bmatrix}. \tag{131}$$

To this end, assume that there exist a vector $\boldsymbol{v}_1 \in \mathbb{R}^3$, and scalars $v_2, v_3 \in \mathbb{R}$ such that

$$\begin{bmatrix} \boldsymbol{v}_1^T & v_2 & v_3 \end{bmatrix} \begin{bmatrix} \hat{\mathbf{s}}_{\mathrm{f}}^{\times} & \hat{\mathbf{t}}_{\mathrm{f}} & \hat{\mathbf{s}}_{\mathrm{f}} \\ 0 & 1 & 0 \\ \hat{\mathbf{s}}_{\mathrm{f}}^T & 0 & 0 \end{bmatrix} = 0. \tag{132}$$

Equivalently,

$$\boldsymbol{v}_1^T \hat{\mathbf{s}}_{\mathrm{f}}^{\times} + v_3 \hat{\mathbf{s}}_{\mathrm{f}}^T = 0, \tag{133}$$

$$\boldsymbol{v}_1^T \hat{\mathbf{t}}_{\mathrm{f}} + v_2 = 0, \tag{134}$$

$$\boldsymbol{v}_1^T \hat{\mathbf{s}}_{\mathrm{f}} = 0. \tag{135}$$

Equation (133) holds if and only if $\boldsymbol{v}_1 = 0$ and $v_3 = 0$. From (134) it follows that $v_2 = 0$. This implies that the left null space of the matrix in Eq. (132) contains only the zero vector and thus rank $\mathcal{C}'(0) = 5$ and the proof is completed. □

Notice that Proposition 1 does not ensure the controllability of the linearized system if $\Omega_{\mathrm{f}} = 0$. However, if the initial angular momentum $\mathbf{H}_0$ is not zero, then $\Omega_{\mathrm{f}} \neq 0$ by the momentum conservation law.

6.3.2 Linear Control Design

Next, a linear control law is designed via LQR theory for the linearized system (126). Let the matrices A and B denote the system matrices in Eq. (126). Then we can determine a control gain matrix $K \in \mathbb{R}^{2\times 5}$ such that the static full-state feedback law

$$\boldsymbol{u} = -K[\boldsymbol{\omega}^T, \gamma_e, \phi_e]^T \tag{136}$$

minimizes the performance index

$$\mathcal{J} \triangleq \int_0^\infty \left(\boldsymbol{x}^T Q\, \boldsymbol{x} + \boldsymbol{u}^T R\, \boldsymbol{u}\right) \mathrm{d}t \tag{137}$$

where $\boldsymbol{x} = [\boldsymbol{\omega}^T, \gamma_e, \phi_e]^T$, $Q \in \mathbb{R}^{5\times 5}$ is positive semi-definite, and $R \in \mathbb{R}^{2\times 2}$ is positive definite. The gain matrix K is computed by $K = R^{-1}B^T P$, where P is the solution of the Algebraic Riccati Equation (ARE)

$$A^T P + PA - PBR^{-1}B^T P + Q = 0. \tag{138}$$

No further details are provided since LQR theory is well known in the literature [16].

6.4 Nonlinear System Analysis and Controller Design

The LQR controller of the previous section ensures asymptotic stability only locally about the equilibrium $\boldsymbol{\omega} = 0$ (and thus also $\Omega = \Omega_{\mathrm{f}}$) and $\gamma_e = 0$ and $\phi_e = 0$. In realistic cases, however, one cannot expect that the initial states will be near the equilibrium point. In order to globally achieve the desired stabilization objective, it is therefore necessary to design a controller based on the complete nonlinear equations of motion.

In the sequel a control method which is comprised of a sequence of three stages is suggested. At the first stage, only the angular velocity $\boldsymbol{\omega}$ is controlled to decrease toward zero. When a certain condition is met, the controller switches to the second stage in which both $\boldsymbol{\omega}$ and the gimbal angle γ are controlled to the desired values, according to the sign of the wheel speed. Once $\boldsymbol{\omega}$ and γ are sufficiently close to the values at the desired equilibrium, then the controller switches to the third stage where the LQR controller designed in Section 6.3 regulates the Euler angle ϕ to ϕ_{f}, along with $\boldsymbol{\omega}$ and γ.

Several assumptions are made in order to simplify the analysis.

- **Assumption 1.** The spacecraft is inertially axisymmetric about the gimbal axis $\hat{\mathbf{g}} = \hat{\mathbf{b}}_3$.
- **Assumption 2.** The spacecraft is not inertially symmetric.

Under Assumption 1, the inertia matrix written in the gimbal frame $\mathcal{G}$ takes the form

$$\bar{J} \triangleq \begin{bmatrix} J_{\mathrm{t}} & 0 & 0 \\ 0 & J_{\mathrm{t}} & 0 \\ 0 & 0 & J_{\mathrm{a}} \end{bmatrix} = J, \tag{139}$$

for any gimbal angle γ, where J is the inertia matrix written in the body frame $\mathcal{B}$. Assumption 2 implies that $J_{\mathrm{t}} \neq J_{\mathrm{a}}$.

6.4.1 Angular Velocity Stabilization

Consider the positive definite, continuously differentiable Lyapunov function candidate

$$V_1(\boldsymbol{\omega}) = \tfrac{1}{2}\boldsymbol{\omega}^T J \boldsymbol{\omega}. \tag{140}$$

Its time derivative along the trajectories of the system (109) yields

$$\begin{aligned} \dot{V}_1 &= \boldsymbol{\omega}^T J \dot{\boldsymbol{\omega}} \\ &= \boldsymbol{\omega}^T \left(-\boldsymbol{\omega}^{\times} (J\boldsymbol{\omega} + I_{\mathrm{cg}} \dot{\gamma} \hat{\mathbf{g}} + I_{\mathrm{ws}} \Omega \hat{\mathbf{s}}) - I_{\mathrm{ws}} \Omega \hat{\mathbf{t}} u_1 - I_{\mathrm{ws}} \hat{\mathbf{s}} u_2 \right) \\ &= -\omega_{\mathrm{t}} I_{\mathrm{ws}} \Omega u_1 - I_{\mathrm{ws}} \omega_{\mathrm{s}} u_2 \end{aligned} \tag{141}$$

where $\omega_{\mathrm{s}} = \boldsymbol{\omega}^T \hat{\mathbf{s}}$ and $\omega_{\mathrm{t}} = \boldsymbol{\omega}^T \hat{\mathbf{t}}$ are the projections of the body angular velocity $\boldsymbol{\omega}$ along the spin and transverse axes of the gimbal frame, respectively, that is, $\boldsymbol{\omega} = \omega_{\mathrm{s}} \hat{\mathbf{s}} + \omega_{\mathrm{t}} \hat{\mathbf{t}} + \omega_{\mathrm{g}} \hat{\mathbf{g}}$,

where $\omega_{\rm g} = \boldsymbol{\omega}^T \hat{\mathbf{g}}$. Taking a control law as

$$u_1 = \dot{\gamma} = k_1 \omega_{\rm t} I_{\rm ws} \Omega, \quad k_1 > 0, \tag{142a}$$

$$u_2 = \dot{\Omega} = k_2 I_{\rm ws} \omega_{\rm s}, \qquad k_2 > 0, \tag{142b}$$

yields

$$\dot{V}_1 = -k_1 (\omega_{\rm t} I_{\rm ws} \Omega)^2 - k_2 (I_{\rm ws} \omega_{\rm s})^2 \leq 0. \tag{143}$$

In order to show that the control law (142) provides a stabilizing feedback, we need to show that there exists $c_0 > 0$ such that, for each $c_1 \in (0, c_0)$, no trajectory of the vector field with $\boldsymbol{u} = 0$ is contained inside the set

$$\mathcal{L}_c \triangleq \{\boldsymbol{\omega} : V_1(\boldsymbol{\omega}) = c_1 \text{ and } \omega_{\rm t} I_{\rm ws} \Omega = I_{\rm ws} \omega_{\rm s} = 0\}. \tag{144}$$

In other words, we need to show that no trajectories of the control-free system stay in nontrivial invariant sets of $\dot{V}_1 = 0$, which are characterized by the equations

$$\omega_{\rm t} I_{\rm ws} \Omega = 0 \tag{145a}$$

$$I_{\rm ws} \omega_{\rm s} = 0. \tag{145b}$$

Inside the invariant set $\mathcal{L}_c$, we have that $u_1 = \dot{\gamma} = 0$ and $u_2 = \dot{\Omega} = 0$, and thus γ and Ω are constant. In addition, $\omega_{\rm s} = 0$ from (145b). Because γ is constant, the gimbal frame $\mathcal{G}$ is fixed in the body frame. Rewriting the dynamic equations in the $\mathcal{G}$-frame, one obtains

$$\bar{J} \dot{\boldsymbol{\omega}} = -\boldsymbol{\omega}^{\times} (\bar{J} \boldsymbol{\omega} + I_{\rm ws} \Omega \hat{\mathbf{s}}) = -\boldsymbol{\omega}^{\times} \mathbf{h}, \tag{146}$$

where

$$\boldsymbol{\omega} = [0, \omega_{\rm t}, \omega_{\rm g}]^T, \quad \dot{\boldsymbol{\omega}} = [0, \dot{\omega}_{\rm t}, \dot{\omega}_{\rm g}]^T. \tag{147}$$

Using Eqs. (139) and (147), Eq. (146) can be written as

$$\begin{bmatrix} 0 \\ J_{\rm t} \dot{\omega}_{\rm t} \\ J_{\rm a} \dot{\omega}_{\rm g} \end{bmatrix} = - \begin{bmatrix} h_3 \omega_{\rm t} - h_2 \omega_{\rm g} \\ h_1 \omega_{\rm g} \\ -h_1 \omega_{\rm t} \end{bmatrix} = \begin{bmatrix} \omega_{\rm t} \omega_{\rm g} (J_{\rm t} - J_{\rm a}) \\ -I_{\rm ws} \Omega \omega_{\rm g} \\ I_{\rm ws} \Omega \omega_{\rm t} \end{bmatrix}, \tag{148}$$

where

$$\mathbf{h} = [h_1, h_2, h_3]^T = [I_{\rm ws} \Omega, J_{\rm t} \omega_{\rm t}, J_{\rm a} \omega_{\rm g}]^T \tag{149}$$

is the total angular momentum of the vehicle expressed in the gimbal frame. Comparing the fist element in Eq. (148), one obtains $\omega_{\rm t}\omega_{\rm g} = 0$ for the equilibria. Also, one has $\omega_{\rm t}\Omega = 0$ from Eq. (145a). Thus, there are two different types of the equilibria: i) $\omega_{\rm t} = 0$, $\omega_{\rm g} \in \mathbb{R}$, and ii) $\omega_{\rm g} = \Omega = 0$, $\omega_{\rm t} \in \mathbb{R}$.

i) $\omega_{\rm t} = 0$, $\omega_{\rm g} \in \mathbb{R}$: Comparing the second element in Eq. (148), one has $\Omega\omega_{\rm g} = 0$. If $\omega_{\rm g} = 0$, then $\boldsymbol{\omega} = 0$, which is the desired equilibrium. However, there can still be a nontrivial equilibrium given by $\Omega = 0$, $\boldsymbol{\omega} = [0, 0, \pm H_0/J_{\rm a}]^T$.

ii) $\omega_{\rm g} = \Omega = 0$, $\omega_{\rm t} \in \mathbb{R}$: There can be a nontrivial equilibrium at $\Omega = 0$, $\boldsymbol{\omega} = [0, \pm H_0/J_{\rm t}, 0]^T$.

Therefore, there exist nontrivial equilibria contained in the nontrivial invariant set $\mathcal{L}_c$, thus the global stabilization is not guaranteed. Nonetheless, these nontrivial equilibria can be proved to be unstable using Lyapunov's first method; see the next section 6.4.2 for the proof.

6.4.2 Instability of the Nontrivial equilibria

In this section, it is shown that the nontrivial equilibrium states of Eqs. (109) and (142) are unstable. For simplicity of the ensuing analysis, it is assumed that $\mathbf{h} \triangleq J\boldsymbol{\omega} + I_{\rm cg}\dot{\gamma}\hat{\mathbf{g}} + I_{\rm ws}\Omega\hat{\mathbf{s}} \approx J\boldsymbol{\omega} + I_{\rm ws}\Omega\hat{\mathbf{s}}$, which is justified by the fact that the gimbal angle rate $\dot{\gamma}$ does not contribute significantly to the total angular momentum. The closed-loop system with the proposed nonlinear controller (142) can be written as

$$J\dot{\boldsymbol{\omega}} = -\boldsymbol{\omega}^{\times}(J\boldsymbol{\omega} + I_{\rm ws}\Omega\hat{\mathbf{s}}) - k_1 I_{\rm ws}^2\Omega^2\omega_{\rm t}\hat{\mathbf{t}} - k_2 I_{\rm ws}^2\omega_{\rm s}\hat{\mathbf{s}} \tag{150}$$

$$\dot{\gamma} = k_1 I_{\rm ws}\Omega\omega_{\rm t} \tag{151}$$

$$\dot{\Omega} = k_2 I_{\rm ws}\omega_{\rm s} \tag{152}$$

Linearizing these equations about $\Omega = 0, \gamma_e = 0, \omega_{\rm t} = 0$ and $\omega_{\rm g} = \pm H_0/J_{\rm a}$, one obtains

$$J\Delta\dot{\boldsymbol{\omega}} = \left((J\boldsymbol{\omega})^{\times} - \boldsymbol{\omega}^{\times}J - k_2 I_{\rm ws}^2\hat{\mathbf{s}}\hat{\mathbf{s}}^T\right)\Delta\boldsymbol{\omega} - \boldsymbol{\omega}^{\times}I_{\rm ws}\hat{\mathbf{s}}\Delta\Omega \tag{153}$$

$$\Delta\dot{\gamma} = 0 \tag{154}$$

$$\Delta\dot{\Omega} = k_2 I_{\rm ws}\hat{\mathbf{s}}^T\Delta\boldsymbol{\omega} \tag{155}$$

It is obvious that the dynamics of $\Delta\gamma$ in Eq. (154) is neutrally stable, and can be decoupled from those of $\Delta\boldsymbol{\omega}$ and $\Delta\Omega$. Thus we only need to check the stability of Eqs. (153) and (155). It can be easily shown that the characteristic equation of this linear system is

$$\lambda(\lambda^3 + a_2\lambda^2 + a_1\lambda + a_0) = 0 \tag{156}$$

where

$$a_2 = (1/J_\mathrm{t})k_2 I_\mathrm{ws}^2, \quad a_1 = \frac{H_0^2(J_\mathrm{a} - J_\mathrm{t})^2}{J_\mathrm{t}^2 J_\mathrm{a}^2}, \quad a_0 = -\frac{I_\mathrm{ws}^2 k_2 H_0^2(J_\mathrm{a} - J_\mathrm{t})}{J_\mathrm{t}^2 J_\mathrm{a}^2}.$$

This equation has a single root at the origin, so the system is marginally stable at best. From Routh's stability criterion, a necessary and sufficient condition for stability for the characteristic equation (156) is

$$a_0 > 0, \quad a_1 > 0, \quad a_2 > 0$$

and

$$a_2 a_1 - a_0 = \frac{I_\mathrm{ws}^2 k_2 H_0^2(J_\mathrm{a} - J_\mathrm{t})}{J_\mathrm{a} J_\mathrm{t}^3} > 0$$

Note however that a_0 and $(a_2 a_1 - a_0)$ cannot have a same sign. Therefore, this equilibrium is unstable.

Similarly, consider the equilibrium $\Omega = 0, \gamma_e = 0, \omega_\mathrm{g} = 0$ and $\omega_\mathrm{t} = \pm H_0/J_\mathrm{t}$. The linearized equations about this equilibrium state are

$$J\Delta\dot{\boldsymbol{\omega}} = \left((J\boldsymbol{\omega})^\times - \boldsymbol{\omega}^\times J - k_2 I_\mathrm{ws}^2 \hat{\mathbf{s}}\hat{\mathbf{s}}^T\right)\Delta\boldsymbol{\omega} - k_2 I_\mathrm{ws}^2 \omega_\mathrm{t}\hat{\mathbf{s}}\Delta\gamma - \boldsymbol{\omega}^\times I_\mathrm{ws}\hat{\mathbf{s}}\Delta\Omega \tag{157}$$

$$\Delta\dot{\gamma} = k_1\omega_\mathrm{t} I_\mathrm{ws}\Delta\Omega \tag{158}$$

$$\Delta\dot{\Omega} = k_2 I_\mathrm{ws}\hat{\mathbf{s}}^T\Delta\boldsymbol{\omega} + k_2\omega_\mathrm{t} I_\mathrm{ws}\Delta\gamma \tag{159}$$

The characteristic equation of this linear system is

$$\lambda^2(\lambda^3 + a_2\lambda^2 + a_1\lambda + a_0) = 0 \tag{160}$$

where

$$a_2 = (1/J_\mathrm{t})k_2 I_\mathrm{ws}^2, \quad a_1 = -\frac{k_1 I_\mathrm{ws}^2 k_2 H_0^2}{J_\mathrm{t}^2} \quad a_0 = \frac{I_\mathrm{ws}^2 k_2 H_0^2}{J_\mathrm{t}^3 J_\mathrm{a}}(J_\mathrm{a} - J_\mathrm{t}).$$

One of the necessary conditions for stability is

$$a_1 > 0$$

which is false for this system. Therefore, this equilibrium is also unstable, and the proof is complete.[†]

6.4.3 Stabilization of $\boldsymbol{\omega}$, γ_e and Ω_e

The nonlinear controller designed in the previous section stabilizes $\boldsymbol{\omega}$, but it is not sufficient to achieve the overall control objective, as it controls only the angular velocity vector. Hence, the final orientation of the spacecraft is not controlled. In this section, a nonlinear controller is designed which makes, in addition to $\boldsymbol{\omega} \to 0$, also $\gamma_e = \gamma - \gamma_\mathrm{f} \to 0$.

Notice that in this case there are two possible desired values of the final gimbal angle γ_f, depending on the sign of the final wheel speed Ω_f, as shown in Eq. (116) or Eq. (121). The magnitude of the final wheel speed is given by $|\Omega_\mathrm{f}| = H_0/I_\mathrm{ws}$ as $\boldsymbol{\omega} \to 0$ due to the momentum conservation law, but its sign can be either positive or negative, unless it is explicitly controlled. Thus, we also need to control the wheel speed Ω as well as $\boldsymbol{\omega}$ and γ.

First, let us consider a nonlinear controller which makes $\boldsymbol{\omega} \to 0$, $\gamma \to \gamma_\mathrm{f}^+$ and $\Omega \to \Omega_\mathrm{f}^+$. For this purpose, define a Lyapunov function candidate $V_2^+(\boldsymbol{\omega}, \gamma_e, \Omega_e)$ as

$$\begin{aligned} V_2^+(\boldsymbol{\omega}, \gamma_e, \Omega_e) &\triangleq \tfrac{1}{2}\boldsymbol{\omega}^T J \boldsymbol{\omega} + \tfrac{1}{2}k_\gamma {\gamma_e^+}^2 + \tfrac{1}{2}k_\Omega {\Omega_e^+}^2 \\ &= \tfrac{1}{2}\left(J_\mathrm{t}(\omega_\mathrm{s}^2 + \omega_\mathrm{t}^2) + J_\mathrm{a}\omega_\mathrm{g}^2\right) + \tfrac{1}{2}k_\gamma {\gamma_e^+}^2 + \tfrac{1}{2}k_\Omega {\Omega_e^+}^2, \quad k_\gamma, k_\Omega > 0, \end{aligned} \tag{161}$$

where $\gamma_e^+ \triangleq \gamma - \gamma_\mathrm{f}^+$ and $\Omega_e^+ \triangleq \Omega - \Omega_\mathrm{f}^+$. Its time derivative along the trajectories of the system (109) and (124) yields

$$\begin{aligned} \dot{V}_2^+ &= \boldsymbol{\omega}^T J \dot{\boldsymbol{\omega}} + k_\gamma \gamma_e^+ \dot{\gamma} + k_\Omega \Omega_e^+ \dot{\Omega} \\ &= -(\omega_\mathrm{t} I_\mathrm{ws}\Omega - k_\gamma \gamma_e^+)u_1 - (I_\mathrm{ws}\omega_\mathrm{s} - k_\Omega \Omega_e^+)u_2. \end{aligned} \tag{162}$$

Taking a control law as

$$u_1 = \dot{\gamma} = k_3(\omega_\mathrm{t} I_\mathrm{ws}\Omega - k_\gamma \gamma_e^+), \quad k_3 > 0, \tag{163a}$$

$$u_2 = \dot{\Omega} = k_4(I_\mathrm{ws}\omega_\mathrm{s} - k_\Omega \Omega_e^+), \quad k_4 > 0, \tag{163b}$$

yields

$$\dot{V}_2^+ = -k_3(\omega_\mathrm{t} I_\mathrm{ws}\Omega - k_\gamma \gamma_e)^2 - k_4(I_\mathrm{ws}\omega_\mathrm{s} - k_\Omega \Omega_e)^2 \leq 0. \tag{164}$$

[†]Instability also ensues because of the double zero at the origin.

Now, let us check whether there exist nontrivial equilibria which make $\dot{V}_2^+ = 0$, as we did in Section 6.4.1. These equilibria are characterized by the equations

$$\omega_{\rm t} I_{\rm ws}\Omega - k_\gamma \gamma_e = 0 \quad \text{and} \quad I_{\rm ws}\omega_{\rm s} - k_\Omega \Omega_e = 0. \tag{165}$$

There are three types of nontrivial equilibria, and are shown in Table 2. See Section 6.4.4 for the details.

Table 2: Nontrivial Equilibria of the System Under Controller Eq. (163).

Type	E1	E2	E3
$\omega_{\rm s}$	$-\frac{k_\Omega H_0}{I_{\rm ws}^2}$	$-\frac{2H_0}{J_{\rm t}+I_{\rm ws}^2/k_\Omega}$	$\frac{H_0}{J_{\rm a}-J_{\rm t}-I_{\rm ws}^2/k_\Omega}$
$\omega_{\rm t}$	$\pm\sqrt{\frac{H_0^2}{I_{\rm ws}^4}\left(\frac{I_{\rm ws}^4}{J_{\rm t}^2}-k_\Omega^2\right)}$	0	0
$\omega_{\rm g}$	0	0	$\pm\sqrt{H_0^2\left(\frac{1}{J_{\rm a}^2}-\frac{1}{(J_{\rm a}-J_{\rm t}-I_{\rm ws}^2/k_\Omega)^2}\right)}$
γ_e	0	0	0
Ω	0	$\frac{-2I_{\rm ws}H_0}{J_{\rm t}k_\Omega+I_{\rm ws}^2}+\frac{H_0}{I_{\rm ws}}$	$-\frac{I_{\rm ws}H_0}{k_\Omega(J_{\rm t}-J_{\rm a})+I_{\rm ws}^2}+\frac{H_0}{I_{\rm ws}}$
V_2^+	$\frac{1}{2}H_0^2\left(\frac{1}{J_{\rm t}}+\frac{k_\Omega}{I_{\rm ws}^2}\right)$	$\frac{2k_\Omega H_0^2}{I_{\rm ws}^2+k_\Omega J_{\rm t}}$	$\frac{1}{2}\frac{H_0^2(I_{\rm ws}^2+k_\Omega J_{\rm t})}{J_{\rm a}(k_\Omega(J_{\rm t}-J33)+I_{\rm ws}^2)}$

Similarly, we also consider a nonlinear controller for the negative final wheel speed $\Omega_{\rm f}^-$. Define another Lyapunov function candidate $V_2^-(\boldsymbol{\omega}, \gamma_e, \Omega_e)$ as

$$\begin{aligned} V_2^-(\boldsymbol{\omega}, \gamma_e, \Omega_e) &\triangleq \tfrac{1}{2}\boldsymbol{\omega}^T J \boldsymbol{\omega} + \tfrac{1}{2}k_\gamma {\gamma_e^-}^2 + \tfrac{1}{2}k_\Omega {\Omega_e^-}^2 \\ &= \tfrac{1}{2}\left(J_{\rm t}(\omega_{\rm s}^2+\omega_{\rm t}^2) + J_{\rm a}\omega_{\rm g}^2\right) + \tfrac{1}{2}k_\gamma {\gamma_e^-}^2 + \tfrac{1}{2}k_\Omega {\Omega_e^-}^2, \end{aligned} \tag{166}$$

where $\gamma_e^- \triangleq \gamma - \gamma_{\rm f}^-$ and $\Omega_e^- \triangleq \Omega - \Omega_{\rm f}^-$. This Lyapunov function candidate suggests the control law

$$u_1 = \dot{\gamma} = k_3(\omega_{\rm t} I_{\rm ws}\Omega - k_\gamma \gamma_e^-), \quad k_3 > 0, \tag{167a}$$

$$u_2 = \dot{\Omega} = k_4(I_{\rm ws}\omega_{\rm s} - k_\Omega \Omega_e^-), \quad k_4 > 0, \tag{167b}$$

One can show that the nontrivial equilibria of this control law are identical with those of the control law (163) shown in Table 2, except that ω_s and Ω have opposite sign.

Since it is rather complicated to check the stability of these nontrivial equilibria using Lyapunov's first method as did in Section 6.4.1, here we follow a different approach. The possibility of encountering these nontrivial equilibria is eliminated altogether, by properly

choosing the values of the controller gain and by utilizing the controller designed in Section 6.4.1, which stabilizes the angular velocity $\boldsymbol{\omega}$. To this end, let $V_{2\mathrm{eq}}$ be the minimum of the values of Lyapunov candidates V_2^+ and V_2^- at the nontrivial equilibria, that is, let

$$V_{2\mathrm{eq}} \triangleq \min\{\tfrac{1}{2}H_0^2\left(\tfrac{1}{J_\mathrm{t}}+\tfrac{k_\Omega}{I_\mathrm{ws}^2}\right),\ \tfrac{2k_\Omega H_0^2}{I_\mathrm{ws}^2+k_\Omega J_\mathrm{t}},\ \tfrac{1}{2}\tfrac{H_0^2(I_\mathrm{ws}^2+k_\Omega J_\mathrm{t})}{J_\mathrm{a}(k_\Omega(J_\mathrm{t}-J33)+I_\mathrm{ws}^2)}\}. \tag{168}$$

For any nonzero initial angular momentum $\mathbf{H}_0$ and any spacecraft inertia matrix J, we can choose the control gains k_γ and k_Ω so that

$$V_{2\mathrm{eq}} > \tfrac{1}{2}k_\gamma\pi^2. \tag{169}$$

If we take the value of the gimbal angle γ using the "congruence"-function modulo 2π, that is,

$$\begin{aligned}\gamma^+ = &\quad \mathrm{mod}(\gamma+\pi-\gamma_\mathrm{f}^+,2\pi)-\pi+\gamma_\mathrm{f}^+,\\ \gamma^- = &\quad \mathrm{mod}(\gamma+\pi-\gamma_\mathrm{f}^-,2\pi)-\pi+\gamma_\mathrm{f}^-,\end{aligned} \tag{170}$$

and redefine

$$\gamma_e^+ \triangleq \gamma^+-\gamma_\mathrm{f}^+,\quad \gamma_e^- \triangleq \gamma^--\gamma_\mathrm{f}^-, \tag{171}$$

then the gimbal angle errors are confined as $-\pi \le \gamma_e^+ < \pi$ and $-\pi \le \gamma_e^- < \pi$.

Now, suppose that the control law (142) is applied to make $\boldsymbol{\omega} \to 0$. From momentum conservation, the wheel speed Ω converges to either Ω_f^+ or Ω_f^-, as $\boldsymbol{\omega} \to 0$. If we let $\epsilon \triangleq V_{2\mathrm{eq}} - \frac{1}{2}k_\gamma\pi^2 > 0$ from Eq. (169), then there exist a time $t_\mathrm{s} > 0$ such that

$$\tfrac{1}{2}(\boldsymbol{\omega}^2 J\boldsymbol{\omega}+k_\Omega{\Omega_e^+}^2)\Big|_{t=t_\mathrm{s}} < \epsilon, \quad \text{or} \quad \tfrac{1}{2}(\boldsymbol{\omega}^2 J\boldsymbol{\omega}+k_\Omega{\Omega_e^-}^2)\Big|_{t=t_\mathrm{s}} < \epsilon. \tag{172}$$

At this time t_s, therefore, one of the following equations must hold

$$V_2^+(t=t_\mathrm{s}) < \epsilon+\tfrac{1}{2}k_\gamma{\gamma_e^+}^2 < \epsilon+\tfrac{1}{2}k_\gamma\pi^2 = V_{2\mathrm{eq}}, \tag{173a}$$

$$V_2^-(t=t_\mathrm{s}) < \epsilon+\tfrac{1}{2}k_\gamma{\gamma_e^-}^2 < \epsilon+\tfrac{1}{2}k_\gamma\pi^2 = V_{2\mathrm{eq}}. \tag{173b}$$

Hence, if we switch the controller at $t = t_\mathrm{s}$ from Eq. (142) to Eqs. (163) or (167), depending on the sign of the wheel speed Ω, then we ensure that $\gamma \to \gamma_\mathrm{f}^+$ and $\Omega \to \Omega_\mathrm{f}^+$, or $\gamma \to \gamma_\mathrm{f}^-$ and $\Omega \to \Omega_\mathrm{f}^-$ as $\boldsymbol{\omega} \to 0$, respectively, without encountering any of the nontrivial equilibria. This follows from the fact that control laws (163) and (167) imply $\dot{V}_2^+ \le 0$ and $\dot{V}_2^- \le 0$, respectively.

6.4.4 Characterization of the Nontrivial Equilibria

In this section, the author derives the nontrivial equilibrium states of the closed-loop system under the nonlinear controller (163). These equilibria are characterized by Eq. (165) which is rewritten here as

$$\omega_{\mathrm{t}} I_{\mathrm{ws}} \Omega - k_\gamma \gamma_e = 0 \quad \text{and} \quad I_{\mathrm{ws}} \omega_{\mathrm{s}} - k_\Omega \Omega_e = 0. \tag{174}$$

We consider two cases: i) $\Omega = 0$ and ii) $\Omega \neq 0$.

i) $\Omega = 0$: When $\Omega = 0$, then $\Omega_e = -\Omega_{\mathrm{f}}^- = H_0/I_{\mathrm{ws}}$, and thus $\omega_{\mathrm{s}} = k_\Omega H_0/I_{\mathrm{ws}}^2$ is a nonzero constant. Rewriting the dynamic equations in the gimbal frame $\mathcal{G}$, one obtains $J\dot{\boldsymbol{\omega}} = -\boldsymbol{\omega}^\times J\boldsymbol{\omega}$, where $\boldsymbol{\omega} = [\omega_{\mathrm{s}}, \omega_{\mathrm{t}}, \omega_{\mathrm{g}}]^T$, $\dot{\boldsymbol{\omega}} = [0, \dot{\omega}_{\mathrm{t}}, \dot{\omega}_{\mathrm{g}}]^T$. This equation can be written componentwise as

$$\begin{bmatrix} 0 \\ J_{\mathrm{t}}\dot{\omega}_{\mathrm{t}} \\ J_{\mathrm{a}}\dot{\omega}_{\mathrm{g}} \end{bmatrix} = \begin{bmatrix} (J_{\mathrm{t}} - J_{\mathrm{a}})\omega_{\mathrm{t}}\omega_{\mathrm{g}} \\ -(J_{\mathrm{t}} - J_{\mathrm{a}})\omega_{\mathrm{g}}\omega_{\mathrm{s}} \\ 0 \end{bmatrix} \tag{175}$$

which immediately yields $\omega_{\mathrm{t}}\omega_{\mathrm{g}} = 0$ and $\dot{\omega}_{\mathrm{g}} = 0$. Moreover, since ω_{s} and ω_{g} are constant, $\dot{\omega}_{\mathrm{t}}$ is constant If $\dot{\omega}_{\mathrm{t}}$ is a nonzero constant, ω_{t} will diverge to infinity thus violating the momentum conservation law. Thus, $\dot{\omega}_{\mathrm{t}} = 0$ and $\omega_{\mathrm{g}}\omega_{\mathrm{s}} = 0$. Since $\omega_{\mathrm{s}} = k_\Omega H_0/I_{\mathrm{ws}}^2 \neq 0$, it follows that $\omega_{\mathrm{g}} = 0$. Therefore, the total angular momentum is

$$\mathbf{h} = [\ J_{\mathrm{t}} \frac{k_\Omega H_0}{I_{\mathrm{ws}}^2}\ ,\ \ J_{\mathrm{t}}\ \omega_{\mathrm{t}}\ ,\ \ 0\ ]^T \tag{176}$$

and thus from $\|\mathbf{h}\| = H_0$, we have that

$$\omega_{\mathrm{t}} = \pm\sqrt{\frac{H_0^2}{I_{\mathrm{ws}}^4}\left(\frac{I_{\mathrm{ws}}^4}{J_{\mathrm{t}}^2} - k_\Omega^2\right)}. \tag{177}$$

This is the nontrivial equilibrium E1 in Table 2.

ii) $\Omega \neq 0$: In this case, ω_{t} is constant, as well as ω_{s}. The equation of motion written in the gimbal frame is

$$J\dot{\boldsymbol{\omega}} = -\boldsymbol{\omega}^\times(J\boldsymbol{\omega} + I_{\mathrm{ws}}\Omega\hat{\mathbf{s}}) = -\boldsymbol{\omega}^\times\mathbf{h} \tag{178}$$

where

$$\mathbf{h} = [\ J_{\rm t}\omega_{\rm s} + I_{\rm ws}\Omega\ ,\ \ J_{\rm t}\omega_{\rm t}\ ,\ \ J_{\rm a}\omega_{\rm g}\ ]^T \tag{179}$$

and $\boldsymbol{\omega} = [\omega_{\rm s}, \omega_{\rm t}, \omega_{\rm g}]^T$, $\dot{\boldsymbol{\omega}} = [0, 0, \dot{\omega}_{\rm g}]^T$. Equivalently,

$$\begin{bmatrix} 0 \\ 0 \\ J_{\rm a}\dot{\omega}_{\rm g} \end{bmatrix} = \begin{bmatrix} \omega_{\rm t}\omega_{\rm g}(J_{\rm t} - J_{\rm a}) \\ \omega_{\rm g}\omega_{\rm s}(J_{\rm a} - J_{\rm t}) - I_{\rm ws}\Omega\omega_{\rm g} \\ I_{\rm ws}\Omega\omega_{\rm t} \end{bmatrix} \tag{180}$$

and thus $\omega_{\rm t}\omega_{\rm g} = 0$. Let us consider two cases again: a) $\omega_{\rm g} = 0$ and b) $\omega_{\rm t} = 0$.

ii)-(a) : $\omega_{\rm g} = 0$: Since $\dot{\omega}_{\rm g} = 0$, $\omega_{\rm t} = 0$ and

$$\mathbf{h} = [J_{\rm t}\omega_{\rm s} + I_{\rm ws}\Omega\ , 0\ ,\ 0\ ]^T = [\ \pm H_0\ ,\ 0\ ,\ 0\ ]^T. \tag{181}$$

From Eq. (174), $\Omega_e = I_{\rm ws}\omega_{\rm s}/k_\Omega$, and thus $\Omega = \Omega_e + \Omega_{\rm f}^- = I_{\rm ws}\omega_{\rm s}/k_\Omega - H_0/I_{\rm ws}$. Comparing the first element of (181) yields

$$\omega_{\rm s}(J_{\rm t} + \frac{I_{\rm ws}^2}{k_\Omega}) = 0, \quad \text{or} \quad \omega_{\rm s}(J_{\rm t} + \frac{I_{\rm ws}^2}{k_\Omega}) = 2H_0. \tag{182}$$

If $\omega_{\rm s} = 0$, then it is nothing more than the desired trivial equilibrium. If $\omega_{\rm s} \neq 0$, then

$$\omega_{\rm s} = \frac{2H_0}{J_{\rm t} + I_{\rm ws}^2/k_\Omega}, \tag{183}$$

and

$$\Omega = \frac{2I_{\rm ws}H_0}{J_{\rm t}k_\Omega + I_{\rm ws}^2} - \frac{H_0}{I_{\rm ws}}, \tag{184}$$

and this state corresponds to the nontrivial equilibrium E2 in Table 2.

ii)-(b) : $\omega_{\rm t} = 0$: From Eq. (180), $\dot{\omega}_{\rm g} = 0$, thus,

$$\boldsymbol{\omega}^\times \mathbf{h} = 0, \tag{185}$$

where

$$\boldsymbol{\omega} = [\omega_{\rm s}, 0, \omega_{\rm g}]^T, \quad \mathbf{h} = [J_{\rm t}\omega_{\rm s} + I_{\rm ws}\Omega, 0, J_{\rm a}\omega_{\rm g}]^T. \tag{186}$$

Since $\mathbf{h} \neq 0$, this equation implies $\boldsymbol{\omega} = 0$ or $\mathbf{h} = \lambda\boldsymbol{\omega}$ $(\lambda \neq 0)$. The equilibrium with $\boldsymbol{\omega} = 0$ is the desired state, so we can ignore it. From (186), therefore, one obtains

$$(J_{\rm t} - \lambda)\omega_{\rm s} = -I_{\rm ws}\Omega \tag{187}$$

$$(J_{\rm a} - \lambda)\omega_{\rm g} = 0 \tag{188}$$

The case with $\omega_{\rm g} = 0$ has been examined already, so we only need to check the case $\lambda = J_{\rm a}$. For this case, it is easy to show that

$$\omega_{\rm s} = \frac{-H_0}{J_{\rm a} - J_{\rm t} - I_{\rm ws}^2/k_\Omega}, \tag{189}$$

$$\omega_{\rm g} = \pm\sqrt{H_0^2\left(\frac{1}{J_{\rm a}^2} - \frac{1}{(J_{\rm a} - J_{\rm t} - I_{\rm ws}^2/k_\Omega)^2}\right)}, \tag{190}$$

where we have used the fact that $\Omega = \Omega_e + \Omega_{\rm f}^- = \frac{I_{\rm ws}\omega_{\rm s}}{k_\Omega} - \frac{H_0}{I_{\rm ws}}$ and $\|\mathbf{h}\| = H_0$. These equilibrium states correspond to E3 in Table 2.

6.4.5 Nonlinear control design for stabilization of $\boldsymbol{\omega}$, γ_e and ϕ_e

The final goal of the control design is to globally stabilize ϕ_e, as well as $\boldsymbol{\omega}$ and γ_e. We already have designed three separate controllers and we will used them to fulfill this objective. One is a linear controller, designed in Section 6.3, which locally stabilizes $\boldsymbol{\omega}$, γ_e and ϕ_e. The second one is a nonlinear controller, designed in Section 6.4.1, which globally stabilizes $\boldsymbol{\omega}$. The third one designed in Section 6.4.3 makes $\boldsymbol{\omega} \to 0$, as well as $\gamma \to \gamma_{\rm f}$ and $\Omega \to \Omega_{\rm f}$. Each one of the first and the third controllers has two different versions according to the sign of $\Omega_{\rm f}$. Utilizing these three control laws, we can construct a control logic consisting of three control phases that globally achieves the final control objectives, given in Eq. (122). At the first stage, we use the nonlinear controller (142) to make $\boldsymbol{\omega} \to 0$. While this controller is being applied, the values of the Lyapunov candidates V_2^+ and V_2^- are monitored, and if one of them becomes less than $V_{2\rm eq}$, then the control switches to the second stage, where the controller (163) or (167) results in $\boldsymbol{\omega} \to 0$ and $\gamma \to \gamma_{\rm f}$ where $\gamma_{\rm f} = \gamma_{\rm f}^+$ or $\gamma_{\rm f}^-$, and $\Omega \to \Omega_{\rm f}$ where $\Omega_{\rm f} = \Omega_{\rm f}^+$ or $\Omega_{\rm f}^-$, according to the sign of $\Omega_{\rm f}$. At the third stage, we use the linear controller in Section 6.3 to also stabilize ϕ_e as well as $\boldsymbol{\omega}$,γ_e.

In order to use the linear controller in the third stage, we need all the states to be kept close to their desired equilibrium values, except ϕ_e which is ignorable, that is, it has no effect on the kinetic equations. It follows that

$$\boldsymbol{\omega} \approx 0, \quad \gamma_e \approx 0, \quad \Omega \approx \Omega_{\rm f} \tag{191}$$

at the beginning of and during the third stage. Owing to the nonlinear controller used at the second stage, $\boldsymbol{\omega}$ and γ_e are stabilized at the beginning of the third stage. The wheel

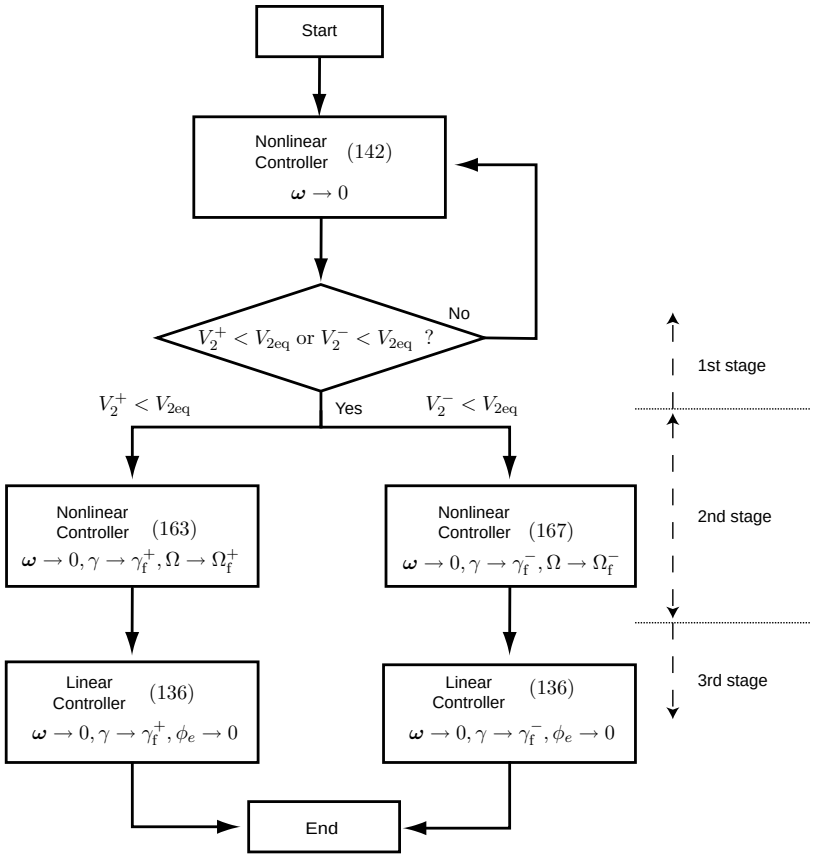

Figure 29: Flow Chart of Entire Control Procedure.

speed Ω also becomes $\Omega = \Omega_{\mathrm{f}}$ to conserve the total angular momentum. In addition, if we determine the weighting matrix Q and R in the performance index (137) so that the weights on $\boldsymbol{\omega}$ and γ_e are large, then the LQR controller which minimizes the performance index in (137) will keep $\boldsymbol{\omega}$ and γ_e small during the third stage. The wheel speed variation also must be kept small, i.e., $\Omega \approx \Omega_{\mathrm{f}}$, but this is not guaranteed by the LQR controller. From the momentum conservation law, however, if we can keep $\boldsymbol{\omega}$ sufficiently small during the third stage, then Ω will also stay close to Ω_{f}. This can be achieved by giving large weight on $\boldsymbol{\omega}$ in the LQR controller designing step.

Figure 29 summarizes the whole control procedure to achieve the control objective.

6.5 Numerical Examples

In this section, we give an illustrative example of the proposed control design method for the spacecraft angular velocity stabilization with the body-fixed line-of-sight control problem.

Table 3: Spacecraft Model Parameters for LOS Control

Symbol	Value	Units
${}^{B}I$	$\begin{bmatrix} 20 & 0 & 0 \\ 0 & 20 & 0 \\ 0 & 0 & 10 \end{bmatrix}$	$\mathrm{kg\,m^2}$
I_{ws}	0.0042	$\mathrm{kg\,m^2}$
$I_{\mathrm{wt}}, I_{\mathrm{wg}}$	0.0024	$\mathrm{kg\,m^2}$
I_{gs}	0.0093	$\mathrm{kg\,m^2}$
$I_{\mathrm{gt}}, I_{\mathrm{gg}}$	0.0054	$\mathrm{kg\,m^2}$
$\hat{\mathbf{s}}_0$	$[1,0,0]^T$	-
$\hat{\mathbf{t}}_0$	$[0,1,0]^T$	-
$\hat{\mathbf{g}}_0$	$[0,0,1]^T$	-

In the previous sections, the simplified equations of motion with the assumptions $\dot{J} = 0$ and $I_{\mathrm{cg}}\ddot{\gamma}\hat{\mathbf{g}} = 0$ were used for control design. In this section the complete nonlinear equations of motion given by Eq.(107) and the acceleration steering law (20) are used to predict and validate the performance of the proposed controllers under realistic conditions. Table 3 summarizes the values of the moments of inertia of the spacecraft and the VSCMG used in all numerical simulations.

The control design parameters, the initial conditions and the desired line-of-sight $\hat{\mathbf{n}}$ used in the simulations are given in Table 4. To describe the attitude of the spacecraft with respect to the inertial frame $\mathcal{I}$, we use the Euler's parameters. The initial values of the quaternion vector in Table 4 implies that the initial body frame $\mathcal{B}$ is aligned with the inertial frame $\mathcal{I}$ at $t = 0$. The controller gains of the nonlinear controller and the weighs of the LQR controller are chosen by trial and error in order to stabilize the system quickly with suitable damping. In particular, the gains k_γ and k_Ω are chosen so that the condition (169) holds.

For the given initial angular velocity $\boldsymbol{\omega}(0)$ and the line-of-sight direction vector $\hat{\mathbf{n}}$, the desired final gimbal angles are calculated from Eq. (121) as $\gamma_{\mathrm{f}}^{+} = 149.7^\circ$ and $\gamma_{\mathrm{f}}^{-} = -30.3^\circ$. The final wheel speeds are given by $\Omega_{\mathrm{f}}^{+} = H_0/I_{\mathrm{ws}} = 13606$ rpm and $\Omega_{\mathrm{f}}^{-} = -H_0/I_{\mathrm{ws}} =$

Table 4: Control Design Parameters and Initial Conditions For LOS Control

Symbol	Value	Units
$\mathbf{q}(0)$	$[0,0,0,1]^T$	-
$\boldsymbol{\omega}(0)^*$	$[-0.3,-0.2,0.1]^T$	rad/sec
$\gamma(0)$	120	deg
$\dot{\gamma}(0)$	0	deg/sec
$\Omega(0)$	3×10^3	rpm
$\hat{\mathbf{n}}^{**}$	$\frac{1}{\sqrt{5}}[1,2,0]^T$	-
Q	$\text{diag}[10^4,10^4,10^4,10^3,10^3]$	-
R	$\text{diag}[10^3,1]$	-
$k_1,\ k_3$	1	-
$k_2,\ k_4$	5×10^4	-
k_γ	0.05	-
k_Ω	1×10^{-6}	-
K_p	1	-

* Written in the body frame $\mathcal{B}$

** Written in the inertial frame $\mathcal{I}$

-13606 rpm. In addition, the inertial frame $\mathcal{H}$, defined from (113) and (118), is given via

$$R_{\mathcal{I}}^{\mathcal{H}} = \begin{bmatrix} \hat{\mathbf{a}}_1^T \\ \hat{\mathbf{a}}_2^T \\ \hat{\mathbf{a}}_3^T \end{bmatrix} = \begin{bmatrix} 0.8889 & 0.4474 & 0.0983 \\ -0.1458 & 0.0729 & 0.9866 \\ 0.4342 & -0.8914 & 0.1300 \end{bmatrix}. \tag{192}$$

Figures 30-35 show the results of the numerical simulations. As mentioned in Section 6.4.5, the whole control procedure consists of three stages. During the first stage, the nonlinear controller (142) is applied so as to stabilize $\boldsymbol{\omega}$, while γ and ϕ are allowed to take any values. For this example, V_2^- becomes less than $V_{2\text{eq}} = 3.1487$ at $t_{\text{s1}} \approx 4.98$ sec, as shown in Fig. 31, so the control mode is switched to the second stage of the nonlinear controller (167). During the second stage, $\boldsymbol{\omega}$ is still under stabilization, and $\gamma \to \gamma_{\text{f}}^-$ and $\Omega \to \Omega_{\text{f}}^-$.

The switching from the second stage to the third one occurs when the norms of $\boldsymbol{\omega}$ and γ_e become smaller than some given tolerances $\epsilon_\omega, \epsilon_\gamma > 0$, respectively. We have used $\epsilon_\omega = 10^{-3}$ and $\epsilon_\gamma = 10^{-2}$ in the simulations, and the switching time for these tolerance was $t_{\text{s2}} \approx 110.66$ sec. At the third stage, the linear LQR controller is applied to achieve the overall control objective by making $\boldsymbol{\omega}$, γ_e and ϕ_e ($= \phi$) all converge to zero.

Figure 30 shows the angular velocity trajectory of the spacecraft. As expected, the angular velocity is stabilized, then momentarily diverges after the switching from the second to the third stage (near $t_{s2} = 110.66$ sec), and converges to zero again. Notice that $\omega_3 = \omega_g$ is kept small even during the second stage. This means that the spacecraft does not rotate significantly about the gimbal axis, but it does rotate about the spin axis in order to make $\phi_e \to 0$.

Figure 32 shows the attitude history of the body frame $\mathcal{B}$. Figure 32(a) is the time history of the quaternion parameters of $\mathcal{B}$ with respect to $\mathcal{I}$. Before the switching from the second to the third stage, the attitude parameters converge to certain constant values because $\boldsymbol{\omega} \to 0$ due to the nonlinear controller, and after switching, they converge to some other values as $\boldsymbol{\omega} \to 0$ again, due to the linear LQR controller. The final quaternion coincides with the desired final quaternion vector. Specifically, we may check that the final $\hat{\mathbf{b}}_1$-axis is

$$\hat{\mathbf{b}}_1 = [0.4472,\ 0.8944,\ 0]^T \approx \hat{\mathbf{n}}$$

which means that the line-of-sight fixed along the $\hat{\mathbf{b}}_1$-axis points at the given direction $\hat{\mathbf{n}}$, as desired.

Figures 32(b)-32(d) show the time history of the Euler angles of $\mathcal{B}$ with respect to $\mathcal{H}$, which are used for the parametrization of the spacecraft orientation at rest. As the angular velocity converges to zero, θ converges to $\theta_f = 90^\circ$ as expected. As shown in Fig. 32(b), ϕ is not controlled in the first and second stage, but after switching to the third stage, ϕ converges to zero as expected in Eq. (119) via the use of the LQR controller. The other Euler angle ψ also converges to $\psi_f = -37.09^\circ$ given in Eq. (119). We can see that only ϕ varies in the third stage while θ and ψ are nearly kept constant, and this implies again that the spacecraft rotates about the spin axis in the third stage.

Figure 33 shows the gimbal angle and the wheel speed trajectories of the VSCMG, respectively. It can be shown that both the gimbal angle changes and the wheel speed changes are exploited by the controller during the first and second stages to stabilize $\boldsymbol{\omega}$ and γ_e. However, in the third stage, only the wheel speed change is exploited to make $\phi \to 0$. The variation of the wheel speed in the third stage is not very large, so the use of

the linearized analysis is justified. In fact, we can make the difference $\Omega - \Omega_{\rm f}$ much smaller by weighting less ϕ or weighting more $\boldsymbol{\omega}$ and/or $\dot{\Omega}$ in the performance index (137), but then the convergence rate of ϕ will become smaller in this case. It is also shown that the gimbal angle γ converges to $\gamma_{\rm f}^- = -52.91^\circ$, which satisfies Eq. (116). Figure 34 shows the trajectories of the control inputs, $\dot{\gamma}$, $\ddot{\gamma}$ and $\dot{\Omega}$.

Finally, Fig. 35 shows a series of snapshots of the whole maneuver of the spacecraft. Note that the total angular momentum vector $\mathbf{H}$ is fixed in inertial space during the maneuver. The angular velocity $\boldsymbol{\omega}$ is stabilized and it is hardly seen in the snapshots after $t = 40$ sec. At $t = 100$ sec., which is just before the switching from the second to the third stage, the gimbal angle γ becomes $\gamma_{\rm f}^- = -52.91^\circ$. See the relative positions of $\hat{\mathbf{b}}_1$ and $\hat{\mathbf{s}}$ about the $\hat{\mathbf{b}}_3$-axis. The spin axis $\hat{\mathbf{s}}$ is perfectly opposite in direction to $\mathbf{H}$, and the wheel speed is $\Omega = \Omega_{\rm f}^- < 0$, which means that the wheel is actually spinning in the direction of $\mathbf{H}$ to conserve the angular momentum. At $t = 120$ sec., which is just after the second switching, we may see that the spacecraft rotates about the $\hat{\mathbf{s}}$-axis to align the $\hat{\mathbf{b}}_1$-axis with $\hat{\mathbf{n}}$, while controlled by the LQR controller. Near $t = 200$ sec., the spacecraft is at rest with the $\hat{\mathbf{b}}_1$-axis pointing at $\hat{\mathbf{n}}$, and the control objective is successfully achieved.

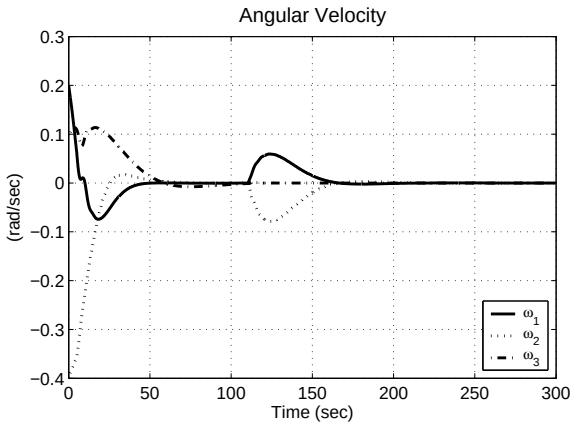

Figure 30: Spacecraft Angular Velocity History $\boldsymbol{\omega}(t)$.

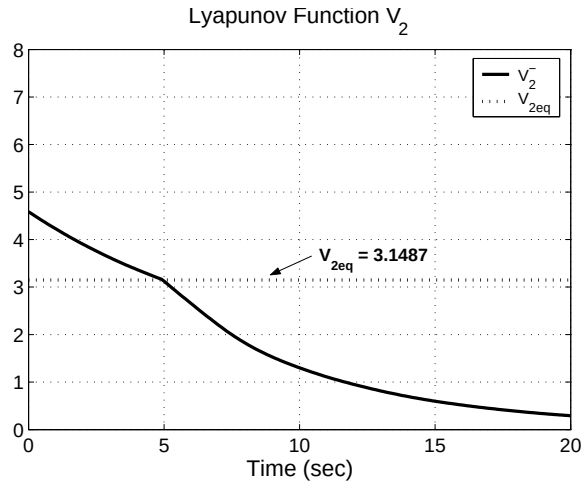

Figure 31: Lyapunov Function Candidate History $V_2^-(t)$.

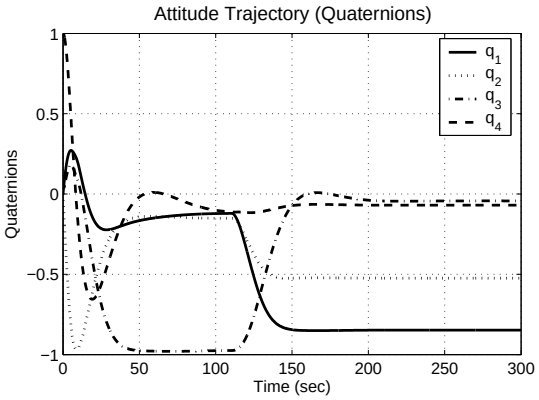

(a) Quaternions (with respect to $\mathcal{I}$).

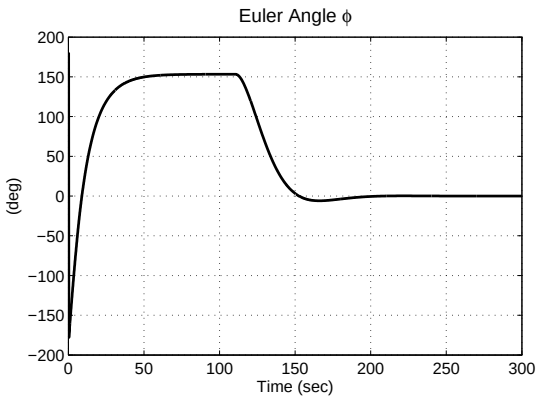

(b) Euler Angle ϕ (with respect to $\mathcal{H}$).

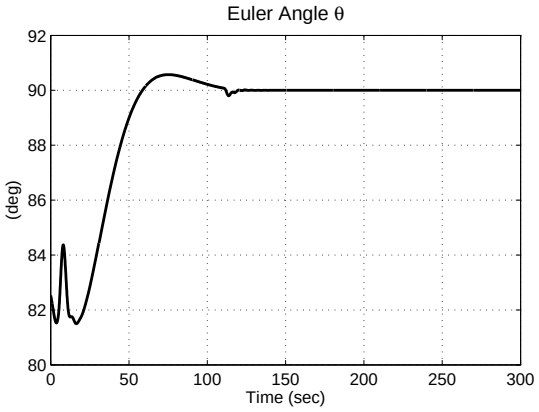

(c) Euler Angle θ (with respect to $\mathcal{H}$).

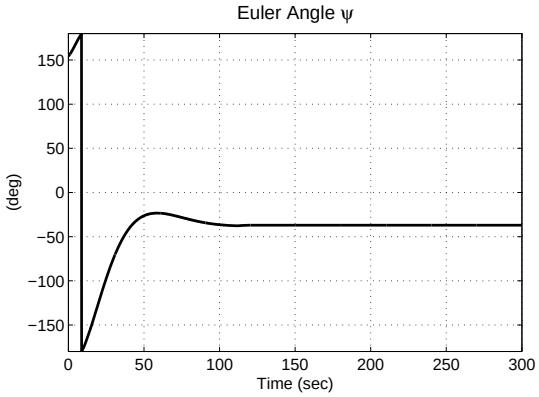

(d) Euler Angle ψ (with respect to $\mathcal{H}$).

Figure 32: Spacecraft Attitude Trajectories.

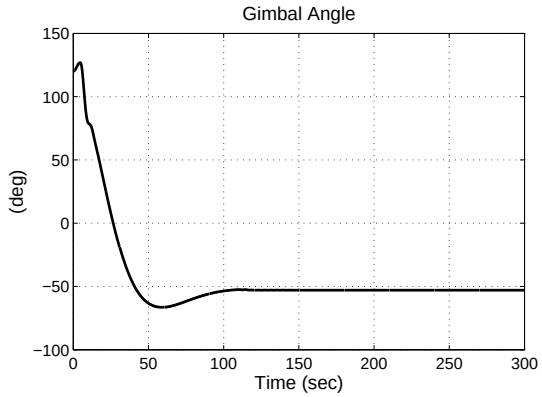

(a) Gimbal angle γ.

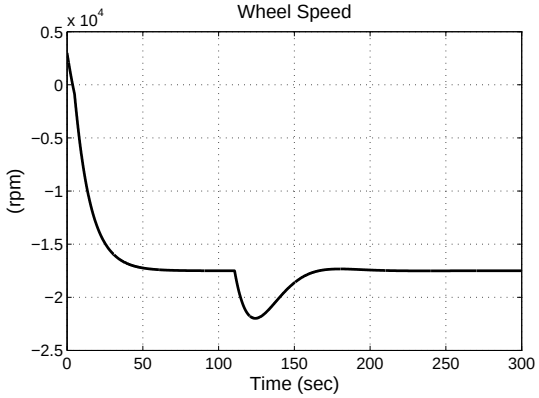

(b) Wheel speed Ω.

Figure 33: Gimbal Angle and Wheel Speed.

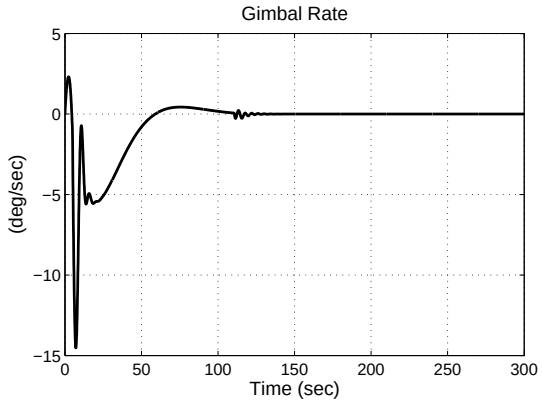

(a) Gimbal rate $\dot{\gamma}$.

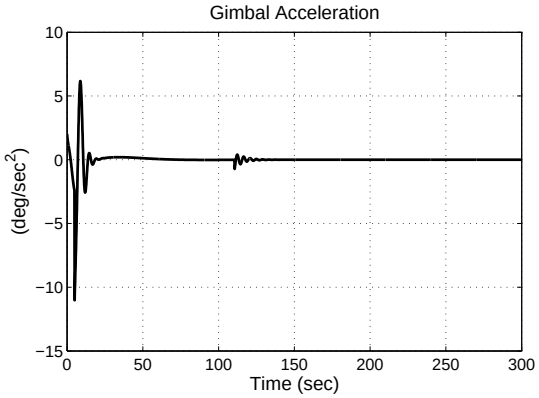

(b) Gimbal acceleration $\ddot{\gamma}$.

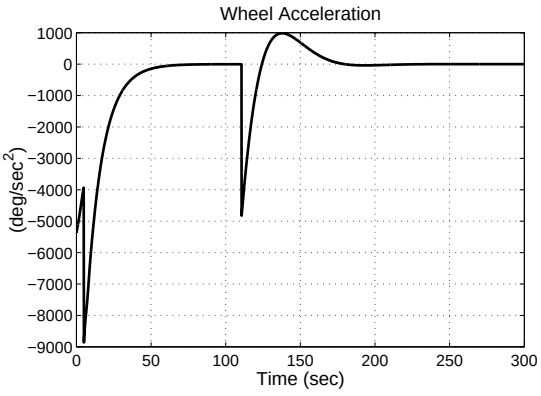

(c) Wheel acceleration $\dot{\Omega}$.

Figure 34: Control Inputs.

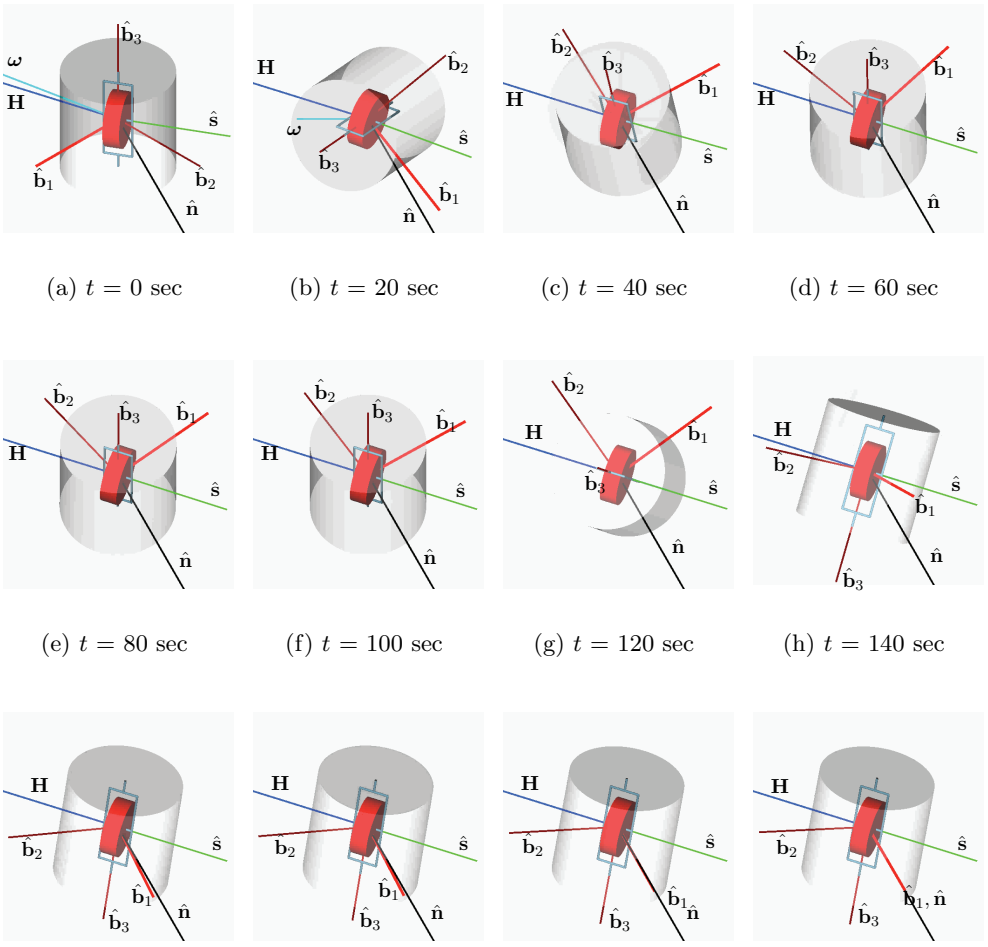

(a) $t = 0$ sec (b) $t = 20$ sec (c) $t = 40$ sec (d) $t = 60$ sec

(e) $t = 80$ sec (f) $t = 100$ sec (g) $t = 120$ sec (h) $t = 140$ sec

(i) $t = 160$ sec (j) $t = 180$ sec (k) $t = 200$ sec (l) $t = 220$ sec

Figure 35: Snapshots of the Spacecraft Orientation During the Maneuver.

CHAPTER VII

ADAPTIVE SPACECRAFT ATTITUDE TRACKING CONTROL WITH ACTUATOR UNCERTAINTIES

7.1 Problem Statement

The dynamic equations of motion of a spacecraft with a cluster of VSCMGs have been fully derived in Chapter 2. In general, the total moment of inertia of the spacecraft will change as the VSCMG rotates about its gimbal axis, so the matrix $J = J(\gamma)$ is a function of a gimbal angle γ; see Eq. (7). However, the dependence of J on γ is weak, especially when the size of spacecraft main body is large. We will therefore assume that J is constant ($\dot{J} = 0$) during controller design. In addition, to simplify the analysis, we assume that the gimbal acceleration term $A_g I_{\rm cg} \ddot{\boldsymbol{\gamma}}$ is ignored. This assumption is standard in the literature [28, 73, 65], and it amounts to gimbal angle rate servo control. It is also useful to assume that the gimbal angle rate term $A_g I_{\rm cg} \dot{\boldsymbol{\gamma}}$ does not contribute significantly to the total angular momentum of the spacecraft and the VSCMGs. Then, one obtains the equation of motion as

$$J\dot{\boldsymbol{\omega}} + C\dot{\boldsymbol{\gamma}} + D\dot{\boldsymbol{\Omega}} + \boldsymbol{\omega}^{\times}\mathbf{h} = 0, \tag{193}$$

where,

$$\mathbf{h} = J\boldsymbol{\omega} + A_s I_{\rm cg}\boldsymbol{\Omega}. \tag{194}$$

and

$$C = A_t I_{\rm cg}\boldsymbol{\Omega}^d, \quad D = A_s I_{\rm cg}. \tag{195}$$

Notice that this equation is for a spacecraft with a VSCMG cluster, but it can be easily converted to the case of reaction wheels by setting $\boldsymbol{\gamma}$ constant, and for conventional CMGs by setting $\boldsymbol{\Omega}$ constant.

As done in Ref. [79], the dynamic equation (193) and the kinematic equation (13) can be combined into a state-space form. By differentiating Eq. (13), one obtains $\boldsymbol{\omega} = G^{-1}(\boldsymbol{\sigma})\dot{\boldsymbol{\sigma}}$

and $\ddot{\boldsymbol{\sigma}} = G(\boldsymbol{\sigma})\dot{\boldsymbol{\omega}} + \dot{G}(\boldsymbol{\sigma}, \dot{\boldsymbol{\sigma}})\,\boldsymbol{\omega}$. The total angular momentum $\mathbf{h}$ written in the body frame can be expressed as $\mathbf{h} = R_{\mathcal{I}}^{\mathcal{B}}(\boldsymbol{\sigma})\mathbf{H}_{\mathcal{I}}$, where $R_{\mathcal{I}}^{\mathcal{B}}(\boldsymbol{\sigma})$ is the rotational matrix from the inertia frame $\mathcal{I}$ to the body frame $\mathcal{B}$, and $\mathbf{H}_{\mathcal{I}}$ is the total angular momentum written in $\mathcal{I}$-frame. If we assume that no external control/disturbance torques are applied to the spacecraft, then the total angular momentum of the spacecraft-VSCMG system is conserved (in both magnitude and direction) during a maneuver, and thus $\mathbf{H}_{\mathcal{I}}$ is constant. From, Eq. (193), one can write

$$G^{-T}JG^{-1}\ddot{\boldsymbol{\sigma}} - G^{-T}JG^{-1}\dot{G}G^{-1}\dot{\boldsymbol{\sigma}} + G^{-T}\boldsymbol{\omega}^{\times}(R_{\mathcal{I}}^{\mathcal{B}}(\boldsymbol{\sigma})\mathbf{H}_{\mathcal{I}}) + G^{-T}(C\dot{\boldsymbol{\gamma}} + D\dot{\boldsymbol{\Omega}}) = 0. \tag{196}$$

and equivalently,

$$\ddot{\boldsymbol{\sigma}} = F^{*}(\boldsymbol{\sigma}, \dot{\boldsymbol{\sigma}}) + G^{*}(\boldsymbol{\sigma}, \dot{\boldsymbol{\sigma}})\boldsymbol{u} \tag{197}$$

where

$$F^{*}(\boldsymbol{\sigma}, \dot{\boldsymbol{\sigma}}) = H^{*-1}\left(G^{-T}JG^{-1}\dot{G}G^{-1}\dot{\boldsymbol{\sigma}} - G^{-T}\boldsymbol{\omega}^{\times}(R_{\mathcal{I}}^{\mathcal{B}}(\boldsymbol{\sigma})\mathbf{H}_{\mathcal{I}})\right) \in \mathbb{R}^{3\times 1} \tag{198a}$$

$$G^{*}(\boldsymbol{\sigma}, \boldsymbol{\gamma}, \boldsymbol{\Omega}) = -H^{*-1}G^{-T}Q \in \mathbb{R}^{3\times 2N} \tag{198b}$$

$$H^{*}(\boldsymbol{\sigma}) = G^{-T}JG^{-1} \in \mathbb{R}^{3\times 3} \tag{198c}$$

$$Q(\boldsymbol{\gamma}, \boldsymbol{\Omega}) = [C(\boldsymbol{\gamma}, \boldsymbol{\Omega})\ ,\ D(\boldsymbol{\gamma})] \in \mathbb{R}^{3\times 2N} \tag{198d}$$

$$\boldsymbol{u} = [\dot{\boldsymbol{\gamma}}^{T}, \dot{\boldsymbol{\Omega}}^{T}]^{T} \in \mathbb{R}^{2N\times 1} \tag{198e}$$

Therefore, the equation of motion in state space form can be written as

$$\frac{\mathrm{d}}{\mathrm{d}t}\begin{bmatrix}\boldsymbol{\sigma}\\ \dot{\boldsymbol{\sigma}}\end{bmatrix} = \begin{bmatrix}0 & \mathbf{I}\\ 0 & 0\end{bmatrix}\begin{bmatrix}\boldsymbol{\sigma}\\ \dot{\boldsymbol{\sigma}}\end{bmatrix} + \begin{bmatrix}0\\ \mathbf{I}\end{bmatrix}\Big(F^{*}(\boldsymbol{\sigma}, \dot{\boldsymbol{\sigma}}) + G^{*}(\boldsymbol{\sigma}, \dot{\boldsymbol{\sigma}})\boldsymbol{u}\Big). \tag{199}$$

Now, suppose that there are uncertainties in the actuator modelling, so that the exact value of the initial axis directions and scaling input gain are unknown. Let us assume that the actual initial axis direction matrices can be expressed as

$$A_{s0} = A_{s0}^{\mathrm{n}} + A_{s0}^{\Delta}, \quad A_{t0} = A_{t0}^{\mathrm{n}} + A_{t0}^{\Delta} \tag{200}$$

where $A_{\bullet 0}^{\mathrm{n}}$ are known nominal values and $A_{\bullet 0}^{\Delta}$ are unknown constant values. Moreover, since we do not know the exact angular momentum of the VSCMGs cluster, the total angular

momentum $\mathbf{H}_{\mathcal{I}}$ can be expressed as

$$\mathbf{H}_{\mathcal{I}} = \mathbf{H}_{\mathcal{I}}^{\mathrm{n}} + \mathbf{H}_{\mathcal{I}}^{\Delta} \tag{201}$$

where $\mathbf{H}_{\mathcal{I}}^{\mathrm{n}}$ is the known nominal value of $\mathbf{H}_{\mathcal{I}}$, and $\mathbf{H}_{\mathcal{I}}^{\Delta}$ is the unknown constant. Then, the system matrices in (198a) and (198b) can be decomposed as

$$F^{*} = F^{*\mathrm{n}} + F^{*\Delta}, \quad G^{*} = G^{*\mathrm{n}} + G^{*\Delta} \tag{202}$$

where,

$$F^{*\mathrm{n}} = H^{*-1}\left(G^{-T}JG^{-1}\dot{G}G^{-1}\dot{\boldsymbol{\sigma}} - G^{-T}\boldsymbol{\omega}^{\times}(R_{\mathcal{I}}^{\mathcal{B}}(\boldsymbol{\sigma})\mathbf{H}_{\mathcal{I}}^{\mathrm{n}})\right) \tag{203}$$

$$F^{*\Delta} = -H^{*-1}\left(G^{-T}\boldsymbol{\omega}^{\times}(R_{\mathcal{I}}^{\mathcal{B}}(\boldsymbol{\sigma})\mathbf{H}_{\mathcal{I}}^{\Delta})\right) \tag{204}$$

and

$$G^{*\mathrm{n}} = -H^{*-1}G^{-T}Q^{\mathrm{n}} \tag{205}$$

$$G^{*\Delta} = -H^{*-1}G^{-T}Q^{\Delta} \tag{206}$$

where Q^{n} and Q^{Δ} are with nominal and uncertain values of the matrix Q in Eq. (198d), respectively.

Notice that $F^{*\Delta}$ is linear in the uncertain parameters of $\mathbf{H}_{\mathcal{I}}^{\Delta}$, thus it can be written as

$$F^{*\Delta} = Y_F\Theta_F \tag{207}$$

where $\Theta_F = \mathbf{H}_{\mathcal{I}}^{\Delta}$. The matrix Y_F is called the "regressor matrix" and can be constructed from the measurements of $\boldsymbol{\sigma}$ and $\dot{\boldsymbol{\sigma}}$. In addition, $G^{*\Delta}$ can also be written similarly as

$$G^{*\Delta} = Y_G\Theta_G \tag{208}$$

where

$$\Theta_G = \mathrm{diag}[\Theta_{G1}, \Theta_{G2}, \cdots, \Theta_{G2N}] \in \mathbb{R}^{12N\times 2N} \tag{209}$$

$$\Theta_{Gi} = \Theta_{G(i+N)} = [\mathbf{t}_{i0}^{\Delta T}, \mathbf{s}_{i0}^{\Delta T}]^{T} \in \mathbb{R}^{6\times 1}, \qquad i = 1, \cdots, N, \tag{210}$$

and

$$Y_G = [Y_{G1}, Y_{G2}, \cdots, Y_{G2N}] \in \mathbb{R}^{3\times 12N} \tag{211}$$

$$Y_{Gi} = -H^{*-1}G^{-T}I_{\rm cg}[\cos\gamma_i \mathbf{I}_3,\ -\sin\gamma_i \mathbf{I}_3] \in \mathbb{R}^{3\times 6}, \quad i = 1, \cdots, N \tag{212}$$

$$Y_{Gi} = -H^{*-1}G^{-T}I_{\rm cg}[\sin\gamma_i \mathbf{I}_3,\ \cos\gamma_i \mathbf{I}_3] \in \mathbb{R}^{3\times 6}, \quad i = N+1, \cdots, 2N. \tag{213}$$

7.2 Adaptive Controller Design

Assume that the attitude to be tracked is given in terms of some known functions $\boldsymbol{\sigma}_d(t)$, $\dot{\boldsymbol{\sigma}}_d(t)$ and $\ddot{\boldsymbol{\sigma}}_d(t)$ for $t \geq 0$. Here $\boldsymbol{\sigma}_d$ is the MRP vector presenting the attitude of a desired reference frame ($\mathcal{D}$-frame) with respect to the inertial frame ($\mathcal{I}$-frame). Defining

$$\mathbf{e} \triangleq \begin{bmatrix} \boldsymbol{\sigma}_e \\ \dot{\boldsymbol{\sigma}}_e \end{bmatrix} = \begin{bmatrix} \boldsymbol{\sigma} - \boldsymbol{\sigma}_d \\ \dot{\boldsymbol{\sigma}} - \dot{\boldsymbol{\sigma}}_d \end{bmatrix} \in \mathbb{R}^{6\times 1}, \tag{214}$$

one can obtain the tracking error dynamics from Eq. (199) as

$$\frac{\mathrm{d}}{\mathrm{d}t}\mathbf{e} = A_0\mathbf{e} + B\left(F^*(\boldsymbol{\sigma}, \dot{\boldsymbol{\sigma}}) + G^*(\boldsymbol{\sigma}, \dot{\boldsymbol{\sigma}})\boldsymbol{u} - \ddot{\boldsymbol{\sigma}}_d\right) \tag{215}$$

where

$$A_0 \triangleq \begin{bmatrix} 0 & \mathbf{I} \\ 0 & 0 \end{bmatrix}, \qquad B \triangleq \begin{bmatrix} 0 \\ \mathbf{I} \end{bmatrix}. \tag{216}$$

It can be easily shown that the pair of (A_0, B) is controllable, so one can choose a gain matrix K such that $A \triangleq A_0 - BK$ is Hurwitz, and rewrite (215) as

$$\dot{\mathbf{e}} = A\mathbf{e} + B\left(K\mathbf{e} + F^*(\boldsymbol{\sigma}, \dot{\boldsymbol{\sigma}}) + G^*(\boldsymbol{\sigma}, \dot{\boldsymbol{\sigma}})\boldsymbol{u} - \ddot{\boldsymbol{\sigma}}_d\right) \tag{217}$$

Let $P = P^T > 0$ be the solution of the Lyapunov equation

$$A^TP + PA + Q = 0, \qquad Q = Q^T > 0 \tag{218}$$

and choose a Lyapunov function as

$$V = \frac{1}{2}\mathbf{e}^TP\mathbf{e} + \frac{1}{2\alpha_F}\tilde{\Theta}_F^T\tilde{\Theta}_F + \frac{1}{2\alpha_G}\mathrm{Tr}(\tilde{\Theta}_G^T\tilde{\Theta}_G), \tag{219}$$

where $\tilde{\Theta}_\bullet \triangleq \hat{\Theta}_\bullet - \Theta_\bullet$, and $\hat{\Theta}_\bullet$ is an estimate of $\Theta_\bullet$ to be determined by the parameter adaptation law.

Since the dynamics $\dot{\mathbf{e}} = A\mathbf{e}$ is stable itself, let us consider a control law to cancel the extra terms in (217), for example,

$$\boldsymbol{u} = (G^{*\mathrm{n}} + Y_G\hat{\Theta}_G)^{\dagger}(-K\mathbf{e} - F^{*\mathrm{n}} - Y_F\hat{\Theta}_F + \ddot{\boldsymbol{\sigma}}_d), \tag{220}$$

where $(\bullet)^{\dagger}$ is the pseudo-inverse. The tracking error dynamics under the control law (220) equals to

$$\begin{aligned}
\dot{\mathbf{e}} &= A\mathbf{e} + B\left(K\mathbf{e} + F^{*\mathrm{n}} + Y_F\Theta_F + (G^{*\mathrm{n}} + Y_G\hat{\Theta}_G - Y_G\tilde{\Theta}_G)\boldsymbol{u} - \ddot{\boldsymbol{\sigma}}_d\right) \\
&= A\mathbf{e} + BK\mathbf{e} + BF^{*\mathrm{n}} + BY_F(\hat{\Theta}_F - \tilde{\Theta}_F) \\
&\quad + B(-K\mathbf{e} - F^{*\mathrm{n}} - Y_F\hat{\Theta}_F + \ddot{\boldsymbol{\sigma}}_d) - BY_G\tilde{\Theta}_G\boldsymbol{u} - B\ddot{\boldsymbol{\sigma}}_d \\
&= A\mathbf{e} - BY_F\tilde{\Theta}_F - BY_G\tilde{\Theta}_G\boldsymbol{u}
\end{aligned} \tag{221}$$

The time derivative of V becomes

$$\begin{aligned}
\dot{V} &= \frac{1}{2}\mathbf{e}^T(A^TP + PA)\mathbf{e} - \mathbf{e}^TPBY_F\tilde{\Theta}_F - \mathbf{e}^TPBY_G\tilde{\Theta}_G\boldsymbol{u} \\
&\quad + \frac{1}{\alpha_F}\dot{\hat{\Theta}}_F\tilde{\Theta}_F + \frac{1}{\alpha_G}\mathrm{Tr}(\dot{\hat{\Theta}}_G\tilde{\Theta}_G) \\
&= -\frac{1}{2}\mathbf{e}^TQ\mathbf{e} + \frac{1}{\alpha_F}\tilde{\Theta}_F^T(\dot{\hat{\Theta}}_F - \alpha_FY_F^TB^TP\mathbf{e}) + \frac{1}{\alpha_G}\mathrm{Tr}[\tilde{\Theta}_G^T(\dot{\hat{\Theta}}_G - \alpha_GY_G^TB^TP\mathbf{e}\boldsymbol{u}^T)] \\
&= -\frac{1}{2}\mathbf{e}^TQ\mathbf{e} + \frac{1}{\alpha_F}\tilde{\Theta}_F^T(\dot{\hat{\Theta}}_F - \alpha_FY_F^TB^TP\mathbf{e}) + \sum_{i=1}^{2N}\tilde{\Theta}_{Gi}^T(\dot{\hat{\Theta}}_{Gi} - \alpha_GY_{Gi}^TB^TP\mathbf{e}\boldsymbol{u}_i)
\end{aligned} \tag{222}$$

so one can choose the parameter adaptation law as

$$\dot{\hat{\Theta}}_F = \alpha_FY_F^TB^TP\mathbf{e} \tag{223}$$

$$\dot{\hat{\Theta}}_{Gi} = \alpha_GY_{Gi}^TB^TP\mathbf{e}\boldsymbol{u}_i, \quad i = 1, \cdots, 2N. \tag{224}$$

to make $\dot{V} = -1/2\mathbf{e}^TQ\mathbf{e} \leq 0$.

One of the serious drawbacks in this adaptation law is that the estimate of the parameter $\hat{\Theta}_G$ can make $(G^{*\mathrm{n}} + Y_G\hat{\Theta}_G)$ singular. If we use more than two VSCMGs with their nominal gimbal axes not parallel to each other [73], the nominal matrix $G^{*\mathrm{n}}$ has full rank. Therefore, if the true value of the parameter uncertainty Θ_G is bounded by a sufficiently small number, and we can also keep its estimation $\hat{\Theta}_G$ small, then we can expect that $(G^{*\mathrm{n}} + Y_G\hat{\Theta}_G)$ will be full rank. Thus, we make two following assumptions.

- **Assumption 1.** The actual value Θ_{Gi} belongs to the set $\Omega_{\Theta_{Gi}} = \left\{\Theta_{Gi} \in \mathbb{R}^6 \mid \Theta_{Gi}^T \Theta_{Gi} < \beta_{Gi}\right\}$, where $\beta_{Gi} > 0$ is known.

- **Assumption 2.** Let $\hat{\Omega}_{\Theta_{Gi}} = \left\{\hat{\Theta}_{Gi} \in \mathbb{R}^6 \mid \hat{\Theta}_{Gi}^T \hat{\Theta}_{Gi} < \beta_{Gi} + \delta_{Gi},\ \delta_{Gi} > 0\right\}$, which contains $\Omega_{\Theta_{Gi}}$ in its interior. If $\hat{\Theta}_{Gi} \in \hat{\Omega}_{\Theta_{Gi}}$ for $\forall\ i = 1, \cdots, 2N$, then $(G^{*\mathrm{n}} + Y_G \hat{\Theta}_G)$ is non-singular.

Now, instead of the adaptation law (224), one can take the alternative rule using the so-called "smooth projection algorithm" [64, 41, 19] as follows.

$$\dot{\hat{\Theta}}_{Gi} = \mathrm{Proj}(\hat{\Theta}_{Gi}, \Phi_{Gi}), \qquad i = 1, \cdots, 2N \tag{225}$$

where

$$\Phi_{Gi} \triangleq Y_{Gi}^T B^T P \mathbf{e} \boldsymbol{u}_i \tag{226}$$

and

$$\mathrm{Proj}(\hat{\Theta}_{Gi}, \Phi_{Gi}) = \begin{cases} \alpha_G \Phi_{Gi} & \text{if (i) } \|\hat{\Theta}_{Gi}\|^2 < \beta_{Gi}\ , \\ & \text{or (ii) } \|\hat{\Theta}_{Gi}\|^2 \geq \beta_{Gi} \text{ and } \Phi_{Gi}^T \hat{\Theta}_{Gi} \leq 0 \\ \alpha_G \left(\Phi_{Gi} - \frac{(\|\hat{\Theta}_{Gi}\|^2 - \beta_{Gi}) \Phi_{Gi}^T \hat{\Theta}_{Gi}}{\delta_{Gi} \|\hat{\Theta}_{Gi}\|^2} \hat{\Theta}_{Gi}\right) & \\ & \text{if (iii) } \|\hat{\Theta}_{Gi}\|^2 \geq \beta_{Gi} \text{ and } \Phi_{Gi}^T \hat{\Theta}_{Gi} > 0 \end{cases} \tag{227}$$

This adaptation law is identical to (224) in case (i) and (ii), and switches smoothly and continuously to another function in case (iii). $\mathrm{Proj}(\hat{\Theta}_{Gi}, \Phi_{Gi})$ is locally Lipschitz in $(\hat{\Theta}_{Gi}, \Phi_{Gi})$, thus the system has a unique solution defined on some time interval $[0, T_0)$. It can be verified that the adaptation rule (225) satisfies

$$\tilde{\Theta}_{Gi}^T (\dot{\hat{\Theta}}_{Gi} - \alpha_G Y_{Gi}^T B^T P \mathbf{e} \boldsymbol{u}_i) \leq 0 \tag{228}$$

and

$$\dot{\hat{\Theta}}_{Gi}(t = 0) \in \Omega_{\Theta_{Gi}} \Rightarrow \dot{\hat{\Theta}}_{Gi}(t) \in \hat{\Omega}_{\Theta_{Gi}}, \quad \forall t \geq 0. \tag{229}$$

The proof of this statement is as follows. In case (i), the proof is trivial. In case (ii), the equality in Eq. (228) trivially holds, and $\dot{\hat{\Theta}}_{Gi}^T \hat{\Theta}_{Gi} = \alpha_G \Phi_{Gi}^T \hat{\Theta}_{Gi} \leq 0$, thus the estimation

$\hat{\Theta}_{Gi}$ moves closer to zero. In case (iii), the left hand side of Eq. (228) becomes

$$\tilde{\Theta}_{Gi}^T(\dot{\hat{\Theta}}_{Gi} - \alpha_G Y_{Gi}^T B^T P \mathbf{e} \boldsymbol{u}_i) = -\alpha_G \frac{(\|\hat{\Theta}_{Gi}\|^2 - \beta_{Gi})\Phi_{Gi}^T \hat{\Theta}_{Gi}}{\delta_{Gi}\|\hat{\Theta}_{Gi}\|^2} \tilde{\Theta}_{Gi}^T \hat{\Theta}_{Gi} \;\leq\; 0, \tag{230}$$

because $\tilde{\Theta}_{Gi}^T \hat{\Theta}_{Gi} \geq 0$ as shown in Fig. 36. On the other hand,

$$\dot{\hat{\Theta}}_{Gi}^T \hat{\Theta}_{Gi} = \alpha_G \Phi_{Gi}^T \hat{\Theta}_{Gi} \left(1 - \frac{(\|\hat{\Theta}_{Gi}\|^2 - \beta_{Gi})}{\delta_{Gi}}\right) \begin{cases} < 0 & \text{if } \|\hat{\Theta}_{Gi}\|^2 > \beta_{Gi} + \delta_{Gi} \\ = 0 & \text{if } \|\hat{\Theta}_{Gi}\|^2 = \beta_{Gi} + \delta_{Gi} \\ > 0 & \text{if } \|\hat{\Theta}_{Gi}\|^2 < \beta_{Gi} + \delta_{Gi} \end{cases} \tag{231}$$

thus $\hat{\Theta}_{Gi}$ does not drift outward $\hat{\Omega}_{\Theta_{Gi}}$.

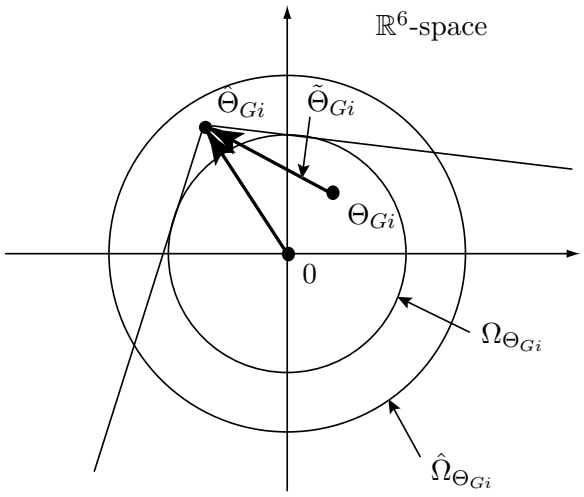

Figure 36: $\tilde{\Theta}_{Gi}^T \hat{\Theta}_{Gi} \geq 0$ in Case (iii).

From the above observations, one concludes that using the feedback law (220) and the adaptation laws (223) and (225), one obtains that

$$\dot{V} \leq -\frac{1}{2}\mathbf{e}^T Q \mathbf{e} \leq 0, \tag{232}$$

and $(G^{*\mathrm{n}} + Y_G \hat{\Theta}_G)$ will not become singular, if we choose the initial parameter guess $\hat{\Theta}_{Gi}(0)$ inside $\Omega_{\Theta_{Gi}}$, for instance $\hat{\Theta}_{Gi}(0) = 0$. Moreover, Eq. (232) implies that $\mathbf{e} \to 0$, since Q is positive-definite.

- **Remark :** It is worth pointing out that the design procedure provided in this section can be easily applied to other general systems which can be written in the form of

Eq. (197), or equivalently in the standard 2nd order form as

$$H(\boldsymbol{x})\ddot{\boldsymbol{x}} + C(\boldsymbol{x}, \dot{\boldsymbol{x}})\dot{\boldsymbol{x}} + g(\boldsymbol{x}) = \tau. \tag{233}$$

Many types of dynamical systems fall into this category, such as robot manipulators or spacecraft attitude dynamics [81, 82].

7.3 Numerical Example

A numerical example for a satellite with a VSCMGs cluster is provided to test the proposed adaptive control algorithm. In the previous section, the simplified equations of motion, given by (193), with several assumptions were used for the adaptive control design, but in this section the complete nonlinear equations of motion given, by Eq.(8), and the acceleration steering law (20) are used to predict and validate the performance of the proposed controllers under realistic conditions. The parameters used for the simulations are chosen as in Table 1, except that the initial gimbal angles are $\boldsymbol{\gamma}(0) = [0, 0, 0, 0]$ rad/sec. We also use a standard four-VSCMG pyramid configuration, shown in Fig. 7.

The nominal values of the axis directions at $\boldsymbol{\gamma} = [0, 0, 0, 0]^T$ in this pyramid configuration are

$$A_{s0}^{\mathrm{n}} = [\mathbf{s}_1, \mathbf{s}_2, \mathbf{s}_3, \mathbf{s}_4] = \begin{bmatrix} 0 & -1 & 0 & 1 \\ 1 & 0 & -1 & 0 \\ 0 & 0 & 0 & 0 \end{bmatrix} \tag{234}$$

$$A_{t0}^{\mathrm{n}} = [\mathbf{t}_1, \mathbf{t}_2, \mathbf{t}_3, \mathbf{t}_4] = \begin{bmatrix} -0.5774 & 0 & 0.5774 & 0 \\ 0 & -0.5774 & 0 & 0.5774 \\ 0.8165 & 0.8165 & 0.8165 & 0.8165 \end{bmatrix}. \tag{235}$$

The (unknown) actual axis directions used in the present example are assumed as*

$$A_{s0} = \begin{bmatrix} 0.0745 & -0.9932 & -0.1221 & 0.9901 \\ 0.9919 & -0.1024 & -0.9911 & -0.1033 \\ 0.1033 & -0.0547 & -0.0536 & -0.0954 \end{bmatrix} \tag{236}$$

$$A_{t0} = \begin{bmatrix} -0.6570 & 0.0029 & 0.6485 & 0.1394 \\ -0.0291 & -0.4929 & -0.1206 & 0.6335 \\ 0.7533 & 0.8701 & 0.7516 & 0.7611 \end{bmatrix}. \tag{237}$$

The reference trajectory is chosen so that the initial reference attitude is aligned with the actual attitude, and the angular velocity of the reference attitude is chosen as

$$\omega_d(t) = 0.02 \times (\ \sin(2\pi t/800),\ \ \sin(2\pi t/600),\ \ \sin(2\pi t/400)\ )^T \text{rad/sec}. \tag{238}$$

Figure 37 shows the time history of the reference attitude using the Euler parameters.

The feedback gain K is chosen so that the eigenvalue of $A = A_0 - BK$ is

$$\text{eig}(A) = \{-0.1 \pm 0.1i,\ -0.1\sqrt{2}, -0.15 \pm 0.15i,\ -0.15\sqrt{2}\},$$

and the other design parameters for the adaptive control law as

$$Q = \mathbf{I}, \quad \beta_{Gi} = 0.1, \quad \delta_{Gi} = 0.05, \quad \alpha_F = 1.0 \times 10^7, \quad \alpha_G = 1.0 \times 10^3.$$

Before applying the designed adaptive control law, we first performed a simulation without adaptation for comparison purposes. Figure 38 shows the attitude error under the control law with the adaptation gains α_F and α_G set all zero.

Figures 39-42 show the simulation results under the designed adaptive control law. As shown in Fig. 39, the attitude error is significantly attenuated by the adaptation law. However, the error does not converge to zero even as time goes infinity, because the adaptation law is designed under the simplified equation of motion and thus there still exist the effects of the ignored dynamics. Figure 40 shows the time history of the parameter estimation $\hat{\Theta}_F$. The flat lines with bold dots are the actual values of these parameters. The estimations

*The actual directions are taken by small angle rotations from the nominal directions, thus the orthogonality $\hat{\mathbf{t}}_i \cdot \hat{\mathbf{s}}_i = 0$ still holds for each VSCMG.

approach the actual values, but do not perfectly converge to these values due to the ignored dynamics. Figure 41 shows the time history of $\|\hat{\Theta}_{Gi}\|^2$. It is shown that $\|\hat{\Theta}_{Gi}\|^2$ does not drift more than $\beta_{Gi} + \delta_{Gi} = 0.15$ due to the smooth projection algorithm.

Similar to other general adaptive algorithms, the designed adaptive law does not guarantee by itself that the parameter estimations should converge to the actual values. Even though the given reference trajectory in Eq. (238) is so-called "coning motion" which generally satisfies the "persistent excitation" condition, it is not sufficient to make the parameter estimates converge to the actual values, because the number of the parameter estimation is so large. Generally speaking, for a linear system, the convergent estimation of m parameters requires at least $m/2$ sinusoids in the reference signal. For the nonlinear case, such simple relation may not be valid [82]. Additionally, in Figs. 40 and 41, chaotic bursting phenomena, where the parameter estimates exhibit intermittent short periods of burst are shown. This phenomena generally occur due to lack of persistency of excitation [6]. Finally, Fig. 42 shows the states of the VSCMGs cluster.

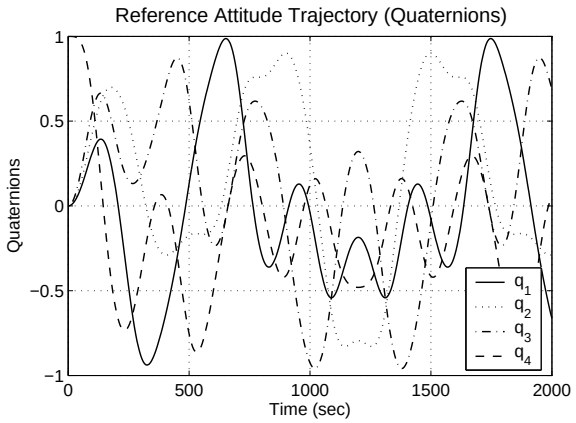

Figure 37: The Reference Attitude Trajectory

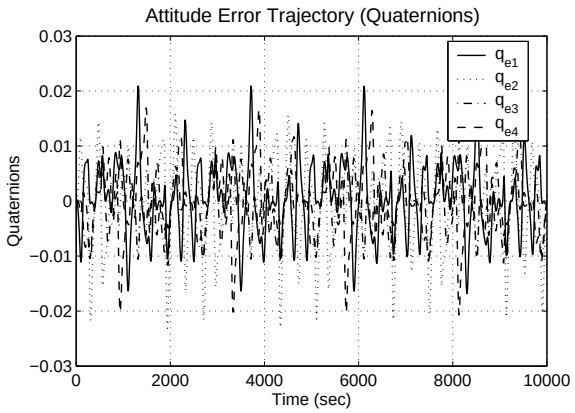

Figure 38: The Attitude Error Trajectory Without Adaptation ($\mathbf{q}_e = \mathbf{q}_d - \mathbf{q}$)

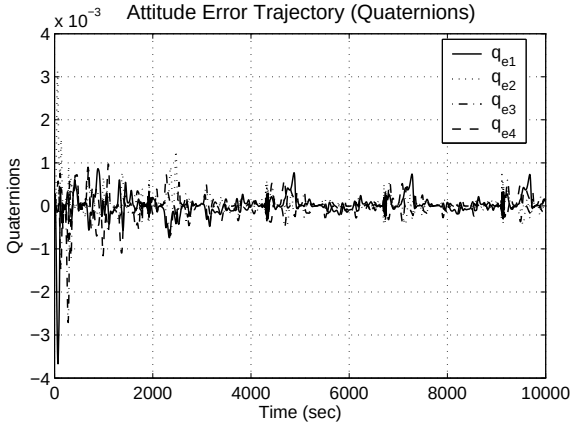

Figure 39: The Attitude Error Trajectory With Adaptation ($\mathbf{q}_e = \mathbf{q}_d - \mathbf{q}$)

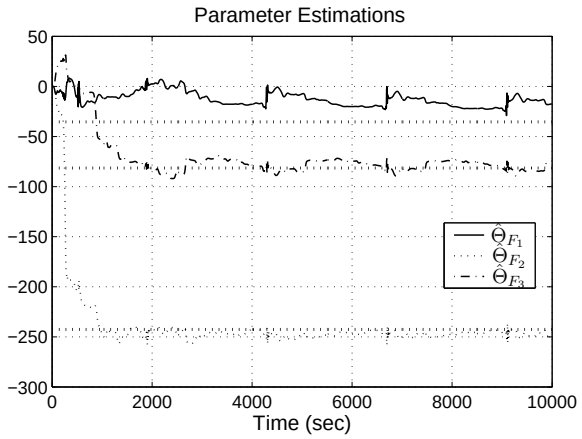

Figure 40: Parameter Estimation $\hat{\Theta}_F$

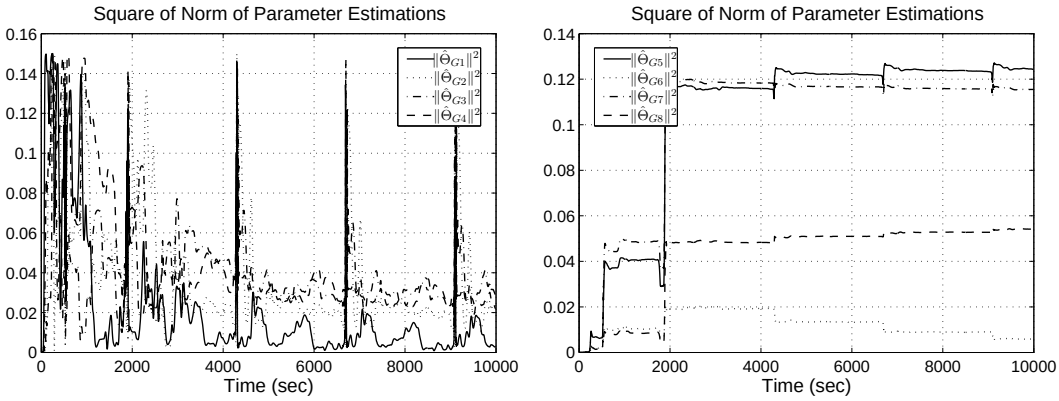

(a) $i = 1, 2, 3, 4$ (b) $i = 5, 6, 7, 8$

Figure 41: Square of Norms of Parameter Estimation $\|\hat{\Theta}_{Gi}\|^2$

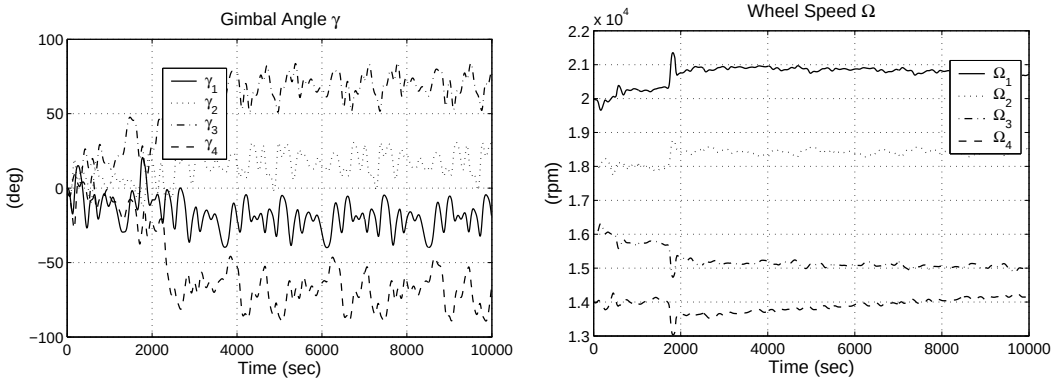

(a) Gimbal angle $\boldsymbol{\gamma}$ (b) Wheel Speed $\boldsymbol{\Omega}$

Figure 42: Gimbal Angle $\boldsymbol{\gamma}$ and Wheel Speed $\boldsymbol{\Omega}$

CHAPTER VIII

CONCLUSIONS AND FUTURE WORK

8.1 Conclusions

The present thesis provided control algorithms and analyses of VSCMGs for the spacecraft attitude and power control problems. The VSCMG system keeps most benefits of the SGCMG system, such as the torque amplification effect and simple mechanism. Moreover, it can be used to track reference attitude trajectories without encountering singular states, using null motion method to avoid singularities. Additionally, the VSCMG system can be used to track not only reference attitude but also reference power trajectory simultaneously. This means that the two subsystems, namely, the attitude control actuator system and the energy storage system, can be integrated into one subsystem using a VSCMGs cluster. In the case with power requirement, it was shown that the VSCMG system may encounter singularities even when a singularity avoidance law applies, but these unavoidable singularities can be anticipated by a simple criterion. This criterion can be used to determine the size of a VSCMGs system for a given attitude/power mission.

The present thesis also dealt with an attitude control problem with a single VSCMG. It was shown that the complete attitude equations are not controllable, but partial attitude control without violating the angular momentum conservation principle is possible. As an example of partial attitude control, the control of a body-fixed line-of-sight is addressed. The developed control law consisting of three stages successfully stabilizes the spacecraft angular velocity while making the line-of-sight aim at any given inertial direction.

This thesis also presented two kinds of adaptive control laws. One was for uncertainties in the spacecraft inertia. Even though the unknown matrix of inertia of the spacecraft is not constant and varies as the gimbal angles of CMGs/VSCMGs change, the proposed adaptive control law successfully attenuates the attitude tracking error. The second one was for a case when the actuator model has unknown bounded constant uncertainties. The adaptive

law is based on the smooth projection algorithm in order to avoid the singularities which may be caused by the drift of the parameter estimates. This algorithm forces the parameter estimates to stay inside a certain convex set containing the unknown actual values. The control algorithm was designed based on the simplified equations of motion, nonetheless, the numerical examples using the full equations showed that the adaptive algorithm reduces the tracking error significantly.

8.2 Future Work

In this section, several possible extensions of the work presented in this dissertation are outlined.

8.2.1 Singularity analysis and avoidance of CMGs/VSCMGs with consideration of the spacecraft dynamics

Although the full equations of motion have been used to design control laws and to conduct numerical simulations, only the simplified, decoupled equations of motion for a VSCMG cluster were used for the singularity analysis in Chapters 4 and 5. Such a use of the decoupled equations of motion is justified when the spacecraft is maneuvering slowly. When the spacecraft maneuvers very fast, the contribution of the spacecraft to the total angular momentum may not be neglected. Many researchers recently have studied the use of CMGs/VSCMGs for agile small spacecraft [34, 52, 53]. For fast maneuvering spacecraft we may need to also take into account the spacecraft dynamics. The use of the full equations of motion will be more complicated in this case and thus it is not easy to mathematically analyze their singularity properties. On the other hand, even though it is shown in Chapter 5 that a CMG cluster has inescapable singularities which cannot be avoided using the null motion method, these singularities may be inescapable if one considers the dynamics of spacecraft.

In addition, for some special cases, e.g., the angular velocity stabilization problem, the consideration of the spacecraft dynamics raises the possibility of an "inverse-free" steering law. To this end, note that the equations of motion of a spacecraft with a CMG cluster can

be written as

$$J\dot{\boldsymbol{\omega}} = -\boldsymbol{\omega}^{\times}(J\boldsymbol{\omega} + A_s I_{\text{ws}}\boldsymbol{\Omega}) - A_t I_{\text{ws}}\boldsymbol{\Omega}^d\dot{\boldsymbol{\gamma}} \tag{239}$$

Let us define a Lyapunov function as $V = 1/2\boldsymbol{\omega}^T J\boldsymbol{\omega}$. Then its time derivative becomes

$$\dot{V} = -\boldsymbol{\omega}^T C\dot{\boldsymbol{\gamma}}, \qquad C = A_t I_{\text{ws}}\boldsymbol{\Omega}^d. \tag{240}$$

Choosing a control law as $\dot{\boldsymbol{\gamma}} = C^T\boldsymbol{\omega}$ yields

$$\dot{V} = -\boldsymbol{\omega}^T CC^T\boldsymbol{\omega} \leq 0, \tag{241}$$

thus the system becomes at least Lyapunov stable. In order to ensure asymptotic stability, one needs to investigate the characteristics of nontrivial equilibria for $C^T\boldsymbol{\omega} = 0$.

8.2.2 Feedback Control for Power Tracking

In this thesis, it has been assumed that the power generated by the flywheels is exactly the same with the time derivative of the kinetic energy stored in the flywheels. The proposed control method for an IPACS can be regarded as a feedforward control, because it does not use any feedback of the *actual* value of the power output. In practice, there may be a discrepancy between the actual and the required power output due to the power loss in the system electromechanical components. Moreover, the VSCMG actuator also consumes electric power to steer or hold the gimbal against the gyroscopic torque along the bearing axis. Therefore, a feedback of the actual power output may be needed to control the flywheels in order to generate electric power more accurately. In fact, this issue has been dealt with in a recently published work of Ref. [24].

Finally, although the focus in this work has been on power tracking, the real objective in an actual IPACS system is voltage regulation. The IPACS algorithm should be able to track power so that the voltage on the spacecraft bus should remain constant in the presence of load variation, external disturbances, etc. The issue of voltage regulation for an IPACS system should include a more detailed analysis of the effect of the power electronics, inverter, motor/generator characteristics etc. Reference [40] gives a good overview of the IPACS voltage regulation problem.

8.2.3 Degenerate Null Motion Problem

In the present thesis, it has been assumed that the existence of null motion guarantees escape from singularities. This assumption is assumed to be valid in the literature, albeit no rigorous mathematical proof is provided. Recently, however a few researchers, including Bedrossian [10] and Wie [106], have mentioned the possibility that the VSCMG configuration remains singular even under the application of null motion. This is the so-called "degenerate null motion" problem. Nonetheless, Bedrossian did not provide any specific example in his work [10]. Wie provided an example in Ref. [106], but this example is only for a very special CMG configuration, namely one in which only two CMGs are installed with their gimbal axes parallel to each other. This CMG cluster can generate only a two-dimensional torque which is normal to the gimbal axes. The author conjectures that with a standard pyramid configuration with four CMGs/VSCMGs, such degeneration of null motion will not occur. This conjecture has been confirmed by an extensive number of numerical simulations. A rigorous mathematical proof of this observation is still needed, however. The author feels that a good starting point would be to investigate the gimbal angle rate $\dot{\boldsymbol{\gamma}}$ which keeps the CMG cluster singular. If one can show that the set of such $\dot{\boldsymbol{\gamma}}$ does not contain the null space of the Jacobian matrix C in Eq. (57), then one should be able to avoid singularities using a null motion in the subspace $\mathcal{N}(C)$.

8.2.4 Reduction Of The Number Of Parameter Estimates In The Adaptive Control Design

In Chapter 7, an adaptive controller was proposed to deal with the uncertainties in the axis directions of the VSCMG cluster. The proposed adaptive control law shows significant performance improvement in numerical simulation, but it needs to estimate a total of $6 \times 2N + 3 = 51$ parameters. (Here $N = 4$ for the pyramid configuration.) In fact, this adaptation method is highly over-estimating, because the actual number of uncertain parameters is only $6 \times N = 24$; that is, three parameters for the initial value of $\hat{\mathbf{s}}_i$ and three for the initial value of $\hat{\mathbf{t}}_i$, for each VSCMG. Moreover, these uncertain parameters can be parameterized by an even smaller number. Using the three rotational parameters from

the nominal to the actual axes frames for each VSCMG, one obtains twelve ($3 \times N = 12$) parameters. The disadvantage of parameter over-estimation becomes worse when there also exist uncertainties in the inertia matrix of a spacecraft. In that case, the proposed adaptive algorithm requires the estimation of hundreds of parameters. Several of these parameters are combinations of the parameters in the inertia matrix and the actuator axes. Therefore, the reduction of the number of parameter estimates during adaptation is an important issue that needs to be explored.

APPENDIX A

DERIVATION OF THE EQUATION OF TOTAL ANGULAR MOMENTUM OF A SPACECRAFT WITH VSCMGs

The equation of motion of a spacecraft with a CMG/VSCMG cluster is more complicated than those with other actuators, such as gas jets or reaction wheels, because the inertia of whole spacecraft varies as the gimbal angles of CMG/VSCMG change. In this appendix, a detail procedure to derive the total angular momentum of whole spacecraft is provided in order to derive the equation of motion.

For this purpose, let us define several coordinate frames as shown in Fig. 6. First, we will derive the equation for the case with only 1 VSCMG (i-th), then expand it to the N-VSCMGs case later. A VSCMG (denoted by C) is assumed to be composed with a rotating wheel (W) and gimbal structure (G) which sustains the wheel. A whole spacecraft body (B) is composed with a platform (P) and VSCMG (C), where 'platform' means a spacecraft body without VSCMG.

Let $\mathcal{G}$, $\mathcal{W}$, $\mathcal{P}$, and $\mathcal{B}$ are reference frames attached to the gimbal structure G, the rotating wheel W, the platform P, the whole spacecraft body B, and respectively. The origins of these reference frames are located at the center of mass of the corresponding body, and denoted by C_{G}, C_{P}, and O, respectively. When $\mathcal{F}$ and $\mathcal{H}$ denote any reference frames, $\boldsymbol{\omega}_{\mathcal{F}/\mathcal{H}}$ means a angular velocity of $\mathcal{F}$ relative to $\mathcal{H}$, and for any vector $\boldsymbol{x}$, ${}^{\mathcal{F}}\{\boldsymbol{x}\}$ is its 3×1 matrix expression written in $\mathcal{F}$. Without loss of generality, $\mathcal{B}$ and $\mathcal{P}$ are defined parallel to each other, and thus $\boldsymbol{\omega}_{\mathcal{P}/\mathcal{N}} = \boldsymbol{\omega}_{\mathcal{B}/\mathcal{N}}$, where $\mathcal{N}$ is the inertial frame, and let $\{\boldsymbol{x}\} \triangleq {}^{\mathcal{P}}\{\boldsymbol{x}\} = {}^{\mathcal{B}}\{\boldsymbol{x}\}$. A velocity vector $\boldsymbol{v}_P$ means a velocity of a point P relative to $\mathcal{N}$. In addition, define $[R_{\mathcal{F}}^{\mathcal{H}}]$ to be a rotational transformation matrix from $\mathcal{F}$ to $\mathcal{H}$, thus ${}^{\mathcal{H}}\{\boldsymbol{x}\} = [R_{\mathcal{F}}^{\mathcal{H}}]{}^{\mathcal{F}}\{\boldsymbol{x}\}$. Especially, the rotational matrix from $\mathcal{G}$-frame to $\mathcal{B}$-frame can be expressed as $[R_{\mathcal{G}}^{\mathcal{B}}] = [\{\hat{\mathbf{s}}_i\}, \{\hat{\mathbf{t}}_i\}, \{\hat{\mathbf{g}}_i\}]$.

Besides, $\mathbf{r}_{PQ}$ denotes a position vector from a point P to Q, and ${}^{\mathcal{F}}[I_{\star/P}]$ is an inertia matrix of $\star$ ($\star$ is wheel, gimbal structure and platform etc.) about a point P expressed in $\mathcal{F}$-frame.

Let us make several mild assumptions for simplicity. The center of mass of whole spacecraft body, O, is assumed to be fixed in $\mathcal{B}$, while the inertia of B may vary as the gimbal angle changes. In addition, we consider only the rotational motion but not the translational motion, thus O is now assumed to be fixed in $\mathcal{N}$-frame. The center of mass of the rotating wheel (W) is assumed to coincide with C_{G}. The wheel (W) and the gimbal structure (G) are balanced, i.e., ${}^{\mathcal{G}}[I_{\mathrm{G}/C_{\mathrm{G}}}] = \mathrm{diag}[I_{\mathrm{gs}_i}, I_{\mathrm{gt}_i}, I_{\mathrm{gg}_i}]$ and ${}^{\mathcal{G}}[I_{\mathrm{W}/C_{\mathrm{G}}}] = \mathrm{diag}[I_{\mathrm{ws}_i}, I_{\mathrm{wt}_i}, I_{\mathrm{wg}_i}]$.

Each angular momentum vector of the platform, gimbal, and wheels about its own center of mass can be expressed in its own frame as

$$ {}^{\mathcal{P}}\{\mathbf{h}_{\mathrm{P}/C_{\mathrm{P}}}\} = {}^{\mathcal{P}}[I_{\mathrm{P}/C_{\mathrm{P}}}]{}^{\mathcal{P}}\{\boldsymbol{\omega}_{\mathcal{P}/\mathcal{N}}\} = {}^{\mathcal{B}}[I_{\mathrm{P}/C_{\mathrm{P}}}]{}^{\mathcal{B}}\{\boldsymbol{\omega}_{\mathcal{B}/\mathcal{N}}\} \tag{242} $$

$$ {}^{\mathcal{G}}\{\mathbf{h}_{\mathrm{G}/C_{\mathrm{G}}}\} = {}^{\mathcal{G}}[I_{\mathrm{G}/C_{\mathrm{G}}}]{}^{\mathcal{G}}\{\boldsymbol{\omega}_{\mathcal{G}/\mathcal{N}}\} \tag{243} $$

$$ {}^{\mathcal{G}}\{\mathbf{h}_{\mathrm{W}/C_{\mathrm{G}}}\} = {}^{\mathcal{G}}[I_{\mathrm{W}/C_{\mathrm{G}}}]{}^{\mathcal{G}}\{\boldsymbol{\omega}_{\mathcal{W}/\mathcal{N}}\}. \tag{244} $$

The total angular momentum vector of whole spacecraft (B) can be written in the $\mathcal{B}$-frame as

$$ \begin{aligned} {}^{\mathcal{B}}\{\mathbf{h}_{\mathrm{B}/O}\} &= {}^{\mathcal{B}}\{\mathbf{h}_{\mathrm{P}/O}\} + {}^{\mathcal{B}}\{\mathbf{h}_{\mathrm{G}/O}\} + {}^{\mathcal{B}}\{\mathbf{h}_{\mathrm{W}/O}\} \\ &= {}^{\mathcal{B}}\{\mathbf{h}_{\mathrm{P}/C_{\mathrm{P}}} + m_{\mathrm{P}}\mathbf{r}_{OC_{\mathrm{P}}} \times \boldsymbol{v}_{C_{\mathrm{P}}}\} + {}^{\mathcal{B}}\{\mathbf{h}_{\mathrm{G}/C_{\mathrm{G}}} + m_{\mathrm{G}}\mathbf{r}_{OC_{\mathrm{G}}} \times \boldsymbol{v}_{C_{\mathrm{G}}}\} \\ &\quad + {}^{\mathcal{B}}\{\mathbf{h}_{\mathrm{W}/C_{\mathrm{G}}} + m_{\mathrm{W}}\mathbf{r}_{OC_{\mathrm{G}}} \times \boldsymbol{v}_{C_{\mathrm{G}}}\} \\ &= {}^{\mathcal{B}}\{\mathbf{h}_{\mathrm{P}/C_{\mathrm{P}}}\} + m_{\mathrm{P}}{}^{\mathcal{B}}\{\mathbf{r}_{OC_{\mathrm{P}}} \times \boldsymbol{v}_{C_{\mathrm{P}}}\} + [R^{\mathcal{B}}_{\mathcal{G}}]{}^{\mathcal{G}}\{\mathbf{h}_{\mathrm{G}/C_{\mathrm{G}}}\} + [R^{\mathcal{B}}_{\mathcal{G}}]{}^{\mathcal{G}}\{\mathbf{h}_{\mathrm{W}/C_{\mathrm{G}}}\} \\ &\quad + (m_{\mathrm{G}} + m_{\mathrm{W}}){}^{\mathcal{B}}\{\mathbf{r}_{OC_{\mathrm{G}}} \times \boldsymbol{v}_{C_{\mathrm{G}}}\} \end{aligned} \tag{245} $$

where m_{P}, m_{G}, and m_{W} are mass of the platform, gimbal, and wheel, respectively.

Since,

$$ \mathbf{r}_{OC_{\mathrm{P}}} \times \boldsymbol{v}_{C_{\mathrm{P}}} = \mathbf{r}_{OC_{\mathrm{P}}} \times (\boldsymbol{\omega}_{\mathcal{B}/\mathcal{N}} \times \mathbf{r}_{OC_{\mathrm{P}}}) = (\mathbf{r}_{OC_{\mathrm{P}}} \cdot \mathbf{r}_{OC_{\mathrm{P}}})\boldsymbol{\omega}_{\mathcal{B}/\mathcal{N}} - (\boldsymbol{\omega}_{\mathcal{B}/\mathcal{N}} \cdot \mathbf{r}_{OC_{\mathrm{P}}})\mathbf{r}_{OC_{\mathrm{P}}} $$

and from a fact that

$$ \{(\mathbf{a} \cdot \mathbf{b})\mathbf{b}\} = \begin{bmatrix} b_1^2 & b_1b_2 & b_1b_3 \\ b_1b_2 & b_2^2 & b_2b_3 \\ b_1b_3 & b_2b_3 & b_3^2 \end{bmatrix} \begin{Bmatrix} a_1 \\ a_2 \\ a_3 \end{Bmatrix} $$

where vectors $\mathbf{a}$ and $\mathbf{b}$ can be expressed as $[a_1, a_2, a_3]^T$ and $[b_1, b_2, b_3]^T$, respectively, we have

$$m_{\mathrm{P}}{}^{\mathcal{B}}\{\mathbf{r}_{OC_{\mathrm{P}}} \times \boldsymbol{v}_{C_{\mathrm{P}}}\} = m_{\mathrm{P}} \begin{bmatrix} y_1^2 + z_1^2 & -x_1 y_1 & -x_1 z_1 \\ -x_1 y_1 & x_1^2 + z_1^2 & -y_1 z_1 \\ -x_1 z_1 & -y_1 z_1 & x_1^2 + y_1^2 \end{bmatrix} {}^{\mathcal{B}}\{\boldsymbol{\omega}_{\mathcal{B}/\mathcal{N}}\} = m_{\mathrm{P}} M_{\mathrm{P}}{}^{\mathcal{B}}\{\boldsymbol{\omega}_{\mathcal{B}/\mathcal{N}}\},$$

and similarly,

$$\begin{aligned}(m_{\mathrm{G}} + m_{\mathrm{W}})^{\mathcal{B}}\{\mathbf{r}_{OC_{\mathrm{G}}} \times \boldsymbol{v}_{C_{\mathrm{G}}}\} &= (m_{\mathrm{G}} + m_{\mathrm{W}}) \begin{bmatrix} y_2^2 + z_2^2 & -x_2 y_2 & -x_2 z_2 \\ -x_2 y_2 & x_2^2 + z_2^2 & -y_2 z_2 \\ -x_2 z_2 & -y_2 z_2 & x_2^2 + y_2^2 \end{bmatrix} {}^{\mathcal{B}}\{\boldsymbol{\omega}_{\mathcal{B}/\mathcal{N}}\} \\ &= m_{\mathrm{C}} M_{\mathrm{C}}{}^{\mathcal{B}}\{\boldsymbol{\omega}_{\mathcal{B}/\mathcal{N}}\}\end{aligned}$$

where ${}^{\mathcal{B}}\{\mathbf{r}_{OC_{\mathrm{P}}}\} = [x_1, y_1, z_1]^T$, ${}^{\mathcal{B}}\{\mathbf{r}_{OC_{\mathrm{G}}}\} = [x_2, y_2, z_2]^T$, $m_{\mathrm{C}} = m_{\mathrm{G}} + m_{\mathrm{W}}$, and

$$M_{\mathrm{P}} = \begin{bmatrix} y_1^2 + z_1^2 & -x_1 y_1 & -x_1 z_1 \\ -x_1 y_1 & x_1^2 + z_1^2 & -y_1 z_1 \\ -x_1 z_1 & -y_1 z_1 & x_1^2 + y_1^2 \end{bmatrix}, \quad M_{\mathrm{C}} = \begin{bmatrix} y_2^2 + z_2^2 & -x_2 y_2 & -x_2 z_2 \\ -x_2 y_2 & x_2^2 + z_2^2 & -y_2 z_2 \\ -x_2 z_2 & -y_2 z_2 & x_2^2 + y_2^2 \end{bmatrix}.$$

We also have

$$\begin{aligned}{}^{\mathcal{G}}\{\mathbf{h}_{\mathrm{G}/C_{\mathrm{G}}}\} &= {}^{\mathcal{G}}[I_{\mathrm{G}/C_{\mathrm{G}}}]^{\mathcal{G}}\{\boldsymbol{\omega}_{\mathcal{G}/\mathcal{N}}\} = {}^{\mathcal{G}}[I_{\mathrm{G}/C_{\mathrm{G}}}]^{\mathcal{G}}\{\boldsymbol{\omega}_{\mathcal{G}/\mathcal{B}} + \boldsymbol{\omega}_{\mathcal{B}/\mathcal{N}}\} \\ &= {}^{\mathcal{G}}[I_{\mathrm{G}/C_{\mathrm{G}}}]^{\mathcal{G}}\{\boldsymbol{\omega}_{\mathcal{G}/\mathcal{B}}\} + {}^{\mathcal{G}}[I_{\mathrm{G}/C_{\mathrm{G}}}][R_{\mathcal{B}}^{\mathcal{G}}]^{\mathcal{B}}\{\boldsymbol{\omega}_{\mathcal{B}/\mathcal{N}}\}\end{aligned}$$

and

$$\begin{aligned}{}^{\mathcal{G}}\{\mathbf{h}_{\mathrm{W}/C_{\mathrm{G}}}\} &= {}^{\mathcal{G}}[I_{\mathrm{W}/C_{\mathrm{G}}}]^{\mathcal{G}}\{\boldsymbol{\omega}_{\mathcal{W}/\mathcal{N}}\} = {}^{\mathcal{G}}[I_{\mathrm{W}/C_{\mathrm{G}}}]^{\mathcal{G}}\{\boldsymbol{\omega}_{\mathcal{W}/\mathcal{G}} + \boldsymbol{\omega}_{\mathcal{G}/\mathcal{B}} + \boldsymbol{\omega}_{\mathcal{B}/\mathcal{N}}\} \\ &= {}^{\mathcal{G}}[I_{\mathrm{W}/C_{\mathrm{G}}}]^{\mathcal{G}}\{\boldsymbol{\omega}_{\mathcal{W}/\mathcal{G}}\} + {}^{\mathcal{G}}[I_{\mathrm{W}/C_{\mathrm{G}}}]^{\mathcal{G}}\{\boldsymbol{\omega}_{\mathcal{G}/\mathcal{B}}\} + {}^{\mathcal{G}}[I_{\mathrm{W}/C_{\mathrm{G}}}][R_{\mathcal{B}}^{\mathcal{G}}]^{\mathcal{B}}\{\boldsymbol{\omega}_{\mathcal{B}/\mathcal{N}}\}.\end{aligned}$$

From Eq.(245) , therefore, the total angular momentum of whole spacecraft becomes

$$\begin{aligned}{}^{\mathcal{B}}\{\mathbf{h}_{\mathrm{B}/O}\} &= {}^{\mathcal{B}}[I_{\mathrm{P}/C_{\mathrm{P}}}]^{\mathcal{B}}\{\boldsymbol{\omega}_{\mathcal{B}/\mathcal{N}}\} + m_{\mathrm{P}} M_{\mathrm{P}}{}^{\mathcal{B}}\{\boldsymbol{\omega}_{\mathcal{B}/\mathcal{N}}\} + [R_{\mathcal{G}}^{\mathcal{B}}]^{\mathcal{G}}[I_{\mathrm{G}/C_{\mathrm{G}}}]^{\mathcal{G}}\{\boldsymbol{\omega}_{\mathcal{G}/\mathcal{B}}\} \\ &\quad + [R_{\mathcal{G}}^{\mathcal{B}}]^{\mathcal{G}}[I_{\mathrm{G}/C_{\mathrm{G}}}][R_{\mathcal{B}}^{\mathcal{G}}]^{\mathcal{B}}\{\boldsymbol{\omega}_{\mathcal{B}/\mathcal{N}}\} + [R_{\mathcal{G}}^{\mathcal{B}}]^{\mathcal{G}}[I_{\mathrm{W}/C_{\mathrm{G}}}]^{\mathcal{G}}\{\boldsymbol{\omega}_{\mathcal{W}/\mathcal{G}}\} + [R_{\mathcal{G}}^{\mathcal{B}}]^{\mathcal{G}}[I_{\mathrm{W}/C_{\mathrm{G}}}]^{\mathcal{G}}\{\boldsymbol{\omega}_{\mathcal{G}/\mathcal{B}}\} \\ &\quad + [R_{\mathcal{G}}^{\mathcal{B}}]^{\mathcal{G}}[I_{\mathrm{W}/C_{\mathrm{G}}}][R_{\mathcal{B}}^{\mathcal{G}}]^{\mathcal{B}}\{\boldsymbol{\omega}_{\mathcal{B}/\mathcal{N}}\} + m_{\mathrm{C}} M_{\mathrm{C}}{}^{\mathcal{B}}\{\boldsymbol{\omega}_{\mathcal{B}/\mathcal{N}}\} \\ &= \left({}^{\mathcal{B}}[I_{\mathrm{P}/C_{\mathrm{P}}}] + m_{\mathrm{P}} M_{\mathrm{P}} + m_{\mathrm{C}} M_{\mathrm{C}} + [R_{\mathcal{G}}^{\mathcal{B}}]\left({}^{\mathcal{G}}[I_{\mathrm{G}/C_{\mathrm{G}}}] + {}^{\mathcal{G}}[I_{\mathrm{W}/C_{\mathrm{G}}}]\right)[R_{\mathcal{B}}^{\mathcal{G}}]\right){}^{\mathcal{B}}\{\boldsymbol{\omega}_{\mathcal{B}/\mathcal{N}}\} \\ &\quad + [R_{\mathcal{G}}^{\mathcal{B}}]\left({}^{\mathcal{G}}[I_{\mathrm{G}/C_{\mathrm{G}}}] + {}^{\mathcal{G}}[I_{\mathrm{W}/C_{\mathrm{G}}}]\right){}^{\mathcal{G}}\{\boldsymbol{\omega}_{\mathcal{G}/\mathcal{B}}\} + [R_{\mathcal{G}}^{\mathcal{B}}]^{\mathcal{G}}[I_{\mathrm{W}/C_{\mathrm{G}}}]^{\mathcal{G}}\{\boldsymbol{\omega}_{\mathcal{W}/\mathcal{G}}\}\end{aligned} \tag{246}$$

Let us define ${}^{\mathcal{B}}I$ as the combined matrix of inertia of the spacecraft platform and the *point mass* of the VSCMG written in the body frame, then it can be written as

$$ {}^{\mathcal{B}}I = {}^{\mathcal{B}}[I_{\mathrm{P}/C_{\mathrm{P}}}] + m_{\mathrm{P}}M_{\mathrm{P}} + m_{\mathrm{C}}M_{\mathrm{C}} = {}^{\mathcal{B}}[I_{\mathrm{P}/O}] + m_{\mathrm{C}}M_{\mathrm{C}} \tag{247} $$

by the parallel axis theorem for inertia [31]. Defining $I_{\mathrm{cs}_i} \triangleq I_{\mathrm{gs}_i} + I_{\mathrm{ws}_i}$, $I_{\mathrm{ct}_i} \triangleq I_{\mathrm{gt}_i} + I_{\mathrm{wt}_i}$, and $I_{\mathrm{cg}_i} \triangleq I_{\mathrm{gg}_i} + I_{\mathrm{wg}_i}$, one can easily show that

$$ [R^{\mathcal{B}}_{\mathcal{G}}] \left({}^{\mathcal{G}}[I_{\mathrm{G}/C_{\mathrm{G}}}] + {}^{\mathcal{G}}[I_{\mathrm{W}/C_{\mathrm{G}}}] \right) [R^{\mathcal{G}}_{\mathcal{B}}] = I_{\mathrm{cs}_i}\{\mathbf{s}\}\{\mathbf{s}\}^T + I_{\mathrm{ct}_i}\{\mathbf{t}\}\{\mathbf{t}\}^T + I_{\mathrm{cg}_i}\{\mathbf{g}\}\{\mathbf{g}\}^T $$

In addition,

$$ {}^{\mathcal{G}}\{\boldsymbol{\omega}_{\mathcal{G}/\mathcal{B}}\} = [0, 0, \dot{\gamma}_i], \quad \text{and} \quad {}^{\mathcal{G}}\{\boldsymbol{\omega}_{\mathcal{W}/\mathcal{G}}\} = [\Omega_i, 0, 0] $$

where $\dot{\gamma}_i$ is a gimbal angle rate and Ω_i is wheel spinning speed of the i-th VSCMG.

Finally, Eq.(246) gives the total angular momentum of a spacecraft with a VSCMG written in the spacecraft body frame as

$$ \mathbf{h} \triangleq {}^{\mathcal{B}}\{\mathbf{h}_{\mathrm{B}/O}\} = \left({}^{\mathcal{B}}I + I_{\mathrm{cs}_i}\{\mathbf{s}\}\{\mathbf{s}\}^T + I_{\mathrm{ct}_i}\{\mathbf{t}\}\{\mathbf{t}\}^T + I_{\mathrm{cg}_i}\{\mathbf{g}\}\{\mathbf{g}\}^T \right) {}^{\mathcal{B}}\{\boldsymbol{\omega}_{\mathcal{B}/\mathcal{N}}\} + I_{\mathrm{cg}_i}\dot{\gamma}_i\mathbf{g} + I_{\mathrm{ws}_i}\Omega_i\mathbf{s}. \tag{248} $$

This equation can be expanded for the case of N VSCMGs cluster as

$$ \mathbf{h} = J\boldsymbol{\omega} + A_g I_{\mathrm{cg}}\dot{\boldsymbol{\gamma}} + A_s I_{\mathrm{ws}}\boldsymbol{\Omega} \tag{249} $$

$$ J \triangleq {}^{\mathcal{B}}I + A_s I_{\mathrm{cs}} A_s^T + A_t I_{\mathrm{ct}} A_t^T + A_g I_{\mathrm{cg}} A_g^T \tag{250} $$

where

$$ \boldsymbol{\gamma} = [\gamma_1, \ldots, \gamma_N]^T, \quad \boldsymbol{\Omega} = [\Omega_1, \ldots, \Omega_N]^T, $$

$$ A_s = [\{\mathbf{s}_1\}, \cdots, \{\mathbf{s}_N\}], \quad A_t = [\{\mathbf{t}_1\}, \cdots, \{\mathbf{t}_N\}], \quad A_g = [\{\mathbf{g}_1\}, \cdots, \{\mathbf{g}_N\}] $$

and $I_{\mathrm{c}\bullet} = I_{\mathrm{g}\bullet} + I_{\mathrm{w}\bullet}$, and $I_{\mathrm{g}\bullet} = \mathrm{diag}[I_{\mathrm{g}\bullet_1}, \ldots, I_{\mathrm{g}\bullet_{\mathrm{N}}}]$, $I_{\mathrm{w}\bullet} = \mathrm{diag}[I_{\mathrm{w}\bullet_1}, \ldots, I_{\mathrm{w}\bullet_{\mathrm{N}}}]$, where $\bullet$ is g, s, or t,

APPENDIX B

PROOFS FOR ANALYSIS OF THE SINGULARITIES OF VSCMGs

B.1 The Gradient of the Condition Number

In this appendix, a detailed procedure for computing the gradients $\frac{\partial \kappa}{\partial \boldsymbol{\gamma}}^T$ and $\frac{\partial \kappa}{\partial \boldsymbol{\Omega}}^T$ needed in the gradient method of Section 5.1 is presented. The condition number is chosen as a measure to the vicinity to the singularity. To this end, let $\kappa(\boldsymbol{\gamma}, \boldsymbol{\Omega})$ be the condition number of the matrix-valued function $C : [0, 2\pi)^N \times \mathbb{R}^N \to \mathbb{R}^{3\times N}$ defined by

$$C \triangleq [I_{\text{ws1}}\Omega_1\mathbf{t}_1, \cdots, I_{\text{wsN}}\Omega_N\mathbf{t}_N]\,.$$

Since the matrix C is a function of $\boldsymbol{\gamma} = [\gamma_1, \cdots, \gamma_N]^T$ and $\boldsymbol{\Omega} = [\Omega_1, \cdots, \Omega_N]^T$, so is κ. Let the matrix C be factored using its singular value decomposition as follows

$$C = U\Sigma V^T$$

where $U = [\mathbf{u}_1, \mathbf{u}_2, \mathbf{u}_3] \in \mathbb{R}^{3\times 3}$ and $V = [\mathbf{v}_1, \mathbf{v}_2, \cdots, \mathbf{v}_N] \in \mathbb{R}^{N\times N}$ are unitary matrices, $\mathbf{u}_i$ is a 3×1 column vector, and $\mathbf{v}_i$ is a $N \times 1$ column vector. In addition, $\Sigma = \text{diag}[\sigma_1, \sigma_2, \sigma_3]$, where $\sigma_1, \sigma_2, \sigma_3$ $(\sigma_1 \geq \sigma_2 \geq \sigma_3 \geq 0)$ are the singular values of C. Since $\kappa = \sigma_1/\sigma_3$, one obtains

$$\frac{\partial \kappa}{\partial x} = \frac{1}{\sigma_3}\frac{\partial \sigma_1}{\partial x} - \frac{\sigma_1}{\sigma_3^2}\frac{\partial \sigma_3}{\partial x}$$

where $x = \gamma_i$ or Ω_i. Junkins and Kim [37] have provided the partial derivatives of the singular values as follows

$$\frac{\partial \sigma_i}{\partial x} = \mathbf{u}_i^T \frac{\partial C}{\partial x}\mathbf{v}_i, \quad i = 1, 2, 3$$

From the fact

$$\begin{aligned}
\frac{\partial C}{\partial \gamma_i} &= [0, \cdots, -I_{wsi}\Omega_i\hat{\mathbf{s}}_i, \cdots, 0], \quad i = 1, \cdots, N \\
\frac{\partial C}{\partial \Omega_i} &= [0, \cdots, I_{wsi}\hat{\mathbf{t}}_i, \cdots, 0], \quad i = 1, \cdots, N
\end{aligned}$$

the gradients of $\kappa(\boldsymbol{\gamma}, \boldsymbol{\Omega})$ can be written as

$$\begin{aligned}\frac{\partial \kappa}{\partial \boldsymbol{\gamma}} &= [\frac{\partial \kappa}{\partial \gamma_1}, \cdots, \frac{\partial \kappa}{\partial \gamma_N}] \\ &= \frac{1}{\sigma_3}\mathbf{u}_1^T \left[\frac{\partial C}{\partial \boldsymbol{\gamma}}\right] \mathrm{diag}[v_{11}, v_{21}, \cdots, v_{N1}] \\ &\quad -\frac{\sigma_1}{\sigma_3^2}\mathbf{u}_3^T \left[\frac{\partial C}{\partial \boldsymbol{\gamma}}\right] \mathrm{diag}[v_{13}, v_{23}, \cdots, v_{N3}]\end{aligned}$$

and

$$\begin{aligned}\frac{\partial \kappa}{\partial \boldsymbol{\Omega}} &= [\frac{\partial \kappa}{\partial \Omega_1}, \cdots, \frac{\partial \kappa}{\partial \Omega_N}] \\ &= \frac{1}{\sigma_3}\mathbf{u}_1^T \left[\frac{\partial C}{\partial \boldsymbol{\Omega}}\right] \mathrm{diag}[v_{11}, v_{21}, \cdots, v_{N1}] \\ &\quad -\frac{\sigma_1}{\sigma_3^2}\mathbf{u}_3^T \left[\frac{\partial C}{\partial \boldsymbol{\Omega}}\right] \mathrm{diag}[v_{13}, v_{23}, \cdots, v_{N3}]\end{aligned}$$

where

$$\left[\frac{\partial C}{\partial \boldsymbol{\gamma}}\right] \triangleq [-I_{\mathrm{ws1}}\Omega_1\mathbf{s}_1, -I_{\mathrm{ws2}}\Omega_2\mathbf{s}_2, \cdots, -I_{\mathrm{wsN}}\Omega_N\mathbf{s}_N]$$

and

$$\left[\frac{\partial C}{\partial \boldsymbol{\Omega}}\right] \triangleq [I_{\mathrm{ws1}}\mathbf{t}_1, I_{\mathrm{ws2}}\mathbf{t}_2, \cdots, I_{\mathrm{wsN}}\mathbf{t}_N]$$

and v_{ij} is the ijth element of the matrix V.

B.2 Solution of the Maximization Problem for the Momentum Envelope of VSCMGs

To show (100)-(101) let $\phi_i \in [0, \pi/2]$ denote the angle between $\hat{\mathbf{u}}$ and $\hat{\mathbf{s}}_i$ at the singular configuration with $\epsilon_i = \mathrm{sign}(\hat{\mathbf{s}}_i \cdot \hat{\mathbf{u}}) = +1$ in Fig. 15. The value of $\alpha_i \triangleq \hat{\mathbf{u}} \cdot \hat{\mathbf{s}}_i$ is maximum at this singular configuration, so we have that

$$\begin{aligned}\alpha_{\max i} &= \max\{\hat{\mathbf{u}} \cdot \hat{\mathbf{s}}_i\} = \cos\phi_i = \sqrt{1 - \sin^2(\phi_i)} \\ &= \sqrt{1 - \cos^2(\pi - \phi_i)} = \sqrt{1 - (\hat{\mathbf{g}}_i \cdot \hat{\mathbf{u}})^2}\end{aligned}$$

Introduce the Lagrange multipliers λ_0 and λ_i for $i = 1, \ldots, N$ and define the Lagrangian $\mathcal{L}$ as

$$\mathcal{L} \triangleq \sum_{i=1}^{N} \alpha_i I_{\mathrm{ws}_i}\Omega_i - \lambda_0(\sum_{i=1}^{N} I_{\mathrm{ws}_i}\Omega_i^2 - 2E) - \sum_{i=1}^{N} \lambda_i(\alpha_i^2 - {\alpha_{\max}}_i^2).$$

Then the necessary conditions for a maximum are

$$\frac{\partial \mathcal{L}}{\partial \Omega_i} = \alpha_i I_{\mathrm{w}s_i} - 2\lambda_0 I_{\mathrm{w}s_i}\Omega_i = 0, \quad i = 1, \ldots, N \tag{251}$$

$$\frac{\partial \mathcal{L}}{\partial \alpha_i} = I_{\mathrm{w}s_i}\Omega_i - 2\lambda_i \alpha_i = 0, \quad i = 1, \cdots, N \tag{252}$$

and the complementary slackness condition

$$\lambda_i(\alpha_i^2 - {\alpha_{\max}}_i^2) = 0, \quad i = 1, \ldots, N \tag{253}$$

also must be satisfied.

If $\lambda_0 = 0$ then (251) implies that $\alpha_i^* = 0$ for all $i = 1, \ldots, N$ and (252) yields that $\Omega_i^* = 0$ for all $i = 1, \ldots, N$ which violates the energy constraint. Hence $\lambda_0 \neq 0$, and thus equation (251) yields that

$$\Omega_i^* = \frac{\alpha_i^*}{2\lambda_0}, \qquad i = 1, \ldots, N \tag{254}$$

Now, let us show that the maximizing solution has $\lambda_i \neq 0, \forall i = 1, \ldots, N$, as follows. Consider two candidates for the maximum solution: The candidate (i) is denoted by a superscript $(\cdot)^*$ and the other candidate (ii) by $(\cdot)^{**}$. Assume that $\exists k \in \{1, \ldots, N\}$ such that $\lambda_k^* = 0$ and thus $\Omega_k^* = 0$ from Eq.(252). Clearly, there exists at least one VSCMG with nonzero wheel speed to keep the energy constraint, thus let this VSCMGs be the $(k+1)$th, without loss of generality. Then, we have

$$\begin{aligned} \lambda_k^* &= 0, \quad \lambda_{k+1}^* \neq 0 \\ \Omega_k^* &= 0, \quad \Omega_{k+1}^* \neq 0. \end{aligned}$$

and in order keep the energy constraint,

$$I_{\mathrm{w}s_{k+1}} {\Omega^*}_{k+1}^2 = 2E - \sum_{\substack{i=1 \\ i \neq k, k+1}}^{N} I_{\mathrm{w}s_i}\Omega_i^{*2} \triangleq 2E'$$

and from (253), $\alpha_{k+1}^* = \alpha_{\max k+1}$, since $\alpha_{k+1}^* = -\alpha_{\max k+1}$ is not the maximum obviously.

Define the second candidate so that

$$\Omega_i^{**} = \Omega_i^*, \ \alpha_i^{**} = \alpha_i^* \quad i = 1, \ldots, k-1, k+2, \ldots, N \tag{255}$$

and

$$\Omega_i^{**} = \frac{\alpha_{\max i}}{2\lambda_0^{**}}, \quad \alpha_i^{**} = \alpha_{\max i}, \quad i = k,\, k+1$$

where

$$\lambda_0^{**} = \frac{1}{\sqrt{8E'}} \left(I_{\mathrm{w}s_k} \alpha_{\max_k}^2 + I_{\mathrm{w}s_{k+1}} \alpha_{\max_{k+1}}^2 \right)^{\frac{1}{2}}.$$

It is easily shown that this candidate (ii) satisfies the constraints (98) and (99).

One can have the cost of each candidate as

$$\begin{aligned} \mathcal{J}_{\mathrm{ME}}^* = (\mathbf{H} \cdot \hat{\mathbf{u}})^* &= \sum_{i=1}^{N} \alpha_i^* I_{\mathrm{w}s_i} \Omega_i^* = \sum_{\substack{i=1 \\ i \neq k,k+1}}^{N} \alpha_i^* I_{\mathrm{w}s_i} \Omega_i^* + \alpha_{k+1}^* I_{\mathrm{w}s_{k+1}} \Omega_{k+1}^* \\ &= \sum_{\substack{i=1 \\ i \neq k,k+1}}^{N} \alpha_i^* I_{\mathrm{w}s_i} \Omega_i^* + \sqrt{2E' I_{\mathrm{w}s_{k+1}} \alpha_{\max_{k+1}}^2} \end{aligned} \tag{256}$$

and

$$\begin{aligned} \mathcal{J}_{\mathrm{ME}}^{**} = (\mathbf{H} \cdot \hat{\mathbf{u}})^{**} &= \sum_{i=1}^{N} \alpha_i^{**} I_{\mathrm{w}s_i} \Omega_i^{**} = \sum_{\substack{i=1 \\ i \neq k,k+1}}^{N} \alpha_i^* I_{\mathrm{w}s_i} \Omega_i^* + \alpha_k^{**} I_{\mathrm{w}s_k} \Omega_k^{**} + \alpha_{k+1}^{**} I_{\mathrm{w}s_{k+1}} \Omega_{k+1}^{**} \\ &= \sum_{\substack{i=1 \\ i \neq k,k+1}}^{N} \alpha_i^* I_{\mathrm{w}s_i} \Omega_i^* + \sqrt{2E'(I_{\mathrm{w}s_k} \alpha_{\max_k}^2 + I_{\mathrm{w}s_{k+1}} \alpha_{\max_{k+1}}^2)}. \end{aligned} \tag{257}$$

It is clear that $\mathcal{J}_{\mathrm{ME}}^* \leq \mathcal{J}_{\mathrm{ME}}^{**}$. Moreover, $\mathcal{J}_{\mathrm{ME}}^* = \mathcal{J}_{\mathrm{ME}}^{**}$ only when $\alpha_{\max_k} = 0$, i.e. $\hat{\mathbf{u}} = \pm \mathbf{g}_k$, but in this case $\Omega_k^* = 0$ regardless of λ_k. Therefore, one can say that the maximizing solution must have $\lambda_i \neq 0, \forall i = 1, \ldots, N$.

From above analysis, we only need to check the case with $\lambda_i \neq 0$ for all $i = 1, \ldots, N$. The complementary slackness condition (253) yields that

$$\alpha_i^* = \alpha_{\max i}, \quad i = 1, \ldots, N$$

and from Eq.(254),

$$\Omega_i^* = \frac{\alpha_{\max_i}^*}{2\lambda_0}, \quad i = 1, \ldots, N$$

In order to satisfy the energy constraint,

$$\sum_{i=1}^{N} I_{\mathrm{w}s_i} \Omega_i^{*2} = \frac{\sum_{i=1}^{N} I_{\mathrm{w}s_i} \alpha_{\max_i}^2}{4\lambda_0^2} = 2E$$

we have

$$\lambda_0 = \frac{1}{\sqrt{8E}} \left(\sum_{i=1}^{N} I_{\mathrm{ws}_i} {\alpha_{\max}}_i^2 \right)^{\frac{1}{2}},$$

which completes the solution.

Next, we show that the maximizer

$$\Omega_i^* = \frac{{\alpha_{\max}}_i^*}{2\lambda_0}, \qquad \alpha_i^* = \alpha_{\max i}, \quad i = 1, \ldots, N \tag{258}$$

occurs if and only if the VSCMG system encounters a singularity with rank $M = 1$, i.e. an inescapable singularity.

Sufficiency follows from the fact that $\alpha_i^* = \alpha_{\max i}$ implies a singularity with $\epsilon_i = +1$ for all $i = 1, \ldots, N$. Then the matrix M defined in Eq. (92) becomes

$$\begin{aligned} M &= \begin{bmatrix} I_{\mathrm{ws}_1} \hat{\mathbf{u}} \cdot \mathbf{s}_1 & I_{\mathrm{ws}_2} \hat{\mathbf{u}} \cdot \mathbf{s}_2 & \cdots & I_{\mathrm{ws}_N} \hat{\mathbf{u}} \cdot \mathbf{s}_N \\ I_{\mathrm{ws}_1} \Omega_1^* & I_{\mathrm{ws}_2} \Omega_2^* & \cdots & I_{\mathrm{ws}_N} \Omega_N^* \end{bmatrix} \\ &= \begin{bmatrix} I_{\mathrm{ws}_1} \alpha_{\max_1} & \cdots & I_{\mathrm{ws}_N} \alpha_{\max_N} \\ I_{\mathrm{ws}_1} \alpha_{\max_1} / 2\lambda_0 & \cdots & I_{\mathrm{ws}_N} \alpha_{\max_N} / 2\lambda_0 \end{bmatrix} \end{aligned}$$

which obviously has rank 1.

To show necessity, notice that when VSCMG system encounters a singularity with rank $M = 1$, then necessarily $\epsilon_i = \mathrm{sign}(\hat{\mathbf{u}} \cdot \hat{\mathbf{s}}_i) = +1$ for all $i = 1, \ldots, N$, and thus

$$\alpha_i = \alpha_{\max i}, \quad i = 1, \ldots, N$$

Moreover, there exists a constant $\eta > 0$ such that

$$\boldsymbol{\Omega}^T = \eta \left[\hat{\mathbf{u}} \cdot \mathbf{s}_1, \cdots, \hat{\mathbf{u}} \cdot \mathbf{s}_N \right]$$

The energy constraint must be satisfied, that is,

$$E = \tfrac{1}{2} \boldsymbol{\Omega}^T I_{\mathrm{ws}} \boldsymbol{\Omega} = \tfrac{1}{2} \eta^2 \textstyle\sum_{i=1}^{N} I_{\mathrm{ws}i} (\hat{\mathbf{u}} \cdot \hat{\mathbf{s}}_i)^2 = \tfrac{1}{2} \eta^2 \sum_{i=1}^{N} I_{\mathrm{ws}_i} {\alpha_{\max}}_i^2$$

thus

$$\eta = \sqrt{\frac{2E}{\sum_{i=1}^{N} I_{\mathrm{ws}_i} {\alpha_{\max}}_i^2}} = \frac{1}{2\lambda_0}$$

which implies that

$$\Omega_i = \frac{\alpha_{\max i}}{2\lambda_0}, \quad i = 1, \ldots, N$$

which completes the proof.

B.3 The Momentum Envelope of VSCMGs in a Pyramid Configuration

Let $\mathrm{c}_\theta \triangleq \cos\theta$ and $\mathrm{s}_\theta \triangleq \sin\theta$. Then the gimbal axes of the VSCMG system in Fig. 7 with angle θ are

$$\mathbf{g}_1 = [\mathrm{s}_\theta, 0, \mathrm{c}_\theta]^T, \qquad \mathbf{g}_2 = [0, \mathrm{s}_\theta, \mathrm{c}_\theta]^T,$$
$$\mathbf{g}_3 = [-\mathrm{s}_\theta, 0, \mathrm{c}_\theta]^T, \qquad \mathbf{g}_4 = [0, -\mathrm{s}_\theta, \mathrm{c}_\theta]^T.$$

Also assume that every wheel has the same moment of inertia I_w. Then, for an arbitrary singular direction vector $\hat{\mathbf{u}} = [u_1, u_2, u_3]^T$, and using Eq. (102), the total angular momentum vector becomes

$$\mathbf{H} = \frac{I_\mathrm{w}}{2\lambda_0}\left(4\hat{\mathbf{u}} - \sum_{i=1}^{4}\hat{\mathbf{g}}_i(\hat{\mathbf{g}}_i\cdot\hat{\mathbf{u}})\right) = \frac{I_\mathrm{w}}{\lambda_0}\begin{bmatrix}(1+\mathrm{c}_\theta^2)u_1\\(1+\mathrm{c}_\theta^2)u_1\\2\mathrm{s}_\theta^2 u_3\end{bmatrix}$$

We also have

$$\mathbf{H}\cdot\hat{\mathbf{u}} = \frac{I_\mathrm{w}}{2\lambda_0}\left(4 - \sum_{i=1}^{4}(\hat{\mathbf{g}}_i\cdot\hat{\mathbf{u}})^2\right).$$

Since,

$$\begin{aligned}\lambda_0^2 &= \frac{I_\mathrm{w}}{8E}\sum_{i=1}^{4}\alpha_{\max_i}^2 = \frac{I_\mathrm{w}}{8E}\left(4 - \sum_{i=1}^{4}(\hat{\mathbf{g}}_i\cdot\hat{\mathbf{u}})^2\right)\\ &= \frac{\lambda_0}{4E}\mathbf{H}\cdot\hat{\mathbf{u}},\end{aligned}$$

it follows that

$$\lambda_0 = \frac{\mathbf{H}\cdot\hat{\mathbf{u}}}{4E}$$

Therefore,

$$(\mathbf{H}\cdot\hat{\mathbf{u}})\mathbf{H} = 4EI_\mathrm{w}A\hat{\mathbf{u}}$$

where $A \triangleq \mathrm{diag}\{1+\mathrm{c}_\theta^2, 1+\mathrm{c}_\theta^2, 2\mathrm{s}_\theta^2\}$, which implies

$$\hat{\mathbf{u}} = \frac{\mathbf{H}\cdot\hat{\mathbf{u}}}{4EI_\mathrm{w}}A^{-1}\mathbf{H}.$$

Finally, taking the dot product with $\mathbf{H}$ in both sides, yields

$$\mathbf{H}\cdot\hat{\mathbf{u}} = \frac{\mathbf{H}\cdot\hat{\mathbf{u}}}{4EI_\mathrm{w}}\mathbf{H}^TA^{-1}\mathbf{H}.$$

We have therefore the following quadratic equation for the possible values of $\mathbf{H}$

$$\mathbf{H}^T B \mathbf{H} = 1 \tag{259}$$

where

$$B \triangleq \frac{1}{4EI_{\mathrm{w}}} A^{-1} = \begin{bmatrix} \dfrac{1}{4EI_{\mathrm{w}}(1+c^2)} & 0 & 0 \\ 0 & \dfrac{1}{4EI_{\mathrm{w}}(1+c^2)} & 0 \\ 0 & 0 & \dfrac{1}{8EI_{\mathrm{w}}s^2} \end{bmatrix}$$

The last equation represents an ellipsoid with the semi-axes of lengths $\sqrt{4EI_{\mathrm{w}}(1+\cos^2\theta)}$, $\sqrt{4EI_{\mathrm{w}}(1+\cos^2\theta)}$ and $\sqrt{8EI_{\mathrm{w}}}\sin\theta$.

REFERENCES

[1] Aeyels, D., "Stabilization by smooth feedback of the angular velocity of a rigid body," *Systems and Control Letters*, vol. 6, no. 1, pp. 59–63, 1985.

[2] Aeyels, D. and Szafranski, M., "Comments on the stabilizability of the angular velocity of a rigid body," *Systems and Control Letters*, vol. 10, no. 1, pp. 35–39, 1988.

[3] Ahmed, J. and Bernstein, D., "Adaptive control of a dual-axis CMG with an unbalanced rotor," in *Proceedings of the 37th IEEE Conference on Decision and Control*, (Tampa, FL), pp. 4531–4536, Dec.1992.

[4] Ahmed, J., Coppola, V., and Bernstein, D. S., "Adaptive asymptotic tracking of spacecraft attitude motion with inertia matrix identification," *Journal of Guidance, Control, and Dynamics*, vol. 21, no. 5, pp. 684–691, 1998.

[5] Ahmed, J., Coppola, V., and Bernstein, D., "Adaptive asymptotic tracking of spacecraft attitude motion with inertia matrix identification," *Journal of Guidance, Control, and Dynamics*, vol. 21, no. 5, pp. 684–691, 1998.

[6] Anderson, B. D. O., "Adaptive systems, lack of persistency of excitation and bursting phenomenon," *Automatica*, vol. 21, pp. 247–258, 1985.

[7] Anderson, W. and Keckler, C., "An integrated power/attitude control system (IPACS) for space application," in *Proceedings of the 5th IFAC Symposium on Automatic Control in Space*, (New York), pp. 81–82, Pergamon, 1973.

[8] Andriano, V., "Global feedback stabilization of the angular velocity of a symmetric rigid body," *Systems and Control Letters*, vol. 20, pp. 361–364, 1993.

[9] Bang, H., Myung, H.-S., and Tahk, M.-J., "Nonlinear momentum transfer control of spacecraft by feedback linearization," *Journal of Spacecraft and Rockets*, vol. 39, no. 6, pp. 866–873, 2002.

[10] Bedrossian, N. S., Paradiso, J., Bergmann, E. V., and Rowell, D., "Redundant single gimbal control moment gyroscope singularity analysis," *Journal of Guidance, Control, and Dynamics*, vol. 13, no. 6, pp. 1096–1101, 1990.

[11] Bedrossian, N. S., Paradiso, J., Bergmann, E. V., and Rowell, D., "Steering law design for redundant single-gimbal control moment gyroscopes," *Journal of Guidance, Control, and Dynamics*, vol. 13, no. 6, pp. 1083–1089, 1990.

[12] Bishop, R., Paynter, S., and Sunkel, J., "Adaptive control of space station with control moment gyros," in *IEEE Control Systems Magazine*, vol. 12, pp. 23–28, Oct.1992.

[13] Boskŏvić, J. D., Li, S.-M., and Mehra, R. K., "Robust stabilization of spacecraft in the presence of control input saturation using sliding mode control," in *AIAA Guidance, Navigation, and Control Conference*, pp. 1960–1970, 1999. Portland, OR.

[14] Bourdache-Siguerdidjane, H., "Further results on the optimal regulation of spacecraft angular momentum," *Optimization, Control, Applications and Methods*, vol. 12, pp. 273–278, 1991.

[15] Brockett, R. W., "Asymptotic stability and feedback stabilization," in *Differential Geometric Control Theory* (Brockett, R. W., Millman, R. S., and Sussman, H. J., eds.), pp. 181–208, Birkhauser, 1983.

[16] Brogan, W. L., *Modern Control Theory*, pp. 515–523. New Jersey: Prentice Hall, 3rd ed., 1991.

[17] Byrnes, C. I. and Isidori, A., "On the attitude stabilization of a rigid spacecraft," *Automatica*, vol. 27, no. 1, pp. 87–95, 1991.

[18] Caswell, P., "Getting flywheels ready to fly," GRC News Release 00-017 [on line] URL:http://www.lerc.nasa.gov/WWW/PAO/pressrel/2000/00-017.html [cited 15 Jan. 2002], NASA Glenn Research Center, March 2000.

[19] Chang, Y.-C., "An adaptive $\mathcal{H}_\infty$ tracking control for a class of nonlinear multiple-input-multiple-output (mimo) systems," *IEEE Transactions on Automatic Control*, vol. 46, pp. 1432–1437, Sep. 2001.

[20] Cormack III, A., "Three axis flywheel energy and control systems," tech. rep., NASA Technical Report TN-73-G&C-8, North American Rockwell Corp., 1973.

[21] Cornick, D. E., "Singularity avoidance control laws for single gimbal control moment gyros," in *Proceedings of the AIAA Guidance and Control Conference*, (New York), pp. 20–33, AIAA, 1979.

[22] Coron, J. M. and Keraï, E. L., "Explicit feedback stabilizing the attitude of a rigid spacecraft with two control torques," *Automatica*, vol. 32, no. 5, pp. 669–677, 1996.

[23] Dalsmo, M. and Egeland, O., "State feedback $\mathcal{H}_\infty$-suboptimal control of a rigid spacecraft," *IEEE Transactions on Automatic Control*, vol. 42, no. 8, pp. 1186–1189, 1997.

[24] DeVon, D., Fuentes, R., and Fausz, J., "Closed-loop power tracking for an integrated power and attitude control system using varialbe-speed control moment gyroscopes," in *AIAA Guidance, Navigation, and Control Conference and Exhibit*, AIAA, Aug. 2004.

[25] Dwyer, T. A. W., Fadali, M. S., and Chen, N., "Single step optimization of feedback-decoupled spacecraft attitude maneuvers," in *Proc. of the 24th Conference on Decision and Control*, pp. 669–671, 1985. Ft. Lauderdale, FL.

[26] Dwyer, T. A. W. and Sena, R. P., "Control of spacecraft slewing maneuvers," in *Proc. of the 21st Conference on Decision and Control*, pp. 1142–1144, 1982. Orlando, FL.

[27] Egeland, O. and Gødhavn, J., "Passivity-based adaptive attitude control of a rigid spacecraft," *IEEE Transactions on Automatic Control*, vol. 39, no. 4, pp. 842–846, 1994.

[28] Ford, K. A. and Hall, C. D., "Flexible spacecraft reorientations using gimbaled momentum wheels," in *Advances in the Astronautical Sciences, Astrodynamics* (Hoots, F., Kaufman, B., Cefola, P. J., and Spencer, D. B., eds.), vol. 97, (Univelt, San Diego), pp. 1895–1914, 1997.

[29] Ford, K. A. and Hall, C. D., "Singular direction avoidance steering for control-moment gyros," *Journal of Guidance, Control, and Dynamics*, vol. 23, no. 4, pp. 648–656, 2000.

[30] Ge, S. S., "Adaptive control of robots having both dynamical parameter uncertainties and unknown input scalings," *Mechatronics*, vol. 6, no. 5, pp. 557–569, 1996.

[31] Ginsberg, J. H., *Advanced Engineering Dynamics*, pp. 171–181. New York, NY: Cambridge University Press, 2nd ed., 1998.

[32] Hall, C., "Momentum transfer in two-rotor gyrostats," *Journal of Guidance, Control, and Dynamics*, vol. 19, no. 5, pp. 1157–1161, 1996.

[33] Hall, C. D., "High-speed flywheels for integrated energy storage and attitude control," in *American Control Conference*, (Albuquerque, NM), pp. 1894–1898, 1997.

[34] Heiberg, C. J., "A practical approach to modeling single-gimbal control momentum gyroscopes in agile spacecraft," in *AIAA Guidance, Navigation, and Control Conference and Exhibit*, (Denver, CO.), Aug., 2000. AIAA Paper 2000-4545.

[35] Heiberg, C. J., Bailey, D., and Wie, B., "Precision spacecraft pointing using single-gimbal control moment gyroscopes with disturbance," *Journal of Guidance, Control, and Dynamics*, vol. 23, no. 1, pp. 77–85, 2000.

[36] Horn, R. and Johnson, C. R., *Matrix Analysis*, pp. 427, 449. Cambridge, United Kingdom: Cambridge University Press, 1985.

[37] Junkins, J. L. and Kim, Y., *Introduction to Dynamics and Control of Flexible Structures*, pp. 48–49. New York: AIAA, 1993.

[38] Junkins, J. L. and Turner, J., *Optimal Spacecraft Rotational Maneuvers*. New York: Elsevier, 1986.

[39] Kailath, T., *Linear Systems*, pp. 135–139. Englewood Cliffs, New Jersey: Prentice-Hall, 1980.

[40] Kenny, B. and Kascak, P. E., "DC bus regulation with flywheel energy storage system," Technical Report NASA/TM-2002-211897, NASA Glenn Research Center, January 2003.

[41] Khalil, H. K., *Nonlinear Systems*. New Jersey: Prentice Hall, 2nd ed., 1996.

[42] Kim, S. and Kim, Y., "Spin-axis stabilization of a rigid spacecraft using two reaction wheels," *Jornal of Guidance, Control, and Dynamics*, vol. 24, no. 5, pp. 321–331, 2001.

[43] Krishnan, H., McClamroch, H., and Reyhanoglu, M., "Attitude stabilization of a rigid spacecraft using two momentum wheel actuators," *Journal of Guidance, Control, and Dynamics*, vol. 18, no. 2, pp. 256–263, 1995.

[44] Krishnan, H., Reyhanoglu, M., and McClamroch, H., "Attitude stabilization of a rigid spacecraft using two control torques: A nonlinear control approach based on the spacecraft attitude dynamics," *Automatica*, vol. 30, no. 6, pp. 1023–1027, 1994.

[45] Kurokawa, H., "Exact singularity avoidance control of the pyramid type CMG system," in *Proceedings of the AIAA Guidance, Navigation and Control Conference*, (Scottsdale, AZ), pp. 170–180, 1994. AIAA Paper 94-3559.

[46] Kurokawa, H. and Yajima, N., "A study of CMG systems - for selection and evaluation," in *Proceedings of 16th International Symposium on Space Technology and Science*, (Japan), pp. 1243–1249, 1988.

[47] Kurokawa, H., Yajima, N., and Usui, S., "A study of single gimbal CMG system," in *Proceedings of 15th International Symposium on Space Technology and Science*, (Japan), pp. 1219–1224, 1986.

[48] Kurokawa, H., "Constrained steering law of pyramid-type control moment gyros and ground tests," *Journal of Guidance, Control, and Dynamics*, vol. 20, no. 3, pp. 445–449, 1997.

[49] Kurokawa, H., "A geometry study of single gimbal control moment gyros - singularity problem and steering law," Tech. Rep. Report No.175, Mechanical Engineering Laboratory, Japan, Jan. 1998.

[50] Lam, Q. M., Pal, P. K., Hu, A., Welch, R., Grossman, W., and Freesland, D. C., "Robust attitude control using a joint quaternion feedback regulator and nonlinear model-follower," in *AIAA Guidance, Navigation, and Control Conference*, pp. 817–827, 1996. San Diego, CA.

[51] Lange, T., "Optimal magnetic bearing control for high-speed momentum wheels," *Journal of Guidance, Control, and Dynamics*, vol. 8, no. 6, pp. 737–742, 1985.

[52] Lappas, V. J., Steyn, W. H., and Underwood, C. I., "Practical results on the development of a control moment gyro based attitude control system for agile small satellites," in *Sixteenth Annual AIAA/USU Conference on Small Satellites*, (Logan, UT), Utah State University, Aug., 2002.

[53] Lappas, V. J. and Underwood, C. I., "Experimental testing of a cmg cluster for agile microsatellites," in *54th International Astronautical Congress of the International Astronautical Federation (IAF)*, (Bremen, Germany), Sep.- Oct., 2003.

[54] Lintereur, B. V. and McGovern, L. K., "Constrained $\mathcal{H}_2$ design via convex optimization applied to precision pointing attitude control," in *Proc. of the 36th IEEE Conference on Decision and Control*, pp. 1300–1304, 1997. San Diego, CA.

[55] Lizarralde, F. and Wen, J. T., "Attitude control without angular velocity measurement: A passivity approach," *IEEE Transactions on Automatic Control*, vol. 41, no. 3, pp. 468–472, 1996.

[56] Margulies, G. and Aubrun, J. N., "Geometric theory of single-gimbal control moment gyro systems," *Journal of the Astronautical Science*, vol. 26, no. 2, pp. 159–191, 1978.

[57] Morin, P., "Robust stabilization of the angular velocity of a rigid body with two controls," *European Journal of Control*, vol. 1, pp. 51–56, 1996.

[58] Morin, P. and Samson, C., "Time-varying exponential stabilization of a rigid spacecraft with two control torques," *IEEE Transactions on Automatic Control*, vol. 42, no. 4, pp. 528–534, 1997.

[59] Notti, J., Cormack III, A., Schmill, W., and Klein, W., "Integrated power/attitude control system (IPACS) study : Volume ii - conceptual designs," tech. rep., NASA Technical Report CR-2384, Rockwell International Space Division, Downey, CA, 1974.

[60] Oh, H. and Vadali, S., "Feedback control and steering laws for spacecraft using single gimbal control moment gyro," *The Journal of the Astronautical Sciences*, vol. 39, no. 2, pp. 183–203, 1991.

[61] Osipchuk, M., Bharadwaj, S., and Mease, K., "Achieving good performance in global attitude stabilization," in *Proceedings of the American Control Conference*, pp. 403–407, 1997. Albuquerque, NM.

[62] Outbib, R. and Sallet, G., "Stabilizability of the angular velocity of a rigid body revisited," *Systems and Control Letters*, vol. 18, no. 2, pp. 93–98, 1992.

[63] Paradiso, J. A., "Global steering of single gimballed control moment gyroscopes using a directed search," *Journal of Guidance, Control, and Dynamics*, vol. 15, pp. 1236–1244, Sep.-Oct. 1992.

[64] Pomet, J.-B. and Praly, L., "Adaptive nonlinear regulation : Estimation from the lyapunov equation," *IEEE Transactions on Automatic Control*, vol. 37, pp. 729–740, June 1992.

[65] Richie, D. J., Tsiotras, P., and Fausz, J. L., "Simultaneous attitude control and energy storage using VSCMGs : Theory and simulation," in *Proceedings of American Control Conference*, pp. 3973–3979, 2001.

[66] Roes, J. B., "An electro-mechanical energy storage system for space application," in *Progress in Astronautics and Rocketry*, vol. 3, pp. 613–622, Academic Press, 1961.

[67] Schaub, H., *Novel Coordinates for Nonlinear Multibody Motion with Application to Spacecraft Dynamics and Control*. PhD thesis, Aerospace Engineering Department, Texas A&M University, May 1998.

[68] Schaub, H., Akella, M. R., and Junkins, J. L., "Adaptive control of nonlinear attitude motions realizing linear closed-loop dynamics," in *Proceedings of the American Control Conference*, pp. 1563–1567, 1999. San Diego, CA.

[69] Schaub, H., Akella, M. R., and Junkins, J. L., "Adaptive realization of linear closed-loop tracking dynamics in the presence of large system model errors," *Journal of the Astronautical Sciences*, vol. 48, pp. 537–551, Oct.-Dec. 2000.

[70] Schaub, H. and Junkins, J. L., "Stereographic orientation parameters for attitude dynamics: A generalization of the Rodrigues parameters," *Journal of the Astronautical Sciences*, vol. 44, no. 1, pp. 1–19, 1996.

[71] Schaub, H. and Junkins, J. L., "Singularity avoidance using null motion and variable-speed control moment gyros," *Journal of Guidance Control, and Dynamics*, vol. 23, no. 1, pp. 11–16, 2000.

[72] Schaub, H., Robinett, R. D., and Junkins, J. L., "Globally stable feedback laws for near-minimum-fuel and near-minimum-time pointing maneuvers for a landmark-tracking spacecraft," *Journal of the Astronautical Sciences*, vol. 44, no. 4, pp. 443–466, 1996.

[73] Schaub, H., Vadali, S. R., and Junkins, J. L., "Feedback control law for variable speed control moment gyroscopes," *Journal of the Astronautical Sciences*, vol. 46, no. 3, pp. 307–328, 1998.

[74] Sheen, J. and Bishop, R., "Adaptive nonlinear control of spacecraft," in *American Control Conference*, (Baltimore, Maryland), pp. 2867–2871, 1994.

[75] Sheen, J. J. and Bishop, R. H., "Spacecraft nonlinear control," in *AIAA/AAS Astrodynamics Conference*, (Hilton Head, SC), Aug. 10-12, 1992. Paper AAS 92-172.

[76] Shen, H. and Tsiotras, P., "Time-optimal control of axi-symmetric spacecraft," *Journal of Guidance, Control, and Dynamics*, vol. 22, no. 5, pp. 682–694, 1999.

[77] Shuster, M. D., "A survey of attitude representations," *Journal of the Astronautical Sciences*, vol. 41, no. 4, pp. 439–517, 1993.

[78] Singh, S. A., "Robust nonlinear attitude control of flexible spacecraft," *IEEE Transactions on Aerospace and Electronic Systems*, vol. 23, no. 2, pp. 380–387, 1987.

[79] Slotine, J. J. E. and Benedetto, M. D. D., "Hamiltonian adaptive control of spacecraft," *IEEE Transactions on Automatic Control*, vol. 35, pp. 848–852, July 1990.

[80] Slotine, J. J. E. and Di Benedetto, M. D., "Hamiltonian adaptive control of spacecraft," *IEEE Transactions on Automatic Control*, vol. 35, pp. 848–852, 1990.

[81] Slotine, J.-J. E. and Li, W., "Adaptive manipulator control : A case study," *IEEE Transactions on Automatic Control*, vol. 33, pp. 995 – 1003, Nov. 1988.

[82] Slotine, J. and Li, W., *Applied Nonlinear Control*. New Jersey: Prentice Hall, 1991.

[83] Sontag, E. and Sussmann, H., "Further comments on the stabilizability of the angular velocity of a rigid body," *Systems and Control Letters*, vol. 12, no. 3, pp. 213–217, 1988.

[84] Spindler, K., "Attitude control of underactuated spacecraft," *European Journal of Control*, vol. 6, no. 3, pp. 229–242, 2000.

[85] Tokar, E. N. and Platonov, V. N., "Singular surfaces in unsupported gyrodyne systems," *Cosmic Research*, vol. 16, no. 5, pp. 547–555, 1979.

[86] Tsiotras, P., "Stabilization and optimality results for the attitude control problem," *Journal of Guidance, Control, and Dynamics*, vol. 19, no. 4, pp. 772–779, 1996.

[87] Tsiotras, P., Corless, M., and Longuski, M., "A novel approach to the attitude control of axisymmetric spacecraft," *Automatica*, vol. 31, no. 8, pp. 1099–1112, 1995.

[88] Tsiotras, P. and Doumtchenko, V., "Control of spacecraft subject to actuator failures: State-of-the-art and open problems," in *Proceedings of the R.H. Battin Astrodynamics Symposium*, (College Station, TX), March 20-21, 2000. AAS Paper 00-264.

[89] Tsiotras, P., Junkins, J. L., and Schaub, H., "Higher order Cayley-transforms with applications to attitude representations," *Journal of Guidance, Control, and Dynamics*, vol. 20, no. 3, pp. 528–534, 1997.

[90] Tsiotras, P. and Luo, J., "Stabilization and tracking of underactuated axisymmetric spacecraft with bounded inputs," *Automatica*, vol. 36, no. 8, pp. 1153–1169, 2000.

[91] Tsiotras, P. and Schleicher, A., "Detumbling and partial attitude stabilization of a rigid spacecraft under actuator failure," in *AIAA Guidance, Navigation and Control Conference*, (Denver, CO), 2000. AIAA Paper 00-4044.

[92] Tsiotras, P., Shen, H., and Hall, C., "Satellite attitude control and power tracking with energy/momentum wheels," *Journal of Guidance, Control, and Dynamics*, vol. 24, no. 1, pp. 23–34, 2001.

[93] Tsiotras, P., Yoon, H., and Marshall, A., "Controllability analysis and control of spacecraft using a single-gimbal variable-speed control moment gyroscope," *Jornal of Guidance, Control, and Dynamics*, submitted for publication.

[94] Vadali, S. R., "Variable-structure control of spacecraft large-angle maneuvers," *Journal of Guidance, Control, and Dynamics*, vol. 9, no. 2, pp. 235–239, 1989.

[95] Vadali, S. R. and Junkins, J. L., "Spacecraft large angle rotational maneuvers with optimal momentum transfer," *Journal of the Astronautical Sciences*, vol. 31, no. 2, pp. 2178–235, 1983.

[96] Vadali, S. R., Kraige, L. G., and Junkins, J. L., "New results on the optimal spacecraft attitude maneuver problem," *Journal of Guidance, Control, and Dynamics*, vol. 7, no. 3, pp. 378–380, 1984.

[97] Vadali, S. R., Oh, H. S., and Walker, S. R., "Preferred gimbal angles for single gimbal control moment gyros," *Journal of Guidance Control, and Dynamics*, vol. 13, no. 6, pp. 1090–1095, 1990.

[98] Wen, J. T. and Kreutz-Delgado, K., "The attitude control problem," *IEEE Transactions on Automatic Control*, vol. 36, no. 10, pp. 1148–1162, 1991.

[99] Wertz, J. R., ed., *Spacecraft Attitude Determination and Control*, pp. 196–203. Dordrecht, Netherlands: D. Reidel Publishing Company, 1986 (reprinted).

[100] Wie, B., *Space Vehicle Dynamics and Control*. Reston, VA: American Institute of Aeronautics and Astronautics, Inc., 1998.

[101] Wie, B., Bailey, D., and Heiberg, C. J., "Singularity robust steering logic for redundant single-gimbal control moment gyros," *Journal of Guidance, Control, and Dynamics*, vol. 24, no. 5, pp. 865–872, 2001.

[102] Wie, B. and Barba, P. M., "Quaternion feedback for spacecraft large angle maneuvers," *Journal of Guidance, Control, and Dynamics*, vol. 8, no. 3, pp. 360–365, 1985.

[103] Wie, B., Weiss, H., and Arapostathis, A., "Quaternion feedback regulator for spacecraft eigenaxis rotation," *Journal of Guidance, Control, and Dynamics*, vol. 12, pp. 375–380, 1989.

[104] Wie, B., *Spacecraft Dynamics and Control : Applications of Dynamical Systems Theory*. Arizona State University, 1995.

[105] Wie, B., "New singularity escape and avoidance steering logic for control moment gyro systems," in *AIAA Guidance, Navigation, and Control Conference*, (Austin, TX), August 2003. Paper No. 2003-5659.

[106] Wie, B., "Singularity analysis and visualization for single-gimbal control moment gyro systems," in *AIAA Guidance, Navigation, and Control Conference*, (Austin, TX), August 2003. Paper No. 2003-5658.

[107] Yoshikawa, T., "Steering law for roof type configuration control moment gyro system," *Automatica*, vol. 13, pp. 359–368, July 1979.

[108] Zaremba, A., "An adaptive scheme with parameter identification for spacecraft attitude control," in *Proceedings of American Control Conference*, pp. 552–556, 1997.